AN APPROACH TO STRUCTURAL ANALYSIS

by

Anthony R. Kjar B.E.(Hons.)

submitted in partial fulfilment of the requirements

for the degree of

Doctor of Philosophy, in the

Faculty of Engineering

UNIVERSITY OF TASMANIA

AUSTRALIA.

- SEPTEMBER, 1967 -

INDEX

The purpose of this thesis is to present to the engineering profession a method of structural analysis which is peculiarly suited to the way engineers think. The range and the power of structural analysis are extended by careful study of the actual deformations of structures, leading to the formulation of simple mathematical models. The theme throughout this thesis is the deliberate effort to look for, and to describe characteristic shapes which define the deformed structure; general statements are obtained similar to the historically valuable models which used "plane sections remain plane" or "radial lines remain radial". Once an appreciation of the deformations of the structure is gained, the forces to sustain these deformations are then found easily.

This is one of the oldest approaches of engineering analysis, and the most powerful methods of analysis of structures have been along these lines. Men like Galileo, Parent, Navier, Bernoulli, and Coulomb developed an appreciation of structural behaviour by looking for simple geometric characteristics which would describe the deformed shape of the structure. (We may note also that Kepler's purely geometric study of the motions of the planets paved the way for Newton's formulation of his laws). And today, when one tries to visualize and calculate the deformations of a bent beam, it is difficult to improve upon the first overall approximation that plane sections remain plane.

The key to obtaining a simple mathematical model of a real problem is to start with a simple physical or laboratory model. Simple geometric approximations are then obtained by fitting an analytic function to the form of the deformations of the simple structure. The functional form is chosen so that the strains,

the stresses, and hence the overall statical equilibrium of the structure can be evaluated. With this basis on which thoughts can be focussed, the laboratory and mathematical models can be improved to be a closer representation of the real problem. This approach reduces the need to test full-size structures, as the geometric functional form acts as the geometric scaling factor. When full size testing is carried out, model tests are still a valuable means of providing a quick overall picture. This picture can then be used to determine which important geometric deformations should be measured. At present, full-size testing, although expensive, is still necessary as the relationships between the strength and the size of the material remain unanswered. Nevertheless, improve-ments in this field can be made; for example R.E. Rowe (Ref. 1) has shown that concrete mixtures can be scaled to produce the same geometric crack pattern as would be expected in the full-size structure.

An engineer is frequently using approximate overall characteristics of a simple model as a basis for obtaining further thoughts on the real problem. However, the inability to measure quickly the overall geometric deformations of a simple model has led to specialized full-size structural tests, not by engineers, but by research workers. The aim of this thesis if to show how to use simple experimental studies to obtain simple mathematical models, and thus fulfil the sentiment expressed by Sir Alfred Pugsley (Ref. 2) that "Drawing and design office staffs can, and like to, play a part in the extension of their methods, and if they could do so directly, not only by theoretical but by simple experiment, would welcome the opportunity".

The design of a through plate girder bridge is taken as the main problem throughout this thesis in order to co-ordinate the whole. Existing mathematical models and methods of design are based on the ideas developed after the buckling failure of several through bridges made with heavy floor beams. Bridges nowadays are being made with lighter floor beams, and model studies are used in the investigations for this thesis to indicate characteristic deformations of these lighter

through bridges. An understanding of the problem is obtained from these model studies, and is used to develop a new mathematical model. The predictions of this new model are then compared with measurements taken on a full-size bridge with strain gauge, spirit level, and rule, and reasonable agreement is obtained. This new mathematical model is then used as the basis for recommendations concerning the design of through bridges made with light floors.

*   *   *   *

In <u>Chapter One</u> the author presents a case for measuring geometric deformations as a means of obtaining a good functional form for the description of the structural problem. Simple and well known examples of stretched, bent, and twisted bars are chosen in order that the main features of the method are not lost in the process of mathematical manipulation.

<u>Chapter Two</u> begins with a detailed analysis of the structural stability of a pin-ended column. This review is used as an introduction to the use of a characteristic geometric describing shape in the study of structures liable to buckling instability. It is shown that for many years engineers have recognized the values of using an infinite Fourier sine series (derived from the differential equation describing the behaviour of the pin-ended column) to describe an arbitrary deformed shape. This method is useful when the structural behaviour can be represented by those differential equations for which sine functions are a solution. However, the existence of other sets of infinite series of buckling modes is not generally exploited by engineers. In this chapter it is shown how one can recognize these series by studying the properties of the differential equations and boundary conditions. The properties of the series are then used

to generalize the well known plot, first developed by Sir Richard Southwell (Ref. 3). This generalization provides a link between the initial and final shape of the structure with the loadings on the structure for a large range of structures liable to instability. With this sound analytical basis, reinforced with measurements taken on actual structures, the Southwell Plot becomes a more valuable experimental and design tool. The author believes that this generalization is original.

Chapter Three is the first of three chapters which are concerned with the design of a through bridge. In this chapter the measurements taken on a simplified light through bridge are outlined. It is found that the model through bridge is liable to lateral and torsional instability. A new mathematical model is developed to describe these lateral and torsional movements, and upper and lower bound solutions to the first buckling load are found. These loads and the corresponding buckling modes are shown to be a reasonable approximation to the measured results. Other original contributions outlined in the chapter include Southwell Plots on rotations and on strains suitable for use with the new mathematical model for the bridge, a method for separating the first buckling mode from the measurements of the total deformed shape, and a method for finding lower bound solutions in some structural problems.

In Chapter Four the effects of minor additions to the laboratory and mathematical model are investigated. The first effect described is that resulting from the inclusion of web stiffeners in the model through bridge. The inclusion of web stiffeners is shown to change only slightly the nature of the deformed shape, and to increase by only a small amount the buckling load. The second effect described is that of loadings applied at points other than through the centroid of the I beam. It is shown that lateral and torsional loadings applied to the bridge can sustain large deformations. An original extension of an existing method, used previously by engineers to estimate the deformations sustained by a lateral loading on a pin ended column, is then developed and an estimate of the effects of these loadings is obtained.

In Chapter Five the author discusses the design of real through bridges. An examination of existing code recommendations indicates that there exists a large difference between these recommendations and the measurements taken on the light through bridge (outlined in Chapter Three). To gain a greater appreciation of these differences, five additional model steel bridges are tested in the elastic and elasto-plastic ranges of deformation. A good fit to these model test results is shown to be the mathematical model developed in Chapter Three and, as a result of the understanding gained from these model test results, a process for use in the design of light through bridges is established. This design process is then checked by comparing these predictions with measurements taken on a full-size structure. In the light of these tests, design recommendations for light and heavy through bridges are made. In Chapter Five the new mathematical model developed in Chapter Three is consolidated, and the limits of this model are found in relation to existing mathematical models for heavy through bridges. Also in the chapter a simple approximation to the buckling load is found, and the concept and use of a line of first yield using simple patterns of the deformed shape of the bridge is presented.

In Chapter Six the range and the power of the method of functional form is illustrated by presentation of a description of torsion, as this problem of torsion arises naturally in the discussion of the deformations of the twisted and bent through bridge. It is shown that present methods to describe torsion depend on analogies (physical and mathematical), and at best describe shear stresses in terms of the slope on a thin film membrane, or in terms of the solution of a high order differential equation.

An effective geometric picture of torsion is obtained by measuring and describing the movement of a line drawn on the

twisted member. Coulomb (Ref. 4) used this approach and obtained the good approximation for a twisted circular bar that "plane sections, perpendicular to the longitudinal axis of the bar, remain plane". This approximation is a poor estimate of the deformations of a rectangular bar, and improving approximations could not be found. Later analysis of the torsion problem has therefore tended towards a more rigorous mathematical treatment. Nevertheless, further consideration of the deformations of the twisted section leads to the first approximation that for small angles of twist all straight lines originally parallel to the sides of the member remain straight after the member has been twisted. The behaviour of many twisted members with open and closed cross sections is investigated by using this basic approximation, and an original, complete, and simple picture of torsion is developed.

<p style="text-align:center">*   *   *   *</p>

Professor A.R. Oliver, the Professor of Civil and Mechanical

  Engineering at the University of Tasmania, and

Dr. M.S. Gregory, Reader in Civil and Mechanical Engineering

  at the University of Tasmania, and supervisor of this research.

The author has also had help in the form of correspondence, or

discussion from the following persons:

Mr. J.P. Hill, Chief Engineer, Maring Board of Devonport, Tasmania

Dr. M. Lay, State Electricity Commission, Victoria.

Mr. G. Sved, University of Adelaide.

Dr. N. Trahair, University of Sydney.

Dr. C. O'Connor, University of Queensland,   and

Professor B. Johnston, University of Michigan, U.S.A.

        *   *   *   *

    I hereby declare that, except as stated herein, this thesis

contains no material which has been accepted for the award of any

other degree or diploma in any University, and that, to the

best of my knowledge or belief this thesis contains no copy or

paraphrase of material previously published or written by another

person, except when due reference is made in the text of this thesis.

                      Anthony R. Kyi

CHAPTER ONE

MEASURING GEOMETRY TO OBTAIN SIMPLE MATHEMATICAL MODELS

1.1   Introduction

The formulation of any engineering problem is very conveniently

thought of as containing ~~any~~ three phases, (Refs. 5 and 6), These

are: the real problem, the physical models, and the mathematical

models. The real problem is initially a vague and undefined notion.

It may be the "investigation, design, and construction of a bridge",

while one of the physical models could be described as the bridge

structure itself, or the simplification of it used for structural

design purposes. The bridge structure may have a certain type and

number of beams, columns and decking, and the physical model is

often further defined and simplified in such a manner as to be

more amenable to description. Any description of the behaviour

of these physical models which depends on logical analysis is called

a mathematical model. In engineering analysis the mathematical

and physical models are gradually modified and used to formulate

and describe the real problem and enable a reasonable mathematical

model to be obtained.

All structural analysis is necessarily approximate, and to

obtain a mathematical description a functional relationship must

be used to connect some of the variables. A specific example is

the stress-strain relationship used in structural analysis. It

is rarely fruitful for the structural analyst to question the

nature of the mutual attraction of molecules or even to use the

Newtonian functional description of the problem, that is that there

are mutual forces of attraction between molecules which can be

described approximately as varying in terms of the inverse of

the square of the distance between the molecules. For most

structural analysts this description is far too specific and

it is sufficient to try to describe the overall stress and

strain relationship by direct measurement, combined with sensible

interpolation. Fortunately, the functional description of this relationship for some materials is sufficiently well described by straight lines over part of the practical range of strains.

Since all structural analysis is approximate, there exists a variety of ways in which the variables of the problem can be considered and manipulated. The method presented in this thesis is one in which a pattern is used to link the important deformations of the problem. This pattern, obtained from detailed measurement of model structures is described in terms of an analytic function, or functional form. With this overall estimate of the deformations, the forces to sustain the prescribed shape are easily found.

This is one of the oldest approaches of engineering analysis and the most powerful methods of analysis of structures have been along these lines. However, the source of the power of the method is not generally recognized. To show that the source lies in the use of a functional form or pattern to describe the deformations of the structure, a few historical estimates of the deformations of a bent beam are outlined.

1.2   The Beginnings of Structural Analysis

Structural analysis had its beginnings in the seventeenth century when mathematicians and geometricians like Mariotte and later Leibniz, Varignon and the Bernoulli brothers (Ref. 4) made approximations with regard to the displacements of bent bars. Jacob Bernoulli, when trying to calculate the deflections of a loaded cantilever took the deflection curve as shown in Fig. 1.1.

Suppose ABFD represents an element of the beam, the axial length is ds. Bernoulli made the approximation that during bending the cross section AB rotates with respect to the cross section FD, about an axis through A, and therefore the elongation of the fibres between two adjacent cross sections is proportional to the distance from the axis A.
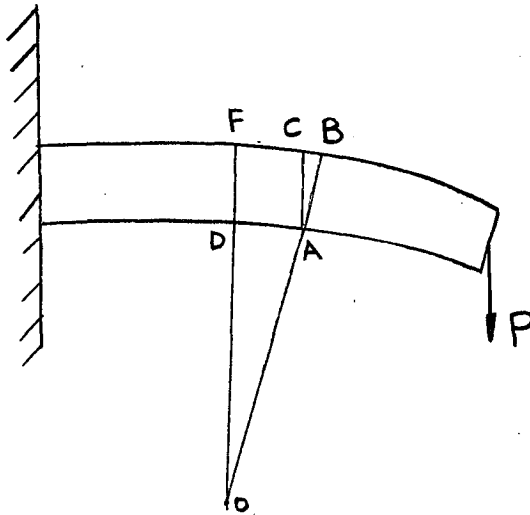
Fig. 1.1. Geometric Approximations for a bent beam: Bernoulli.

Measurements indicate that this approximation is reasonable, as the cross section AB remains reasonably straight. However, we now know that a better approximation for the line of zero strain is obtained by assuming that the cross section rotates about some point inside the beam, the position of this point depending on the particular material and the way it deforms under load.

Bernoulli's approximations allowed advances in structural analysis and the calculus was used to further the study, particularly the Euler column theory. A unified approach was made by Parent and later by Navier using the approximations that cross sections remained plane to describe the bending of plates and bars.

Later mathematicians developed more complicated models to describe the behaviour of structural elements, but they incorporated the smallest possible number of geometric approximations regarding the deformed shape. These developments have led to the mathematical approach involving stress function solutions, biharmonic solutions and high order differential equation solutions.

Improved mathematical models(using the mathematical approach) are obtained when a decrease is achieved in the number of approximations needed to specify the geometrical deformations, or when further account is taken of the complexity of the functional dependence of stress and strain, or when further account is taken of the complexity boundary or loading conditions.

The aim of a mathematical approach is then to make minimal assumptions or guesses of functional dependence, and to develop a complete description of a defined problem from a system of basic axioms, without the need for an appreciation of the deformations of the structure.

The mathematical approach is often useful in obtaining numerical solutions in particular cases, but because of their inherent generality, it can be remarked that

(a) often little understanding of geometric deformations, and load carrying mechanism of the problem is achieved, and hence methods of strengthening the structure are difficult to visualize,

(b) a complete mathematical solution must frequently be obtained before useful information is available,

(c) allowance for second order geometric deformations is often not appreciated,

(d) as regards teaching methods, an engineering attitude is not encouraged and a great deal of time is spent on merely illustrating a routine mathematical calculation.

As a means of overcoming these objections it is useful to look back in history and to glean a few ideas of how the advances and simplifications in structural analysis have been made. When we do so we often find that these advances in analysis have been achieved by the use of approximate descriptions of displacements, and as a result the mathematical complexity of the problem has been considerably reduced.

Throughout this thesis it is shown that patterns or characteristics of the geometrical deformations of structures, (such as displacements and surface slopes)enable good descriptions for a range of structural problems. Analytical functions are used to describe these geometrical characteristics, and from these functions, strains are defined. Estimates for load deformation relationships are used to define stresses and from an integration of these stress patterns the forces which must be applied to the structure, to sustain the specified characteristic shape, are found.

This inverse method has the advantages that the mathematics remains simple. At each stage of the computation the physical significance of the geometrical approximations of functional dependence is obtained very clearly, giving a deeper insight into the effects of the geometrical deformations and the assumptions which have been made about them. This insight enables a good appreciation of the structural behaviour to be developed, and quick and reliable estimates of the effects of stiffening the structure to be made, or of lightening if it is unnecessarily strong in some places, can be made.

1.3 Using Patterns in the geometric deformations to obtain simple Mathematical models

1.3.1 Measuring Devices.

In this chapter the use of geometric information obtained by moire techniques is discussed, particularly measurements showing the position of lines of constant displacement in the plane of the model (Ref. 7) and the position of lines of constant slope on the surface of the model, (Ref. 8). Later in the thesis these ideas will be applied to measurements of an overall shape obtained from many point by point measurements.

Overall detail of geometric deformations using the moire technique is a particularly suitable set of measurements for the following reasons.

(a) The measurements are direct measurements of displacements and deflections, that is geometric deformations. These changes in the geometry can be related to the deformations undergone by sets of straight lines drawn on the model, and hence the change in position of these lines can readily be visualized.

Geometrical effects are always separable from other considerations
and a deformed shape can always be drawn without any consideration
as to how this shape was obtained. Considerable information can
thus be obtained before concepts of stress and statical action
are introduced, the reasoning being thus simpler and more
straightforward than that obtained by introducing stresses too
early. Variables of statics (force variables) are frequently
not separable.

(b)   Lines of constant slope and lines of constant displacement are
      easy to obtain. The patterns suggested by these contour lines
      are usually simple, and suggest the nature of the functional
      form. As they are direct measurement of deformations they can
      then be used to establish a simple mathematical model. The
      order of complexity of the model is then determined by the
      approximations made of the deformed shape of the structure.

(c)   The shape of the moire fringes (or contours), can be used
      to suggest structural behaviour which is common to various
      structural models. When the same functional form is a good
      fit to different size models, then the functional form is
      the scaling function.

(d)   The whole outlook is concentrated on the production of
      simple descriptions of the load and deformation behaviour,
      and is thus suited to an engineering approach. With this
      outlook, simple models, suitable to be incorporated in
      codes of experience or practice, are always kept in mind.

In the following sections very simple structural problems
are investigated as a means of showing that the measurements of the
geometrical deformations of displacements and deflections can be
used to obtain simple structural models. The early problems are
so simple as to be trivial in themselves but deliberately chosen
as having solutions so well known that full attention can be
directed to the process of solution unobscured by algebraic

manipulations involved in the process. It is well known that the shape of an element of a stretched or bent bar, chosen with sides parallel to the edges of the undeformed bar, is approximately the same as the deformed bar. These simple problems are described in terms of a geometric functional form. The simple model for a twisted thin rectangular strip that specifies that the shape of the element is the same as that of the deformed bar is then an easy extension.

1.3.2   A Simple Model for a Stretched Bar.

A rectangular bar is stretched longitudinally. This problem is obvious to the structural analyst; however this simple problem is useful to illustrate the basic ideas.

Measurements of lines of constant displacement (u, v) in the x, y directions are shown in Fig. 1.2a, and Fig. 1.2b. The method used is the method developed in recent years by Oliver, Jenkins and Middleton at the University of Tasmania, and outlined in Ref. 7. For completeness, the optical arrangement used to view the interference pattern is shown in Fig. 1.3a and the interference fringes resulting from rotation, strains, and combined rotation and strain are shown in Fig. 1.3b. A good analytical description of the shape of these lines of constant displacement is given by the functions

$$u = y/a$$
and $$v = x/b \, ,$$

(1.1)

that is, planes originally perpendicular and parallel to the sides of the strip remain straight after the strip is stretched, and hence the shape of a deformed element is similar to the shape of the deformed bar.
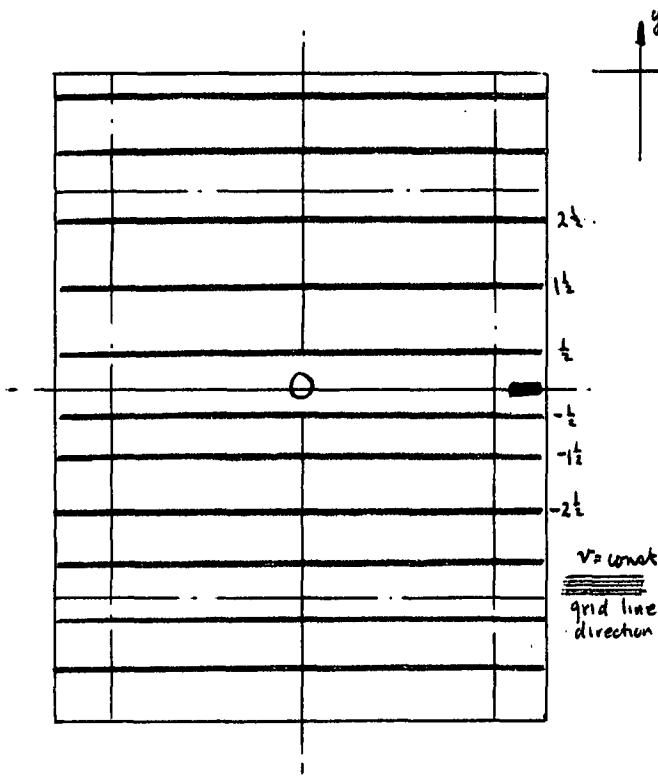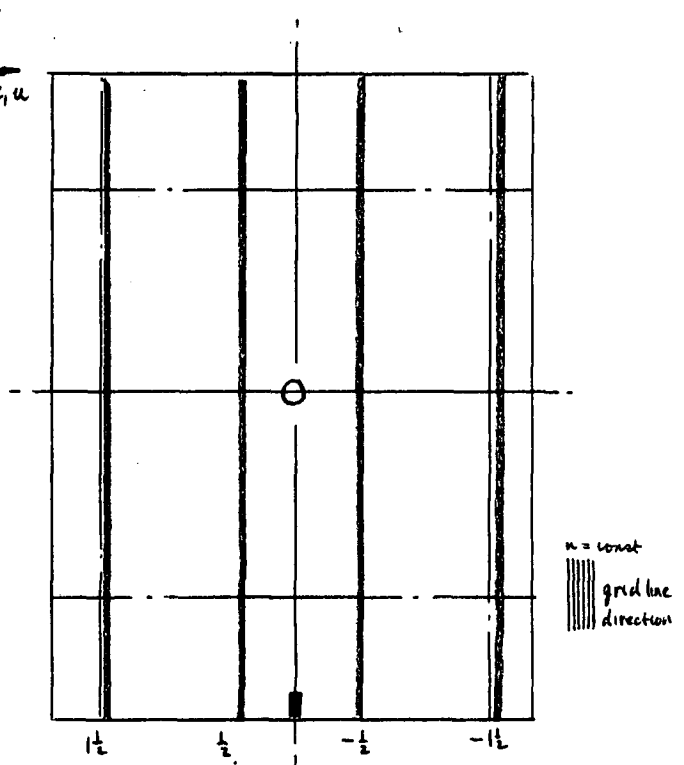
Fig. 1.2a

Fig. 1.2b

Lines of constant displacement for a Stretched Bar.

1.3.3 A Simple Model for a Bent Beam.

Measurement of the surface deflections for the thin beam bent in a manner indicated in Fig. 1.4a indicate that the beam has single curvature in the longitudinal direction. Measurement of the lines of constant displacement u, v in the x, y directions Fig. 1.4a and 1.4b indicate that good approximations to the displacements are

$$u = a_1 \, xy \quad \text{(hyperbolic)}$$

and
$$v = b_1 \, x^2 \quad \text{(parabolic).} \tag{1.2}$$
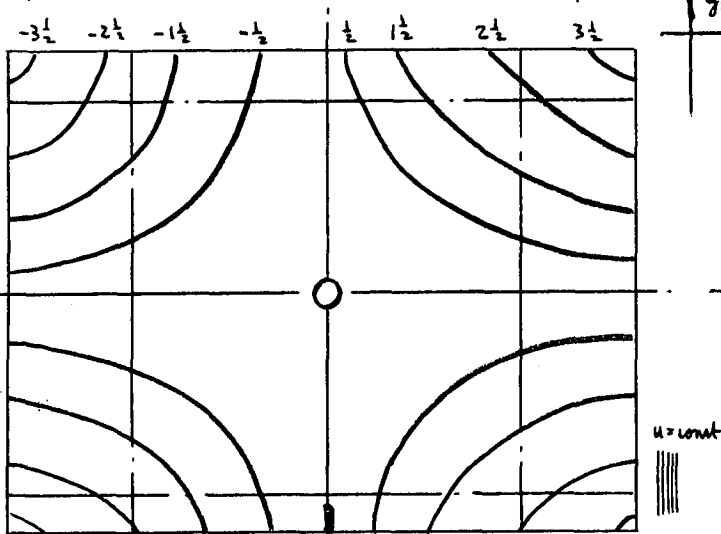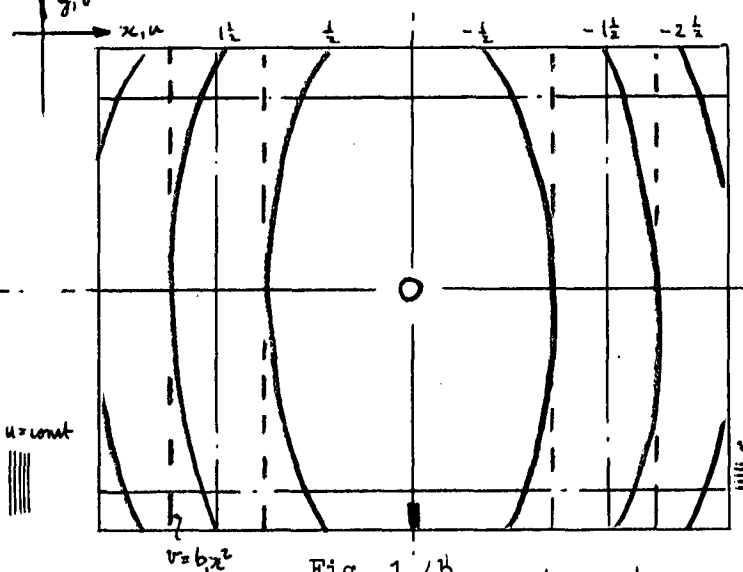

Fig. 1.4a

Fig. 1.4b

Lines of constant displacement for a bent beam
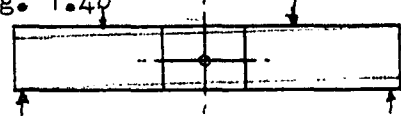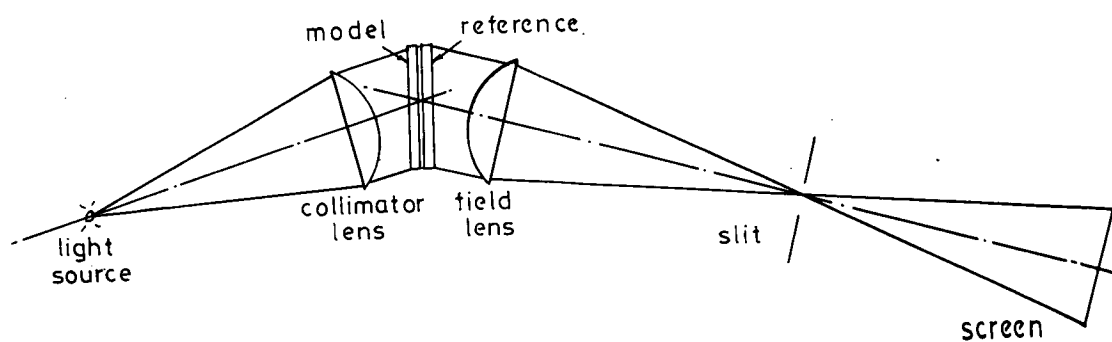
Fig. 1.3a Optical arrangement used to view interference patterns.

59 lines per inch

(a) ROTATION ALONE

(b) DIFFERENCE IN PITCH ALONE

(c) COMBINATION OF ROTATION AND DIFFERENCE IN PITCH

51 lines per inch

Fig. 1.3b Interferences fringes resulting from uniform rotation, uniform strain and a combination of uniform rotation and uniform strain. (Reproduced from "Stress Analysis Manual" *Experimental Mechanics*, Feb. 1967).

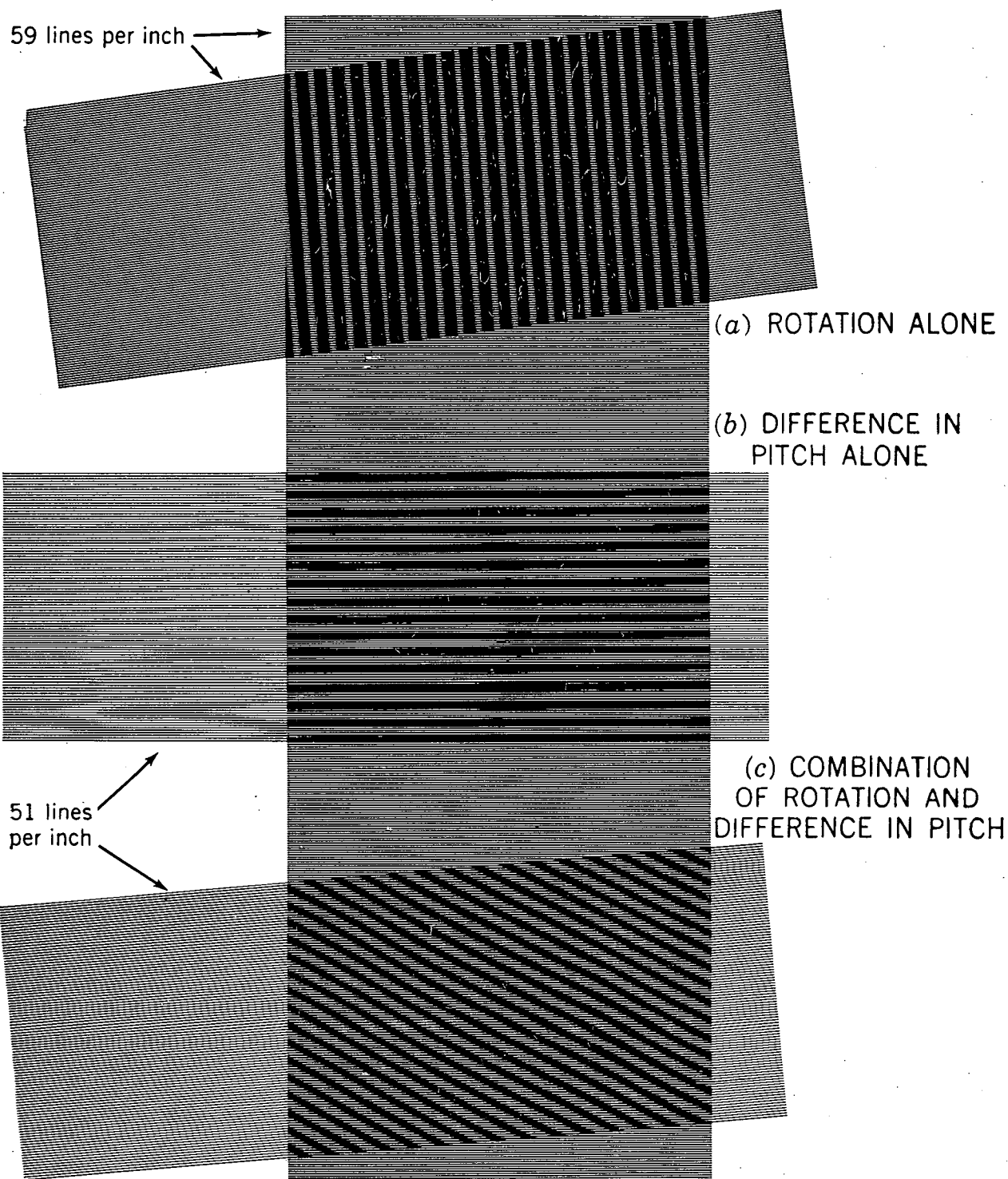These estimates of u, v are particularly simple and as they have been expressed algebraically they may be said to express the functional dependence or the functional form of the displacements.

The strains ϵ_x, ϵ_y in the x, y directions respectively and the shear strain γ_{xy}, consistent with this function form, are calculated from the approximations for small strain

$$\epsilon_x = \partial u / \partial x$$

$$\epsilon_y = \partial v / \partial y \qquad (1.3)$$

and $\qquad \gamma_{xy} = \partial u / \partial y + \partial v / \partial x ,$

and are given by the equations

$$\epsilon_x = a_1 y$$

$$\epsilon_y = 0 \qquad (1.4)$$

and $\qquad \gamma_{xy} = (a_1 + 2b_1)x.$

For the bent beam, the stresses consistent with the functional form (1.2) are

$$\sigma_x = (E/1-\nu^2) \, a_1 y$$

$$\sigma_y = (E/1-\nu^2) \, a_1 y \qquad (1.5)$$

$$\tau_{xy} = G(a_1 + 2b_1)x.$$

The forces necessary to sustain equilibrium are obtained by integration of these stress patterns and are given by the well known equations (using unit width of beam)

Axial load: $\qquad P_x = \int_{-\frac{1}{2}d}^{\frac{1}{2}d}(E/1-\nu^2)a_1 y \; dy = 0$

Vertical shear: $\qquad P_y = \int_{-\frac{1}{2}d}^{\frac{1}{2}d}G(a_1 + 2b_1)x \; dy = 0 \qquad (1.6)$

Bending Moment: $\qquad M = \int_{-\frac{1}{2}d}^{\frac{1}{2}d}(E/1-\nu^2)a_1 \; y^2 \; dy$

$$= (E/1-\nu^2)a_1 \; I \; ,$$

where
$$I = \int_{-\frac{1}{2}d}^{\frac{1}{2}d} y^2 \; dy.$$

If no total shear, P_y , is applied, the relationship between constants a_1 and $2b_1$ can be found. Then, $P_y = 0$ gives

$$a_1 = -2b_1 \; . \tag{1.7}$$

The equation (1.7), when substituted into the last equation of (1.4), indicates that with the guessed functional form and the specification of no total shear we arrive at the obvious statement that the model is one for which no shear strains are present.

To sustain this deformed shape, a constant bending moment M given by the equation

$$M = (E/1-\nu^2) \; a_1 \; I \; , \tag{1.8}$$

must be applied to the beam, and the displacements of the section will be

$$u = (M/EI) \; (1-\nu^2)xy$$
and
$$v = -\tfrac{1}{2}(M/EI)(1-\nu^2) \; x^2 \; . \tag{1.9}$$

It can be seen from Fig. 1.4(a) and equation (1.2) that the specification defines that plane sections perpendicular to the longitudinal axis before deformation remain plane and perpendicular to the longitudinal axis after deformation, and thus the shape of a small element chosen with sides parallel to the beam deforms in a similar shape to that of the whole beam (Fig. 1.5), as Bernoulli assumed.
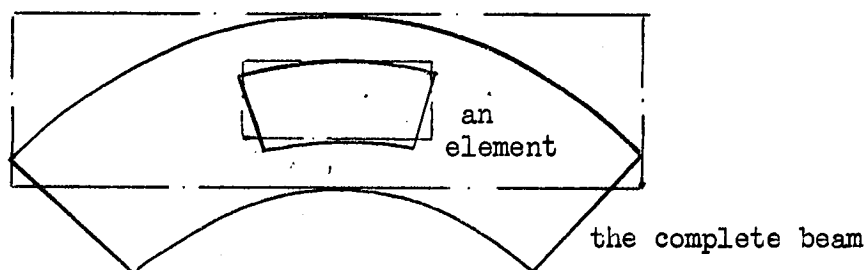

Fig. 1.5. Geometric Approximations for a Bent Beam.

1.3.4 A Simple Model for a Twisted Strip.

Measurement of the surface slope of a twisted strip was carried
out by using the Ligtenberg moire technique (Ref. 8). This technique
is simple and inexpensive to use. A brief summary of the technique
is given in section 3.2. The measurements indicate that lines of
constant slope in the x, z directions can be described approximately
by a series of equally spaced straight lines, as shown in Fig. 1.6.
Thus a good approximation to this surface shape is obtained by
examining the form of the vertical deformation w in the direction
of the y axis, and is given by the equations

$$\partial w/\partial x = kz,$$

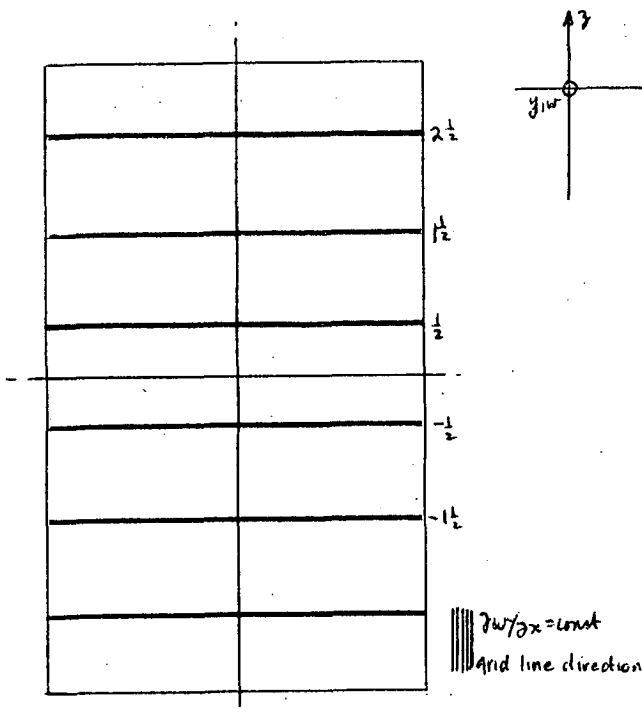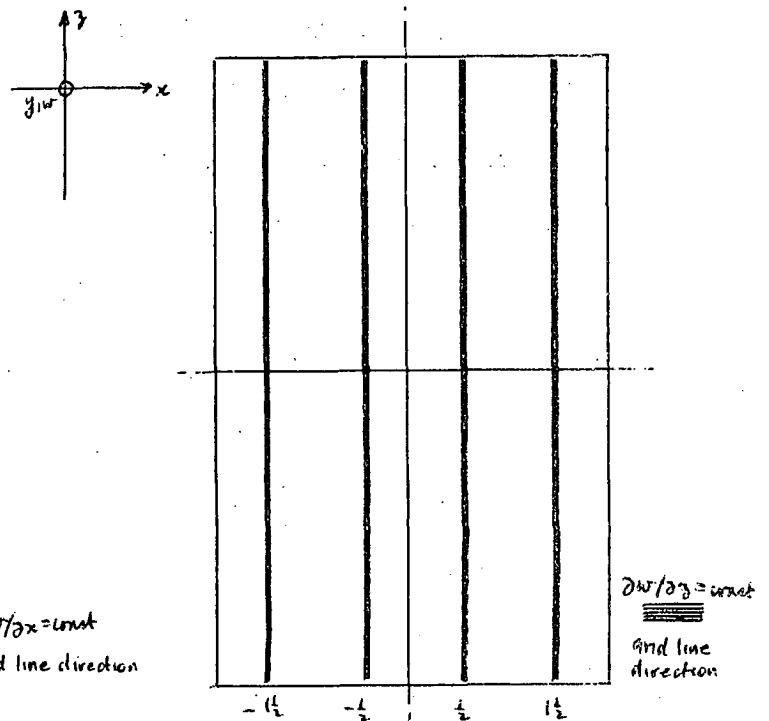and $\quad \partial w/\partial z = kz$.

(1.10)

Fig. 1.6a

Fig. 1.6b

Lines of constant slope on the surface of a twisted strip

Integration of equation (1.10) and choice of axes in the centre of
the strip leads to the specification of the functional form defining
the deflection of the surface as

$$w = k\,xz,$$

(1.11)

that is an anticlastic surface, with zero values for the curvatures $\partial^2 w/\partial x^2$ and $\partial^2 w/\partial z^2$ in directions perpendicular and parallel to the axes. However, rotation of axes by $45°$ to x_1, z_1 gives the deflection as

$$w = /k(x_1^2 - z_1^2)$$

and the curvatures of $\partial^2 w/\partial x_1^2$ and $\partial^2 w/\partial z_1^2$ as equal in magnitude but opposite in sign. As the investigation of the effect of transforming the axes is carried out on the model, or with the model deformations in mind, a better appreciation of the geometrical deformation is obtained.

Measurement of the surface displacements in the xz plane on the top and bottom surfaces of the strip by the method of Ref. (7) indicates that both these surfaces are in approximately pure shear but with opposite sense. A slight inclination of the v lines indicates that a small amount of longitudinal strain is present, (Fig. 1.7a, 1.7b). In this first model we take the lines to be straight and parallel, and thus not consider the shortening of the member.
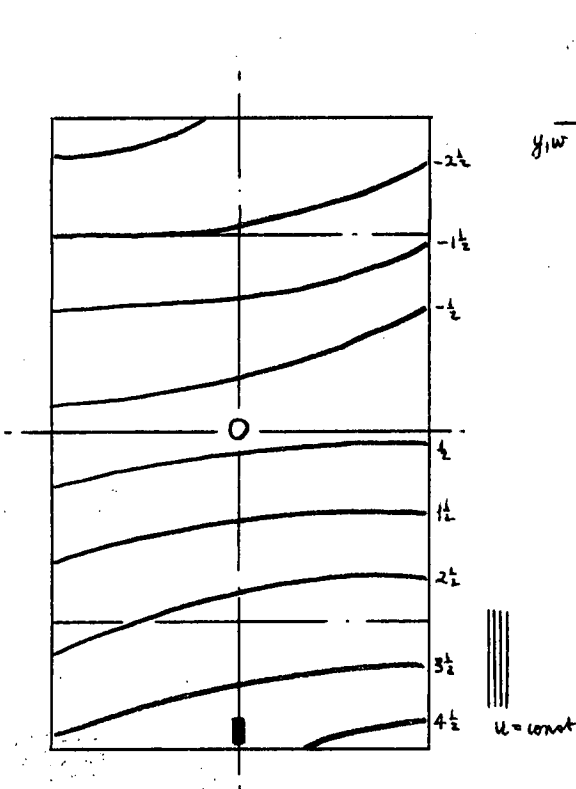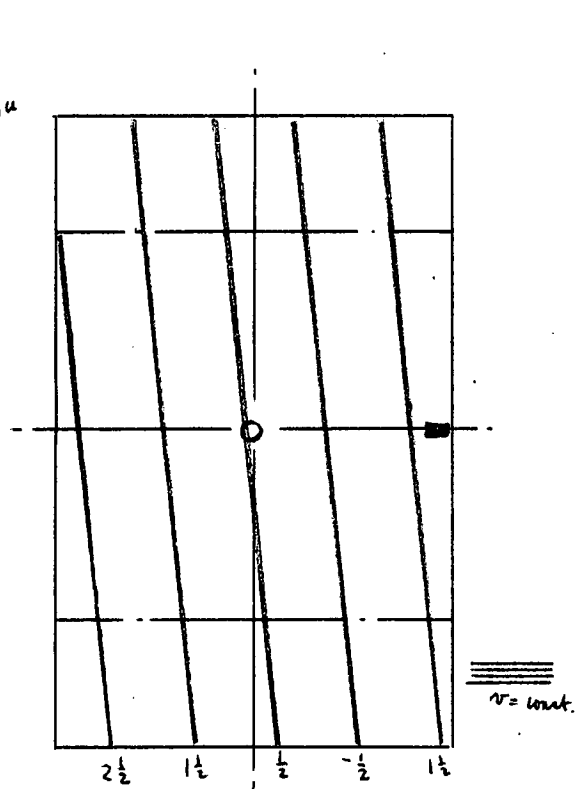
Fig. 1.7a   Fig. 1.7b

Lines of constant displacement on the surface of a twisted strip.

The functional form suggested by the lines of constant displacement is

$$u = cz$$

$$\tag{1.12}$$

$$v = cx$$

and the only strains on the surface of the strip in the x, z plane are shear strains γ_{xz} given by equation (1.13) that is

$$\gamma_{xz} = 2c \quad . \tag{1.13}$$

The approximation that straight lines originally perpendicular to the wide flat surfaces of the strip through the thickness remain straight, after deformation, indicates an element shape as shown in Fig. 1.8. As all lines parallel and perpendicular to the sides of the strip have again remained straight after the twisting, our experience with examples 1.3.2 and 1.3.3 suggests that we try the estimate that the shape of the element in Fig. 1.8 is similar to the shape of the strip. This estimate of the shape of the strip specifies the internal displacements. Each plane originally perpendicular or parallel to the longitudinal line of the strip warps into an anticlastic surface, (Fig. 1.9).

Fig. 1.8. A deformed element   Fig. 1.9. A twisted strip.

The rotations $d\theta_{xy}$ and $d\theta_{yz}$ of one element relative to an adjacent element or one warped cross section perpendicular and one warped cross section parallel to t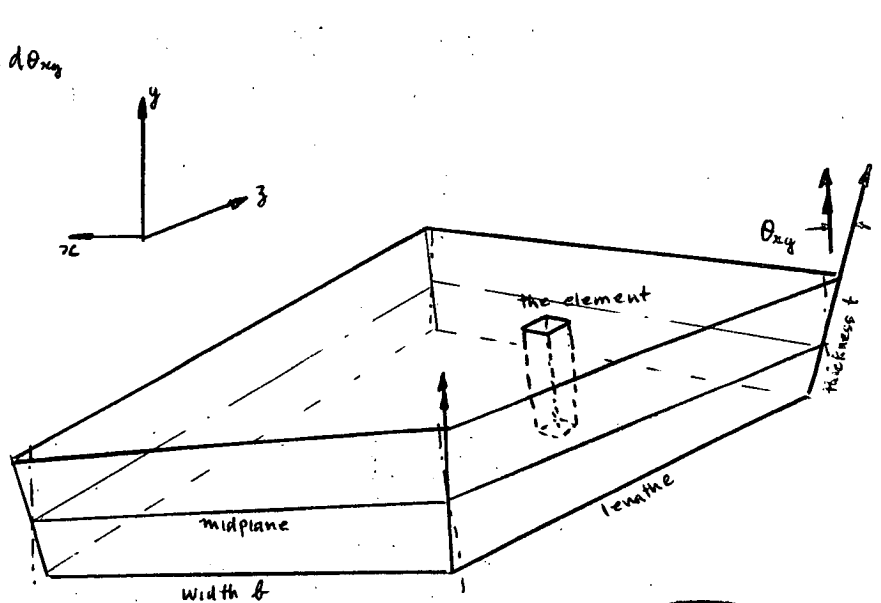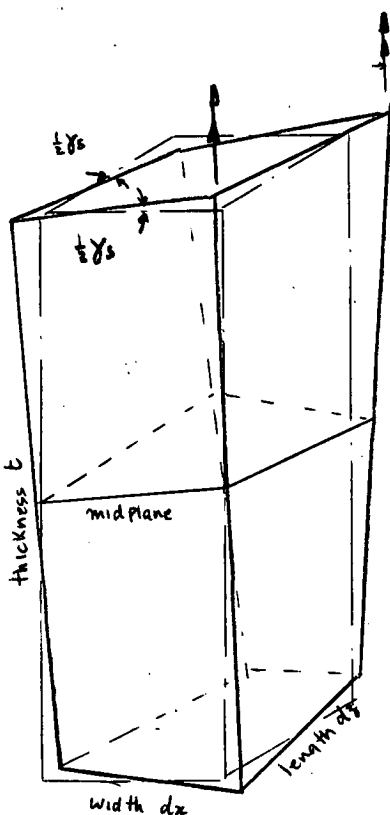he longitudinal axis, relative to another warped cross section is found from the element shape in Fig. 1.8. These rotations are given by

$$d\theta_{xy} = \tfrac{1}{2}\,\gamma_{s}\;dz/\tfrac{1}{2}t \;\;,$$

and

$$d\theta_{yz} = \tfrac{1}{2}\gamma_{s}\;dx/\tfrac{1}{2}t \;\;,$$

and the geometric deformations are completely specified.

The only stresses needed to sustain the shape of this deformed element are shear stresses, which can be specified by $\tau = G\gamma$. The total forces required to sustain the guessed shape are two sets of twsiting moments M_{xy} , M_{yz} as shown in Fig. 1.10. Integration of the stress patterns indicates that the magnitudes of these twisting moments are

$$M_{xy} = [\tfrac{1}{2}\gamma b\,\tfrac{1}{2}t\,\tfrac{2}{3}\,t] \;\;= G[t^{3}b/6]\,(d\theta_{xy}/dz), \quad (1.14)$$

and

$$M_{yz} = [\tfrac{1}{2}\tau\ell\tfrac{1}{2}t\ell\,\tfrac{2}{3}\,t] \;\;= G\,[t^{3}\ell/6]\,(d\theta_{xy}/dz) \; .$$

These twisting moments are statically equivalent to a balanced point load system, as the twisting moments per unit length M_{xy}/b and M_{yz}/ℓ are equal. The applied force F, is given by the equation

$$\tfrac{1}{2}\,F = M_{xy}/b = M_{yz}/\ell \; . \qquad (1.15)$$
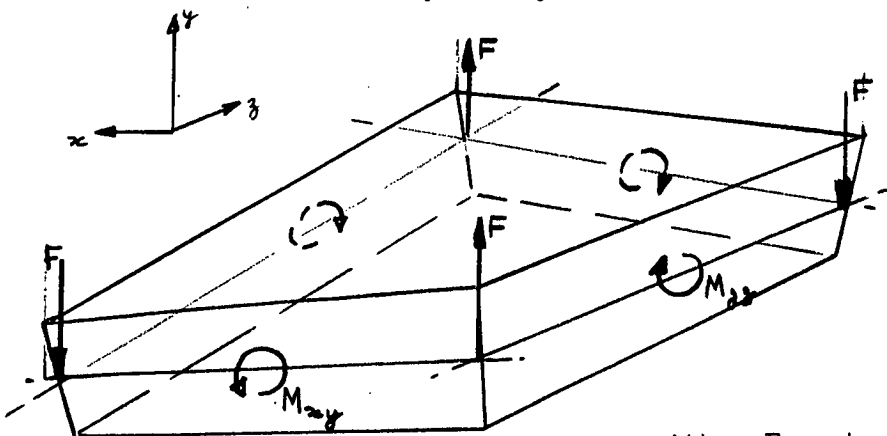
either F system

or M system

Fig. 1.10

Forces necessary to sustain the prescribed twisted shape.

Thus, we obtain the well known relationship linking the end torque Fb with the twist of any element of the section,

$$Fb = G[t^3 b/3] \ (d\theta_{xy}/dz). \qquad (1.16)$$

In Chapter Six, this simple model is extended to include the tapering off effects of shear strains at the corners, to describe the geometrical deformations of any rectangular bar that has been twisted, and to include the shortening effects of twisted members.

It can be seen that the examples chosen are particularly simple, but are basic. Examples, using the twisted strip as the basic element, are now considered to illustrate the power and usefulness of simply functional descriptions of the geometric deformations.

1.3.5   A Simple Model for a Twisted Member Built up from Flat Strips.

Measurement of the surface shape of an angle section twisted by applying four balanced forces on one leg of the angle, indicate that the surfaces deform into shapes which are approximately anticlastic *.   The angle between the legs in the plane of the cross section is almost preserved. A simple model to describe this behaviour can be obtained as follows.

---

* For the purposes of this thesis a surface is called a simple anticlastic surface when the principal curvatures are equal in magnitude, but opposite in sign. The properties and specification of this particular surface are first introduced in 1.3.4. The more general definition of an anticlastic surface is one for which the principal curvatures are opposite in sign but not necessarily equal.

A cut is made in the joining corner as shown in Fig. 1.11, and the surface shape measured as before. It is found that each of the sides still deforms into a simple anticlastic surface, but that the angle between the legs increases slowly, as the slot length is increased.

The results summarized in Fig. 1.12 indicate that a proportion of the moment applied on one leg is transferred to the other leg within a very small region of width, approximately ten times the thickness of the strip. Away from this region a good approximation is to consider the two strips as acted upon by separate sets of forces, the size of the forces being in direct proportion to the width of the leg. The end torque twist relationship is thus

$$Fb = \{G[t^3b/3] \ (d\theta_{xy}/dz) \ . \qquad (1.17)$$

1.3.6   A Simple Model for a Twisted Stiffener in a Twisted I Beam.

Repeating the tests of section 1.3.5 but using an I beam as the built up section, indicates that a similar model can be used, as all surfaces on the I beam again deform in a manner which can be described adequately by the simple anticlastic surface.

When a light transverse stiffener is placed between the flanges, as shown in Fig. 1.13, and the I beam twisted, it is found that the I beam again deforms in approximately an anticlastic manner. Measurement of the surface shape of the stiffener also indicates that the deformed shape of the stiffener can be described adequately by a simple anticlastic surface. The forces required to sustain the estimated deformed shape of the stiffener indicate that a set of forces B which may be called a Vlasov bimoment (Ref. 9), must be applied (Fig.1.14).
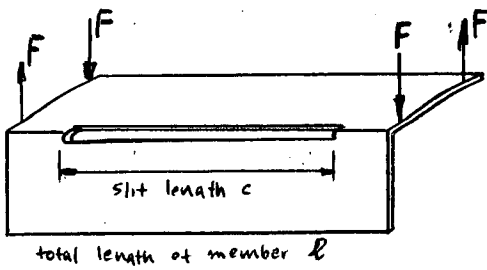
Fig. 1.11 Forces Applied to the angle section.
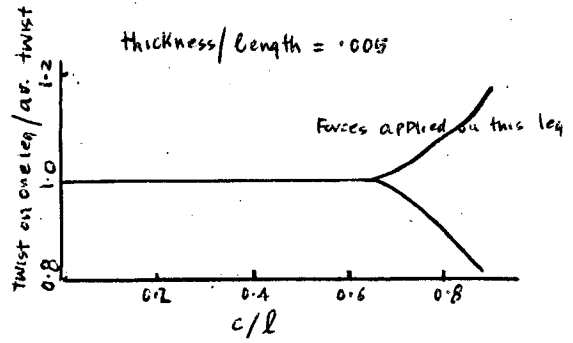
Fig. 1.12 Plot of twist and slit length

light end stiffener
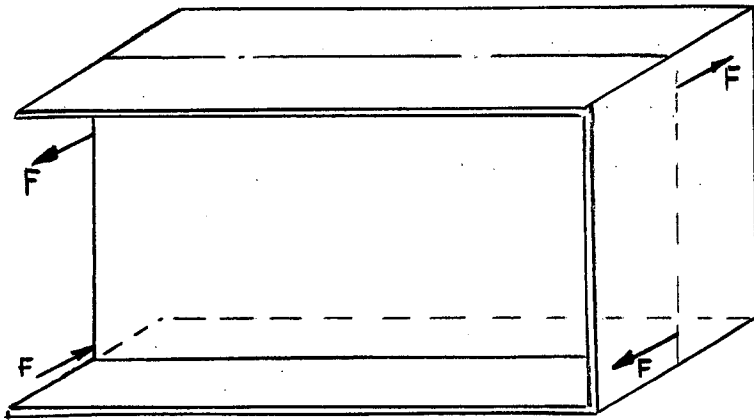
Fig. 1.13. Forces applied to I beam – stiffener arrangement

$$B = K \hbar \ell$$
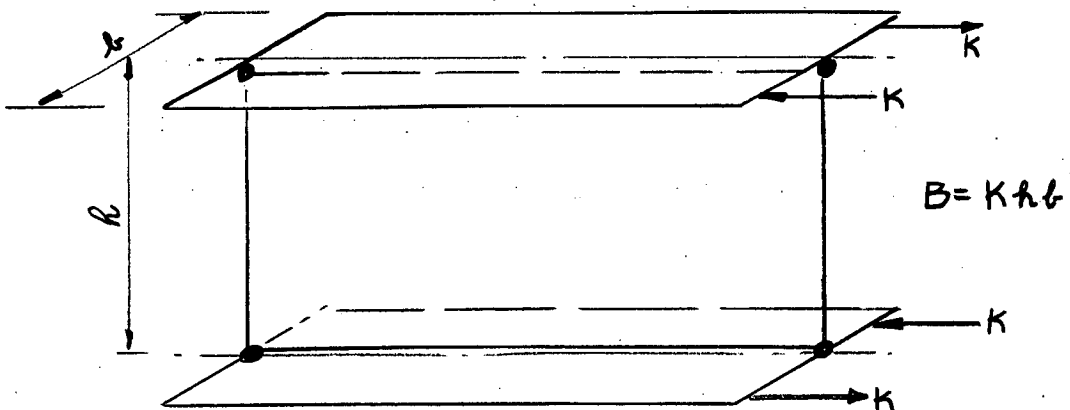
Fig. 1.14 Forces necessary to sustain the stiffener as an anticlastic surface
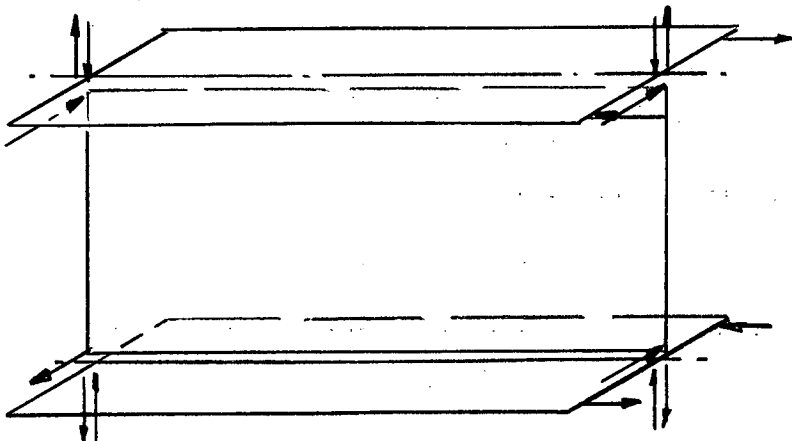
Fig. 1.15 Forces necessary to sustain both the stiffener and the I beam as anticlastic surfaces.

Application of the bimoment to the end of an I beam twists the entire I beam and bends the flanges of the I beam. * When length ℓ of the I beam is short and the width of the flanges b is large, a simple model describing the behaviour is obtained by application of the bimoment to an I beam built from three flat strips, and joined only at the corners of the flange (Fig. 1.14).

Measurement of the surface shape indicates that a reasonable approximation is again the anticlastic surface, with no cross sectional distortion. The forces necessary to sustain the anticlastic shape are shown in Fig. 1.15, and are statically equivalent to the bimoment. Thus, the applied bimoment B and the twist of the I beam can be related by the equation

$$B = K \, h \, b \ = \ G[t^3 b/3] \, \ell \, (d\theta_{xy}/dz) \ . \tag{1.18}$$

A description of the effect of the stiffener can be found using this model. The stiffener slightly reduces the magnitude of the twist, but the overall characteristics of the deformed shape (that is the shape can still be described in terms of anticlastic surfaces) are not altered. The end torque twist relationship for the I beam and stiffener is given by the equation

$$F b \ = \ GJ/[1 - GJ_{STIFF} b/\ell GJ)] \ d\theta_{xy}/dz \tag{1.19}$$

---

* This result may appear at first to be surprising. However, when the twisted member is examined it is seen that the ends of the member warp. If forces are applied similar in magnitude and direction to the form of this warping, that is in the form of a Vlasov bimoment, then twisting of the member is the likely result.

1.4   General Comments.

In the very simple models discussed it has been shown that the determination of scaling factors is inherent in the choice of the geometric functional form used to describe the geometrical deformations. Thus the problem of scaling, that is of relating the behaviour of the small scale model to the behaviour of the full size structure reduces to the problem of choosing a satisfactory functional form. If, when a particular model is studied closely, doubt arises as to whether the geometric deformations measured are a property of that particular size of model or of that type of structure, the problem can be overcome easily by testing several models of different sizes.

The choice of a functional form is especially suitable in any analysis when linear, quadratic or sinusoidal dependence relationships can be established, and when searching for a describing characteristic it is important to measure variables which highlight these types of dependence.

Throughout the history of engineering analysis, functional forms have often been used to describe characteristic features of similar problems. For example, empirical rules have long been used in engineering with considerable success but have usually been restricted to describing a final state, rather than a form or observable pattern that is obvious in the early stages of the description of a problem. However a notable example in structural analysis of using a functional form to describe geometric deformations is the "plane sections remain plane" rule for the bending of beams in metallic or concrete structures. Again in the case of ultimate strength calculations for steel and concrete structures, a functional form for the structure at "collapse", consisting of straight lines joined by hinges, is used to describe the deformed displacements, and the strains, stresses and loads necessary to sustain this deformed shape are then easily found. A recent use of a functional form

to describe geometric displacements has been proposed by J.K. Wilkins (Ref. 10) who uses it as a means of describing and designing for the behaviour of the concrete or bitumen waterproofing layer on the upstream face of decked rock fill dams.

Energy methods of structural analysis are another important use of guessed and measured functional forms of the deformations of the structure. The energy process based on potential energy is merely an averaging device where certain averages of some of the equations of statics are satisfied and are used to obtain good estimates of the variables within the functional form. However, in much modern analysis the functional form chosen is usually an infihite series of sinusoidal waves. Unfortunately, in many problems one or two sine waves are not a good functional description of the deformations, and thus when the infinite series (with no single term being dominant) is used, an appreciation of the deformations is often lost within the mathematical manipulation.

*   *   *   *

Throughout this thesis a deliberate effort is made to look for and describe characteristic shapes which define the deformed structure. The method is used first to gain an understanding of the problem of buckling instability, and a detailed study is made to show that the existence of characteristic shapes can be used to describe this problem. The ideas are then used to measure and describe the behaviour of a real structure, in this instance a through plate girder bridge. In the final chapter, the problem of torsion is tackled in the same manner and simple mathematical models describing torsion are developed.

CHAPTER TWO

AN OUTLINE OF THE INSTABILITY PROBLEM.

2.1 Introduction

The question "Is an engineering structure is stable under the action of the applied loads?" is a question which is easily asked. However, to provide a satisfactory answer, a good appreciation of the possible deformations of the structure is necessary, as the stability of a structure is some measure of how the deformations of the structure increase as the loading of the structure is increased.

All structures deform under the action of loads, and the actual form of the deformation is often the important criterion. Consider, for example, the determination of the stability of a dam. The dam is considered unsatisfactory, or unstable, if the loadings on the dam cause the dam to lift or to overturn. The problem still remains of how much to alter the dam design so that the new shape is stable, and engineers sometimes design the dam so that the joint between the dam and the foundation is everywhere in compression over the complete range of design loads. However, this is not always a satisfactory criterion of stability, as we find when we try to estimate the stability of an axially-loaded slender column. When the column is loaded, points on the column deform in a direction approximately perpendicular to the applied load. One measure of the stability of this structure is by what amount the structure deforms when the load is increased.

This Chapter will be mainly concerned with the problem of the stability of frame and plate structures. In these cases, instability may be considered to be the phenomenon of the occurrence of large relative changes in the geometric deformations of the structure which can be sustained by small relative changes in the loads applied to the structure.

The Chapter is designed to re-inforce and add to the existing work on structural stability as outlined by Euler (Ref. 4), Southwell (Ref. 3), Gregory (Ref. 11 and 12), Ariaratnam, (Ref. 13), Crandall (Ref. 14), Courant and Hilbert (Ref. 15), and Miklin (Ref. 16). Particular attention is focussed on the description and measurement of deformed shapes and of buckling loads and the Southwell Plot, first used by Southwell (Ref. 3) to estimate the first buckling load of a pin ended column, is generalized for a range of mathematical models. Although the mathematical manipulations used are well known by mathematicians, engineers have not taken advantage of the power of the methods used, and the author claims originality for this generalization of the Southwell Plot.

As a first step in the discussion of structural instability, the well known and simple model of an axially loaded column is considered. The description of the behaviour of the loaded column is similar to the approach developed by Gregory (Ref. 12) to describe general buckling phenomena in terms of the simple example of rigid rods and lateral springs. However, the column example has been chosen to emphasize that a continuous system can be thought of in the same manner as a discrete system. Often it is easier to evaluate and find properties of the discrete system and then carry these properties over to the continuum. Hence, the well known column example is outlined thoroughly and the ideas obtained are then used to develop generalizations.

2.2 A Simple Model for the Axially Loaded Slender Column

The design of an axially-loaded slender column will be considered. The first step in this design process is to obtain a description of the deformations of the system. It is well known that for increasing axial loads, larger increments in the lateral deflection of points on the bar arise from the same increment in axial load, but this descriptive form is not sufficient.

The simplest model chosen is shown in Fig. 2.1. This simple and well known model consists of two equal uniform rigid straight rods, joined by a spring which resists the angle change between the rods. The rods are compressed by thrusts which remain axial, and the ends of the rods are considered as pin-ended. This particular model is such that all geometric deformations can be described by one parameter, the central deflection of the rods.
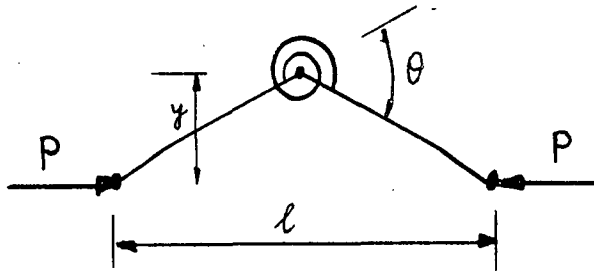
Fig. 2.1. Rod and Single Spring Mechanism.

Examine the stability of the system when a small lateral perturbation y of the hinge is applied. The central lateral deflection y is sufficient to describe the deformed system, consisting of two straight lines and a central hinge. The change of angle θ between the two straight lines at the hinge is, for small values of the lateral deflection

$$\theta = 4y/\ell \tag{2.1}$$

The forces to sustain the deformed system are then found easily. Let us specify a linearly elastic rotational spring. The load deformation relationship is then a relationship(in this case called the spring constant k) between the change of angle at the hinge and the moment M developed by the hinge. The required relationship is

$$M = k\theta$$

i.e. $$M = (4k/\ell)y. \tag{2.2}$$

The conditions for the system to be in statical equilibrium can then be found, as the moment M developed by the spring must be equal to the moment of the applied axial load P taken about the spring. Thus, we obtain the mathematical condition for statical equilibrium, namely,

$$M - Py = 0, \qquad\qquad (2.3)$$

and using equation 2.2, we obtain an equation showing the relationship between the deflection and the load, and

$$(4k/\ell - P)y = 0 . \qquad\qquad (2.4)$$

A mathematical solution to equation (2.4) is obtained from inspection: either $y = 0$, that is the column remains straight, or, at a buckling load P given by

$$P = 4k/\ell \qquad ,$$

the deflection of the hinge is undefined (Fig. 2.2). Nevertheless the form of the deflected shape is defined and consists of the two straight lines with a central hinge (Fig. 2.2). This form is called the buckling mode.
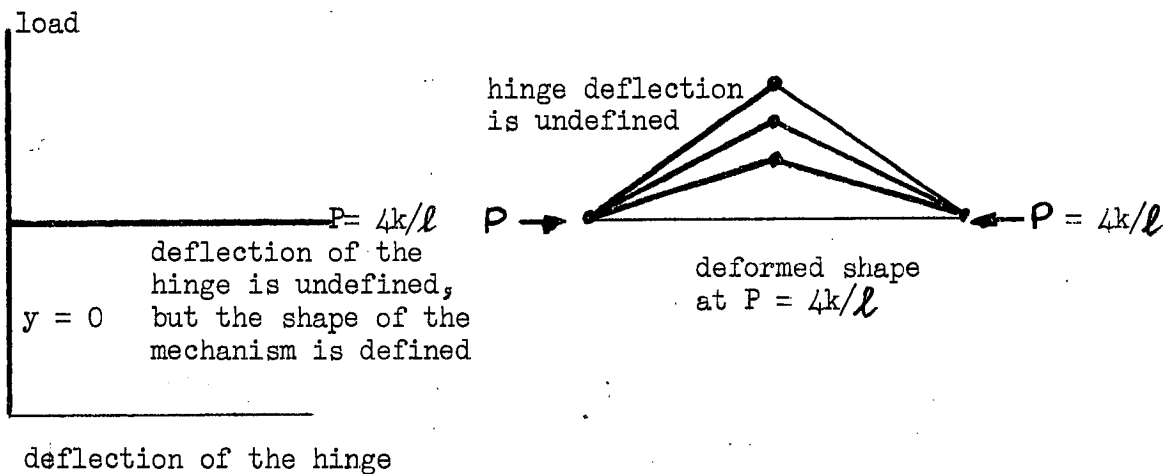
Fig. 2.2 Behaviour of the Mathematical Model (2.4).

However, the foregoing study is inadequate to describe the behaviour of the column for no sudden branch in the load and deflection behaviour is ever measured.

A closer representation of the real problem is obtained by modifying the physical model shown in Fig. 2.1 to include the following: initial crookedness of the column, an increasing number of hinges, and allowance for second order geometric deformations, non-linear load deformation relationships and a closer specification of the loading and boundary conditions. In the following sections, methods which include each of these effects in a large range of mathematical models are examined, and it is shown that a close representation of the behaviour of many real structures subject to instability is obtained.

2.3 Initial Crookedness in the Mathematical Model

The inclusion of initial crookedness in the mathematical model is a worthwhile and well known improvement and adds to the understanding of the real problem. Suppose the initial lateral deflection of the rods is y_o , and the rods between the spring remain straight.

The geometrical estimate of the deformations is again determined by the central lateral deflection. The initial rotation of the hinge θ_o , is given by the equation

$$\theta_o = 4y_o/\ell .$$

The load deformation relationship is dependant on the change of angle between the two straight rods, and is

$$M = k(\theta - \theta_o) \tag{2.5}$$

$$= (4k/\ell)(y - y_o) \bullet$$

The condition for the system to be in statical equilibrium is similar to equation (2.3). The moment developed by the spring is found from equation (2.5), and is equal to the moment of the applied axial load taken about the spring. For the system to be in equilibrium the following condition must apply

$$(4k/\ell)(y - y_o) \quad - \quad P\,y \;=\; 0\,. \tag{2.6}$$

The deflection of the hinge is obtained in terms of the applied load and initial deflection, and we have

$$y \;=\; y_o\big/(1- P\ell/4k) \quad . \tag{2.7}$$

This mathematical model (equation 2.7) indicates a steadily increasing deflection of the hinge for loads ranging from zero to close to the load given by

$$P_1 \;=\; 4k/\ell \; .$$

This load P_1 , called a buckling load in the previous model, is a good describing feature of the two physical models. In Fig. 2.3, a range of values of initial crookedness is plotted and it is seen that for very small initial crookedness values the two mathematical models expressed by equations (2.4) and (2.7) are similar.
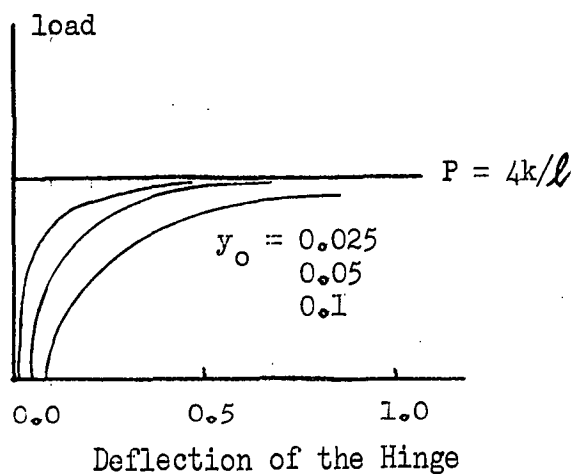
Fig. 2.3. Equation 2.7, with a range of initial crookedness

values.

The description of the real structural behaviour of the column depends on discontinuities in the surface slopes. Improvements in the description are obtained by increasing the number of hinges.

2.4 An Increase in the Number of Hinges.

2.4.1 Two Hinges.

A closer representation of the behaviour of the column is obtained by increasing the number of hinges. When the number of hinges and springs is increased by one, as shown in Fig. 2.4, the geometrical relations between the angles θ_1 and θ_2 and the corresponding deflections, y_1 and y_2, (for small lateral deflections) are

$$\theta_1 = (2y_1 - y_2)/0.66\ell \quad , \quad \text{and} \quad \theta_2 = (2y_2 - y_1)/0.66\ell . \qquad (2.8)$$
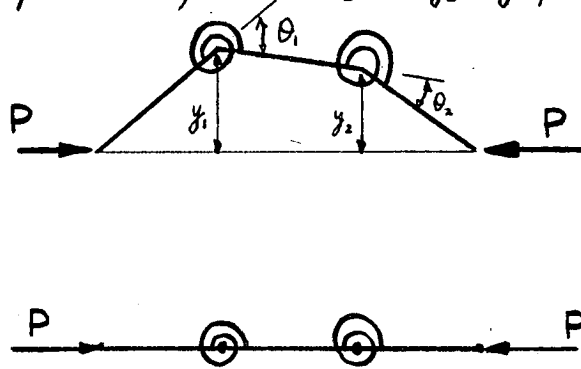
Fig. 2.4 Rod and Two Springs.

The moments sustained by the linear elastic springs are

$$M_1 = k\theta_1 \qquad (2.9)$$

and

$$M_2 = k\theta_2 .$$

The conditions for statical equilibrium are found by considering the equilibrium of the two rods separately, that is

$$M_1 - Py_1 = 0 , \qquad (2.10)$$

and

$$M_2 - Py_2 = 0 .$$

Combining equations (2.8), (2.9) and (2.10) gives the system of linear simultaneous equations that must be satisfied if the system is to remain in statical equilibrium

$$(3k/\ell - P)y_1 \quad - (1.5k/\ell)y_2 = 0 \qquad (2.11)$$

and

$$(-1.5k/\ell)y_1 \quad + (3k/\ell - P)y_2 = 0 ,$$

that is in matrix notation

$$\begin{bmatrix} 3k/\ell - P & -1.5k/\ell \\ -1.5k/\ell & 3k/\ell - P \end{bmatrix} \begin{bmatrix} y_1 \\ y_2 \end{bmatrix} = \begin{bmatrix} 0 \\ 0 \end{bmatrix} , \qquad (2.12)$$

or simply

$$\begin{bmatrix} & A & \end{bmatrix} \begin{bmatrix} y \end{bmatrix} = \begin{bmatrix} 0 \end{bmatrix} . \qquad (2.13)$$

The solution of these two linear simultaneous equations is given either by the trivial solution that the hinges do not move, $(y_1 = y_2 = 0,)$ or

$$(3k/\ell - P)^2 - (1.5k/\ell)^2 = 0 , \qquad (2.14)$$

that is the determinant of $[A]$ is zero. The two non trivial values of load which are solutions of equations (2.14) are either $P_1 = 1.5k/\ell$ or $P_2 = 4.5 \ k/\ell$, and the corresponding buckling modes can be determined from the lateral deflection ratios of the hinges, $y_1 = y_2$ and $y_1 = -y_2$ (Fig. 2.5).

Deflection of a hinge
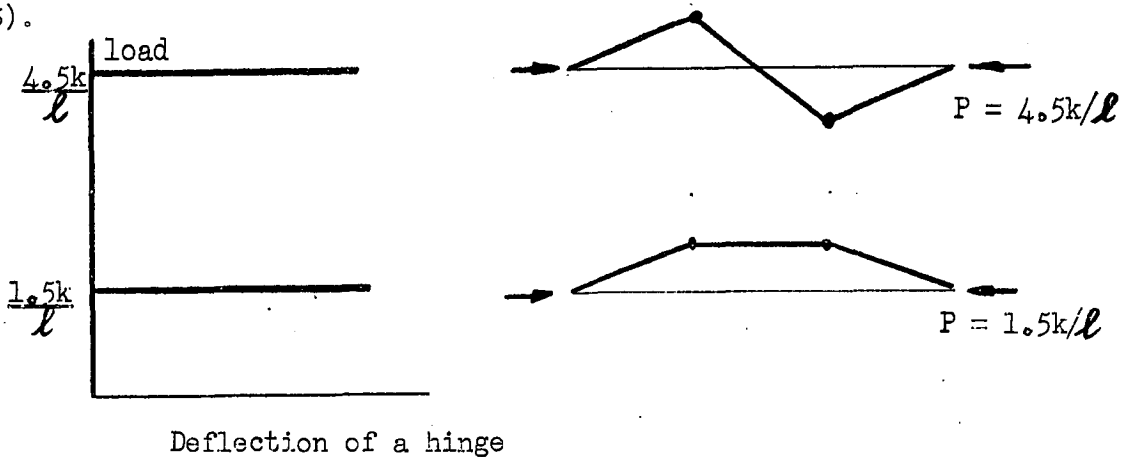
Fig. 2.5 Behaviour of the Mathematical Model 2.13.

2.4.2. Initial Crookedness and Two Hinges.

A method to describe the effects of initial crookedness may now be obtained by use of the buckling modes for the initially straight structure. When the initial crookedness consists only of initial lateral crookedness at the hinges, two variables are needed to specify the shape. A linear combination of the two buckling modes is used to describe this initial crookedness.

An initial crookedness of the form $y_{10} = 1.0$, $y_{20} = 0.5$, is expressed as a linear combination of the buckling modes, and

$$\begin{bmatrix} 1.0 \\ 0.5 \end{bmatrix} = a_1 \begin{bmatrix} 1.0 \\ 1.0 \end{bmatrix} + a_2 \begin{bmatrix} 1.0 \\ -1.0 \end{bmatrix} . \tag{2.15}$$

initial   first buckling   second buckling
crookedness   mode: symmetric   mode:antisymmetric.

The constants a_1 and a_2 are found easily by multiplying by the transpose of the column vectors $\begin{bmatrix} 1.0 \\ 1.0 \end{bmatrix}$ and $\begin{bmatrix} 1.0 \\ -1.0 \end{bmatrix}$ respectively.

Then
$$\begin{bmatrix} 1.0 & 1.0 \end{bmatrix} \begin{bmatrix} 1.0 \\ 0.5 \end{bmatrix} = a_1 \begin{bmatrix} 1.0 & 1.0 \end{bmatrix} \begin{bmatrix} 1.0 \\ 1.0 \end{bmatrix} + a_2 \begin{bmatrix} 1.0 & 1.0 \end{bmatrix} \begin{bmatrix} 1.0 \\ -1.0 \end{bmatrix} \tag{2.16}$$

That is $1.5 = 2a_1 + 0\,a_2$

or $a_1 = + 0.75.$

Similarly, $a_2 = 0.25.$

The initial shape, in terms of the buckling modes, is therefore

$$\begin{bmatrix} 1.0 \\ 0.5 \end{bmatrix} = 0.75 \begin{bmatrix} 1.0 \\ 1.0 \end{bmatrix} + 0.25 \begin{bmatrix} 1.0 \\ -1.0 \end{bmatrix} . \tag{2.17}$$

The separation of the initial crookedness into a combination of the buckling mode components is useful in the solution of the mathematical model for the initially crooked structure, as it indicates the way in which the structure deforms.

The mathematical model for the initially crooked structure consisting of three straight rods and two hinges is obtained in a manner similar to the one hinge case. The initial rotations θ_{1o} and θ_{2o} are linked to the initial deflections y_{1o} and y_{2o} by equation (2.8). The load deformation relationships are then

$$M_1 = k(\theta_1 - \theta_{10})$$
$$= (4k/\ell)(y_1 - y_{10}) \;, \tag{2.18}$$

and
$$M_2 = (4k/\ell)(y_2 - y_{20}) .$$

For the structure to be in statical equilibrium, the moment resisted by the springs must balance the applied moments (equation 2.10). On substitution of equation (2.18) into (2.10) we obtain the equations

$$\begin{bmatrix} 3k/\ell - P & -1.5k/\ell \\ -1.5k/\ell & 3k/\ell - P \end{bmatrix}\begin{bmatrix} y_1 \\ y_2 \end{bmatrix} = \begin{bmatrix} 3k/\ell & -1.5k/\ell \\ -1.5k/\ell & 3k/\ell \end{bmatrix}\begin{bmatrix} y_{10} \\ y_{20} \end{bmatrix} \qquad (2.19)$$

With values for the initial lateral crookedness of the hinges(y_{10} and y_{20}) as 1.0 and 0.5, equation (2.19) becomes

$$\begin{bmatrix} 3k/\ell - P & -1.5k/\ell \\ -1.5k/\ell & 3k/\ell - P \end{bmatrix}\begin{bmatrix} y_1 \\ y_2 \end{bmatrix} = 0.75 \begin{bmatrix} 3k/\ell & -1.5k/\ell \\ -1.5k/\ell & 3k/\ell \end{bmatrix}\begin{bmatrix} 1.0 \\ 1.0 \end{bmatrix} + 0.25 \begin{bmatrix} 3k/\ell & -1.5k/\ell \\ -1.5k/\ell & 3k/\ell \end{bmatrix}\begin{bmatrix} 1.0 \\ 1.0 \end{bmatrix}$$

The right hand side of equation (2.20) is simplified by using the two solutions of equation (2.12), which are

$$\begin{bmatrix} 3k/\ell & -1.5k/\ell \\ -1.5k/\ell & 3k/\ell \end{bmatrix}\begin{bmatrix} 1.0 \\ 1.0 \end{bmatrix} = 1.5k/\ell \begin{bmatrix} 1.0 \\ 1.0 \end{bmatrix} \qquad (2.21)$$

and $$\begin{bmatrix} 3k/\ell & -1.5k/\ell \\ -1.5k/\ell & 3k/\ell \end{bmatrix}\begin{bmatrix} 1.0 \\ -1.0 \end{bmatrix} = 4.5k/\ell \begin{bmatrix} 1.0 \\ -1.0 \end{bmatrix} .$$

The left hand side of equation (2.21) is simplified by separating the final shape into a linear combination of the buckling modes, and

$$\begin{bmatrix} y_1 \\ y_2 \end{bmatrix} = b_1 \begin{bmatrix} 1.0 \\ 1.0 \end{bmatrix} + b_2 \begin{bmatrix} 1.0 \\ -1.0 \end{bmatrix} . \qquad (2.22)$$

Then; from equations (2.20), (2.21) and (2.22) we have the equation

$$\begin{array}{l} b_1 \begin{bmatrix} 3k/\ell - P & -1.5k/\ell \\ -1.5k/\ell & 3k/\ell - P \end{bmatrix}\begin{bmatrix} 1.0 \\ 1.0 \end{bmatrix} \\ b_2 \begin{bmatrix} 3k/\ell - P & -1.5k/\ell \\ -1.5k/\ell & 3k/\ell - P \end{bmatrix}\begin{bmatrix} 1.0 \\ -1.0 \end{bmatrix} \end{array} = \begin{array}{l} 0.75(1.5k/\ell)\begin{bmatrix} 1.0 \\ 1.0 \end{bmatrix} + \\ 0.25(4.5k/\ell)\begin{bmatrix} 1.0 \\ -1.0 \end{bmatrix} \end{array} \qquad (2.23)$$

which simplifies to

$$\begin{array}{l} b_1 \quad (1.5k/\ell - P) \begin{bmatrix} 1.0 \\ 1.0 \end{bmatrix} \\ b_2 \quad (4.5k/\ell - P) \begin{bmatrix} 1.0 \\ -1.0 \end{bmatrix} \end{array} = \begin{array}{l} 0.75(1.5k/\ell)\begin{bmatrix} 1.0 \\ 1.0 \end{bmatrix} + \\ 0.25(4.5k/\ell)\begin{bmatrix} 1.0 \\ -1.0 \end{bmatrix} . \end{array} \qquad (2.24)$$

Equating terms with the same buckling mode, we obtain the values of the two buckling modes, and

$$b_1 = 0.75 \ (1.5k/\ell)/(1.5k/\ell - P) \qquad (2.25)$$

and $$b_2 = 0.25 \ (4.5k/\ell)/(4.5k/\ell - P).$$

From equations (2.22) and (2.25) the co-ordinates of the hinges of the final shape are given by the equation showing the magnification of the

buckling modes of the structures, and

$$\begin{bmatrix} y_1 \\ y_2 \end{bmatrix} = 0.75/(1-P\ell/1.5k)\begin{bmatrix} 1.0 \\ 1.0 \end{bmatrix} + 0.25/(1-P\ell/4.5k)\begin{bmatrix} 1.0 \\ -1.0 \end{bmatrix} \quad (2.26)$$

final deflections of the hinges   first buckling mode co-ordinates of the hinges   second buckling mode co-ordinates of the hinges

The predicted behaviour is shown in Fig. 2.6. For loads less than

the first buckling load, the deflection always increases with load,

and has the same sign as the first mode initial crookedness. However,

because of its discontinuous nature the buckled shape is still not an

adequate description of the shape of the deflected column, and thus

it is necessary to increase the number of hinges.
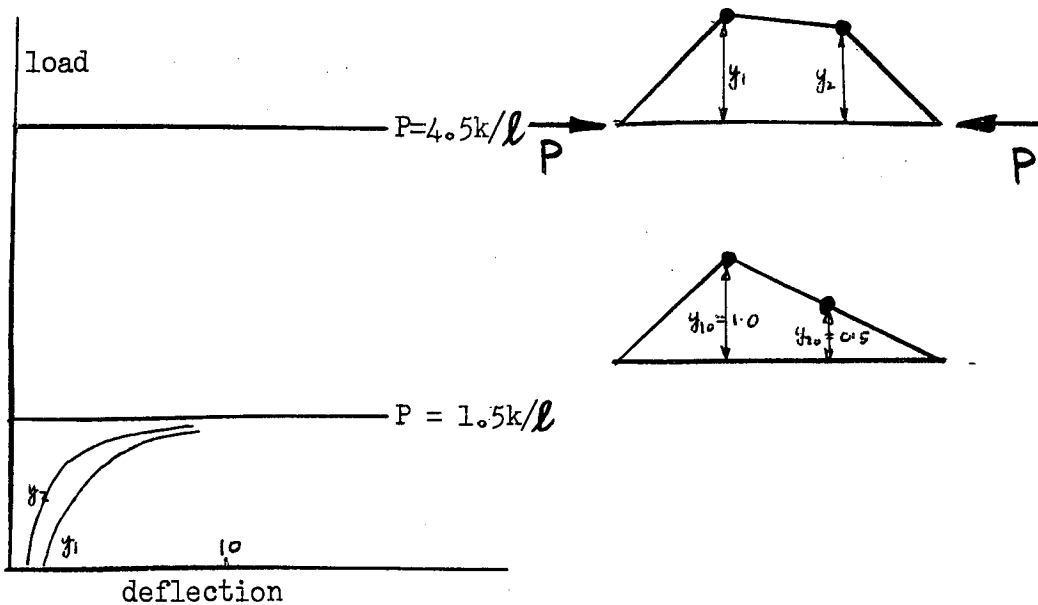
Fig. 2.6. A Graph of Axial Load and hinge deflection, for
the initially crooked column.

2.4.3 A Further increase in the Number of Hinges.

The number of hinges can be increased indefinitely. In

the continuum, the change of angle per unit length along the bar is

approximated by the lateral curvature (d^2y/dx^2) of the bar, and the

moment rotational deformation relationship is related by the flexural

stiffness of the bar, EI. The condition for statical equilibrium of

the initially straight bar is then

$$EI\ d^2y/dx^2 + P\ y = 0 \ . \tag{2.27}$$

The behaviour of the mathematical model (2.27) near the end of the bar is obtained separately. To be of value these descriptions should be at the same level of approximation as the differential equation itself. For the differential equation model of the slender column, the boundary conditions are *

$$x = 0 \ \text{and} \ \ell \ ; \ \ y = 0. \tag{2.28}$$

The solution of the differential equation (2.27) is

$$y = A\ \sin x \sqrt{P/EI} + B\ \cos x\sqrt{P/EI} \tag{2.29}$$

and with the boundary conditions (2.28), particular solutions are obtained.

Use of the boundary condition $x = 0$, $y = 0$ gives $B = 0$, and the boundary condition $x = \ell$, $y = 0$ gives

$$0 = A\ \sin\ell\sqrt{P/EI} \ , \tag{2.30}$$

that is either $A = 0$, and the continuous system remains straight, or the deformations of the system are sustained by a load given by the equation

$$0 = \ \sin \ell \sqrt{P/EI} \ , \tag{2.31}$$

i.e. $P = n^2\pi^2 EI/\ell^2$.   where $n = 0, 1, 2, 3, 4, \ldots$,

These discrete values of load are called eigen values, latent roots, buckling loads or, as this particular family was found by Euler, Euler buckling loads. To each buckling load there corresponds a buckling mode (which is found by substituting into the equation) and the eigen functions, latent vectors, or buckling mode are

buckling mode y: $\sin\pi x/\ell$, $\sin 2\pi x/\ell$, $\sin 3\pi x/\ell$, ...

buckling load P: $\pi^2 EI/\ell^2$, $4\pi^2 EI/\ell^2$, $9\pi^2 EI/\ell^2$, ...

---

* It should be noted that when the models for finite numbers of hinges are used, these boundary conditions and conditions of statical equilibrium are incorporated in one statement, for example equation 2.12.

2.4.4 Describing Initial Crookedness in the Continuum.

A description of the effects of an initial crookedness of the continuous column can be obtained by using ideas obtained from the systems which had only a finite number of variables. For example, including the initial crookedness in the mathematical model for the continuous column, we obtain the differential equation

$$EI d^2(y - y_o)/dx^2 + P y = 0. \tag{2.32}$$

Again the aim is to describe the initially crooked shape as a linear combination of the buckling modes. Southwell (Ref. 3) first developed this method for the pin ended column, but for completeness and to outline the method the solution is given below.

The existence of a unique linear expansion for the initial crookedness y_o , is used, that is the initial crookedness is expressed as an infinite series expansion

$$y_o = \sum_{n=1}^{\infty} a_n \sin n\pi x/\ell . \tag{2.33}$$

This exapnsion is the well known Fourier Series and the justification and properties have been investigated by many authors (see for example Miklin, Ref. 16).

The coefficients a_m are found by multiplying both sides of equation (2.33) by the m buckling mode, and integrating over the length of the structure. Then

$$\int_0^\ell y_o \sin m\pi x/\ell \, dx = \sum_{n=1}^{\infty} a_n \int_0^\ell \sin n\pi x/\ell \, \sin m\pi x/\ell \, dx . \tag{2.34}$$

As before, the product of two different buckling modes is zero. This property is called the orthogonal property of the buckling modes and enables a simplification of equation (2.34). The value of a_m is given by the ratio

$$a_m = \int_0^\ell y_o \sin m\pi x/\ell \, dx \bigg/ \int_0^\ell \sin m\pi x/\ell \, dx . \tag{2.35}$$

The final shape, y and the initial shape y_0 are expressed as linear combinations of the buckling modes,

$$y = \sum_{n=1}^{\infty} b_n \sin n\pi x/\ell \qquad (2.36)$$

and

$$y_0 = \sum_{n=1}^{\infty} a_n \sin n\pi x/\ell \qquad . \qquad (2.37)$$

Equation (2.32) is simplified using equations (2.36) and (2.37) and becomes

$$EI\sum_{n=1}^{\infty}(b_n-a_n)d^2(\sin n\pi x/\ell)/dx^2 + P\sum_{n=1}^{\infty} b_n \sin n\pi x/\ell = 0 \qquad (2.38)$$

But as

$$EI\, d^2(\sin n\pi x/\ell)/dx^2 + n^2\pi^2 EI/\ell^2 \sin n\pi x/\ell = 0 \qquad (2.39)$$

then

$$-\sum_{n=1}^{\infty} n^2\pi^2 EI/\ell^2 (b_n - a_n)\sin n\pi x/\ell + P\sum_{n=1}^{\infty} b_n \sin n\pi x/\ell = 0. \qquad (2.40)$$

Equating terms with the same buckling modes, we have on simplification

$$b_n = a_n/(1-P/P_n) \text{ , where } P_n = n^2\pi^2 EI/\ell^2 \text{ , } \qquad (2.41)$$

The final shape, given in terms of an infinite series expansion of the buckling modes of the initially straight system, is

$$y = [a_1/(1-P/P_1)]\ \sin\pi x/\ell + [a_n/(1-P/P_2)]\ \sin 2\pi x/\ell + \ldots \qquad (2.42)$$

2.5 Comparisons between Experimental Readings and the Mathematical Model

The mathematical model is now at the stage where comparisons can be made with experimental measurements. Southwell (Ref. 3) has presented a reliable method of comparison subject to the restrictions that the structure remain elastic, and that the value of the first term in the infinite series is far greater than the combined effects of the other terms. When these conditions are satisfied, the mathematical model is given approximately by the finite series

$$y \approx [a_1/(1 - P/P_1] \sin \pi x/\ell \ .\qquad\qquad (2.43)$$

The mathematical model is easily manipulated into a form from which the measured results can be compared. The form is

$$\big((y - a_1)\sin \pi x/\ell\big)\big/P = \big((y - a_1)\sin \pi x/\ell\big)\big/P_1 + \big(a_1 \ \sin \pi x/\ell\big)\big/P_1 \ , \qquad (2.44)$$

that is the mathematical model indicates that a plot of the ratio of the measured deflection to applied load against the measured deflection is a straight line. The slope of this line is equal to the reciprocal of the first buckling load, with the intercept on the load axis determined by the initial crookedness and the first buckling load.

Experimental readings of the load P and of the change in deflection $(y - y_o)$ at the centre of the column are found to be approximately hyperbolic. (Fig. 2.7). A horizontal asymptote to the hyperbola, that is

$$P = P_{crit}$$

is found from the reciprocal of the slope of the line of best fit to the Southwell Plot of the ratio of measured deflections to load against measured deflection (Fig. 2.8). The value of the horizontal asymptote P_{crit} found by this device is then used as a measure of P_1 , the first buckling load of the structure. The experimental results do not in general give a linear Southwell Plot, and hence a constant value for the horizontal asymptote P_{crit} is not obtained, but often the deviations from a straight line are sufficiently small to enable a correlation to be made between experimental results and the mathematical models. A few of these correlations are now outlined.
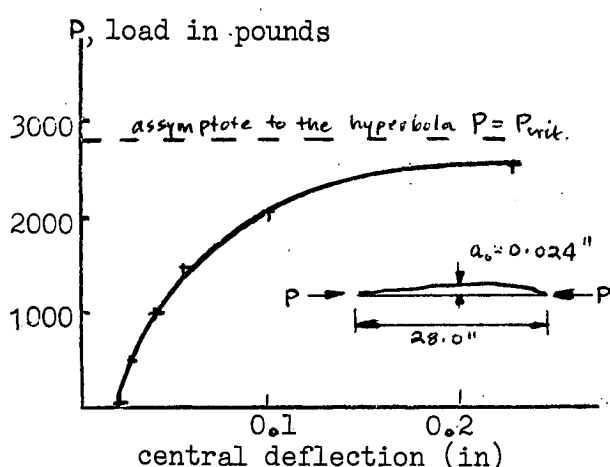

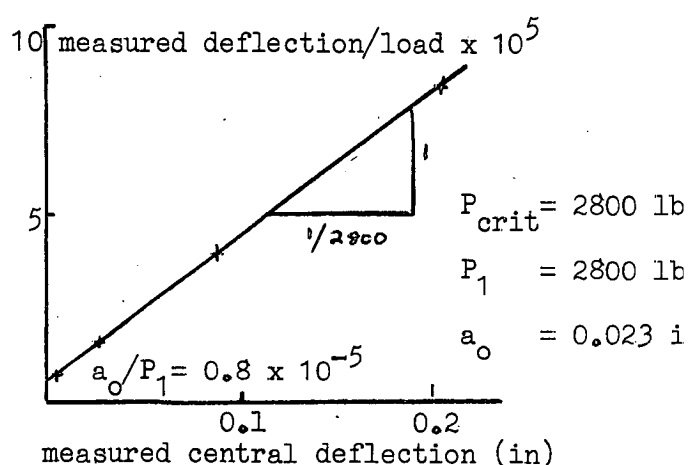Fig. 2.7 Experimental readings of the central deflection of a pin ended column.

Fig. 2.8 A Southwell Plot of the experimental readings.

2.6   History of the use of the Southwell Plot.

Southwell (Ref. 3) was the first to observe that a plot of the load and corresponding mid point deflection of an axially loaded column was approximately hyperbolic in the neighbourhood of the smallest critical load of the mathematical model of the Euler column. He showed that the approximate position of the horizontal asymptote to this hyperbola could be obtained by a suitable transformation, namely plotting $(y - y_0)/P$ against $y - y_0$ where $(y - y_0)$ was the measured deflection and P the applied load, and drawing a line of best fit.

Southwell used the reciprocal of the slope of the line of best fit as a measure of the first critical load of the Euler mathematical model. He justified this comparison by showing that when an arbitrary initial crookedness is included in the mathematical model for the Euler column (as outlined in section 2.4.4) the resulting model is a reasonable description of the experimental behaviour.

Donnell (Ref. 17) suggested that the Southwell straight line plot was a good measure of the first critical load in all cases of buckling, provided that appreciable second order stresses were not introduced, (such stresses occur when a developable surface buckles into a non developable surface) and assumed the validity of the Southwell Plot method in all cases where the corresponding differential equations were linear. However, it is shown in the following sections that to obtain reliable correlations between experimental results and mathematical models, the mathematical model must satisfy several other conditions besides linearity.

Dumont and Hill (Ref. 18) tested some aluminium alloy I-section beams loaded about the major axis by a uniform bending moment. They found that the beams were subject to lateral instability, and to obtain an estimate of the critical bending moment they plotted the ratio of the measured central rotation to the bending moment against the measured rotations. The reciprocal of the slope of the line of best fit to these plots was then approximated to the critical bending moment. They did not justify mathematically this comparison and later Massey (Ref. 19)

showed that the reciprocal of the slope of the line of best fit of a plot of measured rotation to the square of the bending moment against the measured rotation gave a better indication of the square of the critical bending moment.

Galletly and Reynolds (Ref. 20) measured the elastic circumferential strains and internal pressures for ring stiffened cylindrical shells subject to external hydrostatic pressure, and using Southwell's method were able to obtain the horizontal asymptote to the experimental readings. They were then able to compare measured critical buckling loads with buckling loads calculated from a variety of mathematical models.

Greogry (Ref. 21 and 22) showed that for structures bending in their plane and for triangular structures bending and twisting out of their plane a correlation exists between the predicted first critical load and the asymptote obtained from measured axial loads and curvatures by using the transformation as suggested by Southwell. Later, Ariaratnam (Ref. 13) justified mathematically the use of the Southwell Bot of measured deflections, (and hence curvatures) and axial loads as a means of measuring critical loads in framed structures.

Thus, the Southwell Plot method has been of great benefit in the study of instability problems as reasonable estimates of initial crookedness and buckling loads have been obtained for a range of structures.

The plot has the property that almost any curve similar in shape to a hyperbola can be linearized to a certain degree and the fit of the experimental points to a straight line has often been used as a justification of the mathematical model. This approach is not rigorous, and in the next section a set of sufficiency conditions to be satisfied by the mathematical model is outlined. These conditions provide a sound basis for comparisons between experimental results and mathematical models.

2.7.1 Extensions to the Southwell Plot

The ideas outlined in the previous sections indicate that the Southwell Plot is a useful device for the comparison of some experimental results and some mathematical models. These ideas are based on the properties of the differential equation

$$EI \ d^2(y + y_o)/dx^2 \ + P \ y = 0. \qquad (2.45)$$

Many structures behave in a manner similar to that indicated by the experimental points shown in Fig. (2.8), but not all of these structures can be described adequately by the one differential equation and set of boundary conditions. A general test is proposed in the following section whereby any mathematical model, consisting of linear differential equations and boundary conditions can be examined, to see if a basis exists to compare experimental readings. After this basis has been established, firm design rules can be made with confidence.

When the analysis developed by Southwell is examined closely, it is seen that the power of Southwell's analysis lies in the specification of the arbitrary initial crookedness. Southwell uses the terms of an infinite Fourier series to define the crookedness, as each of these Fourier terms is a solution of the mathematical model for the initially straight structure. The description of an arbitrary initial crookedness for a different mathematical model, as an infinite series, with each term a solution of this new mathematical model is now investigated.

2.7.2 Mathematical conditions sufficient to justify the Southwell
Plot as a method of comparison of mathematical models and
experimental results.

The method proposed by Southwell may be extended only when the possibility of expressing the initial deformations ϕ_o in terms of the buckling modes ϕ_r of the particular problem has been investigated; that is, validity has been established for the expansion

$$\phi_0 = a_1 \phi_1 + a_2 \phi_2 + a_3 \phi_3 + \circ \circ a_r \phi_r + \circ \circ \quad (2.46)$$

Expansion (2.46) is valid if the following conditions are satisfied:

(a)   a means exists to find the constants a_1 , a_2 , a_3 $\circ$ $\circ$,

(b)   the expansion is unique, that is the expansion is linear independent,

(c)   there exists an infinite number of solutions ϕ_r ,

and   (d)   the expansion will converge as a_n is increased.

It is shown in the following section that when the mathematical model satisfies the well known mathematical conditions of Rule No. 1, then the conditions (a) to (d) are satisfied and hence the validity of the expansion (2.46) is established.

Rule No. 1.   When the mathematical model for the initially undeformed structure can be expressed as a linear differential equation of the form

$$L(\phi) - \lambda N(\phi) = 0 , \quad (2.47)$$

where $L(\phi)$ and $N(\phi)$ are both self adjoint and positive definite differential operators and λ is a load parameter, then the expansion (2.46) is valid.

Although the conditions required are readily available elsewhere (Ref. 16) for completeness an outline is now given of why the differential equation and boundary condition system satisfying Rule No. 1 satisfies the properties (a) to (d).

Condition (a) is established when the operators $L(\phi)$ and $N(\phi)$ are self adjoint.   One definition of self adjointness is given in by Crandall (Ref. 14) and involves the behaviour of two functions u, v which satisfy the boundary conditions but do not necessarily satisfy the differential equation between the boundary.   When the operators $L(\phi)$ and $N(\phi)$ are self adjoint, the expressions

$$\int_{a}^{b}[u\,L(v) - vL(u)]\,dz, \qquad \text{and} \qquad \int_{a}^{b}[uN(v) - vN(u)]\,dz \quad \text{are both zero.}$$

(The points a, b define the positions of the boundaries.)

The implications of this condition can be seen when two separate solutions of the differential equation (2.46) are examined, i.e.

$$L(\phi r) - \lambda_r N(\phi r) = 0 \qquad\qquad (2.48)$$

and

$$L(\phi s) - \lambda_s N(\phi s) = 0 \quad . \qquad\qquad (2.49)$$

Multiply (2.48) by (ϕ_s) and (2.49) by (ϕ_r), subtract, and then integrate between the boundaries; the expressions become

$$\int_{a}^{b}[\phi_s L(\phi r) - \phi_r L(\phi_s)]\,dz - \int_{a}^{b}[\lambda_r\phi_s N(\phi_r) - \lambda_s\phi_r N(\phi_s)]\,dz = 0 \quad . \qquad (2.50)$$

When $L(\phi)$, and $N(\phi)$ are both self adjoint, equation (2.50) can be reduced to the equation

$$\int_{a}^{b}(\lambda_r - \lambda_s)\,\phi_s\,N(\phi_r)\,dz = 0 \qquad\qquad (2.51)$$

i.e. when $\lambda_r \neq \lambda_s$, $\displaystyle\int_{a}^{b}\!\phi_s\,N(\phi_r)\,dz = 0 \quad . \qquad\qquad (2.52)$

Similarly, the relationship

$$\int_{a}^{b}\phi_s\,L(\phi_r)\,dz = 0 , \qquad\qquad (2.53)$$

can be established. Equations (2.52) and (2.53) are called the orthogonality relationships *. These relationships enable a separation of the variables a_1, a_2, a_3. For example, to evaluate the constants a_r, multiply equation (2.47) on both sides by $N(\phi r)$ and integrate.

---

* A self adjoint differential equation is really another way of stating that the equation obeys the Maxwell Reciprocal Theorem - that is the cross product of generalized deformation U_A at the point A multiplied by the generalized force $L(U_B)$ at the point B is equal to the cross product of the generalized deformation U_B at the point B multiplied by the generalized force $L(U_A)$ at the point A. This statement may be expressed in the form

$$U_A\,L(U_B) = U_B\,L(U_A) .$$

When the self adjoint differential equation describes a buckling phenomenon, the integral of two cross products over the whole structure is equal to zero. (See also the Appendix A).

This gives a_r as the ratio

$$a_r = \int_a^b \phi_o \, N(\phi_r) dz \Big/ \int_a^b \phi_r \, N(\phi_r) dz \, ,$$

Similarly, by multiplying by $L(\phi_r)$ and integrating, the constant a_r is obtained as the ratio

$$a_r = \int_a^b \phi_o \, L(\phi_r) dz \Big/ \int_a^b \phi_r \, L(\phi_r) \, dz.$$

A means of ensuring that a_r is defined is to specify that the integrals $\int_a^b \phi_r \, N(\phi_r) dz$ and $\int_a^b \phi_r \, L(\phi_r) dz$ are never zero. The condition is called the positive definite condition.

The linear independence of the terms of the expansion (condition b) ensures that the expansion is unique. As an outline of this condition, assume that the terms of the expansion are not independent, that is there exists an expansion for zero, for which at least one value of c_r is non zero and

$$c_1 \phi_1 + c_2 \phi_2 + c_3 \phi_3 + \ldots c_r \phi_r + \ldots = 0 \, .$$

Multiply this expansion by $N(\phi_r)$ and integrate. Use of the orthogonality relationships then give the integral $c_r \int_a^b \phi_r N(\phi_r) dz$ as zero i.e. either c_r or $\int_a^b \phi_r N(\phi_r) dz$ is zero. These statements conflict and hence the uniqueness of the expansion is established.

The existence of an infinity of solutions ϕ_r of the equation (2.47) (condition c) is obtained by examining the properties of some systems of linear simultaneous equations. Compare the self adjoint differential equation system with the linear symmetric equation system

$$[A] \, [x] - \lambda \, [B] \, [x] = 0 \, , \tag{2.54}$$

where $[A]$, $[B]$ are symmetric real $n \times n$ matrices, x is a column vector and λ some load parameter. The orthogonality relationships in the linear simultaneous equation case are; $[x_r][A][x_s]$ and

$\left[x_r\right]\left[B\right]\left[x_s\right]$ are zero, where $\left[x_r\right]$ and $\left[x_s\right]$ are particular solutions of (2.54). The positive definite condition becomes; $\left[x_r\right]\left[A\right]\left[x_r\right]$ and $\left[x_r\right]\left[B\right]\left[x_r\right]$ are always positive. For this system there exists n solutions, λ_r and corresponding $\left[x_r\right]$. In the differential equation system the number n is expanded to infinity so that finally in the Hilbert space the linear equations represent the differential equation (Ref. 16).

The absolute and uniform convergence of the expansion (condition d) is more difficult to justify but attempts have been made to show that these convergence conditions hold in particular cases of second order Sturm Liouville equations (Ref. 15) and some higher order equations (Ref. 14, 15). Hilbert and Schmidt (Ref. 16), have proposed a general test for convergence using the equivalent class of integral equations. The theorem and some examples relevant to the mathematical models developed in this thesis are covered in the Appendix B. However, at this stage it should be noted that certain classes of integral equations, differential equations and linear simultaneous equations exhibit similar properties, as the following table indicates:

Linear simultaneous equations	Differential equations	Integral equations
$\left[A\right]\left[x\right] - \lambda\left[B\right]\left[x\right] = 0$ $\left[A\right], \left[B\right]$ are symmetric, positive definite matrices	$L(\phi) - \lambda N(\phi) = 0$ $L(\phi), N(\phi)$ are self adjoint positive definite differential operators	$\phi - \lambda \int_a^b K(x,s)\,\phi(s)\,N(\phi)\,ds = 0$ $K(x, s)$ is a symmetric kernel. $N(\phi)$ is a self adjoint positive definite differential operator.
The boundary conditions are included in the matrices $\left[A\right], \left[B\right]$ and are included in the equations $\left[A\right]\left[x\right] - \lambda\left[B\right]\left[x\right] = 0$	The boundary conditions are included in the self adjoint conditions, but are separate from the equation $L(\phi) - \lambda N(\phi) = 0$	The boundary conditions are included in the kernel, and are included in the equation $\phi - \lambda \int_a^b K(x,s)\,\phi(s)\,N(\phi)\,ds = 0$

Linear simultaneous equations	Differential equations	Integral equations
There exist n solutions $[x_r]$, λ_r where n is the size of the square matrices $[A]$, $[B.]$.	There exist a denumerable infinity of solutions ϕ_r, λ_r	There exist a denumerable infinity of solutions ϕ_r , λ_r

Table 2.1

The Hilbert Schmidt theorem states that if the kernel $K(x, s)$ exists and is bounded then the convergence of the infinite series to any continuous shape is established. However, when infinite series expansion is differentiated, it appears reasonable to impose the additional restrictions that the initial shape should have the same boundary conditions as the solutions ϕ_r , to the highest order of $L(\phi)$ or $N(\phi)$.

The establishment of the properties (a - d) allows the use of the expansion property, i.e. any continuous shape with continuous derivatives up to the highest order of $L(\phi)$ or $N(\phi)$, can be expanded as a linear combination of the solutions of equations (2.47), whence

$$\phi_o = a_1 \phi_1 + a_2 \phi_2 + a_3 \phi_3 + \ldots a_r \phi_r + \ldots$$

The facility to examine the effect of an arbitrary initial deformation pattern in terms of a combination of solutions of the initially undeformed mathematical model has thus been established when the mathematical model satisfies the conditions of Rule No. 1.

Rule No. 2 An adequate description of the effects on the mathematical model of the initial crookedness is obtained when the initial crookedness can be included in the mathematical model in the form

$$L(\phi - \phi_0) - \lambda N(\phi) = 0 \ . \tag{2.55}$$

where $L(\phi)$ and $N(\phi)$ are again both self adjoint and positive definite differential operators. General statements concerning the deformation behaviour can be made, and a plot of $(\phi - \phi_0)/\lambda$ against $(\phi - \phi_0)$ can be used to find the values of λ_1 and $a_1 \phi_1$.

For example: Put $\phi_0 = a_1 \phi_1 + a_2 \phi_2 + a_3 \phi_3 + \ldots$

and put $\phi = b_1 \phi_1 + b_2 \phi_2 + b_3 \phi_3 + \ldots$

The values b_1, b_2, b_3 ... are determined in terms of the constants a_1, a_2, a_3 ... by substituting the expansion for ϕ, and ϕ_0 into the differential equation (2.55). Then $L(\phi - \phi_0) - \lambda N(\phi) = 0$ becomes, on substitution

$$\sum_{r=1}^{\infty} (b_r - a_r) L(\phi_r) - \lambda \sum_{r=1}^{\infty} b_r N(\phi_r) = 0 \ . \tag{2.56}$$

But $L(\phi_r) - \lambda_r N(\phi_r) = 0$ as ϕ_r and λ_r have been determined by this equation and therefore equation (2.56) becomes

$$\sum_{r=1}^{\infty} (b_r - a_r) \lambda_r N(\phi_r) - \lambda \sum_{r=1}^{\infty} b_r N(\phi_r) = 0 \ . \tag{2.57}$$

Equating term by term in (2.57) gives

$$b_r = a_r / [1 - (\lambda/\lambda r)] \ .$$

The differentiation and equation term by term of this infinite series is possible if the series remains absolutely convergent at each level of differentiation, and the initial shape satisfies the boundary conditions of the problem.

The final solution ϕ becomes

$$\phi = a_1 \phi_1 / [1 - (\lambda/\lambda_1)] + a_2 \phi_2 / [1 - (\lambda/\lambda_2)] + a_3 \phi_3 / [1 - (\lambda/\lambda_3)] + \ldots$$

and when

$$a_1 \phi_1 / [1 - (\lambda/\lambda_1)] \gg a_2 \phi_2 / [1 - (\lambda/\lambda_2)] + a_3 \phi_3 / [1 - (\lambda/\lambda_3)] + \ldots$$

that is, at a point on the structure where ϕ_1 is large, and where λ is close to λ_1, then

$$\phi \approx a_1 \phi_1 / [1 - (\lambda / \lambda_1)] \; .$$

(2.58)

Equation (2.58) can be modified to emphasize measured values, and we obtain the generalized Southwell Plot form

$$(\phi - a_1 \phi_1) / \lambda = (\phi - a_1 \phi_1) / \lambda_1 + a_1 \phi_1 / \lambda_1 \; .$$

(2.59)

This . a plot of the ratio of the deformation $(\phi - a_1 \phi_1)$ to the load parameter λ against the deformation $(\phi - a_1 \phi_1)$ is a straight line. When the mathematical model (2.59) is a good representation of the structural behaviour, and the first buckling mode effects predominate, then the measured change in deformation $(\phi - \phi_0)$ is approximately equal to the deformation $(\phi - a_1 \phi_1)$. The reciprocal of the slope of the line of best fit to the plot of the ratio of the measured deformation $(\phi - \phi_0)$ to the load parameter λ against the measured deformation $\phi - \phi_0$, (the reciprocal of the slope of the line being denoted by λ_{crit}) is then a good measure of the lowest buckling parameter λ_1 .

In the Appendix C a short list of mathematical models is given for which a Southwell Plot is a useful device to measure and compare mathematical model and experimental results. Several other mathematical models are investigated in this thesis.

2.8   Second Order Geometric Effects.

In the mathematical models considered so far only the geometric effects which lead to linear simultaneous or linear differential equations have been included. No mathematical model can fully describe real structural behaviour, as there are always unsatisfied derivatives, and always geometrical approximations. Thus, the mathematical models in the previous sections describe characteristics of the mathematics, rather than the real structural behaviour. It is worthwhile to examine the effect of large deformations on the properties of the mathematics by considering the equilibrium of the structure in the deflected position and noting the effects on the mathematical models.

The case of the elastica for the pin-ended column is well known. The change of angle of the rods at the hinges is linked to the lateral deformations of the hinges by the equation

$$d\theta/ds = d\,(dy/ds)/ds$$

where s is measured along the deflected column. For the continuous structure, this relationship can be manipulated and

$$d\theta/ds = d^2y/ds^2 / \left[1 + (dy/dx)^2\right]^{3/2} .$$

Then for the initially straight structure, the conditions to be satisfied if the structure is to remain in equilibrium is

$$EI\; d^2y/dx^2 + Py\,[1+ (dy/dx)^2]^{3/2} = 0 \qquad . \tag{2.60}$$

This well known non linear differential equation (Ref. 23) has a unique solution for every load. The solutions for the initially straight structure (the elastica) and for the initially crooked structure are plotted in Fig. 2.9. It can be seen from the graphs that large deformations are required before any marked difference occurs between this mathematical model and the mathematical model obtained by expressing the equilibrium of the structure in terms of the initial position. In most mathematical models representing structures made from reasonably flat plates and bars, it is unnecessary to include the geometric non-linearies in the model, provided deflections are small. However, judgement must be exercised because, although structures often stiffen as a result of second order geometric effects, sometimes a weakening takes place (Ref. 24).
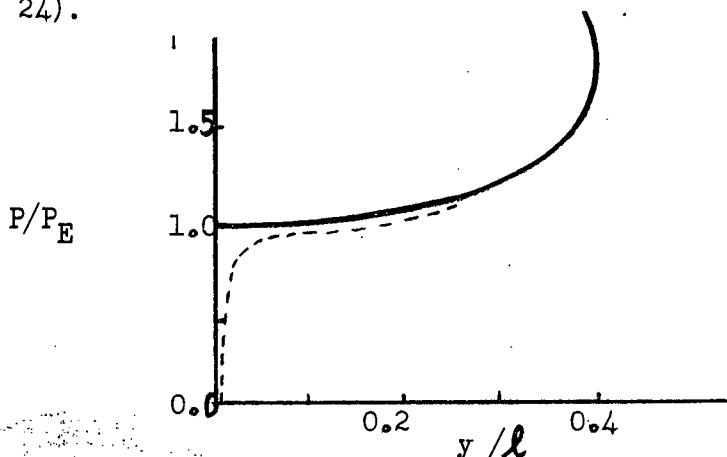

Fig. 2.9. Load and central deflection of a pin ended column, for large elastic deflections.

2.9 Non Linear Load Deformation Relationships

2.9.1. Introduction

Most engineering materials exhibit a reasonably linear load verses deformation relationship for a small range of deformations. Therefore, reasonable approximations of the overall behaviour are usually obtained by approximating the stress strain relationship within the elastic range with a single straight line.

Outside the linearly elastic range the linear differential equations developed for the elastic case do not in general describe adequately the structural behaviour as the behaviour is markedly dependent on the previous deformations.

Various models have been proposed in attempts to define the position on the load-deformation graph that is characteristic of each portion of the structure. For stability studies on compressed bars or framed structures the main models proposed for the initially straight structure are the tangent modulus and the reduced modulus models (Ref. 25). In the tangent modulus model, the strain of each portion of the structure is defined, and the slope of the stress strain relationship at that particular strain is used. In the reduced modulus model, account is taken of the unloading of the structure, and the unloading path is assumed to be linearly elastic.

It has been shown (Ref. 25) that the tangent modulus gives an upper bound estimate of the buckling load of the initially straight frame. In recent years it has also been suggested that the effects of residual stress can be included easily in the tangent modulus model (Ref. 25). As the formation of residual stresses is relevant in this context, it will be discussed before any further mathematical study is developed.

2.9.2 The formation of Residual Stresses.

In the fabrication of structural members, heat is applied in the
rolling and welding processes. As a result of differential expansion and
contraction in the heating and cooling process, residual stresses are
introduced.

For example, if in the fabrication of a built up girder the web
and flange are joined by welding, localized heating near the longitudinal
centreline results. The result of this differential expansion is to
induce tension in the outside of the flanges. While the outside of the
flanges is in tension, some plastic deformations close to the welding
zone occurs. As the section cools, the material near the weld may contract
faster than the material on the oustide of the flanges and compression of
the web flange joint results, while away from the weld tensile forces are
present. A good summary of measurements taken of residual stress effects
is given in Ref. 26 and 27.

2.9.3 Mathematical Models allowing for Residual Stresses.

The following are the main models that are used to describe the
effects of residual stresses

(a) The effect of residual stress is included as an initial
crookedness . Although this approach may first appear irrational,
reasonable design estimates can be made. For example, in Fig. 2.10
the calculations of the Column Research Council are shown (Ref. 25);
a model with no initial crookedness and no residual stress, a model
with initial crookedness and no residual stress, and a model with
initial crookedness and residual stress. The load to first yield
the structure is plotted against the value of the total length
divided by the radius of gyration. A similarly shaped graph
is obtained in the latter two cases, and a close estimate of
load carrying capacity which includes the effects of residual
stress may be obtained by specifying an effective crookedness
(Fig. 2.10).

An effective crookedness , obtained directly from measured

test results, is the basis of the well known Perry-Robertson

formulae, used in British Standard 449: "The Use of

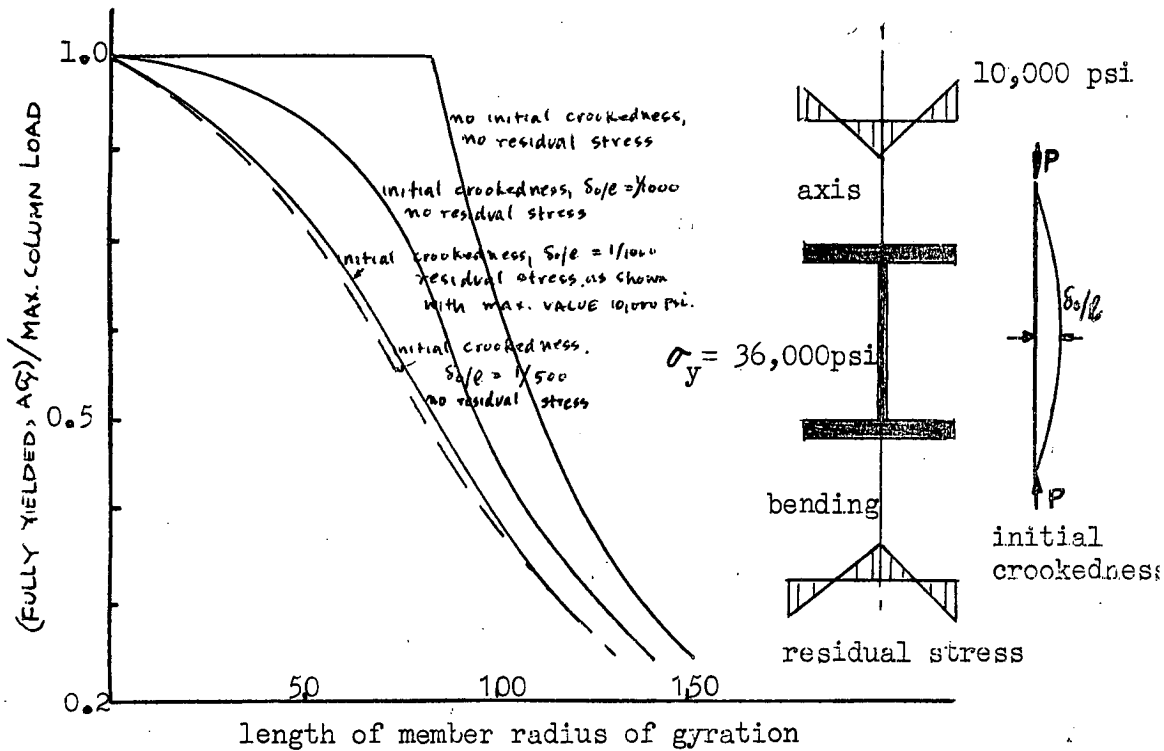Structural Steel in Building".

Fig. 2.10. Effects of initial crookedness, and residual

stress on the load carrying capacity of a

pin ended column (from Ref. 25).

(b) The effect of residual stresses is minimized by

preloading and yielding the structure. A permanent

deformation results, but the structure exhibits a

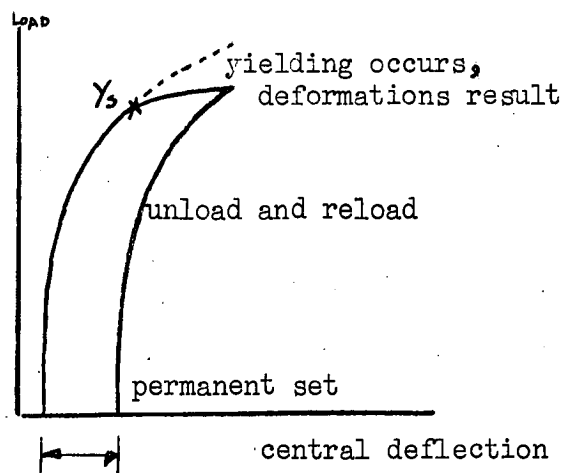larger elastic range (Fig. 2.11).

Fig. 2.11 Preloading the Structure.

(c) Recent methods include the effect of residual stress by using
an effective section modulus (Ref. 27). A guessed residual
pattern is used, and the buckling load is expressed as

$$P = \pi^2 EI_T / \ell^2 \quad ,$$

where E_T is the tangent modulus of the effective section.
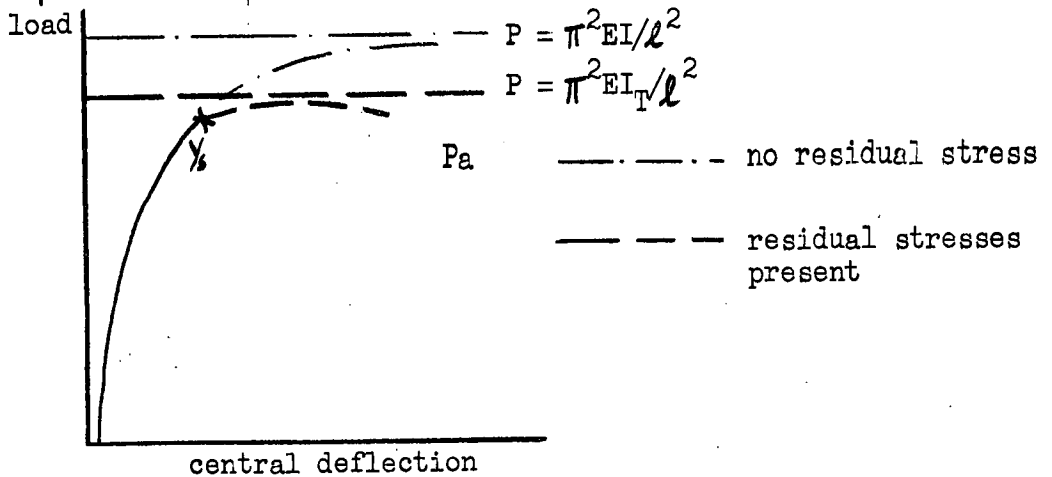
Fig. 2.12. Using an effective section modulus.

For pin-ended columns, the residual stresses induced in
fabrication tend to reduce the load required to produce first
yield of the structure by up to 10% (Fig. 2.12).

Residual stresses are also important when the life of
the structure requires consideration. If the residual stresses
complement the induced stresses, portions of the structure may
yield under repeated loadings. Thus, the evaluation of the fatigue
of the structure may be an important consideration in the design
of the structure.

2.10. Design of Structures Liable to Instability

A structure can be designed to allow for instability
effects when a satisfactory mathematical description of the structural
deformations under load is obtained. Briefly, the criteria which have
been used in the past to calculate working loads are:

(a) A safe working load = some fraction of the first buckling
load of the structure.

(b)   A safe working load = some fraction of the load to cause

first yield of the structure.

(c)   A safe working load = some fraction of the load which

causes a limiting deformation of

the structure.

A safe working load based on some fraction of the first buckling load of the structure is easy to calculate, provided that reasonable estimates of the fraction are available. When the structure is loaded so that the form of the deformation is simple, and the likely value of the initial deformations can be reliably predicted, then it is easy to find for any particular structure the suitable fraction to use in the method (a), by using either method (b) or (c). However, when loads are applied to the system so that the form of the deformations is at all complicated, the use of a fixed fraction, say, 0.66 or 0.5 is unsatisfactory, as the designer has then no idea of the likely deformations that exist for any loading of the structure. Another disadvantage of method (a) is that the buckling load of the structure is usually found by assuming that the structure always remains elastic. Thus, the design of the structure must always be checked to ensure that the structural material can sustain the predicted elastic stresses.

As a means of overcoming these disadvantages design methods based on (b) and (c) are used in this thesis. In both these methods, the deformed shape of the structure is found, and thus a deeper insight into the instability problem is obtained.

CHAPTER THREE

A MATHEMATICAL MODEL FOR A THROUGH BRIDGE.

3.1   Introduction

An engineering investigation of a real problem is illustrated
in the following three chapters and the design of a through bridge is
considered. This problem arose during the design of a very light
through plate girder bridge to serve as a connection between ship
and shore at the ferry terminal at Devonport, Tasmania; the
designer wished to know the deformations that would be present
when the bridge was loaded.

However, little published work appears to exist on this
subject, and thus the design of the bridge was based on suggestions
contained in Ref. 28, which in turn appear to have arisen from the
investigation and description of the failure of several railway
bridges in Western Europe and Russia in the early twentieth century.
(Ref. 4). These railway bridges had heavy floors, but only light
sides and top chords or flanges, and the failures appeared to
result from the lateral movements of the top members of the
bridge. Thus the mathematical models developed by Jasinski
and Engesser (Ref. 29) and Timoshenko (Ref. 30) are all
efforts to determine loading conditions for which the top
member of the bridge will be unstable, and, in these models
the top member of the bridge is isolated and considered as
an axially loaded column with lateral restraints offered by
the sides and bottom of the bridge. The load applied to the
bridge is then limited to some fraction of the load at which
the system becomes unstable.

These mathematical models have been used for
many years to design all types of through bridges. These
bridges usually had floors which strongly resisted rotation

in the plane of the cross section (Fig. 3.1). However, in recent

years, there has been an increasing use of the cheaper and lighter

through bridges having very light bottom floors, as used at

Devonport (Fig. 3.2), and as used as a pedestrian overpass

(Fig. 3.3). With this increasing tendency to lighten the through

bridge, particularly the floor, it appeared desirable that an

examination should be made of the likely deformations of these

newer types of bridges.
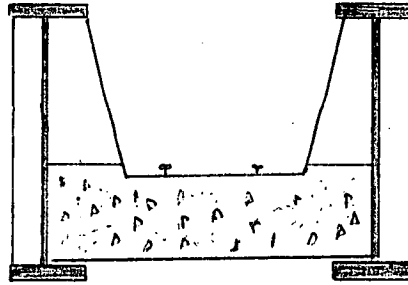
Fig. 3.1. Cross section of a heavy through bridge.

In this Chapter the measurement carried out on the

deformations of a light model through bridge is outlined. A

mathematical model to describe these deformations is then

developed, by including the torsional stiffness of the floor

beam restraints in the existing differential equations

describing the lateral stability of single I beams. The

solution of this new differential equation is then carefully

investigated as an exact mathematical solution does not appear

to exist. Approximate solutions are obtained by using existing

methods of weighting the differential equation, and the energy

method is used to find an upper bound to the first buckling

load. A method used by Southwell (Ref. 31) to find the

natural frequency of a spinning disc is modified, and it is

shown that good lower bounds to the buckling load, in an

algebraic form, can be obtained. This lower bound method

does not appear to have been used previously in structural

problems, and the author feels it could be used for many

other linear differential equations which consist of many

terms.
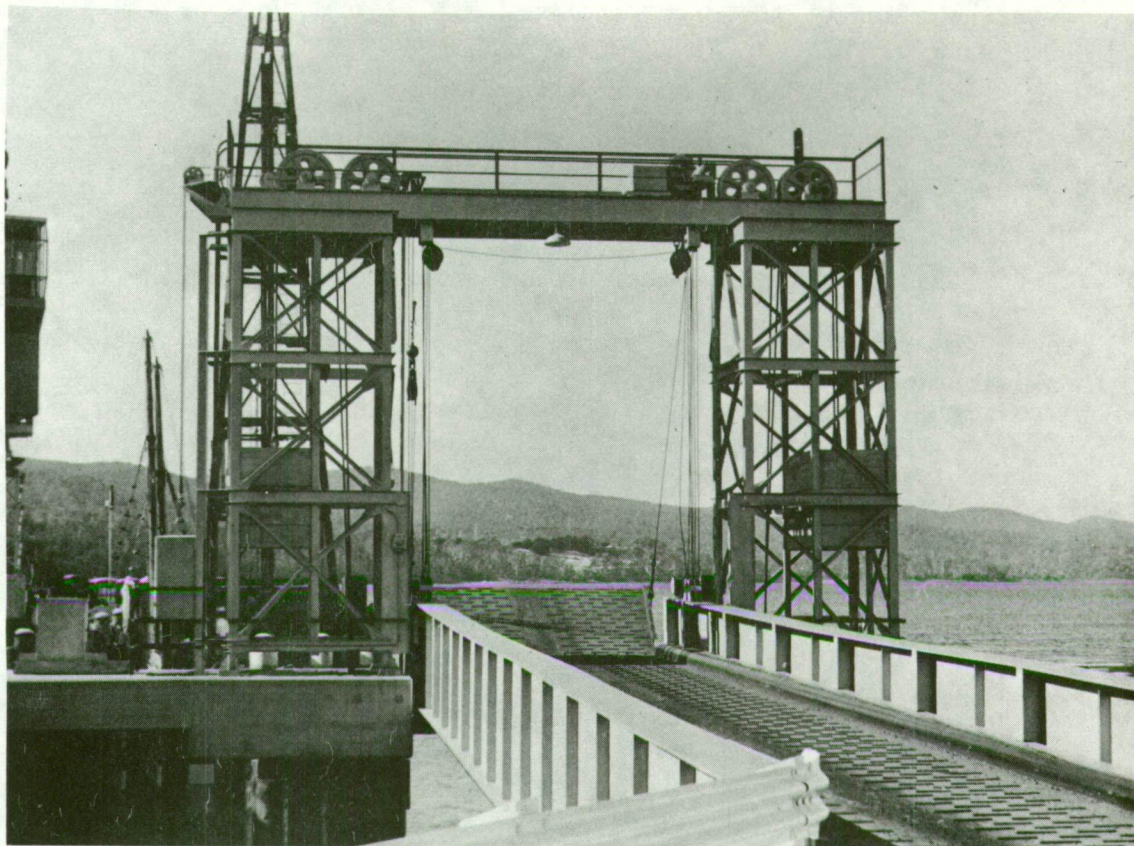
Fig. 3.2 A through plate girder bridge used as a connection between ship and shore, at Bell Bay, Tasmania. A similar type of bridge is used for the same purpose at Devonport, Tasmania.
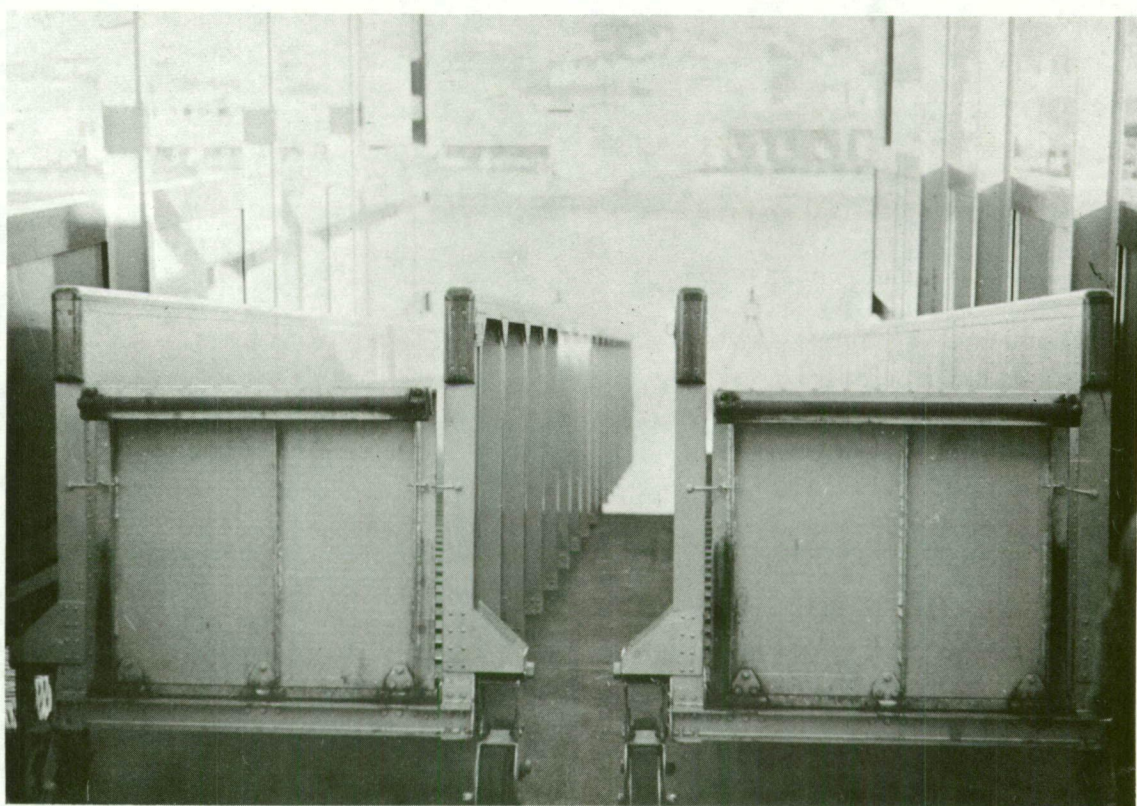
Fig. 3.3 A light through bridge used as a pedestrian overpass.

The mathematical solutions of buckling load (upper and lower bounds) are then compared with the buckling loads measured by using a modified Southwell plot. The modification of the plot involves plotting the ratio of the measured change of rotation of the web of the I beam to the square of the load against the measured change of rotation of the web of the I beam, or plotting the ratio of the measured change in lateral curvature of the centroid of the I beam to the load against the product of the measured change in curvature and the load. The justification for these plots has been outlined in general terms in Chapter Two, but the specific examples are also included in this chapter. The author claims originality for these plots, and also for the generalization outlined in Chapter Two. The measured and calculated buckling loads are found to be close, and therefore the mathematical model is taken to be a good approximation of the structural behaviour.

As a further comparison of the closeness of the mathematical model and the structural behaviour the predicted buckling mode and the measured buckling mode are compared. A technique to separate the first buckling mode from the measurements of the total deformed shape is developed, and it is shown that even for structures with a comparatively large second mode initial crookedness, good estimates of the first buckling mode can be obtained. The comparison of measured and predicted buckling modes shows that the mathematical model is a good approximation to the structural behaviour.

3.2   First Laboratory Model of the Real Bridge Structure

The first model bridge (Fig. 3.4) was constructed from brass strip and brass plate. This material was chosen as it has a high yield strain and when used in the bridge structure measurable elastic deformations were obtained before the structure yielded. Two brass I beams, with a

ratio of depth to thickness of 66 and a ratio of depth to length of 24,
were constructed by milling a groove (.020" x .030") along the flanges,
fitting the brass sheet into the groove and silver soldering the joint.
The floor beams were brazed to the bottom flange of the I beams. The
completed bridge was neither stress relieved nor straightened after
manufacture, but careful measurement was made of the initial rotational
and displacement crookedness.
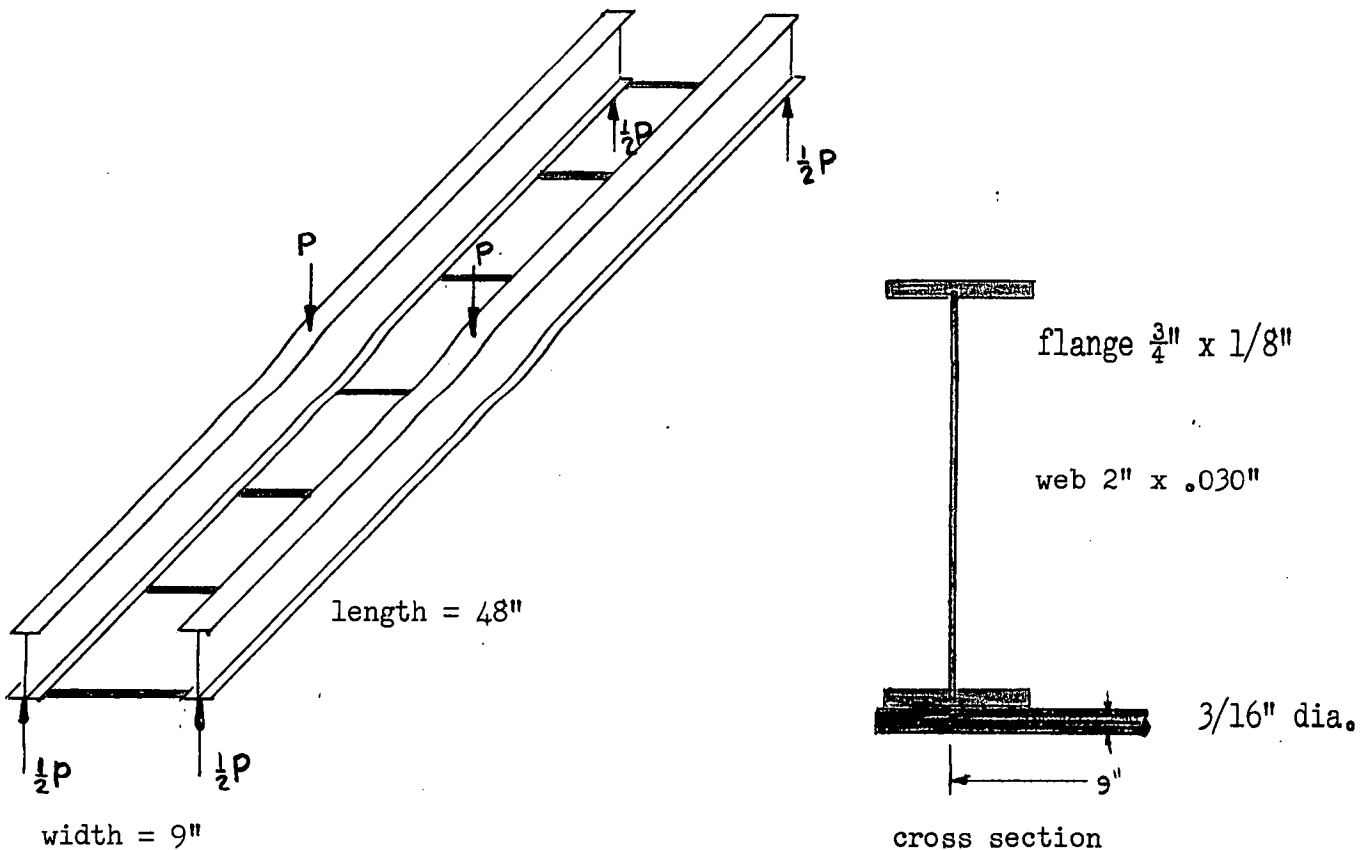
Fig. 3.4. Brass Model Bridge Dimensions.

The structure was loaded by a system of dead loads applied to
the top flange of the structure. (Fig. 3.5). This system was chosen
in order to keep the lateral forces low. Care was also taken to keep
the lateral forces from the measuring devices low as it was noticed
that even the forces exerted by dial gauges affected the lateral
deformations, especially when the bridge was loaded. A general
description of the effects of the lateral forces is considered
more fully in Chapter Four.

P Dead Weights
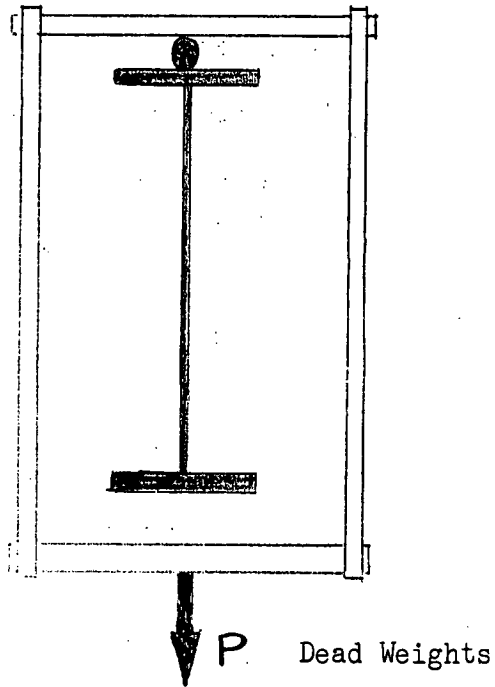
Fig. 3.5 Mechanism used to Load the Model Bridge.

3.3 Measuring Devices Used to Record Deformations of the Model Bridge.

Loading of the bridge resulted in elastic deformations similar
to those shown in Fig. 3.6. An intensive measuring program was
carried out to describe these deformations. Techniques used included:
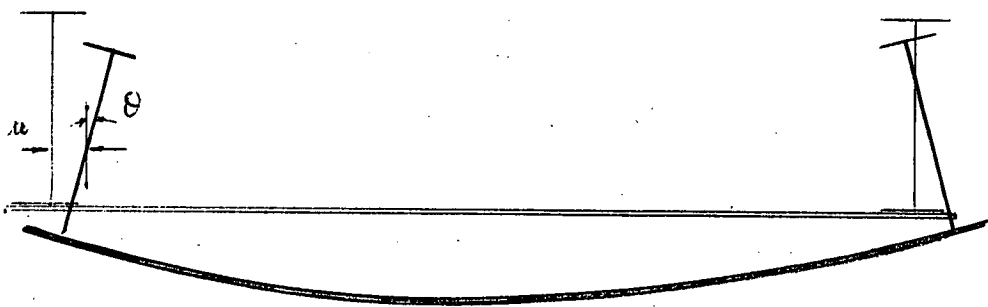
Fig. 3.6. Deformations of the Model Bridge.

(i) Point by point measurements using sixteen Huggenberger
mechanical strain gauges. The lateral and vertical
curvatures of the top and of the bottom flanges of the
I beams and the lateral and vertical curvatures of the
round floor beams were measured.

(ii) Point by point measurements with dial gauges. The
gauges were placed on the top and bottom flanges to
measure lateral and vertical displacements. The

spring return of the dial gauges was sufficient to induce

measurable deformations, especially at higher loads and

the dial gauges were used only as redundant checks on

the double integration of the lateral and vertical curvature

readings.

(iii)   Point by point measurements of the rotation of the web using

light rays reflected from small mirrors placed on the web.

(iv)   Continuous slope measuring devices of the rotation of the

web.   The simplest system consisted of three cameras

arranged along the bridge, as in Fig. 3.7. The position
                        *
of a line, reflected   from the unloaded model was

recorded. The bridge was then loaded and the new position

of the line recorded. The difference in position of the

two lines was then related to the rotation of the bridge.

The Ligtenberg technique (Ref. 8) is a logical extension

of the above method. A number of lines (from 6 to 11 per

inch) were used as a screen and photographs of the grid of

lines, (Fig. 3.8), before and after deformation were taken.

When the two photographs are superimposed an interference

pattern is produced. This pattern represents lines of

constant slope.**

---

* Note: A continuous reflective surface along the web was

obtained by glueing an aluminized terylene (commonly called

Melinex, a product of I.C.I.A.N.Z., or Mylar) to the web,

with a pressure sensitive glue, (Kodaflat, a product of

Kodak Australia).

** Note: When a fixed ray from the photoplane, through the

camera lens on to the screen is examined it is found that

in the unloaded position the ray comes from the line 1,

(Fig. 3.7) whereas in the loaded position the ray comes

from line 2. Thus, the intersection of the lines,
marked by the interference fringe, represents an
angle change of θ of the model and 2θ of the
light ray. The change of slope is then related
to the line spacing d and the distance of the screen
from the model, by the ratio

$$2\theta = d/a.$$

plan of the bridge

Fig. 37.

record

Fig. 3.8

Fig. 3.9

⌐ ·05 radians

⌐ ·05 radians

side No. 1

$\phi = \frac{\pi}{2} \pm ·005$ rad.

- - - - equivalent initial first mode deflection
(calculated from measured initial
rotations)

———— initial rotations as measured by a straight
edge and square
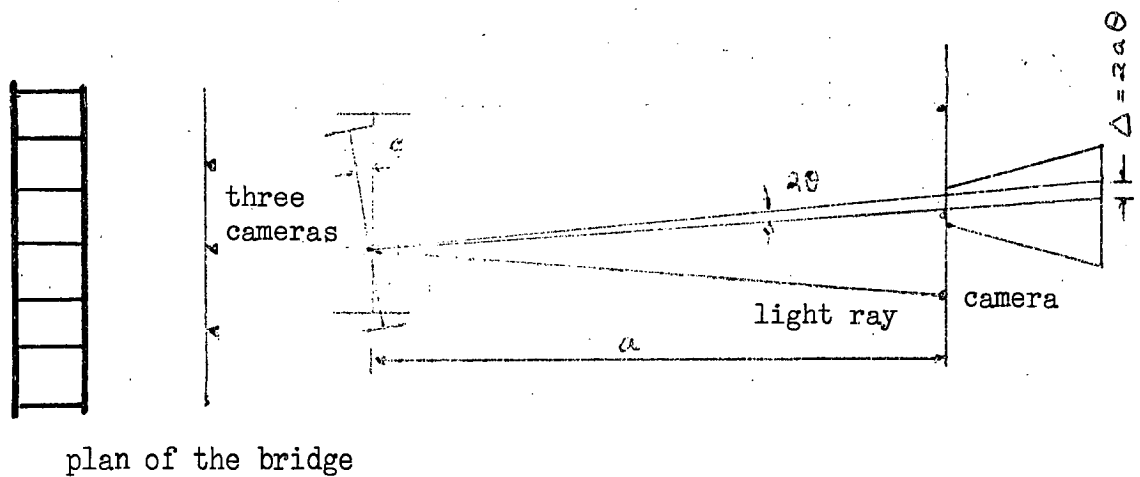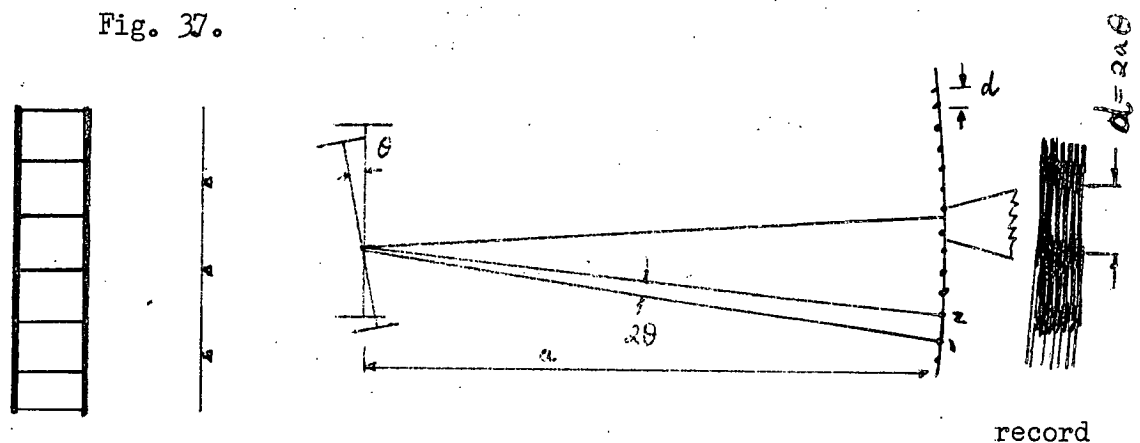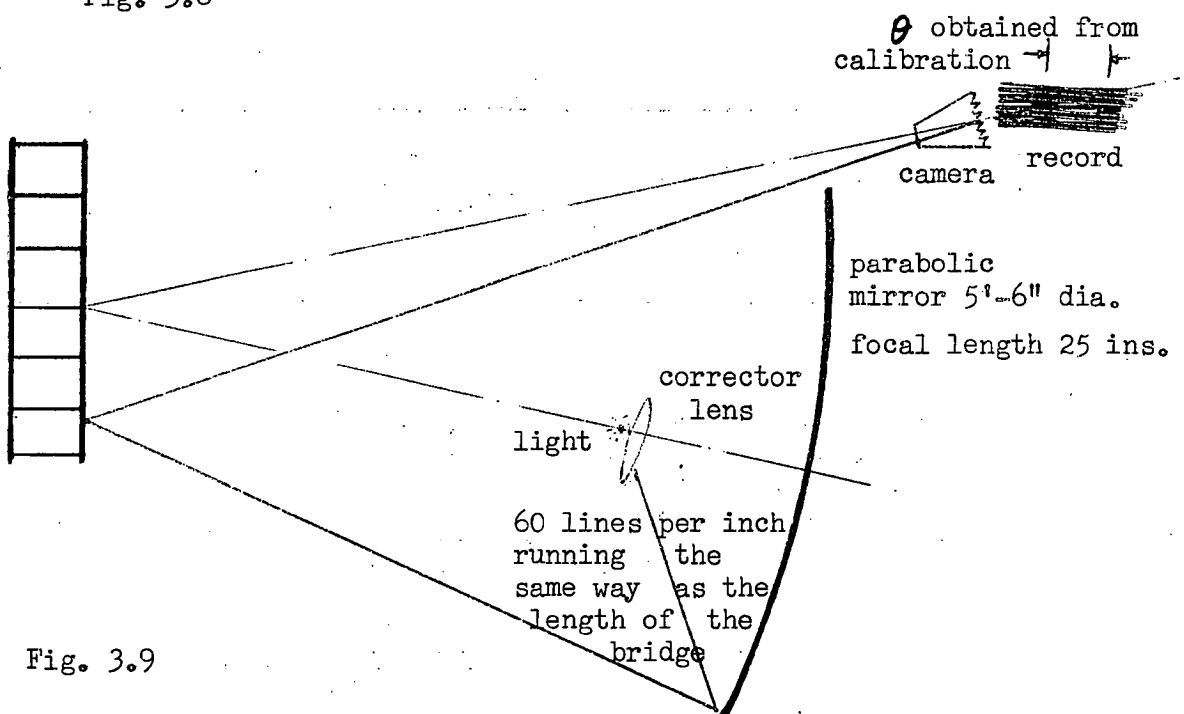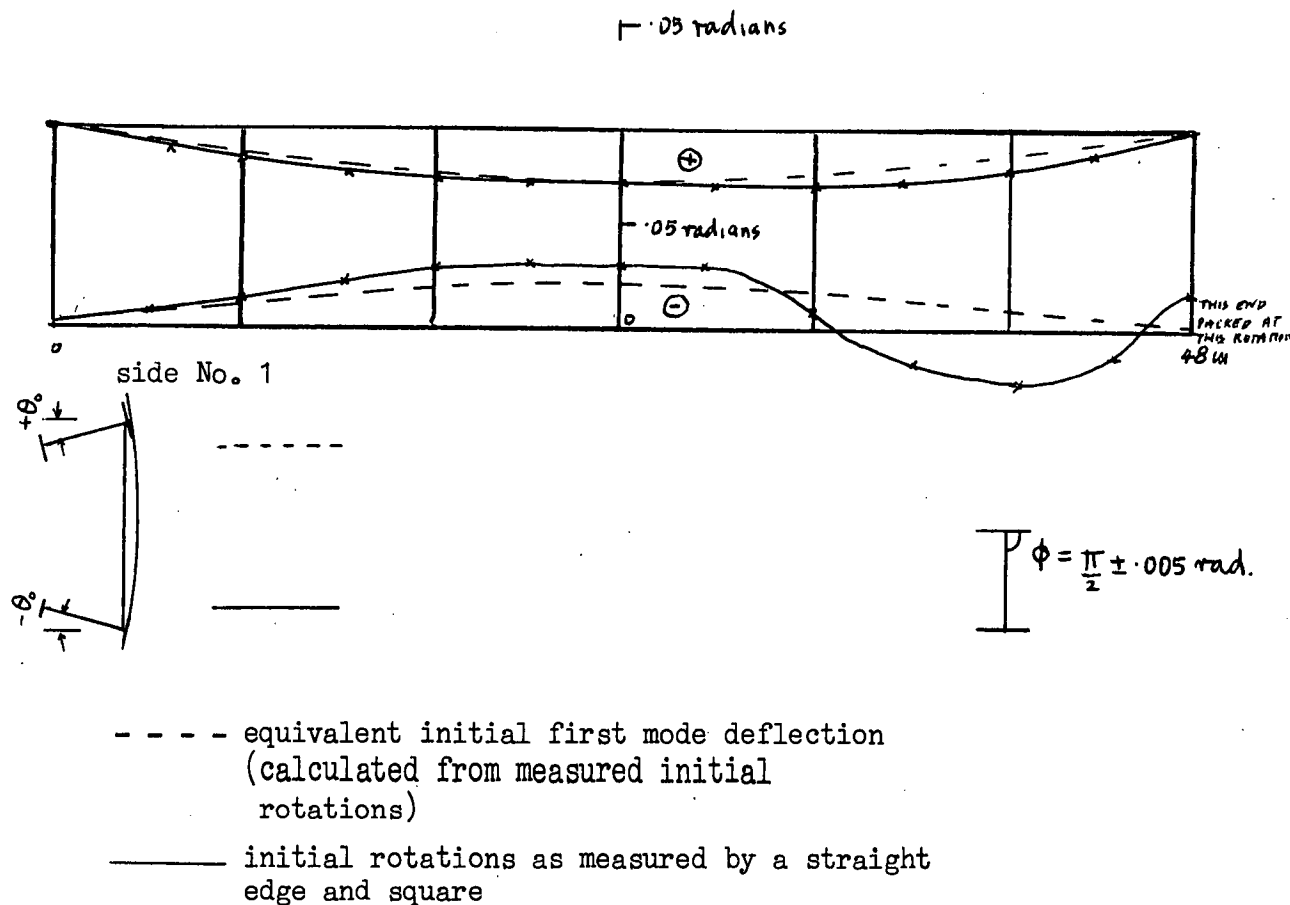
INITIAL ROTATIONS OF THE FLANGES.
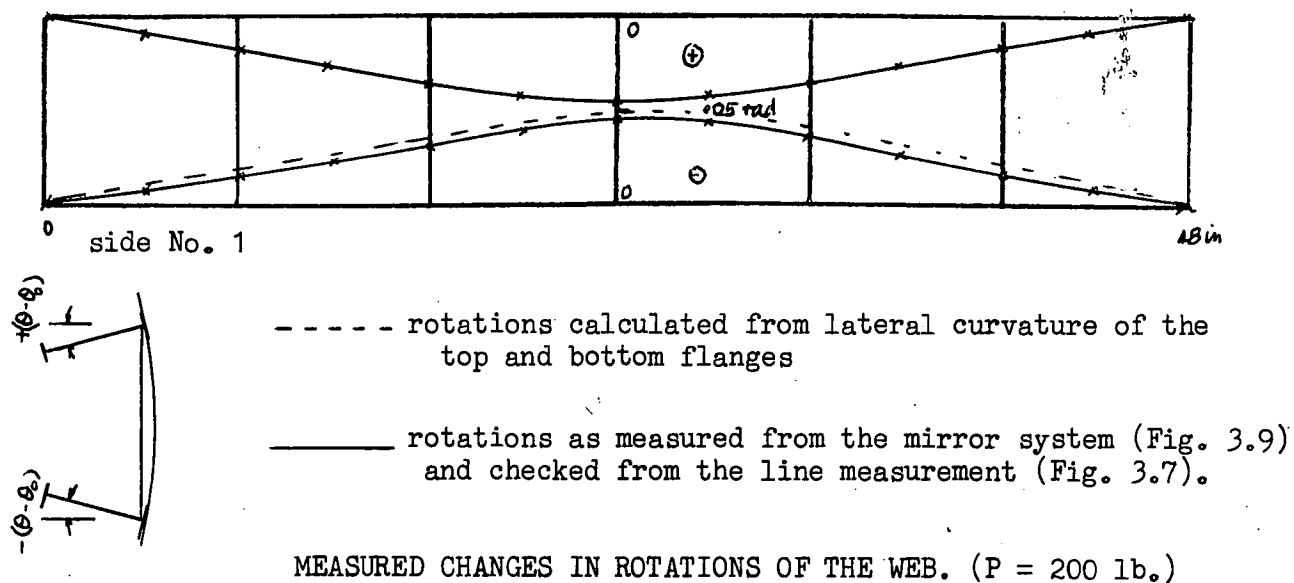
·05 rad

side No. 1   48 in

- - - - - rotations calculated from lateral curvature of the
top and bottom flanges

———— rotations as measured from the mirror system (Fig. 3.9)
and checked from the line measurement (Fig. 3.7).

MEASURED CHANGES IN ROTATIONS OF THE WEB. (P = 200 lb.)

Fig. 3.10. Measured Deformations of First Model Through Bridge.

side No. 1

feeler gauge
readings
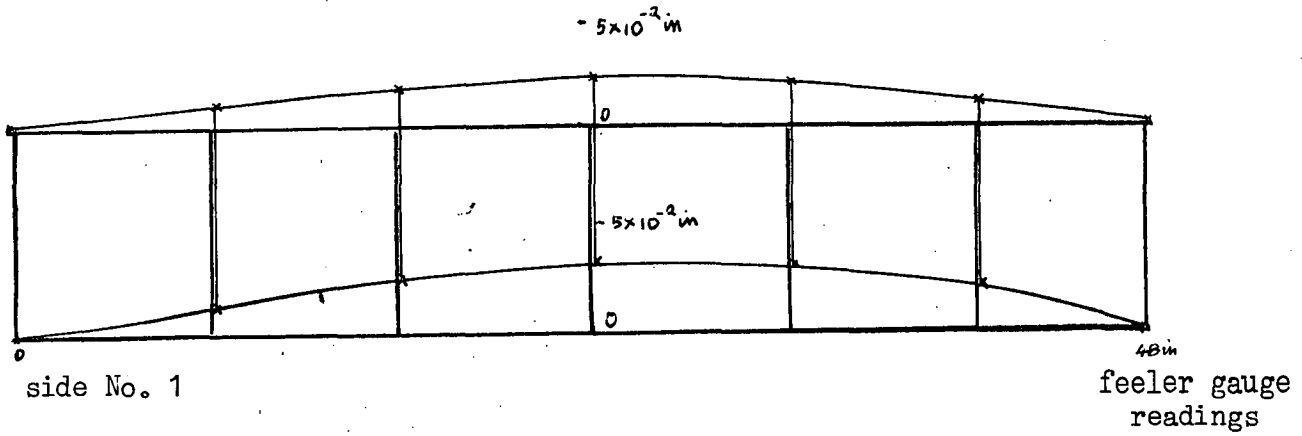
Initial lateral deflections of the centroid

side No. 1

dial gauge
readings,
integration of
lateral curvatures
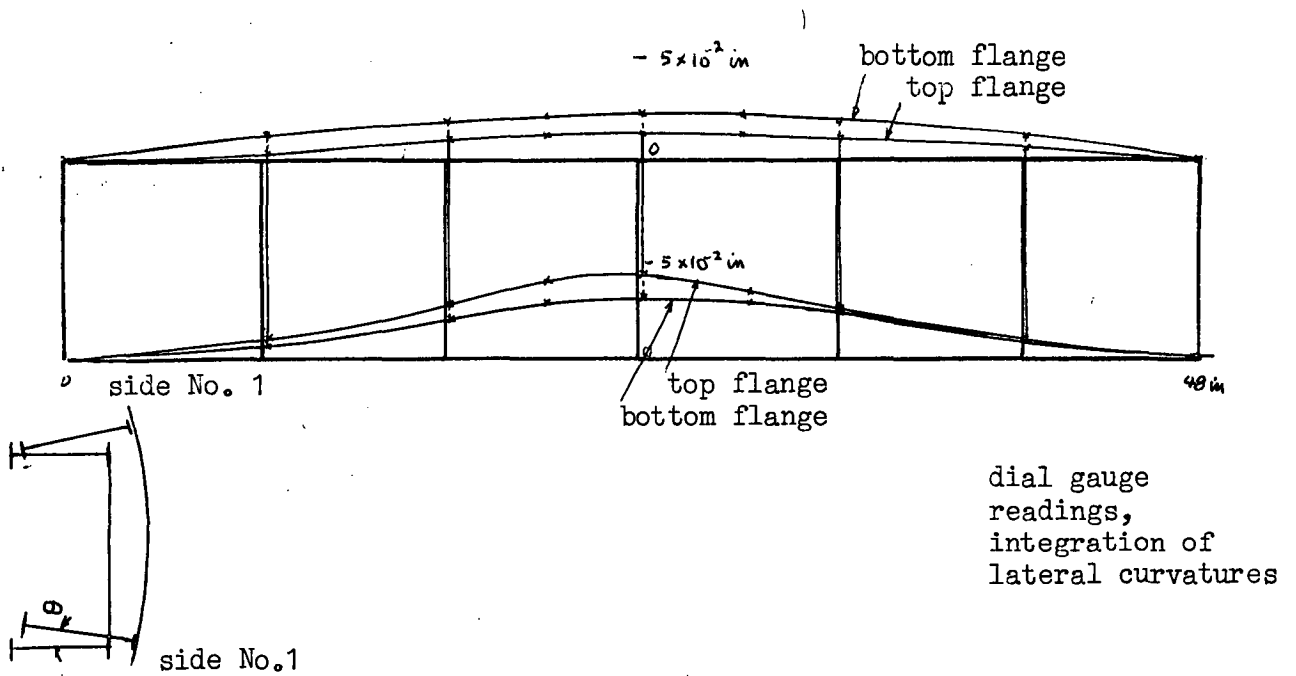
Change in deflections of the flanges, (P = 200 lb.)

side No.1   top flange
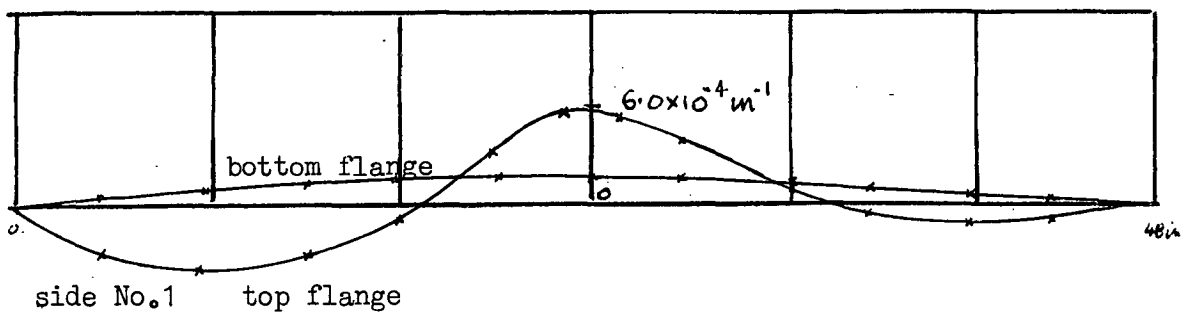
Measured changes in lateral curvatures of the flanges (P = 200 lb.)

Fig. 3.10. Measured Deformations of First Model Through Bridge.

Lines of constant slope obtained from measurements of the web
deformations indicate that the web did not distort in the plane of
the cross section of the I beam. The measurable limit, at a central
rotation of 5×10^{-2} radian was approximately 0.2 of a fringe, each
fringe spacing representing a change of rotation of 2×10^{-2} radians.

The sensitivity of the Ligtenberg technique was improved by
developing on a modified system. The large optical system constructed
is shown in Fig. 3.9. Sensitivities of 2×10^{-3} radians per fringe
with a total range of 20 fringes over a model length of 48 inches
were obtained.[*] As the model surface was not sufficiently flat to
enable measurement over the total length of the bridge, and as the
range of measurement was not sufficient to measure total angle changes,
the bridge was deformed in increments of rotation and the final
shape was calculated by addition of these increments.

3.4   Descriptions of the Measured Results

Sufficient redundant information was obtained from the various
measuring devices to enable a cross checking of curvatures,
displacements and rotations. A detailed summary of the initial
shape of the bridge and the shape of the bridge under the action
of the central loading is given in Fig. 3.10, and from these
graphs the following pattern of the deformed shape of the bridges
can be seen:

(i)   the web remained straight in the plane of the cross section,

(ii)   the ends of the I beam at the supports did not rotate,

(iii) the rotations and lateral displacements were approximately
       sinusoidal in shape,

(iv)   the floor beams rotated and remained integral with the flanges,

---

[*] Note: The calibration of the system was carried out by measuring
the deformations of a twisted glass plate (24 in. x 24 in.). The
resulting surface was anticlastic, and the spacing of the interference
fringes of lines of constant slope was then compared with the movement
of the corners of the plate, as measured by four dial gauges.

(v) the centroid of the I beam when it moved was displaced laterally,

(vi) the initial crookedness in rotation and the final rotation were of similar sign. Both I beams deformed with approximately equal rotations.

3.5 A Mathematical Model for the Model Bridge.

The measured deformations suggest that the I beams bent laterally and twisted, and that a twisting restraint was offered by the floor beams. A good mathematical model suitable to describe the observed deformations is obtained by adding the floor beam restraint, as if it were continuous, to the mathematical model for a single simply supported I beam free to deform with lateral and torsional deformations.

The model for the initially straight system including the torsional restraint offered by the floor beams is obtained by modifying expressions obtained by Mitchell (Ref. 32), Timoshenko (Ref. 30), and O'Connor (Ref. 33); others as summarized by Lee (Ref. 34). The I beam is bent in the yz plane, the plane of maximum rigidity, and a small lateral deflection and twist is assumed.

Sufficient geometric approximations are obtained by using first order approximations for the rotations i.e. using the direction cosines to relate the two sets of axes x, y, z (unloaded state) and ξ, η, ζ (loaded state). A tabulation is given in table 3.1, with θ_x, θ_y, θ_z the rotations in the original axis (Fig. 3.11).

section A-A
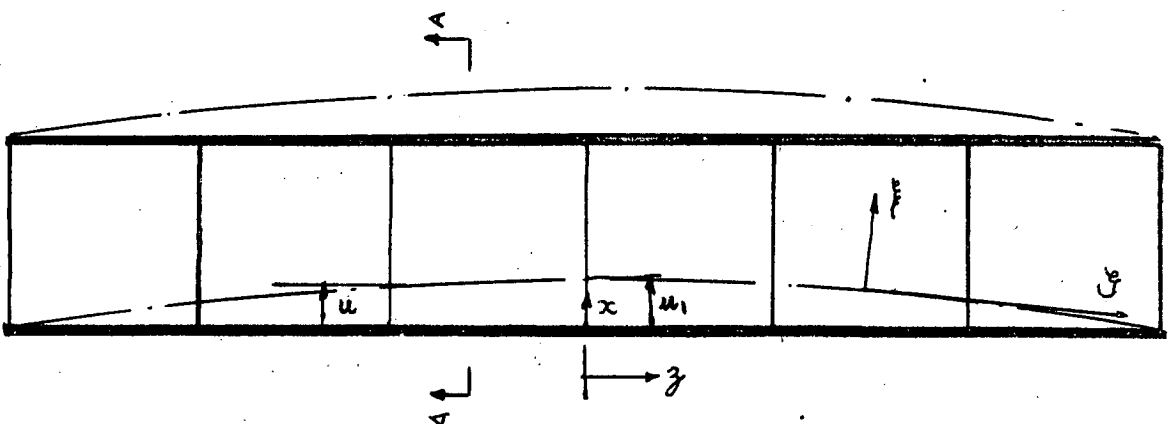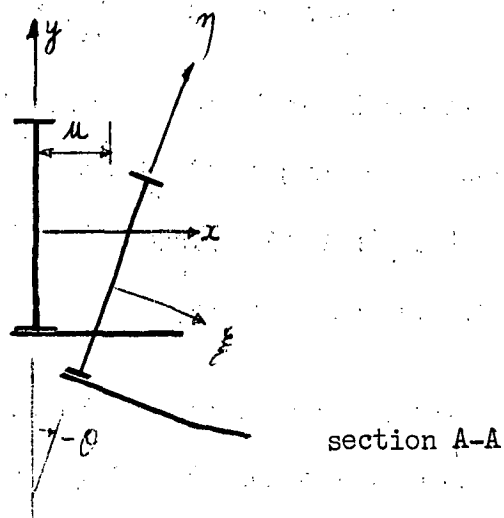
Fig. 3.11 Co-ordinate axes.

	x	y	z
ξ	1	θ_z	$-\theta_y$
η	$-\theta_z$	1	θ_x
ζ	θ_y	$-\theta_x$	1

Table 3.1 Cosine of the angles between the original and final

axes.

The curvatures are then linked by the equations

$$\phi_x = \phi_\xi + \phi_\eta \theta_z$$

$$\phi_y = -\phi_\xi \theta_z + \phi_\eta .$$

(3.3)

A satisfactory model is obtained when the load
deformation relationships are referred to the deformed structure.
The moment curvature relationships needed are

$$M_\xi = EI_\xi \phi_\xi$$

$$M_\eta = EI_\eta \phi_\eta \tag{3.2}$$

and
$$M_\zeta = Cd\theta_\zeta/dz - c_1 d^3\theta_\zeta/dz^3 + \int_0^z c_0\theta_\zeta \, dz,$$

where EI_ξ, EI_η are vertical and lateral bending rigidities,

ϕ_ξ, ϕ_η are curvatures in the $\zeta\eta$ and $\xi\zeta$ planes,

θ_ζ is a rotation in the $\xi\eta$ plane,

and C, C_1 and C_0 are St. Venant, warping, and floor stiffness values.*

For the twisted and bent beam to be in statical equilibrium under the action of a central point load P, acting at the centroid of the I beam, the following equations of statics must be satisfied. (Fig. 3.11).

Bending moment in the
vertical direction; $\qquad\qquad Mx = \frac{1}{2}P(\frac{1}{2}\ell-z)$.

Bending moment in the
lateral direction; $\qquad\qquad My = 0$.

$$\tag{3.3}$$

Torque in the axial
direction; $\qquad\qquad Mz = -\frac{1}{2}P(-u_1 + u)$.

The equations of statics in the new and old axes are therefore

$$M_\xi = \frac{1}{2}P(\frac{1}{2}\ell-z) + \theta_y\frac{1}{2}P(-u_1 + u)$$

$$M_\eta = \frac{1}{2}P(\frac{1}{2}\ell-z)\theta_z - \theta_x\frac{1}{2}P(-u_1 + u) \tag{3.4}$$

and
$$M_\zeta = -\frac{1}{2}P(\frac{1}{2}\ell-z)\theta_y - \frac{1}{2}P(-u_1 + u).$$

Combining the equations (3.1), (3.2), (3.3) and (3.4), we obtain the equations

$$\phi_x = [\frac{1}{2}P(\frac{1}{2}\ell-z) + \theta_y\frac{1}{2}P(-u_1 + u)]/EI_\xi + \theta_z[\frac{1}{2}P(\frac{1}{2}\ell-z)\phi_z -\theta_x\frac{1}{2}P(-u_1 +u)]/EI_\eta$$

$$\tag{3.5}$$

$$\phi_y = -\theta_z[\frac{1}{2}P(\frac{1}{2}\ell-z)-\theta_y\frac{1}{2}P(-u_1 + u)]/EI_\xi + [\frac{1}{2}P(\frac{1}{2}\ell-z)\phi_z -\theta_x\frac{1}{2}P(-u_1 +u)]/EI_\eta$$

and

$$-\int_{-\ell}^{z} c_0\theta_z \, dz + C\,d\theta_z/dz - C_1 d^3\theta_z/dz^3 = -\frac{1}{2}P(\frac{1}{2}\ell-z)\theta_z - \frac{1}{2}P(-u_1 +u).$$

---

* A discussion on the evaluation of the St. Venant torsional stiffness is given in Chapter Six, the warping stiffness in Chapter Four and the floor stiffness in Chapter Five.

Then, neglecting in equation (3.5) second order small

terms, in a manner indicated by O'Connor, (Ref. 33) we obtain

the conditions for the bridge to be in equilibrium, and

$$\phi_x = \tfrac{1}{2}P(\tfrac{1}{2}\ell-z)/EI_\xi$$

$$\phi_y = \tfrac{1}{2}P(\tfrac{1}{2}\ell-z)\theta_z (EI_\xi - EI_\eta)/EI_\eta EI_\xi \qquad (3.6)$$

$$\approx \tfrac{1}{2}P (\tfrac{1}{2}\ell-z)\theta_z/EI_\eta$$

and

$$-\int_{\tfrac{1}{2}\ell}^{z} C_o\theta_z dz + Cd\theta_z/dz - C_1 d^3\theta_z/dz^3 = -\tfrac{1}{2}P(\tfrac{1}{2}\ell-z)\theta_z - \tfrac{1}{2}P(-u_1 + u).$$

The standard method of solution of these three equations is to

differentiate the last equation of (3.6) with respect to z, and to

substitute this equation into the second last equation of (3.6),

and hence obtain a single differential equation expressing the

unbalanced torque per unit length, at any section z, that is

$$C_1 d^4\theta/dz^4 - Cd^2\theta/dz^2 + C_o\theta - (P^2/4EI_\eta)(\tfrac{1}{2}\ell-z)^2\theta = 0 \text{ for } \tfrac{1}{2}\ell \leqslant z \leqslant 0$$

$$(3.7)$$

and

$$C_1 d^4\theta/dz^4 - Cd^2\theta/dz^2 + C_o\theta - (P^2/4EI_\eta)(\tfrac{1}{2}\ell+z)^2\theta = 0 \text{ for } 0 \leqslant z \leqslant -\tfrac{1}{2}\ell.$$

When the differential equation represents the behaviour of the

I beam structure the boundary conditions to be satisfied are

$$z = \pm \tfrac{1}{2}\ell \quad ; \quad \theta = 0 , \quad C_1 d^2\theta/dz^2 = 0. \qquad (3.8)$$

3.6   Examination of the Properties of the Mathematical Model

The first step in the solution of the mathematical model

(3.7) and (3.8) is to check to see if the behaviour of the

differential equation and the associated boundary conditions

is in an Euler manner; that is, to check to see if for the

initially straight system there exists an infinite number of

real buckling loads and modes. The next step is to see if

reliable means can be found to compare the first buckling load

and mode as predicted by the mathematical model and as measured

on the model structure.

Use of the ideas developed in Chapter Two shows that these questions are answered if the mathematical model (3.7) and (3.8) satisfies Rules No.1 and No. 2. Rule No. 1 can be checked, by replacing $L(\phi)$ by the operators

$$c_1 \, d^4\theta/dz^4 - c \, d^2\theta/dz^2 + c_0\theta, \quad N(\phi) \text{ by } (\tfrac{1}{2}\ell - z)^2\theta \quad \text{and } \lambda \text{ by}$$

$P^2/4EI_\eta$. The self adjoint condition is then checked by integration by parts, which gives

$$\int_a^b [\phi_r L(\phi_s) - \phi_s L(\phi_r)] \; dz = \int_{-\frac{1}{2}\ell}^{\frac{1}{2}\ell} \theta_r [c_1(d^4\theta_s/dz^4) - c(d^2\theta_s/dz^2) + c_0\theta_s] \; dz -$$

$$\int_{-\frac{1}{2}\ell}^{\frac{1}{2}\ell} \theta_s [c_1(d^4\theta_r/dz^4) - c(d^2\theta_r/dz^2) + c_0\theta_r] \; dz$$

$$= [\theta_r c_1 (d^3\theta_s/dz^3)]_{-\frac{1}{2}\ell}^{-\frac{1}{2}\ell} - [\theta_s c_1 (d^3\theta_r/dz^3)]_{-\frac{1}{2}\ell}^{\frac{1}{2}\ell} -$$

and

$$[\theta_r c(d\theta_s/dz)]_{-\frac{1}{2}\ell}^{\frac{1}{2}\ell} + [\theta_s c(d\theta_r/dz)]_{-\frac{1}{2}\ell}^{\frac{1}{2}\ell}$$

$$\int_a^b [\phi_r N(\phi_s) - \phi_s N(\phi_r)] dz = \int_{-\frac{1}{2}\ell}^{\frac{1}{2}\ell} \theta_r (\tfrac{1}{2}\ell - z)^2 \theta_s \; dz - \int_{-\frac{1}{2}\ell}^{\frac{1}{2}\ell} \theta_s (\tfrac{1}{2}\ell - z)^2 \theta_r \; dz$$

Both these operators are self adjoint subject to the boundary conditions given in equation (3.8).

The positive definite quality is also easily checked by integration by parts, and

$$\int_a^b \phi_r L(\phi_r) dz = \int_{-\frac{1}{2}\ell}^0 \theta_r [c_1(d^4\theta_r/dz^4) - c(d^2\theta_r/dz^2) + c_0\theta_r] dz$$

$$= [\theta_r c_1 (d^3\theta_r/dz^3)]_{\frac{1}{2}\ell}^0 - [(d\theta_r/dz)c_1(d^2\theta_r/dz^2)]_{\frac{1}{2}\ell}^0 + \int_{\frac{1}{2}\ell}^0 c_1(d^2\theta_r/dz^2)^2 dz$$

$$- [\theta_r c(d\theta_r/dz)]_{\frac{1}{2}\ell}^0 + \int_{\frac{1}{2}\ell}^0 c(d\theta_r/dz)^2 \; dz +$$

$$\int_{\frac{1}{2}\ell}^0 c_0 \theta_r^2 \; dz .$$

and

$$\int_a^b \phi_r N(\phi_r) \; dz = \int_{\frac{1}{2}\ell}^0 \theta_r^2 (\tfrac{1}{2}\ell - z)^2 \; dz .$$

Clearly, both operators are greater then zero for the defined set of boundary conditions between $\tfrac{1}{2}\ell$, 0 and 0 , $-\tfrac{1}{2}\ell$.

Therefore, as indicated by Rule 1, in Chapter Two, there exists a denumerable infinity of solutions, θ_r and corresponding buckling values, λ_r (Fig. 3.12).
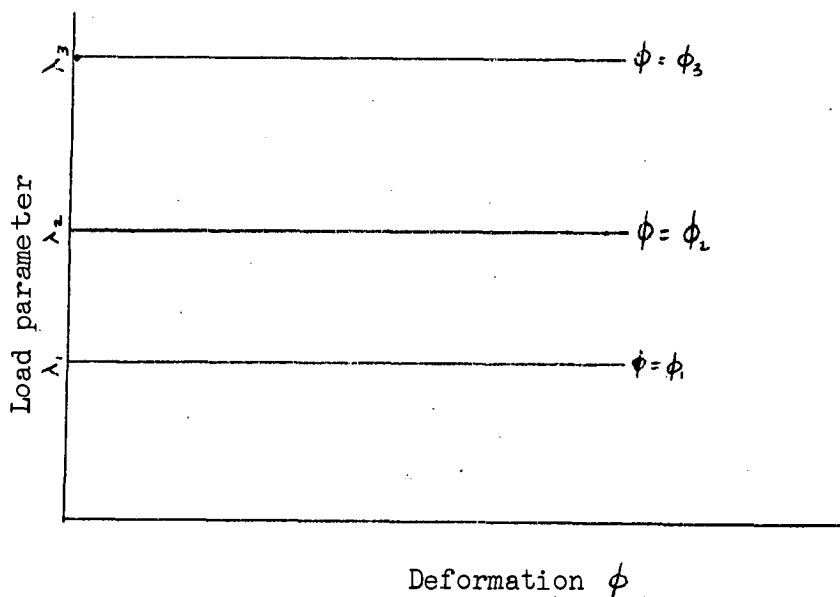
Fig. 3.12   Load and corresponding central rotation

deformations for the initially straight bridge.

Thus there exists a possibility of expressing the buckled

shape as an infinite series, of the form

$$\theta_o = a_1 \theta_1 + a_2 \theta_2 + a_3 \theta_3 + \ldots a_r \theta_r + \ldots$$

where a_r is obtained from the orthogonality properties. In the

Appendix (B) it is shown that this expansion is convergent when

the function θ is continuous and differentiable and satisfies the

boundary conditions of equation (3.8).

When the effect of initial lateral crookedness u_o and

an initial rotational crookedness θ_o is included in the

mathematical model (3.7), we obtain the equations

$$EI_\eta \, d^2(u-u_o)/dz^2 = \tfrac{1}{2}P(\tfrac{1}{2}\ell-z)\theta \qquad (3.9)$$

and

$$\int_{\frac{1}{2}\ell}^{z} C_o(\theta-\theta_o)dz + C \, d(\theta-\theta_o)/dz - C_1 d^3(\theta-\theta_o)/dz^3 = \tfrac{1}{2}P(u_1-u) - \tfrac{1}{2}P(\tfrac{1}{2}\ell-z)du/dz.$$

The equations (3.9) can be reduced to the single differential equation

$$C_1 d^4(\theta-\theta_o)/dz^4 - C d^2(\theta-\theta_o)/dz^2 + C_o(\theta-\theta_o) - (P^2/4EI_\eta)(\tfrac{1}{2}\ell-z)^2\theta = \tfrac{1}{2}P(\tfrac{1}{2}\ell-z)d^2u_o/dz^2.$$
$$(3.10)$$

When the approximation is made that the initial lateral curvature

effect, (that is the term $\tfrac{1}{2}P(\tfrac{1}{2}\ell-z)d^2 u_o/dz^2$), does not significantly

alter this equation *, the single equation becomes

$$C_1 d^4(\theta-\theta_0)/dz^4 - Cd2(\theta-\theta_0)/dz^2 + C_0(\theta-\theta_0) - (P^2/4EI_\eta)(\tfrac{1}{2}\ell-z)^2\theta = 0. \qquad (3.11)$$

Equation (3.11), satisfies the conditions of Rule No. 2, as outlined in Chapter Two, and thus the final rotations, θ , can be expressed as an infinite eigen function expansion containing the initial shape θ_0 . The final shape is

$$\theta = a_1 \theta_1 /[1-(P/P_1)^2] + a_2 \theta_2/[1-(P/P_2)^2] + \ldots \qquad (3.12)$$

where the initial shape θ_0 is given by the infinite series expansion

$$\theta_0 = a_1\theta_1 + a_2\theta_2 + \ldots$$

and θ_r, P_r are solutions of equation (3.7). The infinite series expansion is readily approximated by the finite expansion

$$(3.13)$$

$$\theta \approx a_1 \theta_1/[1-(P/P_1)^2] \quad ,$$

and a rearrangement of equation (3.12), to examine the measured values, is

$$(\theta - a_1 \theta_1)/P^2 = (\theta - a_1\theta_1)/P_1^2 + a_1\theta_1/P_1^2 \quad . \qquad (3.14)$$

Equation (3.14) is similar in form to the usual Southwell Plot. However, the value of the square of the load is plotted, rather than the load itself. The difference arises because of the nature of the differential equation (3.7). We can see from equation (3.7) that the internal change of torque per unit length, given by the expression

$$L(\phi) = C_1 d^4\theta/dz^4 - Cd^2\theta/dz^2 + C_0\theta \quad ,$$

is proportional to the product of the rotation and the square of the first critical load, that is

$$L(\phi) \propto P_1^2 \theta.$$

---

* The effect of the initial lateral curvature is investigated more fully in the Appendix D. It is shown that a reasonable approximation is to use an equivalent initial rotational crookedness and thereby include the effect of the initial lateral curvature.

However, from the differential equation for the pin ended column

(2.32), we find that the internal bending moment is proportional

to the product of the deflection and the first critical load,

that is

$$L(\phi) = EI \, d^2y/dz^2 \propto P_1 y.$$

These differences give rise to different Southwell Plots, and the

analysis presented in Chapter Two is designed to be a rigorous means

of obtaining the correct variables to use in a Southwell Plot. A $^{(N \cdot Paragraph)}$

combination of lateral curvatures are also suitable to use in a

Southwell Plot as a means of finding the buckling load of the

bridge. The lateral deflection of the top flange (Fig. 3.13) is

given by $\quad U_T = u + \frac{1}{2} h \theta$ $\hfill (3.15)$

and of the bottom flange by $U_2 = u - \frac{1}{2}h\theta$, where u is the lateral

deflection of the centroid, h is depth of the I section beam, and θ

is the rotation of the cross section. Differentiating twice and

adding these two expressions gives the curvature of the centroid

and

$$d^2u/dz^2 = \frac{1}{2}[d^2u_T/dz^2 + d^2u_B/dz^2] \hfill (3.16)$$
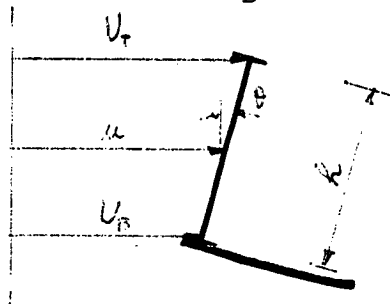
Fig. 3.13 Lateral Deflections of the Bridge.

For the initially crooked structure, the measured

lateral curvature of the centreline is given as the sum of the

measured lateral curvatures of the top and bottom flanges, that is

$$d^2(u-u_o)/dz^2 = \frac{1}{2}[d^2(u-u_o)_T/dz^2 + d^2(u-u_o)_B/dz^2]. \hfill (3.17)$$

But, from the first equation in (3.9) the measured lateral curvature

of the centre line is related to the applied load and the rotation

of the I beam, in the form

load (lb.)

(a)

(b)
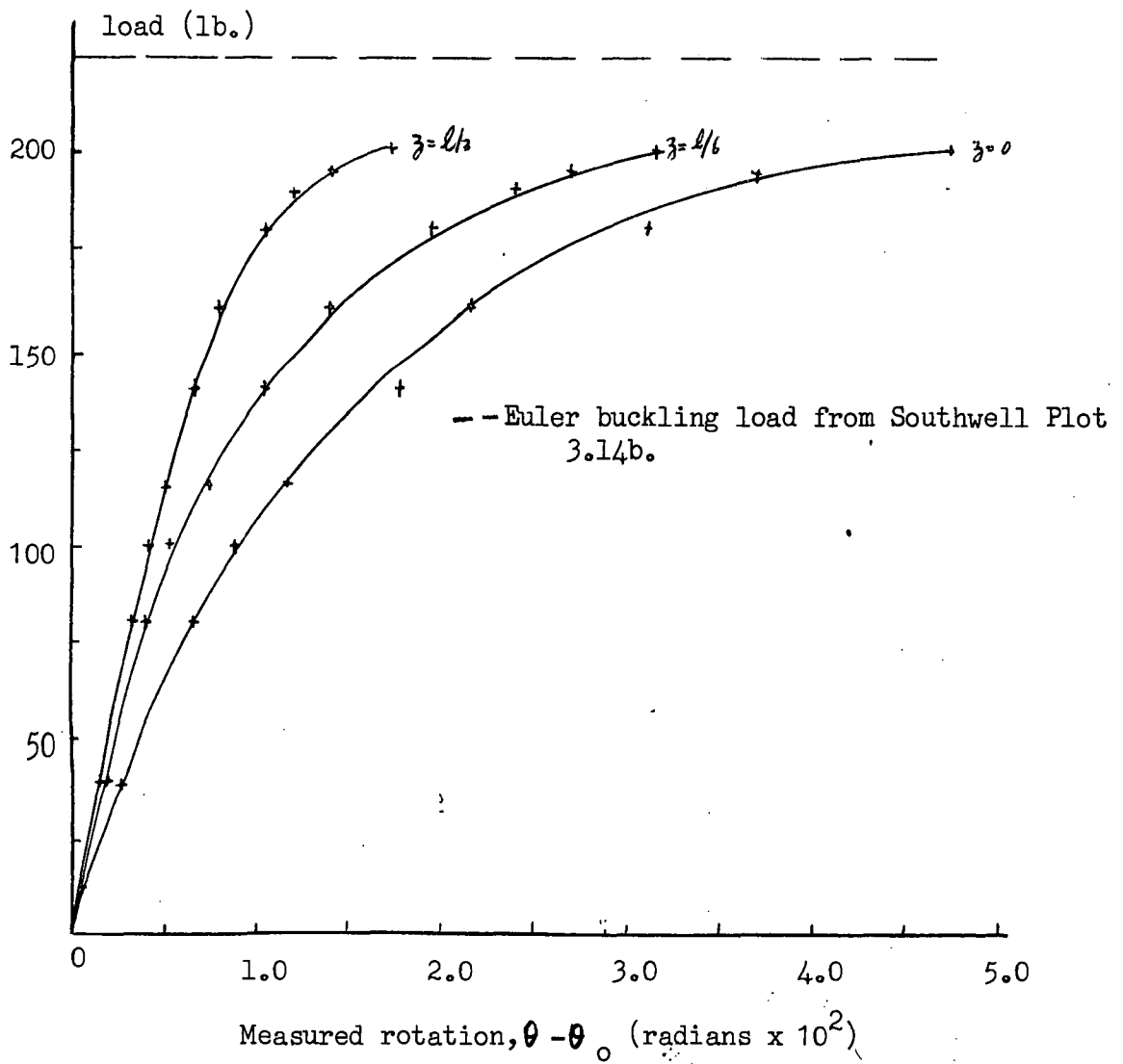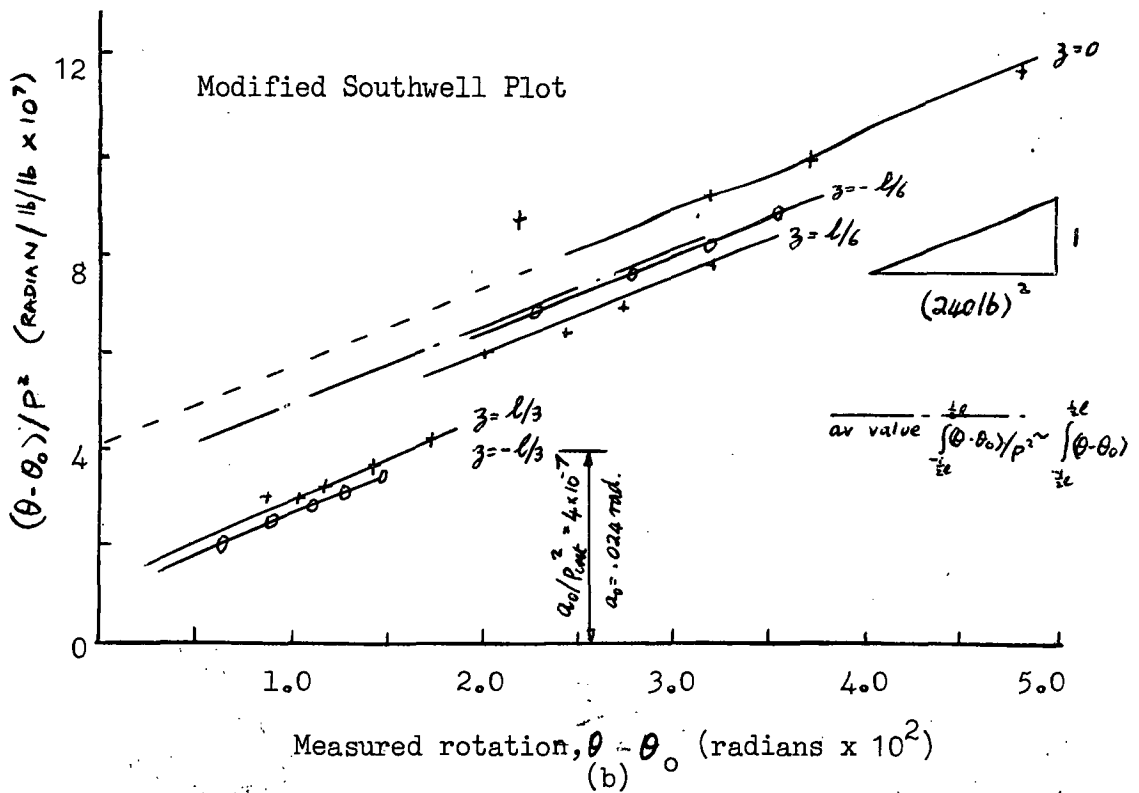
Fig. 3.14 Plots of Measured values of rotation and load.

(c)

Measured lateral curvature (in^{-1}x 10^4)

(d)

Measured lateral bending curvature (in^{-1} x 10^4) x load (1bxin^{-1}x10^2)
of the centroid$\frac{1}{2}(\epsilon_1 + \epsilon_2 + \epsilon_3 + \epsilon_4)$/b
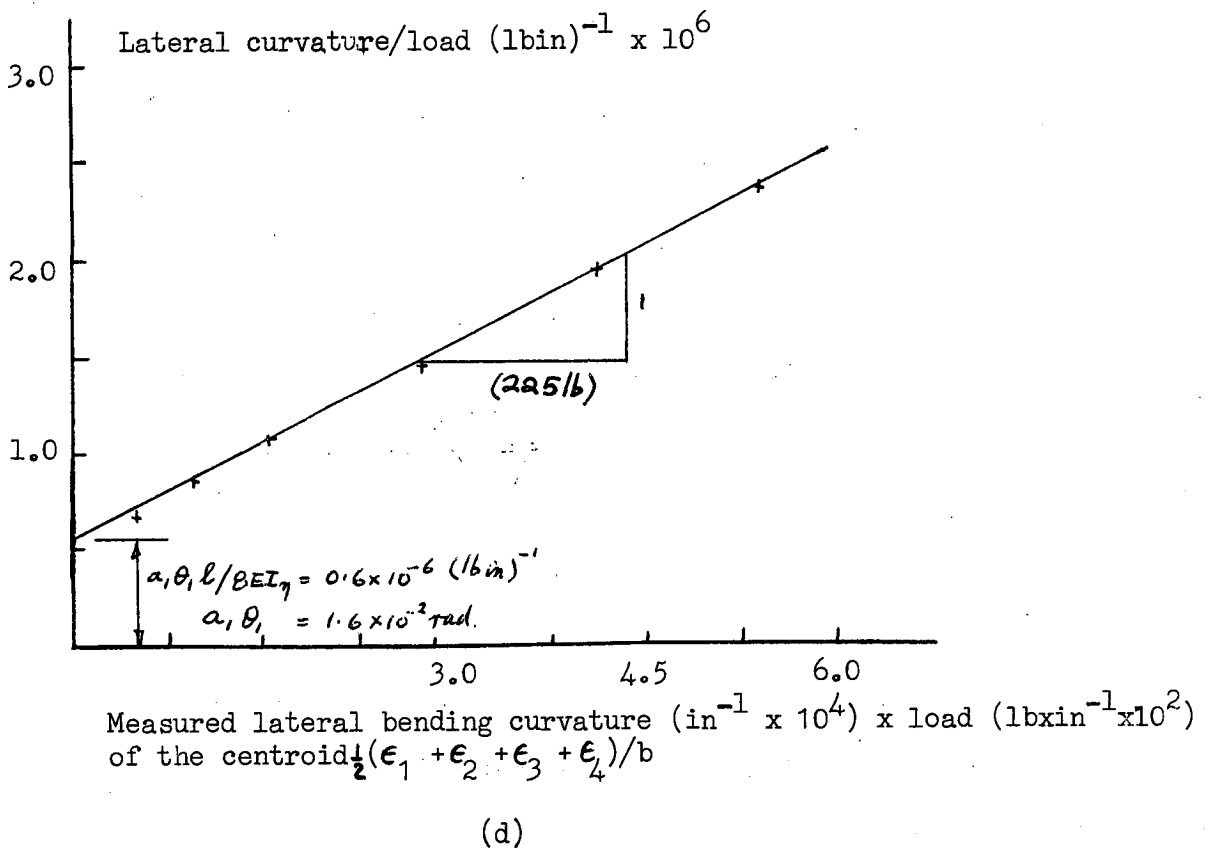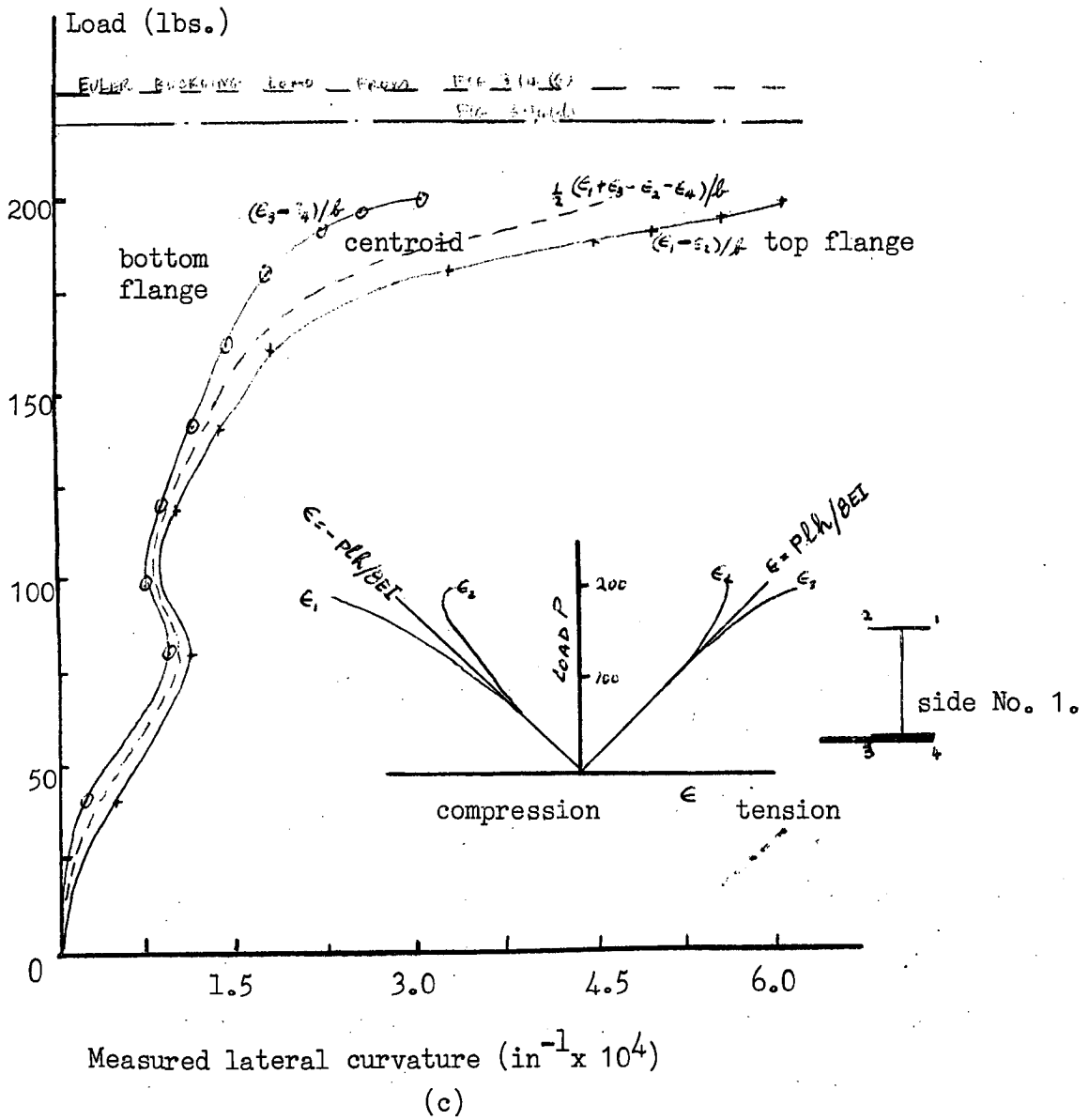
Fig. 3.14. Measured values of lateral curvature and load.

$$EI_\eta \, d^2(u-u_o)/dz^2 = \tfrac{1}{2}P(\tfrac{1}{2}\ell-z)\boldsymbol{\theta} \tag{3.18}$$

$$\approx \tfrac{1}{2}P(\tfrac{1}{2}\ell-z) \, a_1 \boldsymbol{\theta}_1/(1-P/P_1)^2) \; .$$

Therefore substituting equation (3.14) into (3.15) and rearranging,

we obtain the equation

$$\tfrac{1}{2}\left[d^2(u-u_o)_T/dz^2 + d^2(u-u_o)_B/dz^2\right]\Big/ P = \tfrac{1}{2}P\left[d^2(u-u_o)_T/dz^2 + d^2(u-u_o)_B/dz^2\right]\Big/P_1^2 + a_1\theta_1(\tfrac{1}{2}\ell-z)^2/4EI \tag{3.19}$$

which shows that certain combinations of the lateral curvatures can

be used in a Southwell Plot to measure the first buckling load P_1 and

the initial rotational crookedness, $a_1\theta_1$.

3.7   Comparisons between Mathematical Models and
           <u>Experimental Results</u>

3.7.1 Buckling Loads

Examination of the mathematical model (3.7) and (3.8) has

indicated that a satisfactory comparison between experimental results

and the mathematical model is possible by use of modified Southwell Plots.

Modified Southwell Plots of lateral bending strains and

rotations are shown in Fig. 3.14. The author claims originality for

the presentation and justification for these two types of Southwell Plot.

The modified Southwell Plot (Fig. 3.14a) using measured

rotations, at the points z = 0, z = $\pm\ell/6$ and z = $\pm\ell/3$ indicates a

buckling load of approximately 240 lb. The modified Plot using

lateral curvatures (Fig. 3.14b) obtained by separating the vertical

bending strains from the total strain readings taken at the outside

edges of the flanges and assuming that plane sections in the flanges

remained plane when the I beam deformed, also indicates a buckling load

of approximately 225 lb.

Fig. 3.14b shows that not all points on the structure

indicate the same buckling load, but that an average value is a good

approximation to the buckling load. The particular average to be used

is obtained from a consideration of the whole deformed structure. A

plot given by the equation

$$\int_{\frac{1}{2}\ell}^{z}(\theta-\theta_o)dz/P^2 = \int_{-\frac{1}{2}\ell}^{z}(\theta-\theta_o)dz/P_{crit}^2 + \int_{\frac{1}{2}\ell}^{z}\theta_o \, dz/P_{crit}^2 \tag{3.20}$$

is useful in emphasising the geometric deformations of the structure,
rather than the movements of isolated points. It is possible to separate
the antisymmetric from the symmetric mode components by suitable choice
of length over which the integration is performed. An integration of the
rotations over the total length of the bridge, and hence a separation of
the antisymmetric components from the symmetric components is shown in
Fig. 3.14. Again a reasonable straight line is obtained, indicating
a buckling load of 240 lb.

3.7.2 Buckling Modes.

The initial value of the first buckling mode, at the centre of
the bridge, is obtained from the vertical intercept on the graph of
the ratio of the measured rotation to the square of the applied load
against the measured rotation. The initial value found by this
intercept method was 2.4×10^{-2} radians, which is higher than the
value obtained by direct measurement of the initial rotational
crookedness (2.0×10^{-2} radians). This value was obtained by
measuring the initial rotations by the optical means shown in
Fig. 3.7 and also by using a spirit level to define a vertical
line and measuring with feeler gauges the difference in lateral
displacement of the top and bottom flanges. Part of the difference
can be accounted for by including the effect of the initial lateral
crookedness, which was neglected in equation (3.10) and in the
subsequent Southwell Plot analysis. In the Appendix D the measured
results of rotation and load are compared with the predicted values
of rotation and load using different methods to estimate the initial
crookedness values. From this graph it is clear that, provided a
reasonable equivalent initial crookedness is used, (for instance a
good choice is that initial crookedness obtained from the Southwell
Plot), then a reasonable description of the relationship between
load and rotation is obtained *.

When the initial lateral crookedness effects are considered, the analysis presented by equation 3.10 is still a good estimate of the structural behaviour (see Appendix D). The initial lateral crookedness is found to have an effect similar to the initial rotational crookedness, and thus an equivalent rotational crookedness is used. The very light through bridges discussed in this section have an initial rotational crookedness of .02 radians, and an initial lateral crookedness of $\ell/1000$. The equivalent initial rotational crookedness is found to be approximately .025 radians. For bridges with heavier floors the contribution of the initial lateral crookedness to the equivalent rotational crookedness is approximately .0025 radians.

An indication of the first buckling mode is obtained by direct measurement of the deformed shape. However, the shape indicated by these readings changes with load, as the magnitude of the buckling modes present in the initial and final shape vary. The following method is an attempt to rinse the first buckling mode from the deformed shape.

The underlying ideas can be obtained from a study of the behaviour of a pin ended column, with a large second mode crookedness. For the column, the final shape is

$$y = a_1/(1-P/P_1) \sin \pi x/\ell + a_2/(1-P/P_2) \sin 2\pi x/\ell + \ldots \ldots \quad (3.21)$$

When $a_i/(1-P/P_i) \sin \pi x/\ell$ is of the same order as $a_2/(1-P/P_2) \sin 2\pi x/\ell$, and $a_3 = a_4 \ldots = 0$, the deflection is as shown below. Thus, a good approximation to the final shape is

$$y = a_1/(1-P/P1) \sin \pi x/\ell + b_1 P \sin 2\pi x/\ell . \quad (3.22)$$

Differentiating equation (3.22) to obtain the changes of the shape with load, we obtain the equation

$$dy/dP = a_1 \sin \pi x/\ell / P_1 (1-P/P_1)^2 + b_1 \sin 2\pi x/\ell , \quad (3.23)$$
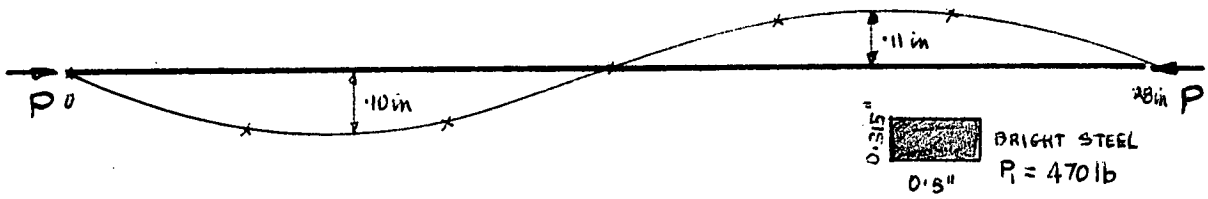
Approximate initial shape in deflection

Southwell Plots on
curvatures

1,2	520 lb
3,4	462 lb
5,6	430 lb
1,2,3,4, 5,6	475 lb

$(\epsilon_2 - \epsilon_1)/0.315$ $(\epsilon_4 - \epsilon_3)/0.315$ $(\epsilon_6 - \epsilon_5)/0.315$

$\epsilon = P/EA$ $\epsilon = P/EA$ $\epsilon = P/EA$

d(Mode)/dP — Mode/P
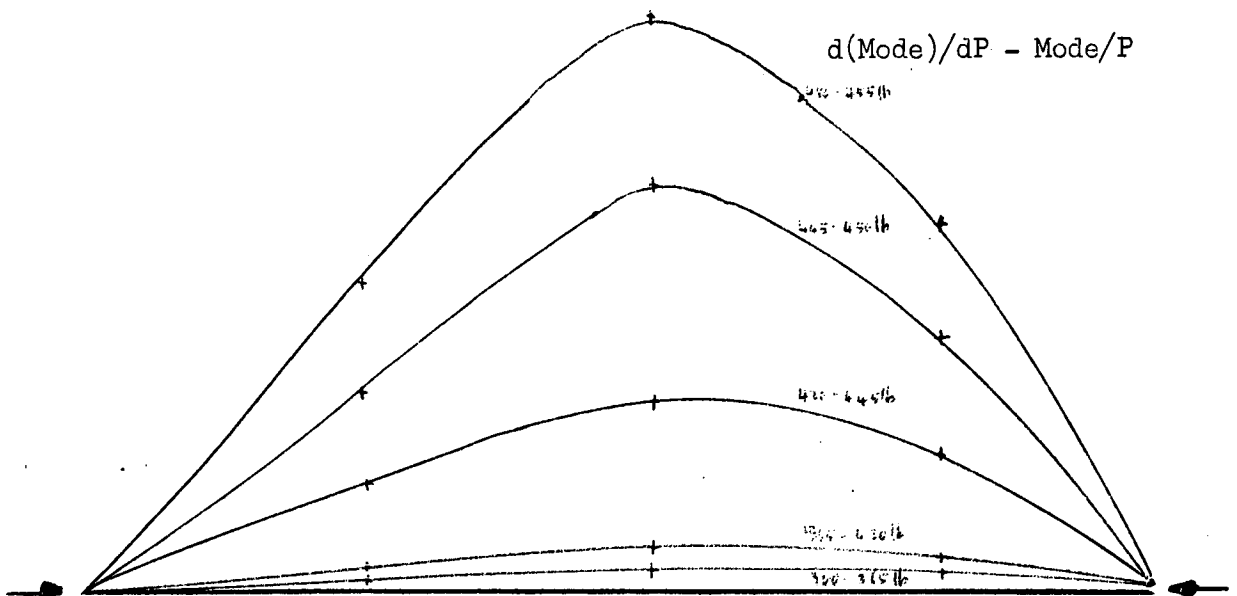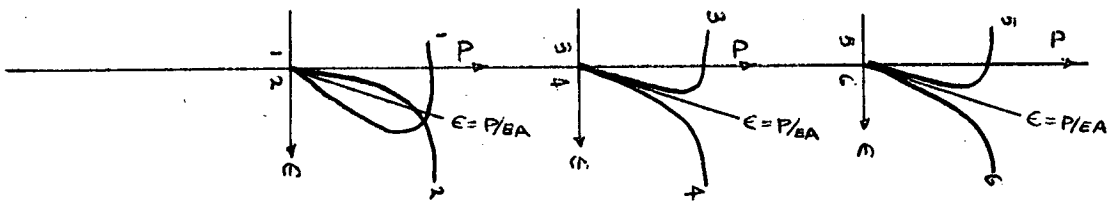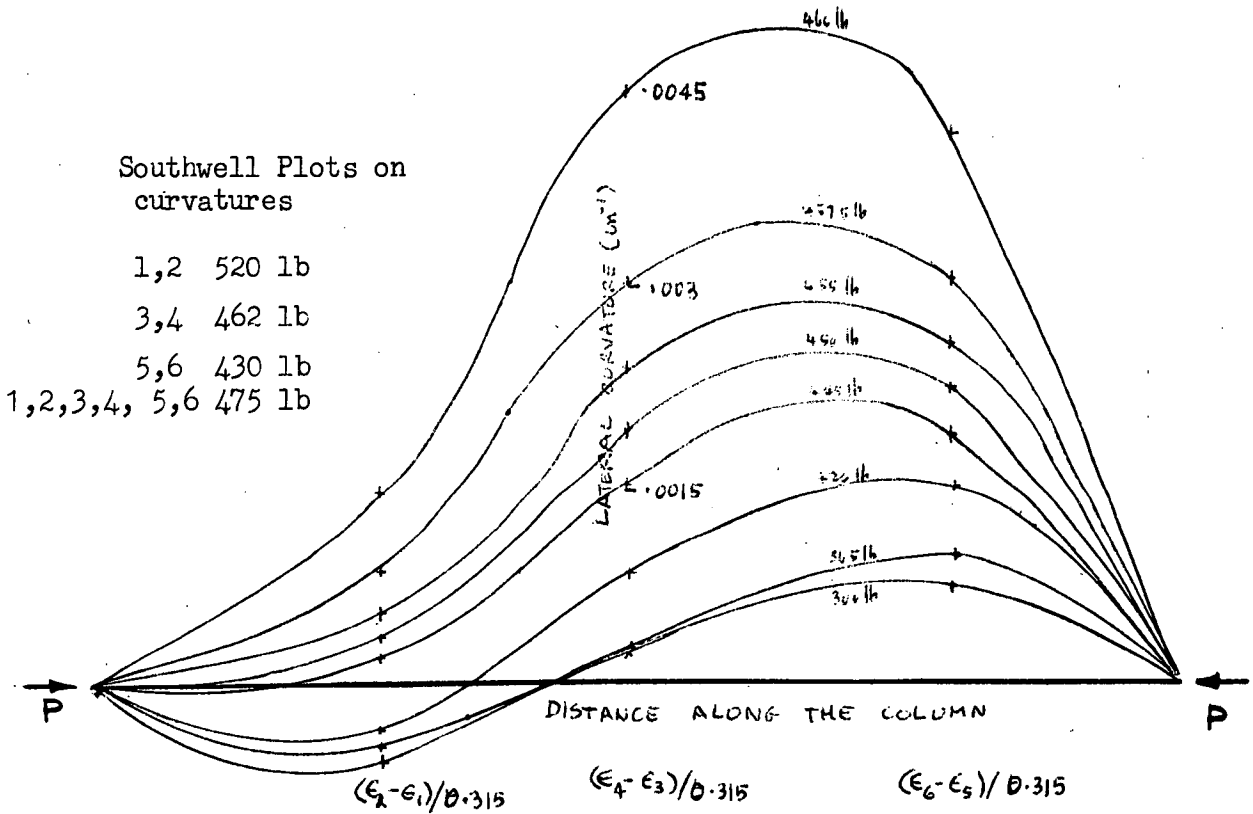
Approximate first lateral curvature
Buckling Mode

Fig. 3.15. Measurement of the first buckling mode of curvatures of a pin
ended column. The column has a large second mode initial
crookedness.
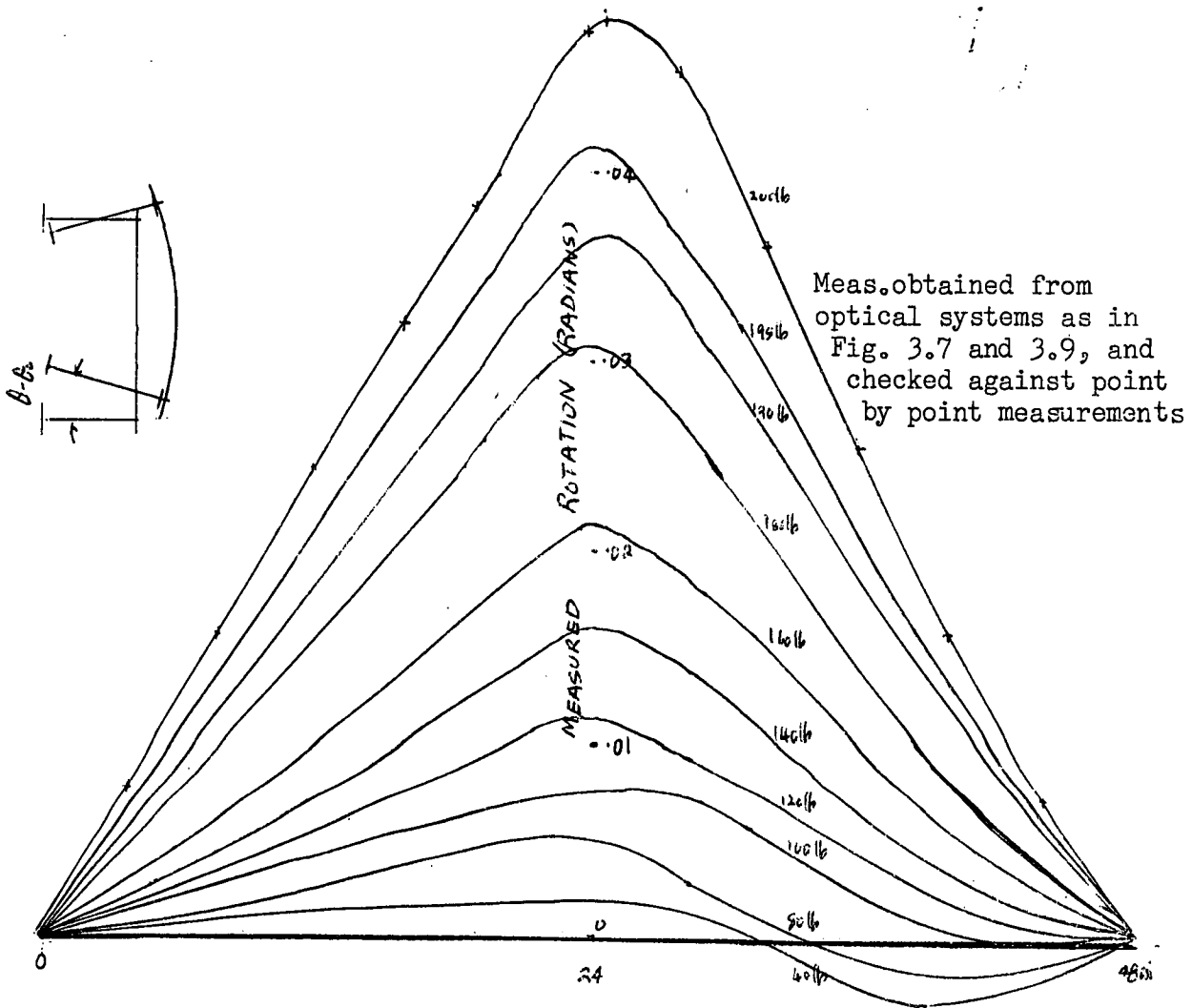
Rotation of side No. 1, first brass bridge
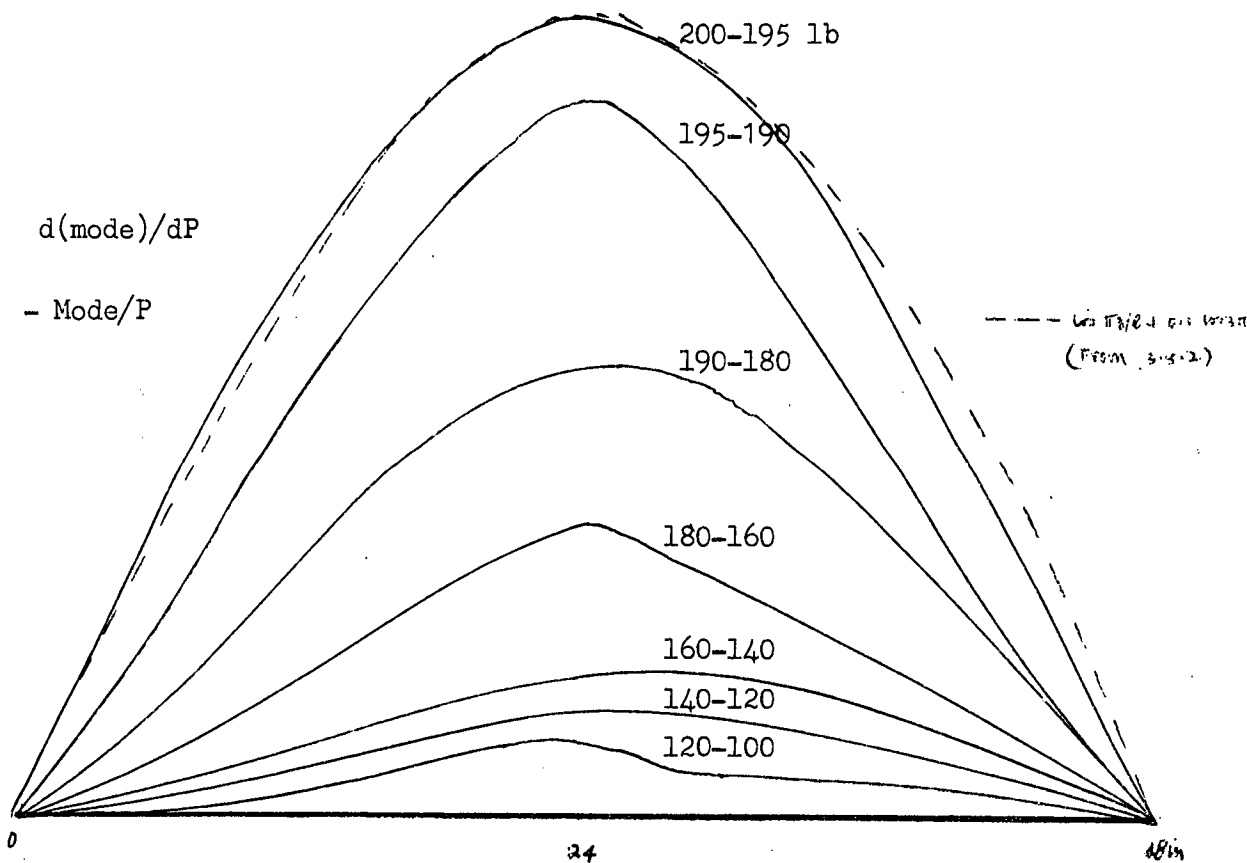
Approximate first buckling mode in rotation.

Fig. 3.16. Measurement of the first buckling mode in rotation of
the model through bridge.

Multiplying the equation (3.23) by P, and subtracting equation (3.22) establishes the proportionality

$$\sin \pi x/\ell \propto y/P - dy/dP .$$ (3.24)

The plot using measured values of curvature instead of the total curvature, was tried for the pin ended column, (Fig. 3.15). The column had a large second mode initial crookedness but the final shape resembled the first mode. The plots of measured curvatures are shown in Fig. 3.15, which shows that this plot gives a closer indication of the first buckling mode than does a direct recording of the readings. Thus the method appears to be a reasonable technique. The method, generalized to find the first buckling mode is:

First Buckling Mode $\propto$ [Deformation/Load] - [Change in Deformation per unit load.]

The initial crookedness readings for the bridge structure (Fig. 3.10) indicate a large antisymmetric rotational crookedness, and a plot of rotations was tried (Fig. 3.16). A reasonably symmetric buckling mode is indicated. The mode has little rotation at the supports with no noticeable reverse curvature away from the supports and is approximately a cosine wave over the total length of the structure. These observations are compared with those predicted by an approximate solution of the mathematical model (3.7) and (3.8) in the following sections.

3.8   Solution of the Mathematical Model of the Model Bridge.

3.8.1.   Introduction

An exact mathematical solution for the differential equation (3.7) , that is

$$C_1 d^4\theta/dz^4 - Cd^2\theta/dz^2 + C_0\theta - (P^2/4EI_\eta)(\tfrac{1}{2}\ell - z)^2\theta = 0$$ (3.25)

subject to the boundary conditions

$$z = \pm \tfrac{1}{2}\ell \; ; \quad \theta = 0 \; , \quad C_1 d^2\theta/dz^2 = 0 \; ,$$ (3.26)

has not been found, so far as the author can discover.

Various approximate methods were tried to gain the maximum possible information concerning the mathematical model. The methods enabled

(i)   an estimate of an upper bound for the first buckling load to be obtained by use of a guessed buckling mode,

(ii)   an estimate of a finite number of buckling loads and modes to be obtained, by use of the approximation that the continuous curve is a series of straight lines,

(iii)   an estimate of a lower bound for the first buckling load to be obtained by use of a weaker mathematical structure than that indicated by the equation (3.25).

A summary of the methods outlined above is presented in the following sections, and a reasonable estimate for the first buckling load and mode is obtained.

3.8.2 Upper Bound Estimates.

Approximate solutions for the differential equation (3.25) are obtained by using estimates for the deformed shape. Unless the correct shape has been used, residuals on the right hand side of the differential equation will be obtained, and the value of buckling load obtained depends on the particular methods used to minimize these residuals.

Consider the approximate * methods of solution for the mathematical model obtained by neglecting the warping and torsional stiffness in equation (3.25), that is

$$C\, d^2\theta/dz^2 + (P^2/4EI_\eta)(\tfrac{1}{2}\ell - z)^2 \theta = 0. \tag{3.27}$$

---

* A mathematically exact solution to equation (3.27) subject to the boundary conditions (3.26) is the Bessel Function of the first kind, and of order $\tfrac{1}{4}$ and $-\tfrac{1}{4}$, (Ref. 30). This solution is

buckling load: $P_1 = 16.94 \sqrt{EI_\eta C}/\ell^2$,

buckling mode: $\theta_1 = (\tfrac{1}{2}\ell - z)^{\frac{1}{2}} J_{\frac{1}{4}}\, 1.05\, [(\tfrac{1}{2}\ell - z)/\tfrac{1}{2}\ell]^2.$

When a guessed shape, given by the equation.

$$\theta = a \cos \pi z/\ell$$

is substituted into the differential equation (3.27), an estimate
of the load P is obtained from the modified equation, in terms
of the residual function R necessary to satisfy the differential
equation. Then

$$C \, d^2(a \cos \pi z/\ell)dz^2 \; + \; (P^2/4EI_\eta)(\tfrac{1}{2}\ell - z)^2 \, a \cos \pi z/\ell = R \quad . \tag{3.28}$$

Methods available to minimize this residual, and their effect
on the load P, are elaborated fully by Crandall, (Ref. 14),
and in an excellent review article by Finalyson and Scriven,
(Ref. 35). For completeness and to introduce further ideas
the methods are outlined again in this thesis.

(a)   Collocation

The residual R can be defined at r different points,
where r is the number of undefined variables. A system of r
equations with r unknowns is obtained and a unique solution
for P is found. In this particular case r is equal to one.
A common choice is to set R equal to zero at the boundaries.
Thus

$$P^2/4EI_\eta = -Cd^2(a \cos \pi z/\ell)/dz^2 \Big/ (\tfrac{1}{2}\ell - z)^2 \, a \cos \pi z/\ell \quad . \tag{3.29}$$

Now if $z = 0$, $P = 2 \pi \sqrt{EI_\eta \, C}/\ell^2$ whereas if
$z = \tfrac{1}{2}\ell$, P is infinite .

Difficulties arise in this method as it is often difficult
to estimate whether the value of the load obtained is higher or
lower than the exact solution of the mathematical model. Also,
the estimation of the best positions to specify the residual
values, and the problem of discontinuities are usually too
great and this method is not usually used to obtain solutions
for buckling problems.

(b)   Subdomain

The average of the residual R, over a subdomain, is defined.
The number of sub domains is made equal to the number of undefined variables,
and a system of equations is obtained. For one variable, the subdomain is
equal to the domain, and the integral of the residual over the domain is
set equal to zero. Thus, we have

$$P^2/4EI_\eta = \int_{\frac{1}{2}\ell}^{0} C \, d^2(a \cos \pi z/\ell) \, dz^2 \Big/ \int_{\frac{1}{2}\ell}^{0} (\tfrac{1}{2}\ell - z)^2 \, a \cos \pi z/\ell$$

i.e. $P = 8.8 \sqrt{EI_\eta C} \Big/ \ell^2$

(c)   Galerkin

An investigation of a method which places more emphasis
on the larger deformations than on the smaller values appears reasonable.
Any weighting function can be chosen. However, use of the deformation
itself as the weighting function often leads to good approximations.
Then choose the sub domain as the complete domain, (in the case of one
variable), and equate the integral of the weighted residual to zero.
We then obtain the equation

$$P^2/4EI_\eta = \int_{\frac{1}{2}\ell}^{0} C \, d^2(a \cos \pi z/\ell)/dz^2 \, a \cos \pi z/\ell \, dz \Big/ \int_{\frac{1}{2}\ell}^{0} (\tfrac{1}{2}\ell - z)^2 (a \cos \pi z/\ell)^2 \, dz \qquad (3.30)$$

i.e. $P = 21.8 \sqrt{EI_\eta C} / \ell^2$

An alternative slant on this method is to examine the
form of the solution if correct values of θ were used, and to find the
variation in P for perturbations of the guessed shape. In this form,
it is easier to investigate the convergence of the load to the first
critical load. Thus the value of the load P , given by the equation

$$P^2/4EI_\eta = \int_{\frac{1}{2}\ell}^{0} C \, d^2\theta/dz^2 \, \theta \, dz \Big/ \int_{\frac{1}{2}\ell}^{0} (\tfrac{1}{2}\ell - z)^2 \, \theta^2 \, dz \qquad (3.31)$$

is examined.

It was shown in 3.6 that continuous differential
equation (3.25) and boundary conditions (3.26) is self adjoint and
positive definite system and therefore the ratio for load P can be

easily modified, by integration by parts, to the Rayleigh Ritz form,

$$P^2/4EI_\eta = \int_{\frac{1}{2}\ell}^{0} C(d\theta/dz)^2 dz \bigg/ \int_{\frac{1}{2}\ell}^{0} (\tfrac{1}{2}\ell-z)^2 \theta^2 dz \quad . \qquad (3.32)$$

In the form (3.32), the mathematical model is equivalent to finding the changes in potential energy as the load moves downwards,(using the deflections as found by Timoshenko in Ref. 30) i.e.

$$U = \tfrac{1}{2} \int_{\frac{1}{2}\ell}^{0} (\tfrac{1}{2}\ell-z)^2 \theta^2 (P^2/4EI_\eta) dz$$

and the changes in interal energy of the structure as the structure deforms, i.e.

$$V = \tfrac{1}{2} \int_{\frac{1}{2}\ell}^{0} C(d\theta/dz)^2 dz$$

and specifying that for loads on the system equal to the buckling load there is no total change in the total energy of the system.

In the Rayleigh Ritz form (Ref. 36), it is easy to obtain values of P. These values are always greater than the first critical buckling load as is seen in the following explanation. (Southwell (Ref. 23)has also proposed a method similar to the method outlined below for differential equations representing framed structures).

The differential equation (3.25) is self adjoint and positive definite and therefore it is well known that any shape can be expreseed as an infinite series expansion of the buckling modes of the system, i.e.

$$\theta = a_1\theta_1 + a_2\theta_2 + a_3\theta_3 + \ldots a_r\theta_r + \ldots$$

The expansion for θ can be differentiated term by term, provided each of the individual terms satisfies the same boundary conditions as in 3.26. Then equation (3.32) can be expressed in the form

$$P^2/4EI_\eta = \frac{a_1^2 \int_{\frac{1}{2}\ell}^{0} (d\theta_1/dz)^2 dz + a_2^2 \int_{\frac{1}{2}\ell}^{0} (d\theta_2/dz)^2 + \ldots}{a_1^2 \int_{\frac{1}{2}\ell}^{0} (\tfrac{1}{2}\ell-z)^2 \theta_1^2 dz + a_2^2 \int_{\frac{1}{2}\ell}^{0} (\tfrac{1}{2}\ell-z)^2 \theta_2^2 dz + \ldots}$$

when the following orthogonality relationships are used:[*]

$$\int_{\frac{1}{2}\ell}^{0} d^2\theta_r/dz^2 \ \theta_s \ dz \ = \ 0$$

and

$$\int_{\frac{1}{2}\ell}^{0} (\tfrac{1}{2}\ell - z)^2 \ \theta_r \ \theta_s \ dz \ = \ 0 \ .$$

Every term of the numerator and denominator is positive (since the corresponding differential operators are positive definite) and thus by using a well known property of fractions, the inequality (3.33) is obtained, that is

$$P_1^2/4EI_\eta \ = \ \int_{\frac{1}{2}\ell}^{0} (d\theta_1/dz)^2 dz \Big/ \int_{\frac{1}{2}\ell}^{0} (\tfrac{1}{2}\ell - z)^2 \ \theta_1^2 \ dz \ \leqslant \ P^2/4EI_\eta \ .$$

(3.33)

Means of obtaining this minimum value of P from the Rayleigh Ritz method are readily available. One method is to choose approximating function, φ_i and several undefined parameters, g_1, g_2, g_3 ... such that the guessed solution, θ is a linear combination of these parameters, i.e.

$$\theta \ = \ g_1\varphi_1 \ + \ g_2\varphi_2 \ + \ g_3\varphi_3 \ + \ \ldots$$

and φ_i are the approximating functions (in general, not the buckling modes) and g_i are the undefined parameters.

For the value of the first buckling load to be obtained from the Rayleigh Ritz expression, g_i is chosen to give a stationary value of P, that is the equation

$$\partial P/\partial g_i \ = \ 0$$

(3.34)

is satisfied. Substituting in the value of P from the Rayleigh Ritz expression, we have

$$\partial(U/V)/\partial gi \ = \ 0 \, ,$$

and this statement is equivalent to the statement

$$\partial U/\partial gi \ - \ P \, \partial V/\partial gi \ = \ 0 .$$

(3.35).

[*] The orthogonality relationships are determined by the differential equation. The particular form of these relationships is obtained in section 2.7.2.

The formulation of the problem (3.35) is called the RITZ formulation (Ref. 30), and does not, in general, determine an upper bound for the first buckling load, but merely a stationary value. The formulation is equivalent to the Rayleigh Ritz form and hence can be used to determine an upper bound only when the differential operators are positive definite (Ref. 35).

The conditions under which the load P found by the Ritz formulation converges to the first buckling load of the differential equation are of considerable significance. As the number of terms g_i is increased, it is usually found that for convergence, the φ_i must satisfy the same boundary conditions as are used to establish the self adjoint property of the differential equation. Other methods, notably the method of Lagrangian multipliers (Ref. 29, and Ref. 35) are useful when the individual φ_i's are not sufficient to describe the boundary conditions.

Frazer et al. (Ref. 37) have shown that when the number of terms of the approximating function is large the methods of collocation and Galerkin are equivalent and both methods will either determine loads which converge or diverge.*

The convergence of the load P to a buckling load may be obtained when the corresponding differential operators representing a continuous structure are self adjoint, and positive definite and the approximating functions satisfy the same boundary conditions as are used to establish the self adjoint property. Under these conditions the value of P for a particular choice of g_i such that $i_{max} = r + 1$, cannot

---

* The possibility of divergence is a real danger in any numerical procedure. For example, the Lagranian interpolation formulae, which is based on the collocation method, fails for the classic case of the polynomial approximation to the function $f(x) = 1/(1 + x^2)$ for intervals greater than $(0, 3.63)$.

be greater than the value of P corresponding to $i_{max} = r$, else a lower

solution for P would be found with the solution $g_{r+1} = 0$. The value

of P is bounded below by P_1 and thus the sequence

$$P_{i\,max} \left\{ l_{max} = 1, 2, 3 \cdots \right\}$$

is monotonic decreasing. Thus the value of the load found from the

Ritz method converges to a limit * when the differential equation

is self adjoint and positive definite.

The Ritz method (essentially similar to the Timoshenko

method, (Ref. 30)) was used to obtain upper bound solutions to the

differential equation (3.25). The corresponding weighted differential

equation (with rotation) is the energy expression

$$C_1 \int_{\frac{1}{2}l}^{0} (d^2\theta/dz)^2 dz + C \int_{\frac{1}{2}l}^{0} (d\theta/dz)^2 dz + \int_{\frac{1}{2}l}^{0} C_0 \theta^2 \, dz = P^2/4EI_\eta \int_{\frac{1}{2}l}^{0} (\tfrac{1}{2}l - z)^2 \theta^2 \, dz \, . \quad (3.36)$$

The guessed shape (symmetric) used was based on the measured observations,**

and was chosen as

$$\theta = g_1 \cos \pi z/l + g_3 \cos 3\pi z/l + g_5 \cos 5\pi z/l \, .$$

and the following linear simultaneous equations are obtained:

$$\begin{bmatrix} 1 + c_1\pi^2/cl^2 + c_0 l^2/c\pi^2 \\ 9 + 81 c_1\pi^2/cl^2 + c_0 l^2/c\pi^2 \\ 25 + 625 c_1\pi^2/cl^2 + c_0 l^2/c\pi^2 \end{bmatrix} \begin{bmatrix} g_1 \\ g_3 \\ g_5 \end{bmatrix} = -\left(P^2 l^3/\pi^4 EI_\eta^6 \right) \begin{bmatrix} \frac{1}{8} + \frac{\pi^2}{48} & \frac{1}{32} + \frac{1}{8} & \frac{1}{72} + \frac{1}{32} \\ \frac{1}{32} + \frac{1}{8} & \frac{1}{72} + \frac{\pi^2}{48} & \frac{1}{128} + \frac{1}{8} \\ \frac{1}{72} + \frac{1}{32} & \frac{1}{128} + \frac{1}{8} & \frac{1}{200} + \frac{\pi^2}{48} \end{bmatrix} \begin{bmatrix} g_1 \\ g_3 \\ g_5 \end{bmatrix} \, . \quad (3.37)$$

* This buckling load may not be the lowest, as is seen in this section

where the choice of only antisymmetric shapes leads to an antisymmetric

mode, which does not correspond to the lowest buckling load.

** The boundary conditions of the individual terms of the guessed shape

satisfies the boundary conditions necessary for the differential equation

(3.25) to be self adjoint.

These linear simultaneous equations were solved by hand and by computer. By increasing the number of the cosine terms (to include $\cos 7\pi z/\ell$ and $\cos q\pi z/\ell$) in a few cases it was found that to obtain values of P within 1% there was no need to include these further cosine terms in the expansion for θ . The results are shown in graph form in Fig. (3.17), and the buckling mode is shown in Fig. (3.18).

A guessed shape of only antisymmetric terms,

$$\theta = g_2 \cos 2\pi z/\ell + g_4 \cos 4\pi z/\ell + g_6 \cos 6\pi z/\ell \, ,$$

was also tried, and the first antisymmetric buckling mode was found to be approximately twice the first symmetric buckling load (Fig. 3.17).

For the model bridge structure, the calculated buckling load was found to be 263 lb. The following constants were used * ,

$$EI_\eta = 120,000 \text{ lb in}^2$$
$$C = 4,000 \text{ lb in}^2$$
$$C_1 = 120,000 \text{ lb in}^4$$
$$h = 2.1 \text{ in.}$$
$$C_0 = 26.0 \text{ in lb/rad/in}$$
$$\ell = 48 \text{ in}$$

and $$EI = 3,000,000 \text{ lb in}^2 \text{ (where EI is the moment}$$
of inertia in the plane of the major axis).

---

* Measured and calculated values for the bridge section constants were found to be within 5%. The values used are the average of the measured and calculated values.

The values of the lateral stiffness EI_η were obtained by

(i) direct measurement of $E(= 13.5 \times 10 \text{ lb in}^2)$ obtained from
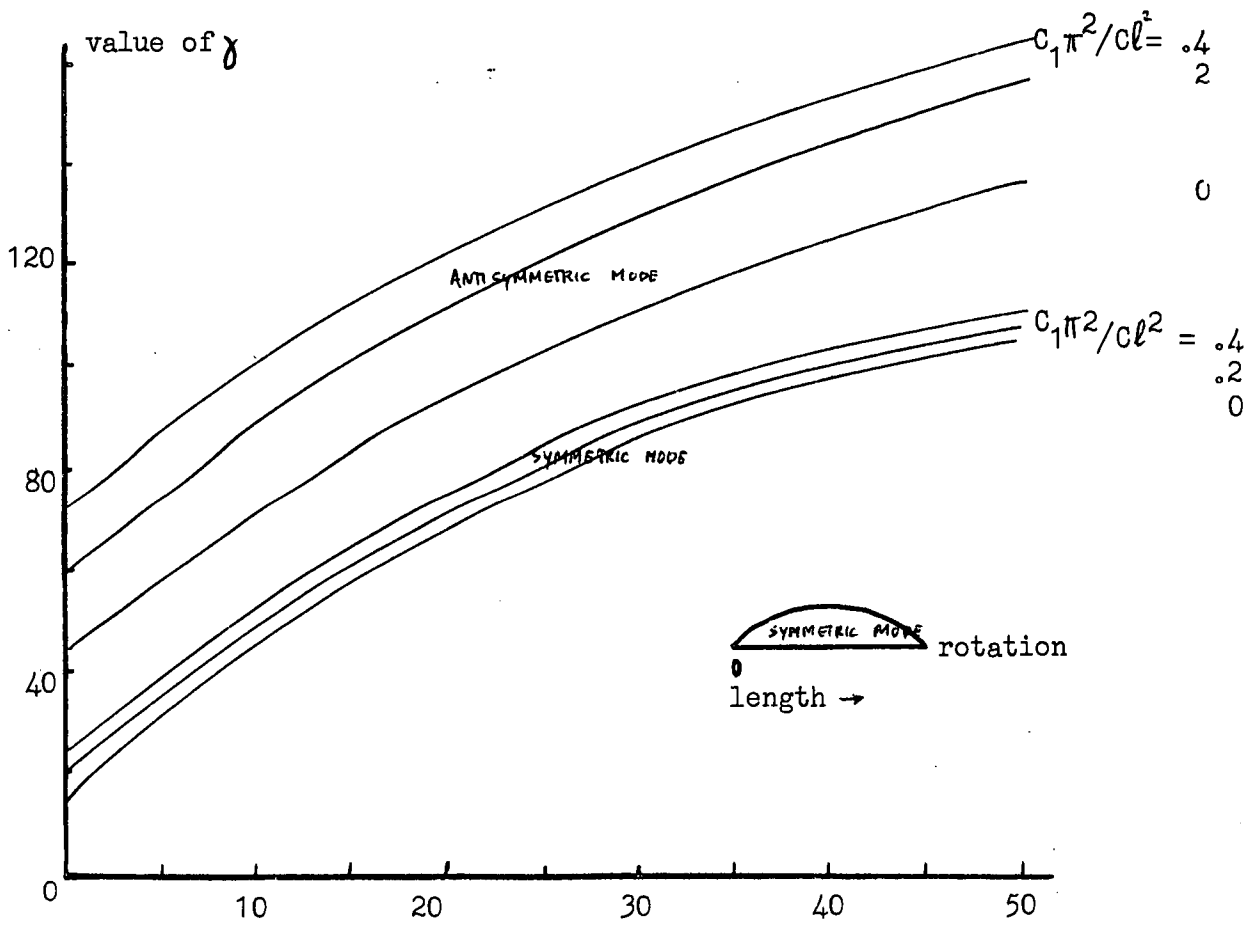
Fig. 3.17. Values of   to use in $P_1 = \gamma \sqrt{EI_\eta} \, C / \ell^2$.
as a solution of equation 3.25.

first buckling mode $\theta =$ +   +   + ...
(symmetrical)
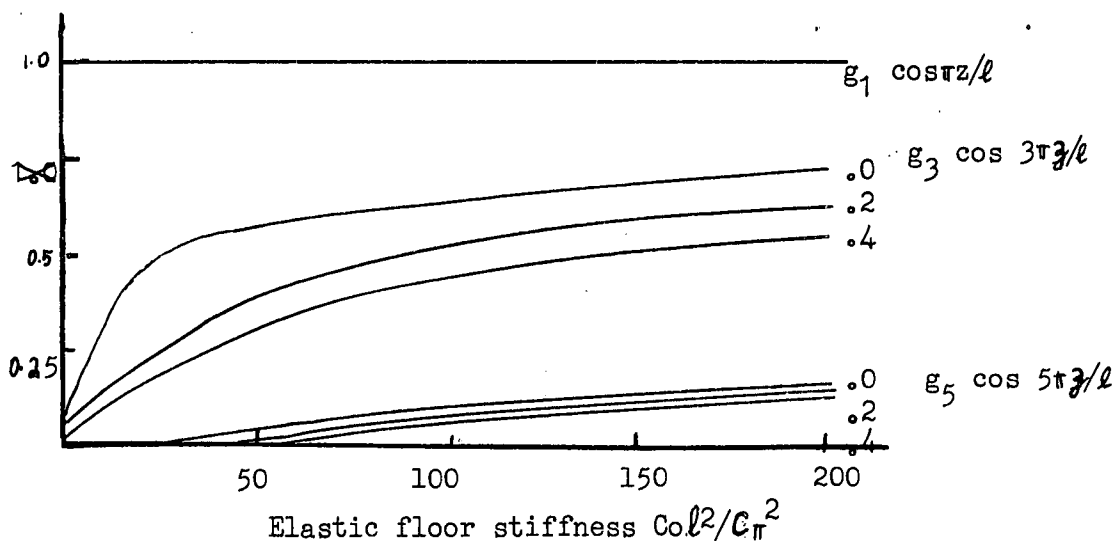
Fig. 3.18. Functional form values for an approximate weighted
residual solution of equation 3.25.

the slope of a graph of measured tensile axial load and measured
extension (Fig. 3.19) and a calculated moment of inertia,

(ii)   the slope of a graph of measured central lateral loads F
and measured central lateral deflections Δ, $(EI_\eta = F\ell^3/48\,\Delta)$.

The values of torsional stiffness C were obtained by

(i)   direct measurement of E and Poisson's ratio $(= .26)$
and a calculated torsional rigidity, $(C = \left[E/2(1+\nu)\right] \lesssim \frac{1}{3}\, b\, t^3)$.

(ii)   the addition of the measured values of torsional stiffness
values of the web and the two flanges, These values were obtained
from the slope of the graph of two end torques and rotations per
unit length. Another check was to find the torsional frequency
of each section. A length of the member was suspended vertically
and was loaded with a known mass. Then the natural frequency of
the system is approximately

$$w = C/(\text{moment of inertia of mass x length}$$
$$\text{of suspended section})$$

(iii)   the slope of a graph of measured end torques and measured
rotations per unit length (obtained by the Ligtenberg technique) .

The value of warping stiffness C_1 was obtained from the approximation
(Ref. 30)

$$C_1 = \tfrac{1}{2}\, EI_\eta\, h^2 .$$

The value of the floor stiffness C_0 was obtained from the approximation

$$C_0 = 2EI_F/\Delta\, a .$$

This approximation assumes that the floor beams are very close to
each other (actually spaced at 8 in. centres over a total length
of 48 in.), and that the initial rotational crookedness for each
I beam is equal (a reasonable estimate for this bridge, as can be
seen from Figure 3.10).

The next improvement in the mathematical model is to consider the effect on the buckling load of a load placed at the top of the I beam, instead of at the centroid of the I beam. The weighted differential equation expression (3.36) can be altered to include the extra lowering of the load, as the I beam rotates, and the new expression is

$$C_1 \int_{\iota}^{o} (d^2\theta/dz^2)dz + C \int_{\iota}^{o} (d\theta/dz)^2 dz + \int_{\iota e}^{o} C_o \theta^2 dz = P^2/4EI_\eta \int_{\iota}^{o} (\tfrac{1}{2}\ell - z)^2 \theta^2 dz + \tfrac{1}{2}Ph\theta \quad (3.38)$$

at $z=0$.

The new buckling load is found by solving a quadratic equation.

The weighted differential equation expression (3.38) gives an estimate of the buckling load of 245 lb. This estimate is probably an upper bound (as the 263 lb. was an upper bound) to the mathematical model. However no checks can be made, as the weighted differential equation expression cannot be expressed in the Rayleigh Ritz form, because the corresponding differential equation is not self adjoint. This non self adjointness arises not because of changing geometrical terms, as is usually the case with non self adjoint differential equations, but because the load P is included in the weighted differential equation in two forms, that is as P^2 and as P. It is difficult to see how a transformation could be made in order that equation 3.38 might be expressed in the self adjoint form. This example illustrates that the calculation of upper bounds is concerned with the calculation of upper bounds of the mathematical models and it is difficult to say what relationship this value bears to the buckling load (if any) of the real structure, particularly when the boundary conditions of the real structure are not measured.

3.8.3 Approximations to the Continuous Differential Equation.

The continuous curve is approximated by a series of discrete straight lines in this method. The ordinates of the straight lines are obtained by satisfying the differential equation away from the boundaries, and the boundary conditions close to the boundaries. The method of central differences was used by the author (Ref. 38) to obtain a set of linear simultaneous equations of the form

$$
\begin{bmatrix} \text{symmetric } n \times n \text{ matrix} \end{bmatrix}
\begin{bmatrix} \theta_a \\ \theta_4 \\ \theta_c \\ \cdot \\ \cdot \\ \cdot \end{bmatrix}
- P^2 \ell^c / c_1 E I_\eta
\begin{bmatrix} \theta_a \\ 4\theta_c \\ 9\theta_c \\ \cdot \\ \cdot \\ \cdot \end{bmatrix}
=
\begin{bmatrix} 0 \\ 0 \\ 0 \\ \cdot \\ \cdot \\ \cdot \end{bmatrix}
\tag{3.39}
$$

that is in matrix notation

$$
\begin{bmatrix} S \end{bmatrix}\begin{bmatrix} \theta \end{bmatrix}
- P^2 \ell^c / c_1 E I_\eta \begin{bmatrix} T\theta \end{bmatrix}
= \begin{bmatrix} 0 \end{bmatrix}.
$$

In the limit, as the number of terms becomes infinitely large, the linear simultaneous equations (3.29) can be replaced by the self adjoint differential equation (3.25). The symmetric matrix $\begin{bmatrix} S \end{bmatrix}\begin{bmatrix} \theta \end{bmatrix}$ is similar to the differential operator $L(\phi)$. Similarly the matrix $\begin{bmatrix} T\theta \end{bmatrix}$ similar to the operator $N(\phi)$. The first buckling load for the finite difference model was found to be 260 lb. This value is close to the value obtained from the method of weighted residual solution, but it is not possible to determine whether the value is an upper or lower bound to the first buckling load of the differential equation.

Another method, published recently by Taylor and Ojalvo, (Ref. 39) obtains a numerical solution by dividing the length ℓ into elements, specifying redundant boundary conditions at one end, followed by integration along the length in conformity with (3.25), to find the boundary conditions at the middle. When the derived conditions in

the middle are consistent with the mathematical model, a solution is
obtained. The solution obtained by Taylor is within 1% of the weighted
residuals solution outlined above, for all ratios of floor stiffness to
St. Venant torsional stiffness in the range

$$0 \leqslant C_0 \ell^2 / C \pi^2 \leqslant 50,$$

3.8.4 Lower Bound Estimates.

These methods are based on the premise that a load lower than
the first buckling load of the differential equation (3.25) is
obtained when the first buckling load is found for a structure which
is everywhere weaker than the structure represented by the differential
equation (3.25). The standard methods have been developed by Swartz,
(Ref. 40), Temple, (Ref. 41), Collatz, (Ref. 42 and 43), and Southwell
(Ref. 31), respectively. The most common method is the Swartz-Temple
method (Ref. 44). For the differential equation (3.25), the load P
is expressed as the ratio

$$P^2 / 4EI_\eta = L(\phi) / N(\phi)$$
$$= (C_1 d^4\theta/dz^4 - Cd^2\theta/dz^2 + C_0\theta) / (\tfrac{1}{2}\ell - z)^2 \theta.$$

A guessed functional relationship for θ is used, and the
parameters C_1, C, C_0 are varied so that they are everywhere weaker
than the original values. The load P is then sandwiched between the limits

$$L(\phi)/N(\phi) \; \big]_{min} \leqslant P^2 / 4EI_\eta \leqslant L(\phi)/N(\phi) \; \big]_{max} .$$

For the method to have significance it should be possible to obtain
the values of C_1, C, C_0 by cutting away portions of the structure.
However, it is difficult to satisfy this requirement and specify the
values of C_1, C, and C_0 in analytical terms, hence only numerical
solutions for particular configurations were obtained.

An extension to this lower bound method was tried, using the corresponding integral equation formulation. In the Appendix B it is shown that the integral equation corresponding to the differential equation (3.25) and boundary conditions (3.26) is

$$\theta - P^2/4EI_\eta \int_{\frac{1}{2}\ell}^{-\frac{1}{2}\ell} K(z, s)(\frac{1}{2}\ell-z)^2 \theta(s) \, ds = 0, \tag{3.40}$$

where $K(z, s)$ is a symmetric kernel.

The value of $P^2/4EI_\eta$ is sandwiched between the maximum and minimum values of the ratio

$$\theta \Big/ \int_{\frac{1}{2}\ell}^{-\frac{1}{2}\ell} K(z, s)(\frac{1}{2}\ell-z)^2 \theta(s) \, ds \, .$$

This method reduces the boundary problem considerably, but introduces the additional problem of finding the kernel. A few simpler problems were examined, but the complexity of solution for the differential equation (3.40) led to a search for other methods.

A good estimate of a lower bound was obtained by using a variation of a method provided by Southwell (Ref. 31) to find the natural frequency of a rotating system. This method does not appear to have been used previously to find buckling loads. However, when applied in this context it can often lead to valuable lower bound values. Consider the differential equation (3.25), that is

$$C_1 d^4\theta/dz^4 - C d^2\theta/dz^2 + C_o\theta - (P^2/4EI_\eta)(\frac{1}{2}\ell-z)^2\theta = 0$$

This equation suggests that it might be broken into two parts, namely

$$C_1 d^4\theta/dz^4 \div (P_A^2/4EI_\eta)(\frac{1}{2}\ell-z)^2\theta = 0 \tag{3.41}$$

and

$$- C \, d^2\theta/dz^2 + C_o\theta - (P_B^2/4EI_\eta)(\frac{1}{2}\ell-z)^2\theta = 0 \tag{3.42}$$

A lower bound to the first buckling load of the differential equation
(3.25) is then determined by the buckling load solutions P_A and P_B of
equations (3.41) and (3.42), and is defined by the inequality

$$P_1^2 \geqslant P_A^2 + P_B^2 \qquad .$$

The establishment of this inequality is easily obtained by examination
of the equations obtained by weighting the differential equations
(3.25), (3.41) and (3.42) with the rotations, and integrating over the
domain. This approach is similar to that developed by Southwell to
find a lower bound to the natural frequency of vibration of a rotating
system, but for completeness the extension of the method to find a
lower bound to the buckling load of a structure will be outlined. The
equation obtained from equation (3.25) is in the Rayleigh Ritz form,
that is

$$P^2/4EI_\eta = [V_A(\theta) + V_B(\theta)]/T(\theta)$$

where
$$V_A(\theta) = C_1 \int_{\frac{1}{2}l}^{0} (d^2\theta/dz^2)^2 \, dz$$

$$V_B(\theta) = C \int_{\frac{1}{2}l}^{0} (d\theta/dz)^2 \, dz + C_0 \int_{\frac{1}{2}l}^{0} \theta^2 \, dz$$

$$T(\theta) = \int_{\frac{1}{2}l}^{0} (\tfrac{1}{2}l-z)^2 \theta^2 \, dz \quad .$$

When the exact value of θ, corresponding to the solution, θ_1
of equation (3.25) is substituted into equation (3.43), P_1^2
is obtained exactly, and

$$(P_1)^2/4EI_\eta = [V_A(\theta_1)]/T(\theta_1) + [V_B(\theta_1)]/T(\theta_1) \qquad . \tag{3.44}$$

However as equation (3.44) is a minimum of two values it is
possible to obtain lower values of $V_A(\theta)/T(\theta)$ and $V_B(\theta)/T(\theta)$
when each term is considered separately that is, there exists
such that

$$P_A^2/4EI_\eta = [V_A(\theta_A)]/T(\theta_A) \leqslant [V_A(\theta_1)]/T(\theta_1) \tag{3.45}$$

and

$$P_B^2/4EI_\eta = [V_B(\theta_B)]/T(\theta B) \leqslant [V_B(\theta_1)]/T(\theta_1) \ . \tag{3.46}$$

The solutions (θ_A , P_A) and (θ_6 , P_6) (see Fig. 3.19) are solutions of equations (3.41) and (3.42) respectively. From equations (3.41), (3.42), (3.45) and (3.46) we then obtain the inequality

$$P_A^2 + P_B^2 \leqslant P_1^2 \ .$$

Choice of Variables in the Functional Form.
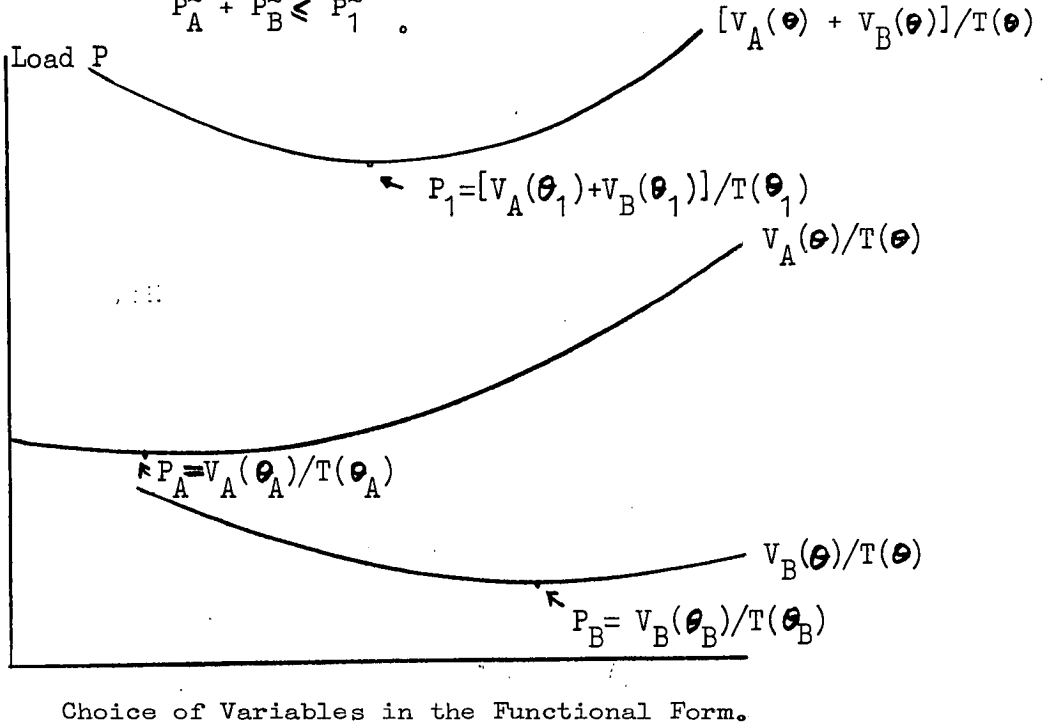
Fig. 3.19. A graph of Load against particular solutions

of equations (3.45) and (3.46).

The equations (3.41) and (3.42) may be easily solved by replacing the torsional stiffness and the warping stiffness by weaker values, of the form

$$C_{00} = [(\tfrac{1}{2}\ell - z)/\tfrac{1}{2}\ell]^2 \ C_0 \ , \ \text{and} \ C_{10} = [(\tfrac{1}{2}\ell - z)/\tfrac{1}{2}\ell]^2 \ C_1 .$$

The equations (3.41) and (3.42) then become

$$C_1 \ d^4\theta/dz^4 \ + (P_A^2 \ \ell^2/16EI_\eta)\theta \ = \ 0 \tag{3.47}$$

and

$$-Cd^2\theta /dz^2 \ - (P_B^2 /4EI_\eta - 4C_0/\ell^2)(\tfrac{1}{2}\ell - z)^2\theta = \ 0 \ . \tag{3.48}$$

The exact mathematical solution to equation (3.47) is obtained by using a cosine shape and the buckling load P_A is given by

the equation

$$P_A^2 = (16EI_\eta C_1/\ell^2)(\pi/\ell)^4 \quad .$$

The exact mathematical solution to equation (3.48) is obtained from a Bessel function solution of the first kind and order $\frac{1}{4}$ and $-\frac{1}{4}$, (Ref. 30) and the buckling load P_B is given by the equation

$$P_B^2 = (16.94/\ell^2)^2 \ EI_\eta C + 16EI_\eta C_o \ell^2 .$$

Thus a lower bound solution to equation (3.25) is *

$$P_1 \geqslant (16.94/\ell^2)\sqrt{ EI_\eta C \ (1 + 0.56 \ C_1 \pi^2/C\ell^2 + 0.55 \ C_o \ell^2/C\pi^2)} \quad . \quad (3.49)$$

For the mathematical model of the bridge structure as given by equation (3.25), a lower bound is found from equation (3.49) and is

$$P_1 \geqslant 233 \ \text{lb} \quad .$$

This load must be adjusted to allow for the decrease in buckling load resulting from the placing of the load at the top of the I beam, instead of the centroid. By making this decrease the same as is found by the method of weighted residuals in section 3.8.2, a lower bound of 215 lb. is obtained.

---

* In section 5.4.2 it is shown that the lower bound given by equation 3.49 can be simplified, especially when the value of the floor stiffness $C_o \ell^2/C\pi^2$ is far greater than unity. This lower bound functional form is then fitted to the upper bound numerical form, and a good estimate of the buckling load of (within 5% of the numerical calculation, for values of $C_o \ell^2/C\pi^2 > 5$) is obtained.

3.9   Further Comparisons Between the Mathematical Model and

Experimental Results

The solutions to the mathematical model (3.25) obtained
in sections 3.8.2 and 3.8.4 sandwich the buckling load between
the limits

$$215 \quad \text{lb} \leqslant P_1 \leqslant 245 \text{ lb.}$$

The measured buckling load (Fig. 3.14) was approximately 240 lb.

A good approximation to the first buckling mode of rotation
is obtained from section 3.8.2, and this approximation is compared
with the measured results in Fig. 3.16.

The comparison of the measured and predicted buckling loads
and modes indicates that the mathematical model developed in this
chapter is a reasonable description of the structural behaviour
of the particular model bridge. In the following chapters, the
ideas gained from the study of this simple bridge structure are
enlarged, and the design of a real through bridge structure is
discussed.

CHAPTER FOUR

REFINEMENTS OF THE MATHEMATICAL MODEL FOR THE THROUGH BRIDGE.

4.1   Introduction

In the previous Chapter a method to predict the structural behaviour of through bridges made from I beams joined by light bottom chords was established. This representation of the real bridge, by a system of I beams with light bottom cross beams can be improved. In this chapter several original improvements are made, each improvement using as a basis small perturbations of the deformed shape of the simple bridge structure.

The first effect described is the effect of including web stiffeners in the I beam structure, while the second effect described is the effect that lateral loadings, applied at points other than through the centroid of the I beam, have on the deformations of the structure.

4.2   Web Stiffeners

4.2.1 The Design of Web Stiffeners.

Web stiffeners are added to the webs of plate girders as an economic means of reducing the total cost of the I beams. The ɛ stiffeners are used to increase to the lateral stiffness of a light web plate, and therefore reduce possible cross sectional distortion (Fig. 4.1). Considerable investigation by previous workers has led to a satisfactory arrangement of stiffeners for plate girders, particularly when the plate girder deforms in the plane of the undeformed web. *

---

* The mathematical models summarizing these observations of the behaviour of stiffened plates are described by Timoshenko,

(Ref. 45) and Gaylord and Gaylord, (Ref. 46). The generally accepted criterion as to when stiffeners are needed for girders made from structural grade mild steel , is when the ratio of the depth of the I beam d to the web thickness t exceeds 60 (Ref. 28). For ratios greater than these values, vertical and horizontal stiffeners are used to limit cross sectional distortions. End or load bearing stiffeners are added to the plate bridge near points of concentrated load. These stiffeners are usually designed to resist most of the vertical loading.
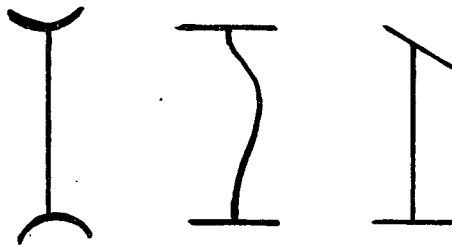
Fig. (4.1) Cross Sectional Deformations.

However, little knowledge exists about the behaviour of stiffeners when the I beam, and hence the stiffener, twists. To investigate the additional effects of twisted stiffeners, a model bridge with stiffeners was loaded and the deformations measured.

4.2.2 The Effect of Stiffeners on the Deformed Structure.

A model bridge, of dimensions similar to the first brass model, was built, and stiffeners designed according to rules recommended in (Ref. 28) were added. This model bridge was loaded, and a deformed shape was measured. The deformed shape was found to be very similar to the measured shape of the first brass bridge. The buckling load, as found from a Southwell Plot of rotations indicated a first buckling load of 290 lb., that is an increase of 20% on the corresponding load for the bridge without stiffeners.

A detailed description of the geometric deformations

of the bridge enabled the main deformations of the stiffeners

to be isolated. It was found that the stiffener size was

sufficient to restrain the distortion of the cross section

of the I beam, but was not sufficient to restrain the relative

warping of the top and bottom flanges. The stiffeners assumed

this warping deformation.

4.2.3 A Mathematical Description of the Effect of Stiffeners.

A close look at the action of warped stiffeners was

taken by breaking down the general problem to simpler specific

problems. One arrangement measured was the deformations of an

I beam with an end stiffener, with a pure twist applied.

Measurement of the surface shape of the stiffeners (Chapter one)

indicated that a reasonable approximation to the deformed

shape of the stiffener was a simple anticlastic surface,

(i.e. one with principal curvatures equal in magnitude, but

opposite in sign).

The forces needed to sustain the stiffener in the

shape of the anticlastic surface are a set of four balanced

forces (Fig. 1.14). A study of the effect of these four

balanced forces on the I beams (Chapter One) leads to

the first mathematical model. However, this model specifies

that all longitudinal lines remain straight. To improve

the mathematical model it is necessary to include some

bending of the flanges. The improved model is well known

and is given by Timoshenko in (Ref. 30) (and 47) but for

completeness the model is outlined again below, in a

manner consistent with the outlook of this thesis.

Measurement of the deformed shape of an I beam, with a heavy end stiffener , Fig. 4.2, indicated that the geometric deformations are separable into two distinct portions. These two geometric deformations may be summarized as follows:

(a)   each surface originally flat deforms into an anticlastic surface, (Fig. 4.3),

and (b)   each flange bends laterally. (Fig. 4.4), and the geometrical specification is the lateral deflection u is determined by the rotation of the web θ ,

and   u = $\frac{1}{2}$ (height of web) θ

$\quad\quad$ = $\frac{1}{2}$ h θ.

The forces necessary to sustain these two separate deformations are

(a)   A St. Venant torque, given by the equation

$$T_1 = C \ d\theta/dz, \quad\quad\quad (4.1)$$

where C is the torsional stiffness of the I beam.

and (b)   Bending moments in each flange, given by the equation

$$M = EI_T \ d^2u/dz^2 \ ,$$

where EI_T is the flexural rigidity of one flange,
d^2u/dz^2 is the lateral curvature of one flange,

The pair of bending moments M have no net statical action on the I beam section, but within the section are a distinct set of forces, called a Vlasov bimoment B, (Ref. 9). The bimoment is then determined by the product of these two moment couples by the distance between them, and

$$\begin{aligned} B &= M \ h \\ &= \tfrac{1}{2}EI_T \ h^2 \ d^2\theta/dz^2 \\ &= C_1 \ d^2\theta/dz^2 \end{aligned} \quad\quad\quad (4.2)$$

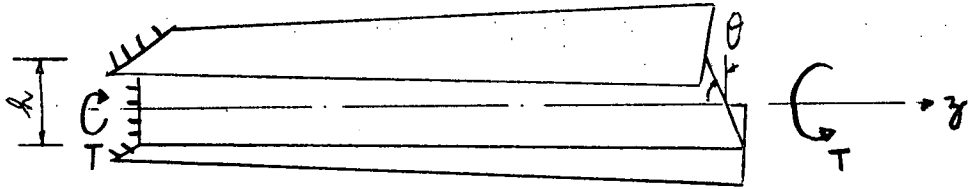The constant C_1 is called the warping stiffness of the I beam.

Fig. 4.2

I beam, with built in end, acted upon by an end torque
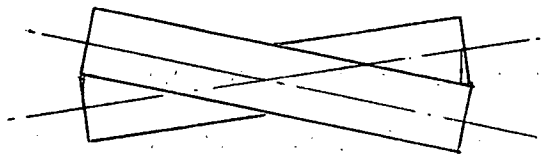

Fig. 4.3

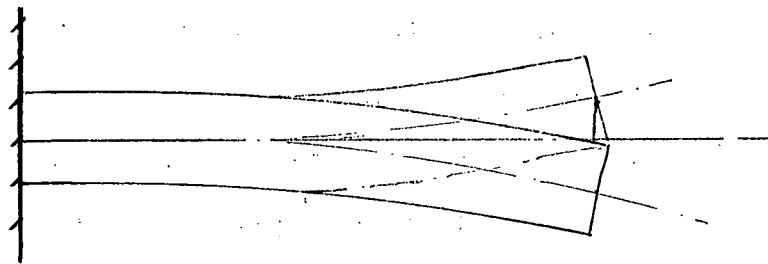I beam deforming into series of anticlastic surfaces

Fig. 4.4

Flanges bend laterally: plane sections remaining plane.

The bimoment is not the only force which must be applied to the cross section. As the curvature of the flanges is changing, shear strains and hence shear stresses must be applied to the flanges. To balance the corresponding shear forces V, which are opposite in direction on each flange, a torque T_2 must be applied, such that

$$T_2 = Vh \ .$$

(4.3)

The shear forces V are found from statical equilibrium of an element of the flange, and

$$
\begin{aligned}
T_2 &= (dM/dz)h \\
&= -(EI_T \ d^3u/dz^3)h \\
&= -\tfrac{1}{2}EI_T \ h^2 \ d^3\theta/dz^3 \\
&= -C_1 \ d^3\theta/dz^3 \\
&= -dB/dz \ .
\end{aligned}
$$

(4.4)

The total forces necessary to sustain the deformations (a) and (b) are therefore a torque T satisfying the equation

$$T = T_1 + T_2$$

(4.5)

$$= Cd\theta/dz - C_1 \ d^3\theta/dz^3 \ ,$$

and the bimoment B, given by the equation

$$B = C_1 \ d^2\theta/dz^2 \ .$$

4.2.4 Including Stiffeners in the Bridge Model.

The effect that the stiffeners have on the deformations of the through bridge can now be found. It has been shown in Chapter One that when the stiffener deforms into a simple anticlastic surface, the forces necessary to sustain this deformation can be found. To a first approximation stiffeners in the through bridge deform into anticlastic surfaces (Fig. 4.5), with principal curvatures equal in magnitude but opposite in sign, the twist of the stiffeners being given by the equation defining the warping of the I beam cross section, that is

$$\phi / \tfrac{1}{2} h = d\theta / dz \ .$$

The stiffener effects can then be mathematically described by altering the differential equation describing the through bridge (3.7). Between the stiffeners, the differential equation expressing the change of torque per unit distance along the bridge remains unaltered, that is in the region $z_i \leqslant z \leqslant z_{i+1}$ (see Fig. 4.5).

$$C_1 d^4\theta / dz^4 - C \, d^2\theta / dz^2 + C_o \theta - (P^2 / 4EI_\eta)(\tfrac{1}{2}\ell - z)^2 \theta = 0 \ , \qquad (4.6)$$

while in the region of the stiffeners a bimoment is applied to the bridge by the stiffeners. The differential equation of the bridge in the region of the stiffeners must be modified. The bimoment necessary to keep the stiffeners twisted is found by considering the twist of the stiffeners, $d\phi/d\ell \ (= d\theta/d_3)$ and the torsional stiffness of the stiffeners, GJ_{STIFF}, and is given by the equation

$$B = -GJ_{STIFF} \ h \ d\theta/dz$$

The extra torque applied to the I beam is therefore

$$T_3 = -dB/dz$$

$$= -GJ_{STIFF} \ h \ d^2\theta/dz^2 \ .$$

The change of this torque per unit distance along the bridge is included in the differential equation showing the change of torque per unit distance, in the region of the stiffeners and we obtain the equation

$$C_1 \, d^4\theta / dz^4 + GJ_{STIFF} \ h \ d^3\theta / dz^3 - C \, d^2\theta / dz^2 + C_o \theta \ -(P^2/4EI_\eta)(\tfrac{1}{2}\ell - z)^2 \theta = 0, \qquad (4.7)$$

$$(\text{for } z_i - dz \leqslant z_i \leqslant z_i + dz) \ .$$

The differential equations (4.6), (4.7) are difficult to solve exactly, and as before the method of weighted residuals is used to obtain an approximate solution.

Weighting the residual with rotation θ and integrating over the

total length of the bridge we obtain the equation

$$\int_{\frac{1}{2}\ell}^{o} c_1\, d^4\theta/dz^4\; \theta\, dz \;+\; \sum_{L=1,2\ldots} \int_{3_L - d_3}^{3_L + d_3} GJ_{STIFF}\, h\, d^3\theta/dz^3\; \theta\, dz \;-\; \int_{\frac{1}{2}\ell}^{o} c\, d^2\theta/dz^2\; \theta\, dz \;-\; P^2/4EI_\eta \int_{\frac{1}{2}\ell}^{o} (\tfrac{1}{2}\ell - 3)^2\theta^2/dz \;=\; 0 \tag{4.8}$$

For a continuous rotation, and first a continuous derivative of

rotation (consistent with the measured results) the equation (4.8)

can be reduced to the equation

$$\int_{\frac{1}{2}\ell}^{o} c_1(d^2\theta/dz^2)^2\, dz \;+\; \sum_{L=1,2} GJ_{STIFF}(d\theta/dz)^2 \;+\; \int_{\frac{1}{2}\ell}^{o} c\,(d\theta/dz)^2\, dz \;-\; P^2/4EI_\eta \int_{\frac{1}{2}\ell}^{o} (\tfrac{1}{2}\ell - 3)^2\theta\, dz = 0, \tag{4.9}$$

which is identical to the expression for the Rayleigh Ritz formulation;

the stiffener term being given by the equation

$$\sum_{L=1,2\ldots} \int_{\phi=o}^{\phi=\phi} T d\phi \;=\; \sum_{L=1,2\ldots} \int_{\phi=o}^{\phi=\phi} GJ_{STIFF}\; d\phi/dz\; d\phi$$

$$=\; \sum_{L=1,2\ldots} \tfrac{1}{2}\; GJ_{STIFF}\; (d\phi/dz)^2$$

$$=\; \sum_{L=1,2\ldots} \tfrac{1}{2}\; GJ_{STIFF}\; (d\theta/dz)^2 \qquad .$$

Thus the approximation for the stiffener action indicates

that the addition of stiffeners increases the St. Venant torsional

stiffness of the cross section. The St. Venant stiffness is

increased because the stiffeners deform (to resist the warping

of the cross section of the I beam) into a simple anticlastic surface

of similar shape to the warping of a rectangular section of the

same outside dimensions as the I beam *.

---

* Warping is the axial deviation from plane sections perpendicular

to a longitudinal axis. The warping deformations of twisted

rectangular bars are described approximately by a simple

anticlastic surface. The general topic of torsion is discussed
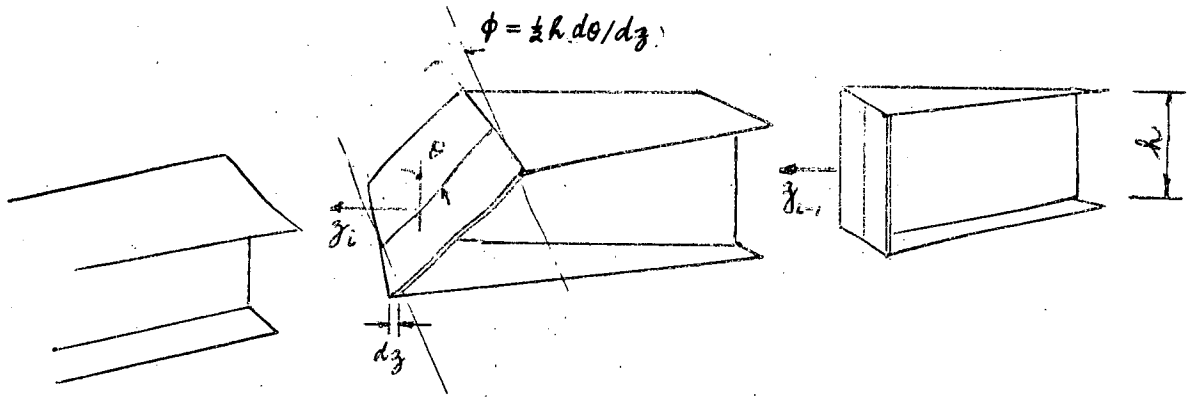
in Chapter Six.

Fig. 4.5. Twisted I Beam and Stiffener.

A guessed buckling mode, specified by a series of
continuous cosine waves indicates that the addition of the
stiffener terms in equation (4.9) increases the buckling
load of the model bridge structure from 245 lb. to
295 lb. (as measured by the modified Southwell Plot on
rotations outlined in Chapter Three). However, these
individual cosine waves have no sharp changes in second derivatives
at the points corresponding to the stiffener locations,
and therefore the convergence of the mode as found by the
method of weighted residuals to the first buckling mode
of the structure is not guaranteed. *

---

* The representation of a discontinuous structural arrangement
by a series of continuous curves is a difficult problem.
The problem is one of determining whether an expansion of
eigen functions (buckling modes) obtained from a continuous
problem is convergent to a shape which has a finite number
of discontinuities in its derivatives. Specific problems
are being considered in present literature (for example
Ref. 48), but much more detailed investigation needs to
be carried out before general statements can be made.

From observation of the warping of the cross section of the

deformed bridge (Fig. 4.6) it is seen that stiffeners placed near

the centre of the span contribute little to the torsional stiffness

of the I beams, while when placed near the ends, where larger

warping deformations are present, a larger increase in torsional

stiffness is obtained. However this increase in torsional

stiffness provided by the stiffeners is not great, and it is

usually not worthwhile to include the stiffener terms when

finding the buckling load of the bridge structure. If it is

felt that the buckling load should be increased significantly,

it is advisable to consider the economics of making portion

of, or the complete sides of, the bridge into a closed box

section, and thus make full use of the high torsional stiffness

of a closed section, [for example see Ref. 49 and subsequent

discussion.]
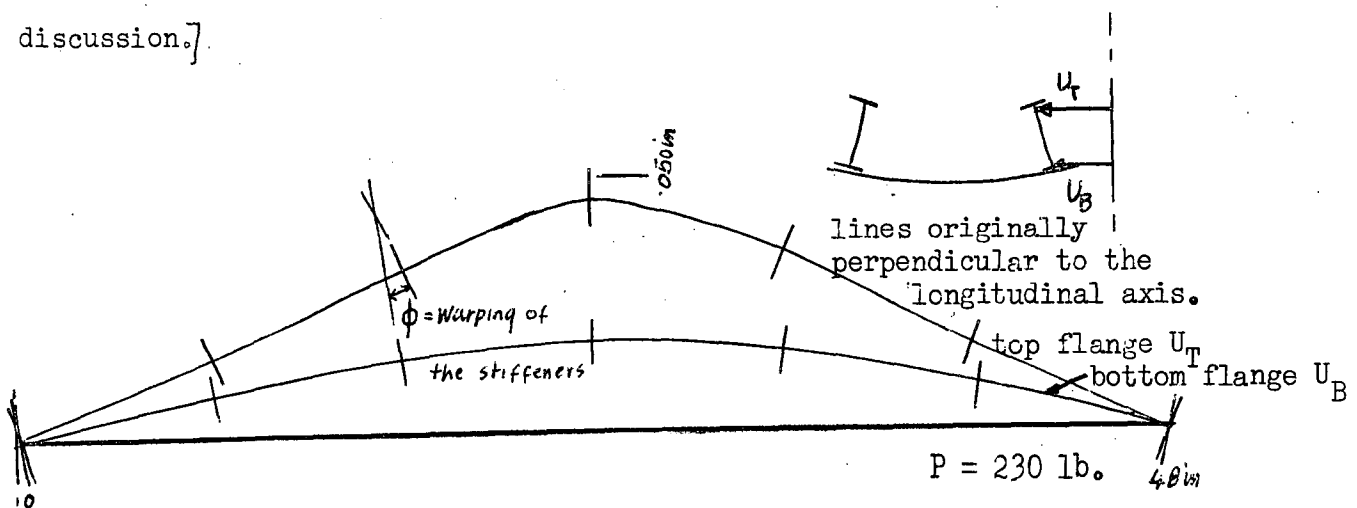
Fig. 4.6. Deformed Bridge showing Warping of the
Cross Section.

4.3 Lateral Loadings.

4.3.1. Introduction

When the model through bridge was loaded, it was noticed that

lateral loadings applied to the structure had an effect on the

rotation and lateral movements, the effect being large when the

bridge was already loaded with vertical loads. Thus, it appears

that the lateral and torsional stiffness of the bridge decreases

with applied vertical loading.

This phenomenon is similar to the behaviour of a laterally and axially loaded pin ended column. It is well known that the lateral stiffness of the column decreases rapidly as the axial load is increased. When the column is loaded by a uniform lateral force system the column deforms into a shape which contains a large component of the first buckling mode of the column. These deformations are then magnified by the instability effects of the axial load, especially when the axial load is close to the first buckling load. Thus, in the design of frame systems liable to instability, particular attention is placed on the effects of lateral loadings. As a result, designers usually limit the loads on the structure to those values for which the instability effects are small.

For some particular structures, however, it is possible that the lateral loadings on the structure do not decrease significantly the lateral stiffness of the structure.

Consider the approximations that are made in the design of through bridges. The questions arise: "Do the wind forces affect the lateral stiffness of the bridge?", or "Do the loadings applied on the floor system, away from the side members, affect the torsional stiffness of the bridge?" Little knowledge concerning these problems exists. The decrease in stiffness has previously been assumed small, as most experience has been with very heavy railway through bridges. However, this does not appear to be the case with light through bridges, with similar proportions to the model bridge outlined in Chapter Three.

In the following sections an original and powerful analysis is presented to describe the effects on through bridges of lateral and torsional loadings which remain constant in magnitude and direction as the bridge deforms. In this analysis, the initial crookedness of the bridge and the deformations induced by the applied loadings are described in terms of an infinite series expansion of the buckling modes. Keeping to the general method of attack used throughout this thesis, the simple problem of the analysis of a pin ended column, under the action of axial and lateral loads is considered first to introduce the necessary ideas, and these ideas are then extended to describe the behaviour of other structures.

4.3.2 . The Effect of Lateral Loadings on an Axially Loaded Column.

Consider the behaviour of an Euler strut of length carrying an axial load P, and having flexural rigidity EI. The inter relationship between the load deformation relations, the equations of statical equilibrium, and the geometrical compatibility of deformations can then be expressed by the differential equation

$$EI \ d^2y/dx^2 \ + \ Py = 0 \ .$$
(4.10)

For this differential equation, together with the boundary conditions $x = 0$ and ℓ, $y = 0$, there exists an infinity of eigen functions (buckling modes)y_n , which are solutions of (4.10). Fortunately in this case the y_n are known precisely, and may be written as

$$y_n \ = a_n \ \sin n\pi x/\ell .$$

The corresponding eigen values λ_n are given by

$$\lambda_n \ = \ P/EI \ = \ n^2\pi^2/\ell^2.$$
(4.11)

The effect of a lateral force is included in the mathematical model in a manner similar to that which was used to handle the initial crookedness, as outlined in Section 2.4.3. The well known lateral model for an initially crooked column (for example (Ref. 50)), acted upon by a uniform load w becomes

$$EI\ d^2(y - y_o)/dx^2 + Py = \tfrac{1}{2}wx(\ell - x) \qquad . \qquad (4.12)$$

The shape of the bending moment induced by this load is then expressed as an infinite series expansion, in terms of the buckling mode solutions. The values of c_n in this expansion, are defined such that

$$c_1 y_1 + c_2 y_2 + c_3 y_3 + \ldots c_n y_n + \ldots = \tfrac{1}{2} wx(\ell - x) \ . \qquad (4.13)$$

The value of the constant c_n is obtained by multiplying both sides by the orthogonalizing function for the differential equation, in this case $\sin(n\pi x/\ell)$, and integrating between the boundaries, i.e.

$$\int_0^\ell c_m\ y_m\ y_n\ dx = \int_0^\ell \tfrac{1}{2}\ wx(\ell - x)\ y_n dx \ . \qquad (4.14)$$

The orthogonalizing function is used because the infinite series expansion $\displaystyle\sum_{m=1}^{\infty} \int_0^\ell y_m\ y_n\ c_m\ dx$ can be simplified, and the term c_m found, using the definition of the orthogonal function, i.e.

$$\int_0^\ell y_m\ y_n\ dx = 0 \qquad\qquad \text{for m not equal to n.}$$

Then, the value of the constant c_n is given uniquely by the equation

$$c_n = \int_0^\ell \tfrac{1}{2}\ wx(\ell - x)\ y_n\ dx \Big/ \int_0^\ell y_n^2\ dx \qquad .$$

The mathematical behaviour of a pin ended column, allowing for both initial crookedness and lateral loading, is obtained by expressing the final shape y as the infinite series expansion

$$y = b_1 y_1 + b_2 y_2 + b_3 y_3 + \ldots$$

The value of b_n is obtained by substitution of the expansions for y and y_o , and lateral loading into the equation (4.12) and b_n is obtained as the ratio

$$b_n = [a_n + c_n/(EI\pi^2/\ell^2)] /[1-(P/P_n)] \quad .$$

Using these values of b_n in the expansion for the final shape, y becomes

$$y= [a_1+ c_1/P_1]/[1- P/P_1] \sin\pi x/\ell + [a_2+c_2/P_2]/[1-P/P_2]\sin 2\pi x/\ell+.. \quad (4.15)$$

and near the first eigen value of the mathematical model, i.e. for P close to P_1 , the final shape, y, is closely represented by the first term in this expression, that is

$$y = [a_1 + c_1/P_1]/[1-P/P_1] \sin \pi x/\ell \quad . \qquad (4.16)$$

Thus, in this well known model, the lateral load is replaced by an equivalent first mode initial crookedness, equal to the crookedness induced by the lateral loading before the axial load is applied. The model is reasonably accurate,especially when the loading produces deformations which contain a large component of the first buckling mode.

For example, the deflections and moments for a uniform loading are calculated using only the first term of the infinite series are compared, in Table 4.1, with the solution of the beam column equation given by Timoshenko (Ref. 30). It is seen that a good estimate of the effect of the lateral load is obtained. It can also be seen from this example of the pin ended column, that as the first buckling mode is very similar to the deflections induced by the lateral loading, the lateral stiffness of the column decreases with increasing axial loads by the factor $(1 - P/P_1)$.

Axial Load	Deflections			Moments
	First term in infinite series	Exact solution of (4)	difference	difference
0	$0.01302w\,\ell^4/EI$	$0.01307w\,\ell^4/EI$	0.4%	3%
0.9P	$0.1307w\,\ell^4/EI$	$0.1307w\,\ell^4/EI$	–	1%

Table 4.1. Comparisons between Mathematical Models.

The ideas outlined in the preceding analysis are now extended by the author to develop mathematical models describing the behaviour of real through bridge structures. An equivalent initial crookedness is found, and a design method is developed to allow for the effects of lateral loadings and initial crookedness.

4.3.3 The effect of lateral loadings on an I beam liable to lateral and torsional instability.

A reasonable model for the behaviour of a light through bridge when it deforms according to Fig. 4.7 is given in section 3.5. Then, when the load is applied vertically through the centroid of each I section, a good model for deformed shape of the initially straight structure in the region $\frac{1}{2}\ell \leq z \leq 0$ is given by the system of equations

$$EI_\eta\, d^2u/dz^2 - \tfrac{1}{2}P(\tfrac{1}{2}\ell - z)\theta = 0$$

$$\int_0^3 -C_o\theta\, d\gamma - C_1 d^3\theta/dz^3 + C\, d\theta/dz + \tfrac{1}{2}P(\tfrac{1}{2}\ell - z)\, du/dz - \tfrac{1}{2}P(u_1 - u) = 0. \quad (4.17)$$

Fig. 4.7. Through bridge deformations, when the light bottomchord provides restraint against rotation but not translation.

When these two equations are combined into a single differential equation, the inter relationship between the load deformation relations, statical equilibrium and geometrical compatibility for the region $\frac{1}{2}\ell < z < 0$, becomes

$$C_1 d^4\theta/dz^4 - C d^2\theta/dz^2 + C_o\theta - (P^2/4EI_\eta)(\tfrac{1}{2}\ell-z)^2\theta = 0 . \tag{4.18}$$

This differential equation, together with the boundary conditions

$$z = -\tfrac{1}{2}\ell \text{ and } \tfrac{1}{2}\ell \; ; \; \theta = 0 \quad , \quad C_1 d^2\theta/dz^2 = 0 \tag{4.19}$$

has been shown in Section 3.6 to be self adjoint and positive definite, and thus there exist an infinity of buckling mode solutions θ_n and buckling load values P_n^2. It was also shown in section 3.6 that any shape provided it satisfies the boundary conditions (4.19),can be expressed in terms of these eigen functions.

The effect on the mathematical model (4.17) of an applied lateral moment M_L which does not change as the structure deforms, is to alter the first equation in (4.17) to the equation

$$\tag{4.20}$$
$$EI_\eta \, d^2u/dz^2 - \tfrac{1}{2}P(\tfrac{1}{2}\ell-z)\theta = M_L \quad .$$

When the moment arises from the action of a central lateral load F and the boundary conditions (4.19) remain unaltered, then the moment is given by the equations

$$M_L = \tfrac{1}{2}F(\tfrac{1}{2}\ell-z) \qquad \text{for} \quad \tfrac{1}{2}\ell \leqslant z \leqslant 0$$

and

$$M_L = \tfrac{1}{2}F(\tfrac{1}{2}\ell+z) \qquad \text{for} \quad 0 \leqslant z \leqslant -\tfrac{1}{2}\ell.$$

Thus, for the central point load equation (4.18) in the region $\frac{1}{2}\ell < z < 0$ becomes

$$C_1 d^4\theta/dz^4 - C d^2\theta/dz^2 + C_o\theta - (P^2/4EI_\eta)(\tfrac{1}{2}\ell-z)^2\theta = (FP/4EI_\eta)(\tfrac{1}{2}\ell-z)^2 . \tag{4.21}$$

in which the right hand side of the equation (4.19) shows the effect of the lateral load. The right hand side of the equation (4.21) is a function of z alone, and this function (Fig. 4.8) can be represented

by the infinite series of eigen function solutions of (4.18).

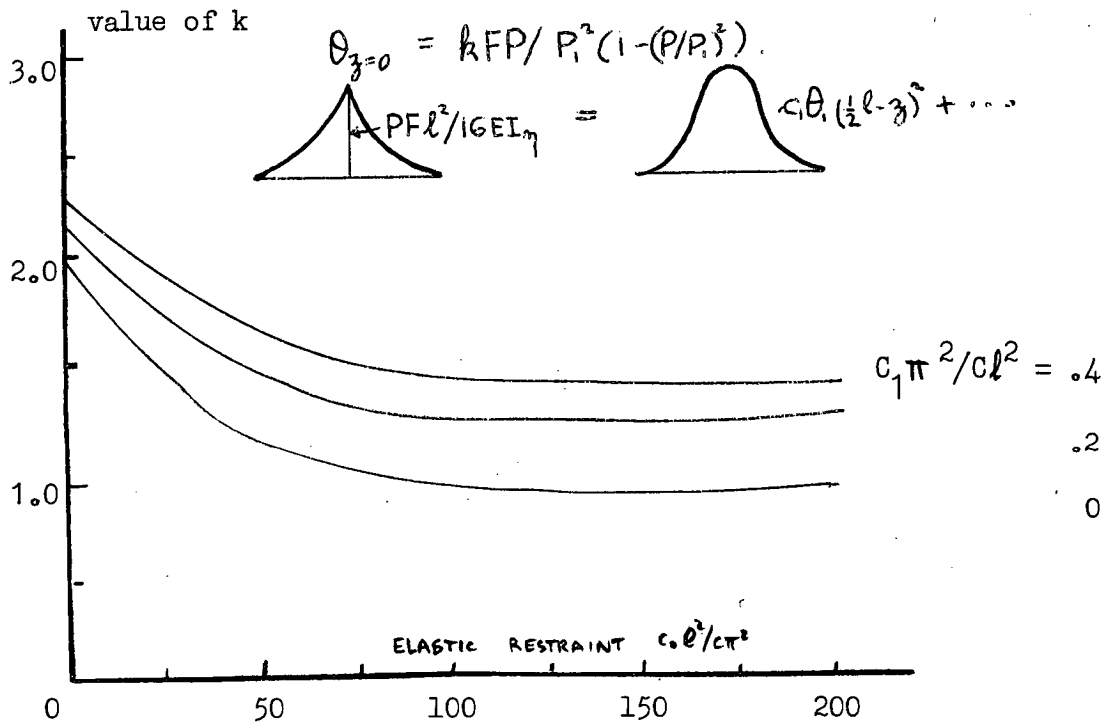The constants c_n are defined in the region $\frac{1}{2}\ell < z < 0$

$$\theta_{z=0} = kFP/P_1^2(1-(P/P_1)^2).$$

$$-PF\ell^2/16EI_\eta = c_1\theta_1(\tfrac{1}{2}\ell-z)^2 + \cdots$$

ELASTIC RESTRAINT $c_0\ell^2/c\pi^2$

$c_1\pi^2/c\ell^2 = .4$

.2

0

Fig. 4.8. Values of k for lateral loadings as
given by equation 4.23.

by the series *

$$c_1\theta_1(\tfrac{1}{2}\ell-z)^2 \;+\; c_3\theta_3(\tfrac{1}{2}\ell-z)^2 + \cdots = (FP/4EI_\eta)(\tfrac{1}{2}\ell-z)^2 \;, \qquad (4.22)$$

and are found by mutliplying both sides of the expansion

by θ_m , using the orthogonalizing function (see section

2.7.2), and integrating between the boundaries. This gives

c_n uniquely, in the form

$$c_n = \int_{\frac{1}{2}\ell}^{0} \theta_n(FP/4EI_\eta)(\tfrac{1}{2}\ell-z)^2 dz \Big/ \int_{\frac{1}{2}\ell}^{0} \theta_n^2 (\tfrac{1}{2}\ell-z)^2 \, dz$$

* The series (4.22) has been chosen with a weighting function

$(\tfrac{1}{2}\ell-z)^2$ on the left hand side in order that the constants c_n and

the final shape are obtained in terms of buckling mode components

only. The weighting function is dependant on the differential

equation. To the author's knowledge the use of a weighting

function in this context has not been successfully tried

previously in structural engineering.

when the orthogonality properties are used, that is

$$\int_{\frac{1}{2}\ell}^{0} (\tfrac{1}{2}\ell - \mathfrak{z})^2 \; C_n \, \theta_n \, \theta_m \, dz = 0 \text{ for m not equal to n.}$$

The final shape, θ given by

$$\theta = d_1 \theta_1 + d_2 \theta_2 + d_3 \theta_3 + \cdots$$

can be found by substitution of this expansion into equation (4.21).
The constants d_n can then be expressed as the ratio

$$d_n = c_n \; (4EI_1)/P_1^2 \; [1-(P/P_1)^2] \quad .$$

Near the first critical loads, $d_1 \theta_1$ dominates and the maximum value of
$d_1 \theta_1$ occurs at $z = 0$. Under these conditions the value $d_1 \theta_1$ is given
by the equation

$$\begin{aligned} d_1 \, \theta_1 &= k \; FP/P_1^2[1-(P/P_1)^2] \\ &= d_{10}/[1-(P/P_1)^2] \quad , \end{aligned} \tag{4.23}$$

where k is a variable depending on the form of the lateral load, and
the values of C_1, C, C_o, and ℓ. Values of k are plotted in Fig.
4.8. The effect of a uniformly distributed load is less than that of
the point load, as the main bending and hence main rotational action
occurs near the centre of the beam but a reasonable estimate for the
rotation is obtained by replacing the lateral load by a central point
load equal to two thirds of the value of the total lateral load. The
overall form of the behaviour is evident in Fig. 4.8. For low values
of the elastic floor stiffness, $C_o \ell^2 /C_1$ lateral loadings have a
relatively large effect, but as the restraint is increased the relative
effect becomes smaller, but not negligible. Thus, in this type of
structure the effects of lateral loadings should be considered in the
design of the structure.

4.3.4 The Effect of Torsional Loadings on an I beam

Liable to Lateral and Torsional Instability.

When the bridge is loaded at points other than through the centroid of the I beam, torsional loadings are imposed. For example, when the load is applied to the floor beam system, the sides of the bridge would rotate, and the centroid of the I beams would move both laterally and vertically even if the bridge was initially straight. The effects of a torsional loading T_z applied along the bridge are included in this section.

The effect of the differential equation (4.17) of a torsional loading T_z is to alter the second equation giving the conditions of torsional loadings for the bridge to be in equilibrium, and

$$EI_\eta d^2u/dz^2 - \tfrac{1}{2}P(\tfrac{1}{2}\ell-z)\theta = 0$$

$$\int_0^{\frac{1}{2}\ell} C\theta dz + Cd\theta/dz - C_1 d^3\theta/dz^3 + \tfrac{1}{2}P(\tfrac{1}{2}\ell-z)du/dz - \tfrac{1}{2}P(u_1-u) = Tz.$$

(4.24)

Using these modified equations, equation (4.19) is altered to the single differential equation

$$C_1 d^4\theta/dz^4 - Cd^2\theta/dz^2 + C\theta - (P^2/4EI_\eta)(\tfrac{1}{2}\ell-z)^2\theta = dT_z/dz .$$

(4.25)

The form of the applied torsional loadings T_z is given by examining the statical equilibrium of an element of the bottom chord, as in Fig. 4.9. The differential equation showing these effects, for a point load applied on the chord, is

$$EI_F d^2y/dx^2 = M\alpha - \tfrac{1}{2} Px\alpha$$

where EI_F is the rigidity in the vertical plane of a bottom chord, and p is the line load per unit distance. Integration of this expression gives the equation

$$EI_F dy/dx = Mx\alpha - \tfrac{1}{2} px^2\alpha + A$$

and fitting the boundary conditions

$$dy/dx = 0 \quad \text{at } x = \tfrac{1}{2}s$$

gives the equation

$$EI_F \, dy/dx = M(x - \tfrac{1}{2}s)a - p(x^2/4 - s^2/16)a \quad .$$

Denoting the slope at the point A by Θ_A , the end moment slope relationship per unit distance along the bridge is then given by the equation

$$M = 2EI_F \, \theta /sa - ps/8 \qquad\qquad (4.26)$$

$$= C_o \theta - ps/8 \qquad .$$

When the loading is applied uniformly in a single vertical line, along the centre of the bridge deck, as in Fig. 4.9 the change in torque per unit length, dTz/dz is obtained from the equation

$$dT/dz = ps/8 \qquad .$$

For the bridge loaded with a single vertical load in the centre of the deck we have the system of equations

$$dT_z/dz = 0$$

and

$$\text{for } \tfrac{1}{2}l < z < dz \; ,$$
$$dT_z/dz = \tfrac{1}{2}P(s/8)/dz$$

$$\text{for } dz < z < 0 \qquad ;$$

and for the bridge loaded uniformly with a load w per unit area over the bridge deck the change in torque per unit length is given by the equation
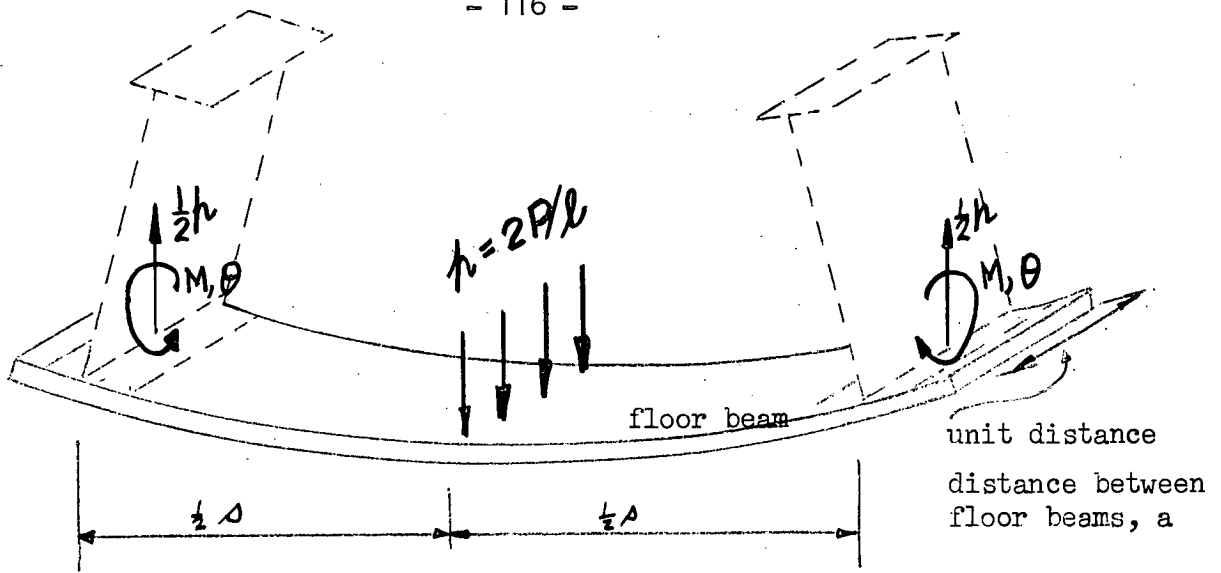
$$dT_z/dz = (ws)\,(s/8) \quad .$$

Fig. 4.9. An element of the bottom chord of the bridge shown in Fig. 4.7, loaded along the centreline

The effect of these torsional loadings is seen by expressing the change in torque per unit length as the infinite series expansion

$$e_1 \theta_1 (\tfrac{1}{2}\ell - z)^2 + e_3 \theta_3 (\tfrac{1}{2}\ell - z)^2 + \ldots = dT_z/dz \, , \qquad (4.27)$$

and solving for the constant e_n by substitution of the expansions into equation (4.25). The value of e_n is thus given by the ratio

$$e_n = \int_{\frac{1}{2}\ell}^{0} (dT_z/dz) \, \theta_n \, dz \Big/ \int_{\frac{1}{2}\ell}^{0} \theta_n^2 \, (\tfrac{1}{2}\ell - z)^2 \, dz \, . \qquad (4.28)$$

The final shape θ , given by the series

$$\theta = f_1 \theta_1 + f_2 \theta_2 + \ldots$$

can be found by proceeding in a similar manner to that outlined above and the value of the first mode component $f_1 \theta_1$ at z = 0 is given, for a central line load, by the ratio

$$f_1 \theta_{1(z=0)} = k(P/\ell)(s/8) \, (4EI)/[(P_1 \ell)^2 (1 - (P/P_1)^2)]$$

$$= f_{10}/[1 - (P/P_1)^2] \, . \qquad (4.29)$$

Values of k are plotted in Fig. 4.10 for a central line load, for a uniform load, and for a

central point load. The central point load is the dominant

case, as can be seen from Fig. 4.10 and loadings of this type

are likely to cause a much earlier first yield of the structure

than other forms of loading. It is also clear from Fig. 4.10

that the torsional loading effect should be considered in the
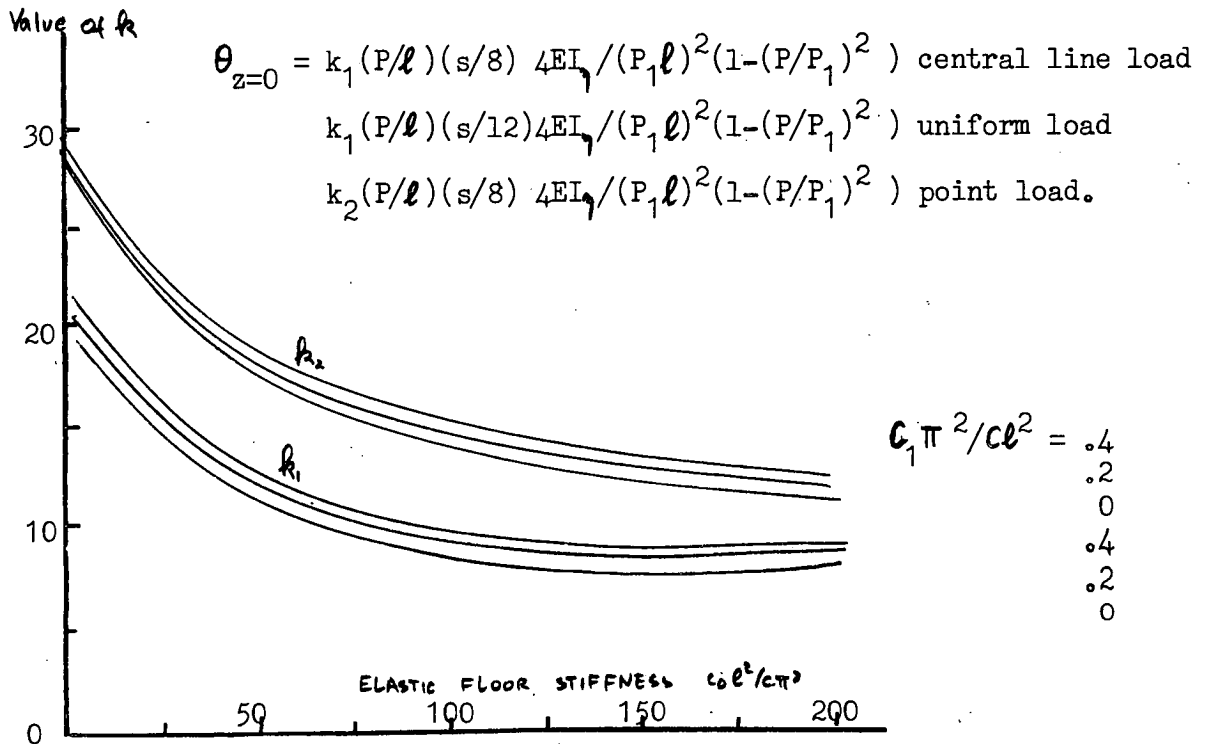
design of this type of structure.

$$\theta_{z=0} = k_1(P/\ell)(s/8) \; 4EI_1/(P_1\ell)^2(1-(P/P_1)^2) \text{ central line load}$$
$$k_1(P/\ell)(s/12)4EI_1/(P_1\ell)^2(1-(P/P_1)^2) \text{ uniform load}$$
$$k_2(P/\ell)(s/8) \; 4EI_1/(P_1\ell)^2(1-(P/P_1)^2) \text{ point load.}$$

$$C_1\pi^2/c\ell^2 = \; .4$$
$$.2$$
$$0$$
$$.4$$
$$.2$$
$$0$$

Fig. 4.10. Values of for Torsional Loadings as
given by equation 4.29.

4.3.5. A Method to add the Effects of Initial Crookedness,
Lateral loadings, and Torsional Loadings.

A solution for a combination of the effects of initial

crookedness, lateral loading and torsional loading is achieved

by incorporating all effects into one differential equation, and

solving this mathematical model in a manner similar to that

used in previous cases. The approximate final shape θ can then

be expressed in terms of the first buckling mode components,

the initial crookedness, and the lateral loads, in the form

$$\theta = [a_1 + d_{10} + f_{10}]\theta_1/[1-(P/P_1)^2]. \tag{4.30}$$

where $a_1\theta_1$ is the initial crookedness in the first mode, $d_{10}\theta_1$ is the equivalent first mode initial crookedness sustained by the lateral load, and $f_{10}\theta_1$ is the equivalent first mode initial crookedness sustained by the torsional load.

The equation (4.30) can be used in design provided it is realized that the expressions for the lateral and torsional loadings are only approximate. In cases where the axial load is zero, the predicted deformations obtained by using one term of the infinite series are likely to differ from the exact solution of the mathematical model. However, as the axial load is increased, the differences between the two solutions become smaller. Thus, the equation (4.30) is a reasonable representation of the solution of the mathematical model (4.17) with initial crookedness, lateral loadings and torsional loadings which remain constant as the structure deforms. Provided the equivalent initial crookedness resulting from the lateral and torsional loadings is small and does not introduce changes in the geometrical terms of equations (4.17), the mathematical model is a good representation of the behaviour of light through bridges.

The foregoing method is used in Chapter Five in the design of through bridges which have light bottom floors. It is shown there that when initial crookedness and torsional loading effects (described in terms of an infinite series of buckling modes) are compared with measurements taken on a real bridge structure, reasonable agreement is obtained.

CHAPTER FIVE

THE DESIGN OF THROUGH BRIDGES.

5.1   Introduction

In this chapter the design of through bridges is discussed. The use of through bridges and present methods of design are investigated first and compared with the measurements outlined in Chapter Three. Large differences between the existing mathematical models used to design through bridges and the measured results are shown to exist, and, as a result, further model tests are carried out to obtain a good appreciation of these differences. Using the ideas outlined in the previous chapters a new mathematical model to describe the behaviour of light through bridges is proposed, and an existing bridge is analyzed by this method. This analysis is then compared with measurements taken by loading the full size bridge.

5.2   The Use of Through Bridges

Through bridges are often used when headroom is an important consideration. This consideration has resulted in the use of through bridges as railway overpasses; present design experience, as tabled in various codes, is largely concerned with structures of this type.

More recently, the through bridge has been used as a pedestrian overpass. The sides of the bridge, usually of truss construction, are used as the hand rail, and the light floor beams are used to connect the trusses.

The advent of roll on roll off cargo ships has resulted in the use of the through bridge as a

connection between ship and shore. This connecting bridge is often longer, wider and of lighter floor beam construction than the railway bridge.

5.3   Current Methods of Design

Most through bridges are designed using ideas summarised by the British Standard 153 (1958) "Steel Birder Bridges" (Ref. 51). These ideas, in turn, are based on the Timoshenko Model, presented in "Theory of Elastic Stability", (Ref. 30). The top flange of each of the I beams is isolated and regarded as an axially loaded column with lateral restraints provided by the web and floor beams. This Timoshenko model will now be outlined for completeness.

Consider the bridge as shown in Fig. 5.1, and assume a deformed shape as shown in Fig. 5.2. The top flange has deformed laterally and the I beams have distorted in the plane of the cross section. The bottom flanges have been completely restrained in the lateral direction.

These estimates of the deformations are used to establish a mathematical model. The buckling load can be found for the top flange as though it were an Euler pin ended strut. The top flange is similar to a column loaded with a changing axial load and restrained elastically in the lateral direction. The buckling load of the top flange system is used to determine a limiting stress in this flange. The axial load P_T that needs to be applied to the initially straight flange, to sustain the buckling mode, is expressed in a form similar to the Euler buckling load; an effective length L is used to allow for the effects of changing axial loads along the bridge and to allow for the effects of the lateral restraints. This load is then given by the equation
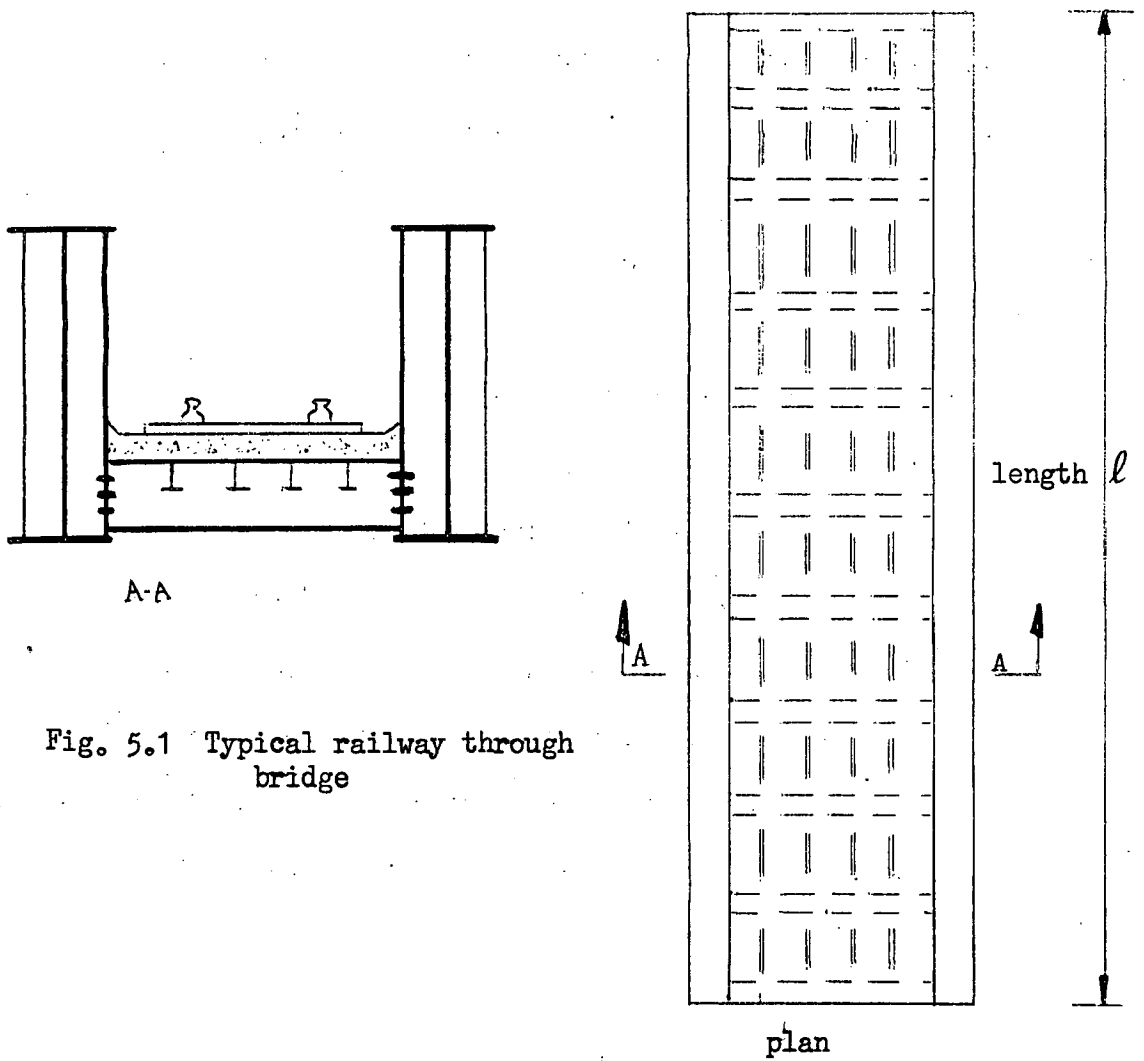
$$P_T = \pi^2 EI / L^2.$$
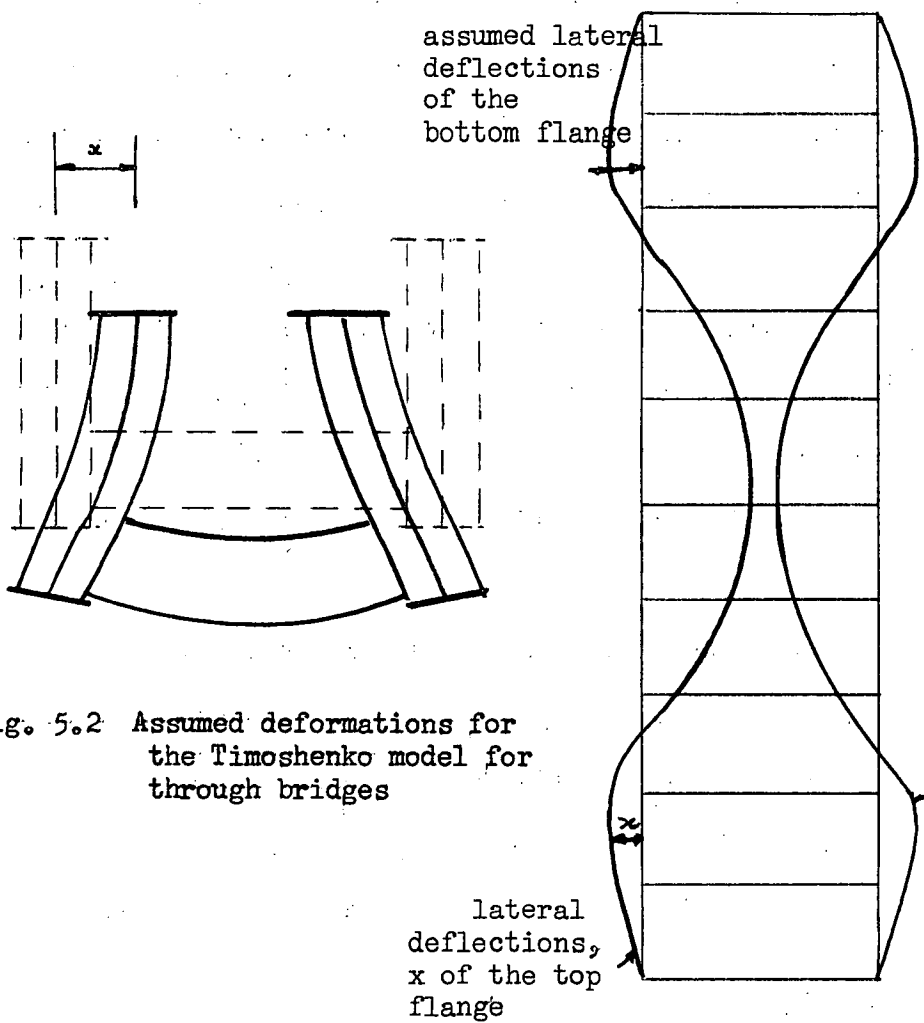
Fig. 5.1 Typical railway through
bridge

plan

length ℓ

assumed lateral
deflections
of the
bottom flange

x

Fig. 5.2 Assumed deformations for
the Timoshenko model for
through bridges

lateral
deflections,
x of the top
flange

When the top flange is considered to be laterally supported by the floor system and web stiffener arrangement, the effective length, as found by British Standard 153, (Ref. 51) is given by the formulae

$$L = 2.5 \sqrt[4]{EI_T \, a \, \delta} \quad , \qquad (5.1)$$

where EI_T = lateral stiffness of the top flange

      a = distance between frames

and δ = the virtual lateral displacement of the compression flange at the frame nearest mid-span of the girder, taken as the horizontal deflection of the stiffener at the point of its intersection with the centroid of the compression flange, under the action of unit horizontal force applied at this point to the frame only.

As an example, consider the through plate girder bridge at the ferry terminal at Devonport, Tasmania, shown in Fig.5.3.

The effective length for the ferry-terminal bridge as shown in Fig. 5.3, calculated from the above formulae, is 250 inches, which is approximately $\frac{1}{4}$ of the length of the bridge and the effective length divided by radius of gyration, L/r. is 54. For a L/r ratio of 54, B.S. 153 recommends a working stress of 16,400 psi for structural grade mild steel.

Comparing this stress with the buckling load of the flange, P_T found from the modified Euler condition $P_T = \pi^2 EI/L^2$, we find that the load corresponding to a working stress of 16,400 psi is 1/6.4 of the buckling load. Thus instability effects for the corresponding buckling deformation are small.

The buckling mode can be either a symmetric lateral deformation of the top flange about the midspan or an anti-symmetric deformation, as the corresponding buckling loads are very close. It can be seen from Fig. 5.2, where the symmetric buckling mode is shown for the particular ferry terminal bridge, that one quarter of the length,
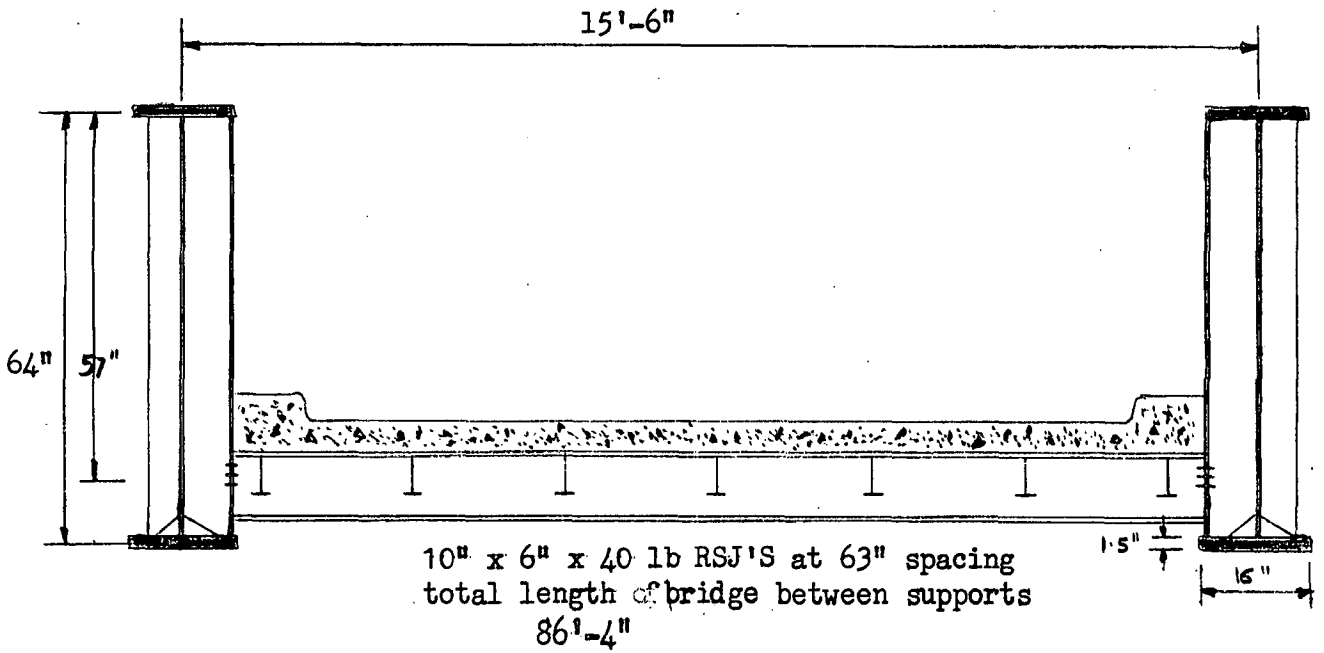
Fig. 5.3   Cross section of the ferry terminal bridge at Devonport,
Tasmania

15'-6"

64"   57"

10" x 6" x 40 lb RSJ'S at 63" spacing
total length of bridge between supports
86'-4"

1.5"

16"

Timoshenko solution

$L = 2 \sqrt[4]{EI\, a\, \delta}$

$L = 2.5 \sqrt[4]{EI\, a\, \delta}$
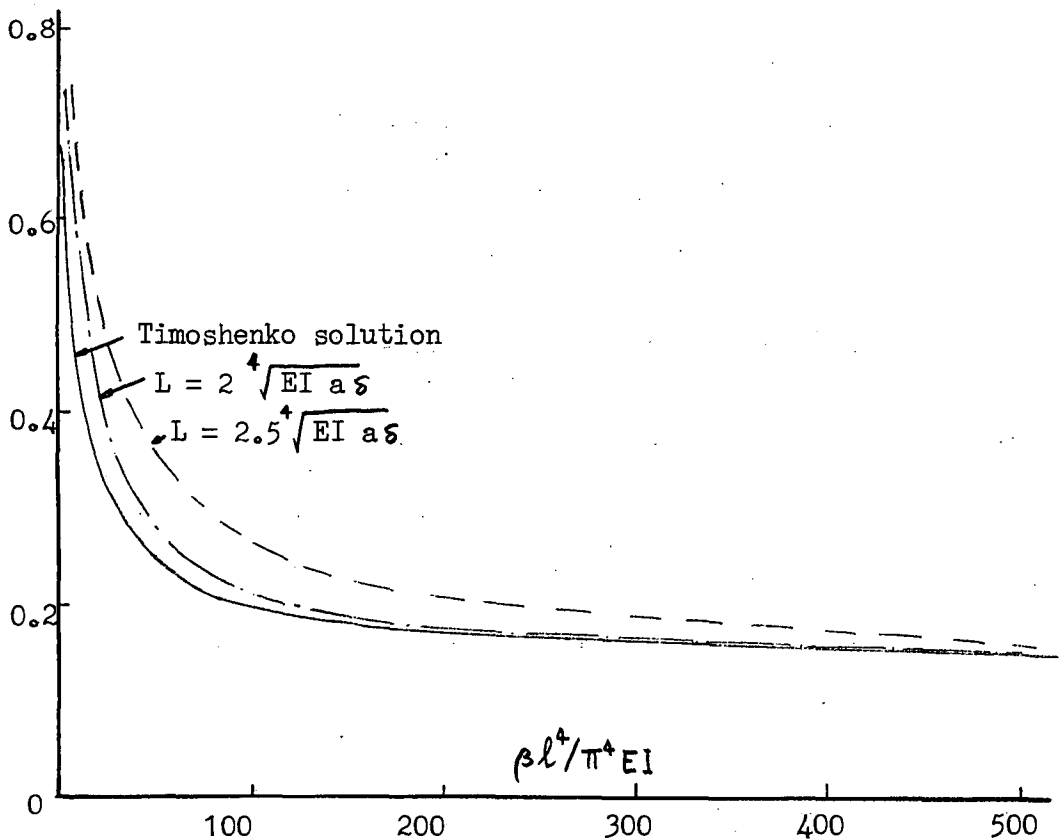
$\beta \ell^4 / \pi^4 EI$

Fig. 5.4   Solutions to Timoshenko model for the lateral stability
of an axially loaded column with elastic lateral restraints

that is L = $\ell/4$, does not represent the distance between points of contraflexure. The lack of correspondence between the effective length and the distance between points of contraflexure in the buckling mode occurs because the buckling mode for the restrained system is not the sinusoidal function buckling mode of the pin ended strut.

A comparison is now made between other codes of practice, the Timoshenko model in "Theory of Elastic Stability" and the British Standard 153. The B.S. 153 expression for the effective length, equation (5.1) can be modified to

$$\beta \ell^4/\pi^4 EI_T = 2.5(\ell/L)^4 \tag{5.2}$$

where $\beta = a/\delta$

In Fig. 5.4, equation (5.1) is plotted against the Timoshenko solution and it is seen that the equation (5.1) given in B.S. 153 is an overestimate of the effective length, for low values of β. A closer estimate, especially for low values of β, is also shown in Fig. 5.4, and this expression is

$$\beta \ell^4/\pi^4 EI_T = 2.0(\ell/L)^4 . \tag{5.3}$$

When equation (5.3) is used to find the buckling load for the ferry terminal bridge of Fig. 5.3, it is found that the ratio of working load, as recommended by B.S. 153, to buckling load is 1/9.2.

The recommendations of the Column Research Council (C.R.C.)(Ref. 52) are based on Engesser's formulation of the problem (Ref. 29). For a perfectly straight system the buckling load is increased by the addition of U frames of a stiffness sufficient to induce a required buckling mode. The stiffness of the U frames required, C_{req}, is given by the equation

$$C_{req} = 1.46 P_a/a , \tag{5.4}$$

where P_a is the Euler pin ended column buckling load of a strut of length equal to the distance a between U frames. The buckling mode
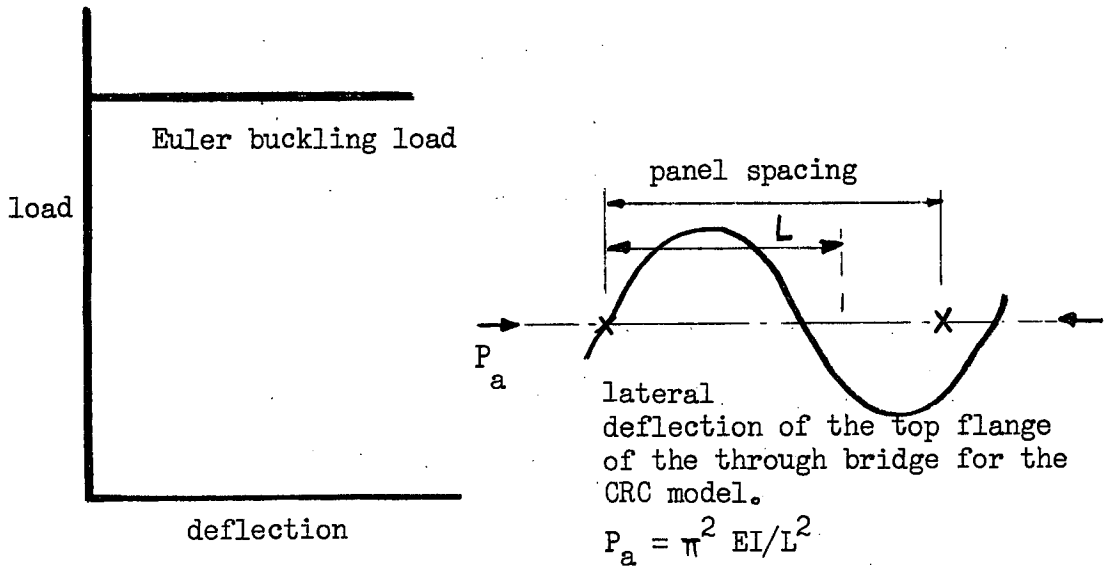
Fig. 5.5a Behaviour of the initially straight bridge.
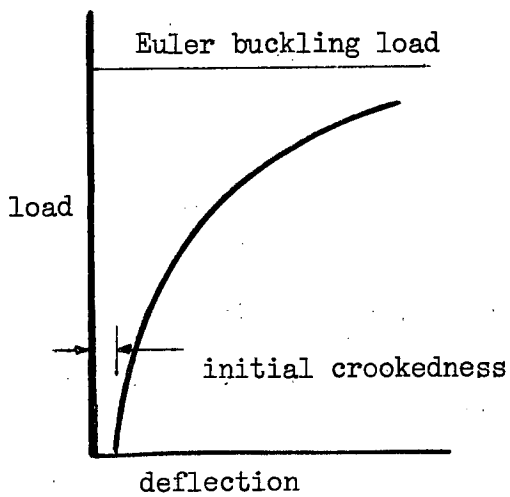

Fig. 5.5b Behaviour of the model for the initially crooked bridge.

and plot of deflection against load are shown in Fig. 5.5. Approximately
similar expressions are given for the equivalent German Code (Ref. 53),
and the required stiffness is

$$C_{req} = 2.50 \ P_a/K_m^2 \ a \ , \tag{5.5}$$

where K_m is a ratio of the effective length to panel length and is
such that

$$1.3 \leqslant K_m \leqslant 3.0 \ . \tag{5.6}$$

Neither the C.R.C. nor the German Code is helpful in the
analysis of the ferry-terminal bridge of Fig. 5.3, as the stiffness
of the U frames (i.e. the stiffeners) is insufficient to enforce
the type of mode implied by the two Codes.

The British Standard 153, C.R.C. Code, and German Code
formulae (5.1), (5.4), and (5.5) are all estimates of the U-frame-
stiffness required to obtain a buckling load and corresponding
buckling mode for an initially straight frame. For the initially
straight frame loaded to less than the buckling load, no deformations
occur (Fig. 5.5a). However when the initially crooked frame is
loaded, the frame deforms under the action of all loads (Fig. 5.5b).
These deformations result in resisting forces in the flanges and
in the web and floor beams.

The British Standard 153 gives an estimate of the lateral
force developed at the junction of the deformed top flange and the
deformed U frames. This lateral force F is given by the equation

$$F = 1.4 \times 10^{-3} \ L/[\ (C_E/fac - 1.7) \ ] \ , \tag{5.7}$$

where C_E = Euler buckling stress for the member
and f_{ac} = calculated working stress in the chord,
and the force is taken as acting in a horizontal direction at the top
of the U frame.

An insight into this formula is obtained by examining the
expression (5.7), by choosing a bridge which has an effective length
equal to the panel length. Expression (5.7) can be rearranged into

the form

$$F = (\ell/2500)(1.7 \text{ fac}/C_E) \Big/ (1/40 - 5/384)(L^3/EI_T)(1 - 1.7 \text{fac}/C_E) , \qquad (5.8)$$

and in this form it can be seen that the design lateral force is obtained

by allowing for the following conditions

(1) an initial crookedness of a half sine wave with a

maximum amplitude of $\ell/2500$, between each panel

point,

(2) an applied load of 1.7 times the working load,

(3) the web resisting the deformations, and the

lateral shear on web being resisted by the U frames.

When the effective length is equal to the panel length,

an alternative simplification for equation (5.7) is

$$F = 5.6 \times 10^{-3} (\pi^2 EI_T/L^2) \Big/ (C_E/f_{ac} - 1.7) \qquad (5.9)$$

and when the working stress is one half of the buckling stress the

value of the lateral force is approximately

$$(5.9)$$

$$F = 0.2\% \ P_a$$

where P_a is the Euler pin ended column buckling load of a strut

of length equal to the panel length.

The C.R.C. and German codes both indicate a value of

lateral force which is approximately 1% P_a[*] , that is a value

higher than the value for the lateral force found in equation

(5.9). The American Association of State Highway Officials

"Standard Specifications for Highway Bridges" (Ref. 54) and the

National Association of Australian State Road Authorities

"Highway Bridge Design Specification", (Ref. 55), both

recommend a force of 300 lbs. per linear foot, to be applied

---

[*] Measurements by Holt (Ref. 52) indicate that this force is

of the order of 0.05% P_a .

to the top chord panel point of each truss, (for a truss bridge) but do
not specify the size of the bridge. This force appears to be a
provision to allow for the forces developed as the bridge deforms, and
the value is approximately equal to the German and C.R.C. Codes * .

The stresses induced by the force F are added to the stresses
induced by the vertical bending of the I beam sides of the bridge.
The maximum stress usually occurs at the corner of the U frame.
For the ferry terminal bridge of Fig. 5.3 the addition of the
tensile stress in the bottom flange and the tensile bending stress
at the corner of the U frame is the maximum stress that occurs in
the bottom flange.

From the preceding calculations it appears that the
ferry terminal bridge satisfies the requirements of the codes
of AASHO, CRC., B.S. 153 and the Australian National Association
of Australian State Road Authorities. "Highway Bridge Design
Specification" 1958. However, these codes do not appear to have
made allowance for a lateral torsional buckling mode. It was
shown in Chapter Three that this type of deformation is possible
for very light through bridges, and thus a close examination of
the overall problem is warranted.

A series of model tests, using small mild steel through
plate girder bridges, was carried out. The models were varied
in size and in the structural arrangement, and the overall pattern

---

* A comparison of the lateral force provisions of the AASHO and
CRC codes indicates the two are equal when

AASHO $(F = 300 \text{ lbs/foot})$ = CRC $(F = 1\%P)$.

Suppose the axial stress in the flange is 15,000 psi, then

$(300/12) \times (\text{panel length in inches}) = (15,000/100) \times (\text{area of flange}$
$\text{in square in.})$

i.e. when the area (in square inches) of the flange is equal
to the panel length(in inches) divided by six then the CRC and AASHO
codes specify a similar lateral force.

---

of deformation was measured. The model tests were used to obtain ideas and an understanding of the problem. When these ideas had been formulated, the real ferry bridge at Devonport was loaded, deformations measured and these measured results were compared with the predicted values. Reasonable agreement was obtained, and hence an improved method of design is suggested. This method is based on the likely form of deformation of the bridge and hence the model studies are presented as a means of describing this form of the deformation.

5.4 Model Studies

5.4.1 Measurements.

Simple mild steel models of plate girder bridges * were

---

* The dimensions and section constants for these model bridges were obtained in a manner similar to that used for the brass bridge, in Chapter Three. The values were:

$h = 1.5$ in., $\ell = 48$ in., flanges 0.5 in x 0.125 in., web 1.5 in x 0.030 in., $EI_\eta = 74,000$ lb in^2, $C_1 = 83,000$ lb.in^4, and $EI_F = 1,850$ lb in^2. A graph of load and extension for the material used to make the flanges of the bridges is shown in Fig. 5.6. Other section properties of the bridges are as follows,

Bridge No.	Width a	C_o (see section 5.4.2)	C	$C_o \ell^2 / C \pi^2$	γ from Fig. 3.17	$P_1 = (\gamma/\ell^2)\sqrt{EI_\eta C}$
A	6 in	$3EI_F/sa$	7400 lb in^2	3.9	27	270 lb
B	8 in	$6EI_F/sa$	7400 lb in^3	5.2	29	290 lb
C	8 in	$3EI_F/sa$	7400 lb in^2	3.0	25	250 lb
D	8 in	$6EI_F/sa$	8700 lb in^2	4.8	28	300 lb.

Load on one I beam (in lbs.)

Fig. 5.8a   Fig. 5.8b   Fig. 5.8c   Fig. 5.8d
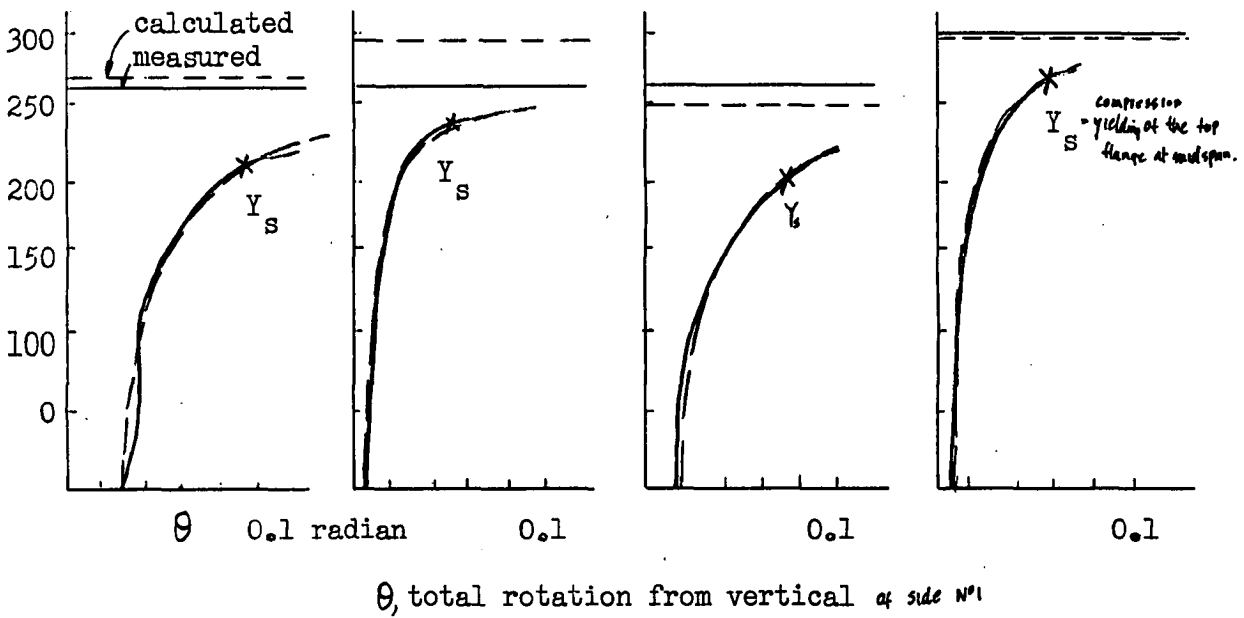
_____ measured result

— — -   replotted from Southwell Plots,
          using measured crookedness and
          measured buckling loads.

Fig. 5.7a   Fig. 5.7b   Fig. 5.7c   Fig. 5.7d

flanges
0.5" x 0.125"

web 1.5" x 0.030"
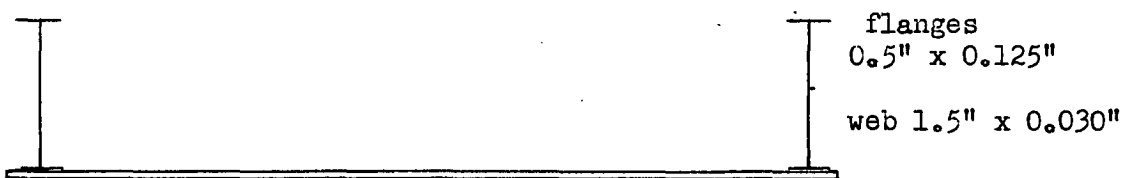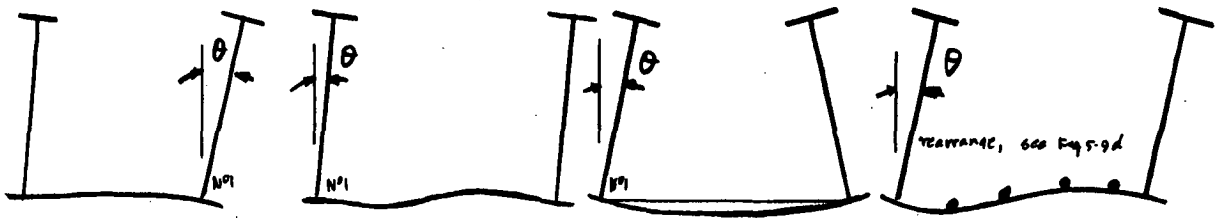
7 bottom chords 9" x 3/16" dia. mild steel,
width between I beams, a, either
6" or 8"
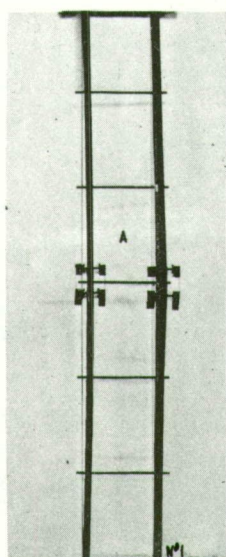length of bridge 48"
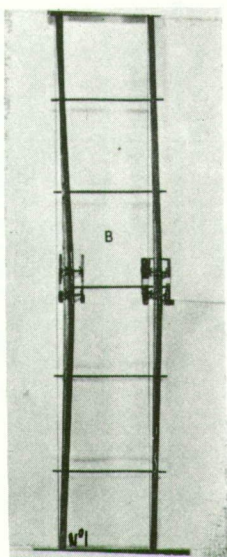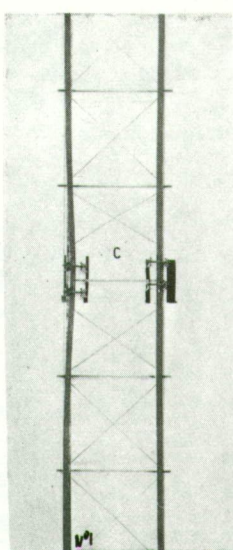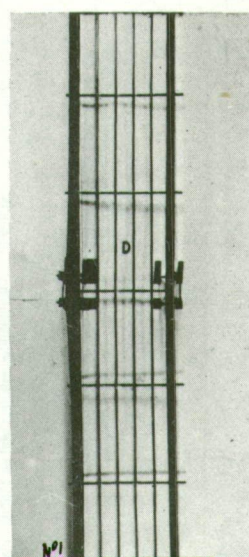
Fig. 5.7a   Fig. 5.7b   Fig. 5.7c   Fig. 5.7d

Shape of the deformed model mild steel bridges, after some yielding of the top flange.
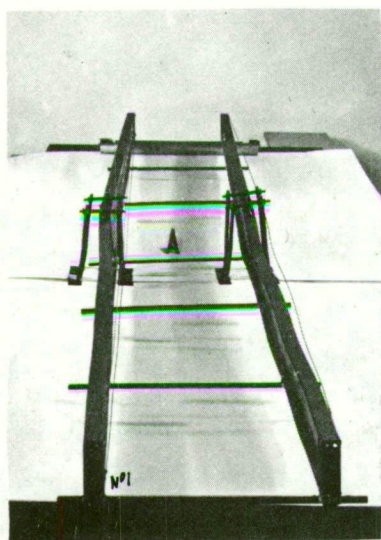
Fig. 5.7a Shape of model bridge 'A',

after some yielding of the top flange.
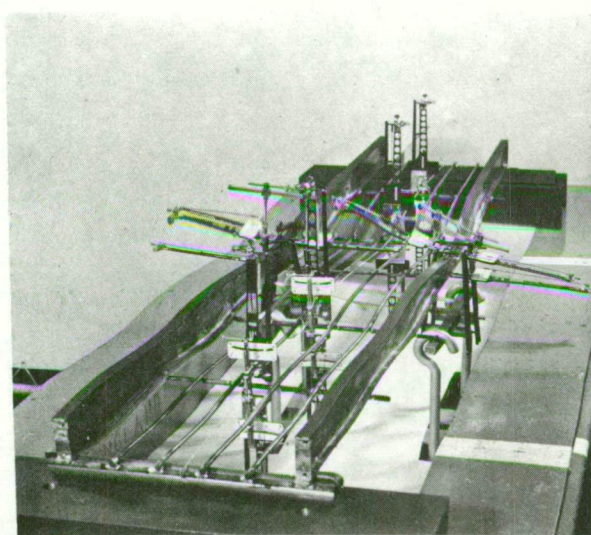
Fig. 5.7d Typical Huggenberger mechanical strain

gauge instrumentation used to measure strains.

1/64" dia. floor bracing. 3/16" dia. floor.

| Fig. 5.9a | Fig. 5.9b | Fig. 5.9c | Fig. 5.9d |

Elastic buckling mode in rotation
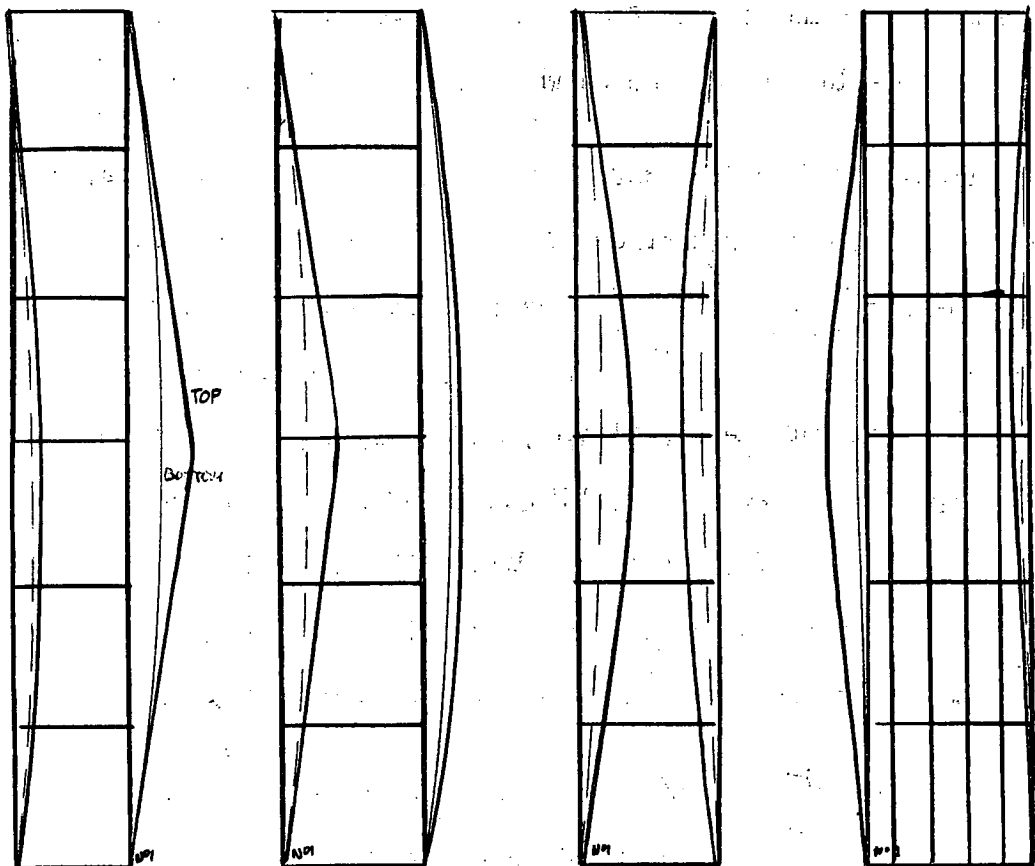
| Fig. 5.10a | Fig. 5.10b | Fig. 5.10c | Fig. 5.10d |

Shape of the top and bottom flanges after some yielding
of the top flange.
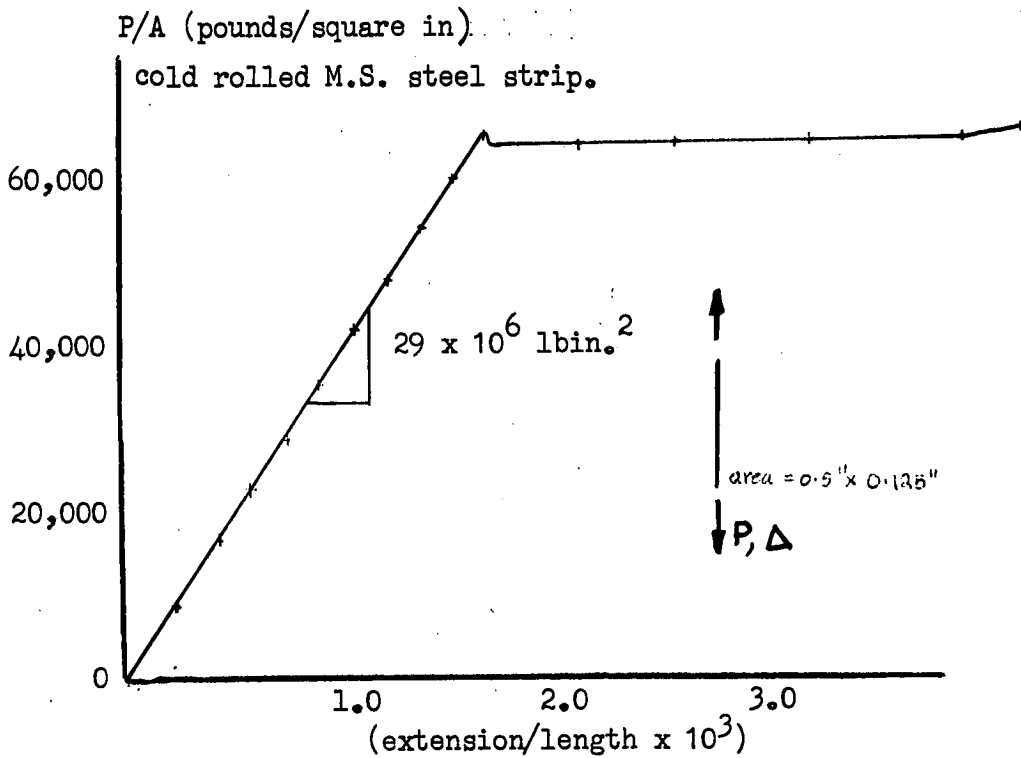
Fig. 5.6 Stress-strain relationship for the Mild Steel
strip used in the flanges of the Model Bridges.

---

tested, up to and beyond the elastic range of the material (Figs.
5.7a, 5.7b, and 5.7c ,5.7d and 5.7e). The floor of the bridge was
placed at the bottom flange and was made from light mild steel round
rods. Some of the models had floors which were not braced against
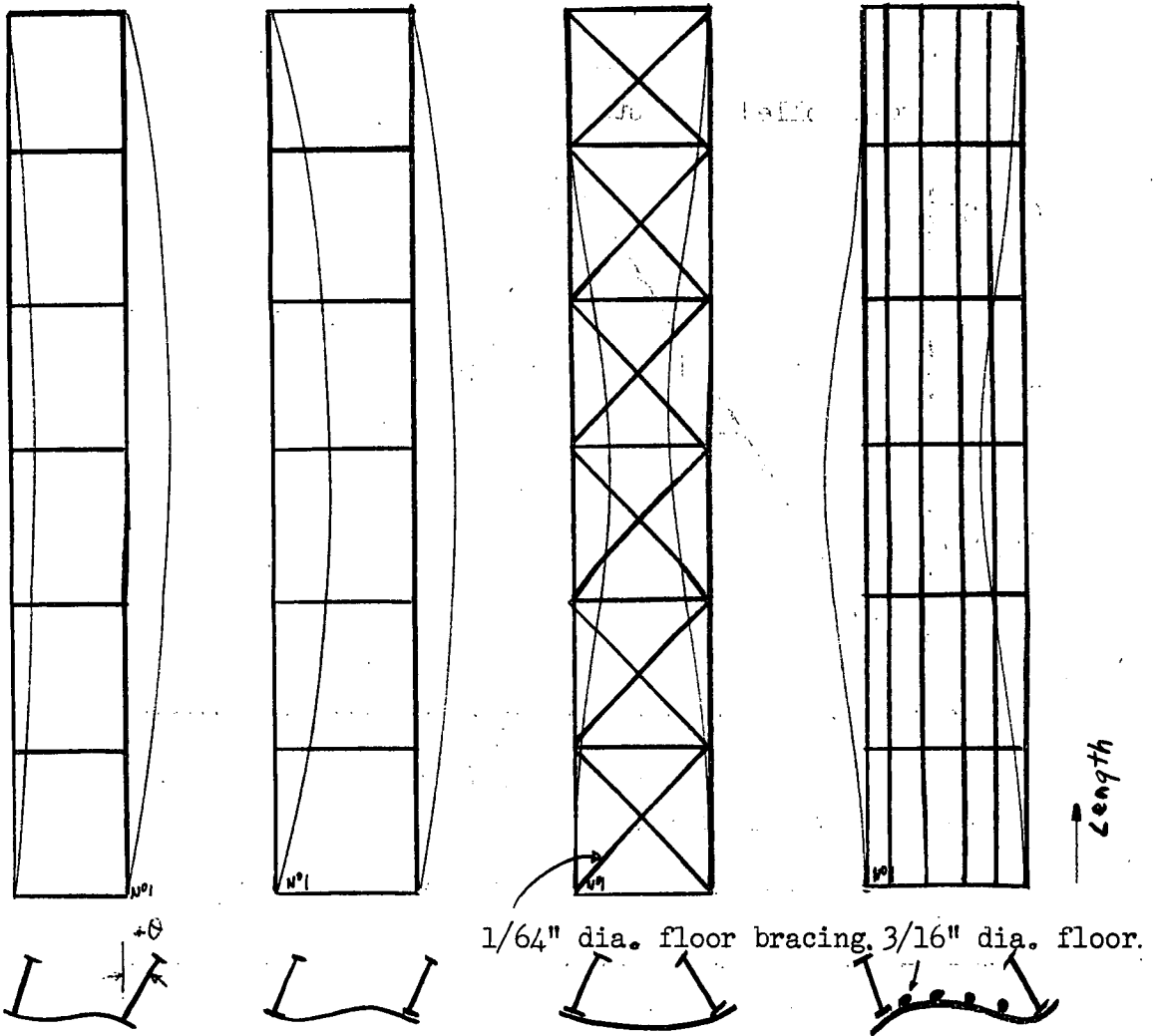movements in the lateral direction while others had floor bracing.

These model bridges deformed as indicated in Figs. 5.8a, 5.8b,
5.8c and 5.8d. The cross section of the I beam did not distort to
any measurable extent. While all strains remained elastic, the
deformed mode was as shown in Figs. 5.9a, 5.9b, 5.9c and 5.9d.
When the outer tip of the top flange yielded the top flange formed
a local hinge, and after some yielding, the deformed shape was similar
to the shape shown in Figs. 5.10a, 5.10b, 5.10c and 5.10d. Further
details concerning the deformed shapes are given in the Appendix E.
Points of interest arising from these model studies are:

(a)   There exist at least two different deformed shapes,
        corresponding to the shapes shown in Figs. 5.7a, 5.7b and
        5.7c. These deformed shapes are in the same sense as
        the initial rotation pattern. The magnitude and direction

of the angles of rotation of the web determine the type of mode which occurs.

(b)   While all strains reamin elastic the cross section of the I beam does not distort. The cross section distorts only when the web-flange joint yields.

(c)   The centroids of the I-beams move laterally.

(d)   While all strains remain elastic the rotation of the cross section of the I beam is approximately a half sine wave.

(e)   After some yielding of the flanges occurs, the shape of the bridge is approximately described by two straight lines for the top flange, and a half sine wave for the bottom flange. The cross section of the I beams at the supports remain vertical. Thus, after some yielding occurs the shape is approximated by the following functions:

lateral deflection of top flange = $2.75h$ $(\theta_{z=0})$ $(1-2z/\ell)$

lateral deflection of bottom flange = $1.75h$ $(\theta_{z=0})\cos \pi z/\ell$

rotation of cross-section of I beam = $1.75 \theta_{z=0} \left[\tfrac{1}{2}\pi - \pi z/\ell - \cos \pi z/\ell \right]$

where $\theta_{z=0}$ = rotation at the centre of the bridge

h = height of the I beam,   and

z = distance along the beam, measured from the midspan of the beam.

(f)   There is little increase of load carrying capacity of the structure beyond the load that corresponds to first yield of the tip of the top flange.

These observations are different from the deformations pictured in Fig. 5.2, corresponding to the Timoshenko model for through bridges, in Ref. 30. An improved mathematical model is needed to describe the new deformations.

5.4.2 Mathematical Descriptions of the model tests.

The model developed in Chapter Three is sufficient to describe adequately the observations, * that is for the initially straight I-beam arrangement

$$C_1 d^4\theta/dz^4 - Cd^2\theta/dz^2 + C_0\theta - (P^2/4EI_\eta)(\tfrac{1}{2}\ell-z)^2\theta = 0 \quad . \qquad (5.10)$$

---

* It is noticed in Fig. 5.7c and Fig. 5.7d that the floor beams may provide considerable lateral restraint to the bottom flange of the I beam. However, even if the sides are braced by U frames, the centroids of the I beams are not rigidly restrained, and the centroid of the section may then twist and bend. The model developed in this thesis approximates the effect of lateral restraints on the bottom flanges on the deformations and buckling loads to being small. This model is suitable when the floor beams offer some torsional restraint, and offer no appreciable lateral restraint to the centroid of the I beams.

An alternative mathematical model, proposed by Schmidt (Ref. 56) is to find the forces necessary to ensure that deformations as shown in Fig. 5.11; that is the floor beams provide complete lateral restraint, but no torsional restraint. As the torsional restraint offered by the floor beams is completely neglected only small buckling loads are needed to sustain the deformations (approx. 100 lb. for the model bridges). Therefore, this model is unsuitable when the floor beams offer any torsional restraint; but Schmidt has shown it to be useful when the floor beams offer large lateral restraint to the I beam section and no appreciable torsional restraint.

The value of C_0 , the equivalent torsional restraint per unit distance offered by the floor system, is found from the initial crookedness pattern and the stiffness of the floor system. When the initial rotations, and hence final rotations, are as shown in Fig. 5.7c the restraint offered by floor beam and adjacent I beam is given by the equation

$$2EI_F/\rho a \;\leqslant\; C_0 \;\leqslant\; 3EI_F/\rho a$$

where EI_F = the rigidity of one cross member of the floor system,

6 = width of the bridge,

a = spacing of the cross members.

The lower value of C_0 occurs when the two initial rotations are equal, and the adjacent I beam is not contributing to the value of C_0 ; the higher value occurs when one rotation is much greater then the other (Fig. 5.12).

Similarly, when the rotations are as shown in Fig. 5.12 the restraint is given by the equation

$$3EI_F/\mathcal{b}\,a \;\leqslant\; C_0 \;\leqslant\; 6EI_F/\mathcal{b}\,a \;.$$

The critical central point buckling, P_1 is obtained from Fig. 5.13. For bridges with a ratio of floor stiffness to St. Venant torsional stiffness greater than 5, that is

$$C_0 \ell^2/C\pi^2 \;>\; 5$$

a good approximation to the buckling load * is obtained by fitting the lower bound functional form (as found in 3.8.4, and putting $C_0 \ell^2/C\pi^2 \gg 1$ and $\gg C_1\pi^2/C\ell^2$) to the upper found numerical form, (as found in 3.8.2). The resulting approximation to the first buckling load P_1 is shown in Fig. 5.13, with

$$P_1 = 5/\ell \sqrt{EI_\eta\, C_0} \;, \tag{5.11}$$

---

* Equation (5.11) gives the buckling load value of a single vertical point load applied in the middle of the beam. Comparisons between this model and that developed by Taylor (Ref. 39), for a uniformly distributed load of $\frac{1}{2}p$ per unit distance along each I beam, indicate that the distributed buckling load on each I beam is approximately

$$\left(\tfrac{1}{2}p\ell\right)_1 = 7.5\sqrt{EI_\eta\, C_0}$$

that is the important variables in determining the buckling load of the
light through bridge are the lateral rigidity of the I beams, the
torsional stiffness of the floor system and the length of the bridge.

$P_1 = 5/\ell \sqrt{EI\ C_o}$
from form of the lower bound
solution
$C_1 \pi^2/C\ell^2 = .4; P_1 = 1/\lambda^2 \sqrt{EI_\eta C}$
$.2$
O
numerical solution by weighted resid
$P_1 = (3.8/\ell)\sqrt{EI_\eta C_o}$
lower bound albegraic solution
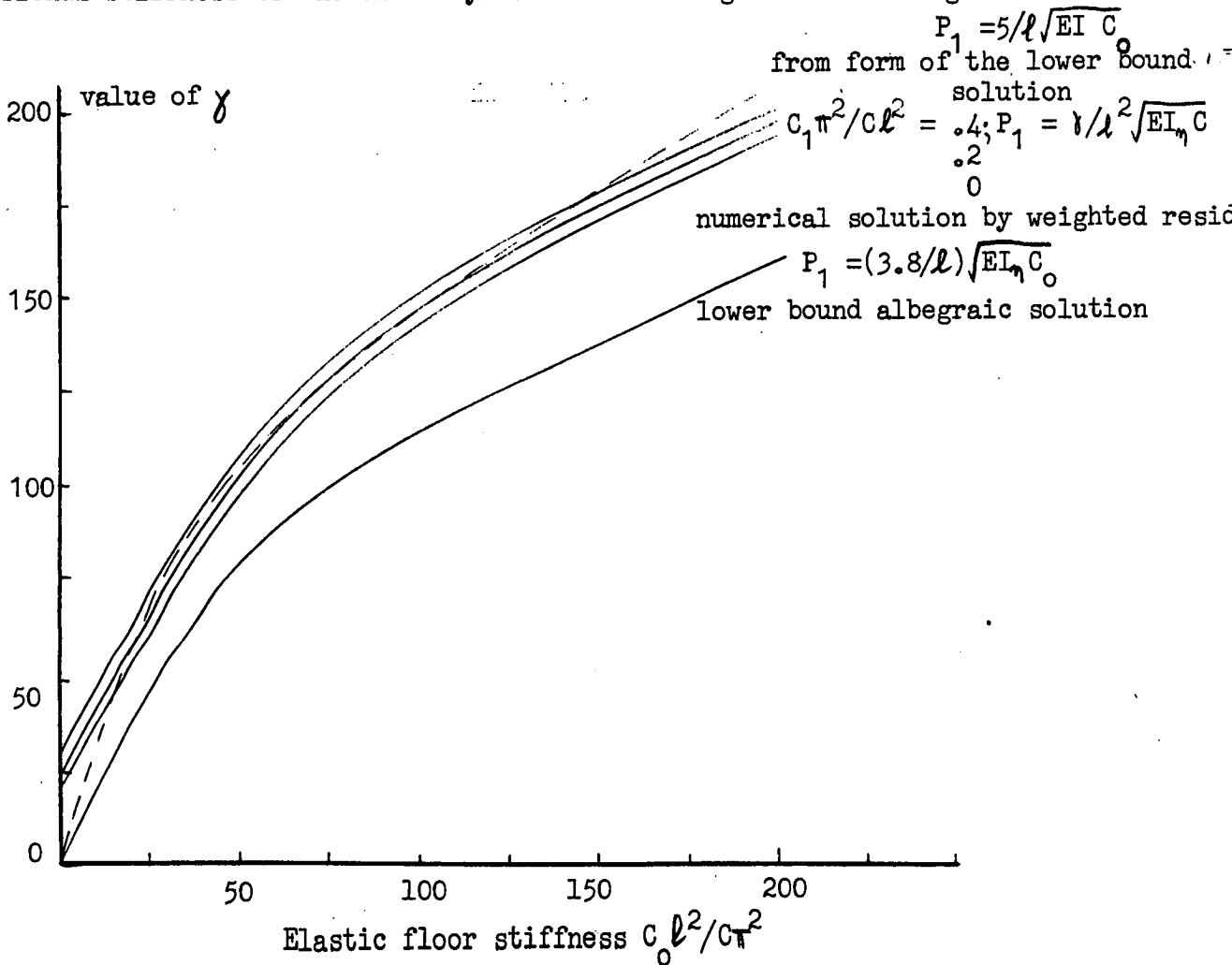
Fig. 5.13. Buckling Load of Mathematical Model (5.10)

The initial crookedness can be included in the mathematical
model, and the final rotations, θ_o , are given approximately by the
equation

$$\theta = \theta_o/[1-(P/P_1)^2] \quad , \tag{5.12}$$

where θ_o is the equivalent first mode initial crookedness, being
determined from the Southwell Plot, or an addition of the measured
initial rotation and the equivalent initial lateral deformation.

These predicted rotations for the model bridges compare
closely with the measured results obtained from the model bridges,
and the two are plotted in Figs. 5.7a, 5.7b, 5.7c and 5.7d. Thus
the mathematical model based on lateral torsional deformations of
the I beams and summarized by the equations (5.11), (5.12) is a
reasonable description of through bridge behaviour.

lateral movement of and
rotation of the top
flange

$\frac{1}{2}P$

P

$\frac{1}{2}P$

no lateral movement of the bottom flange
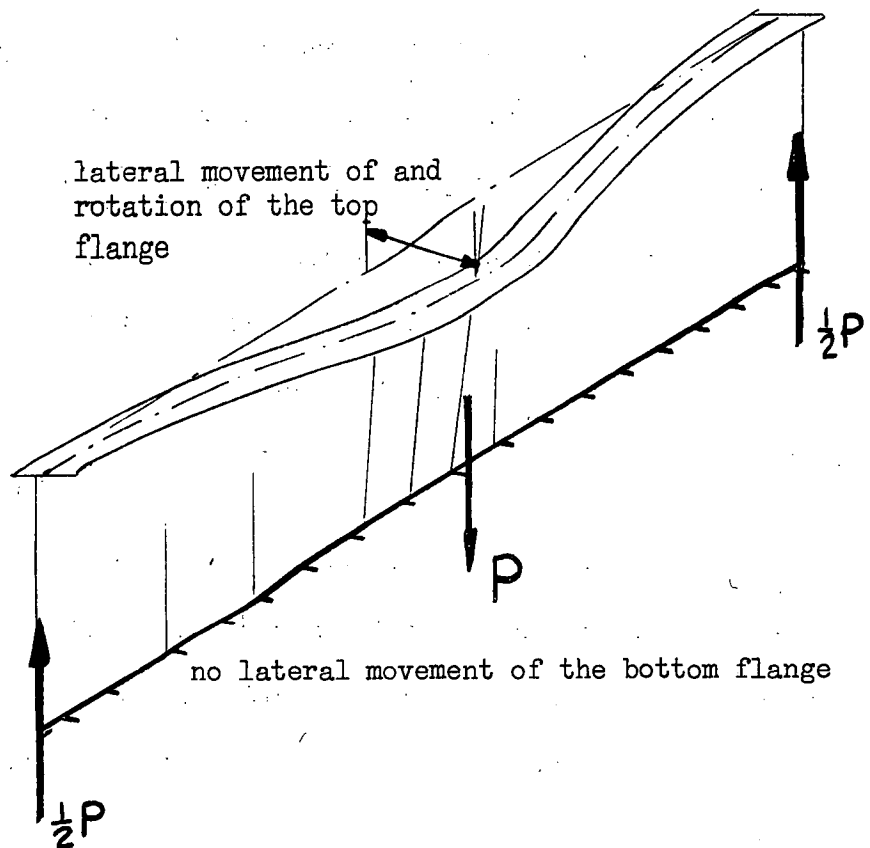
Fig. 5.11. Deformations of bridge as described by Schmidt (Ref. 56).

$M = 2EI_F \, \theta/\Delta$ $M = 3EI_F \, \theta/\Delta$ $M = 6EI_F \, \theta/\Delta$
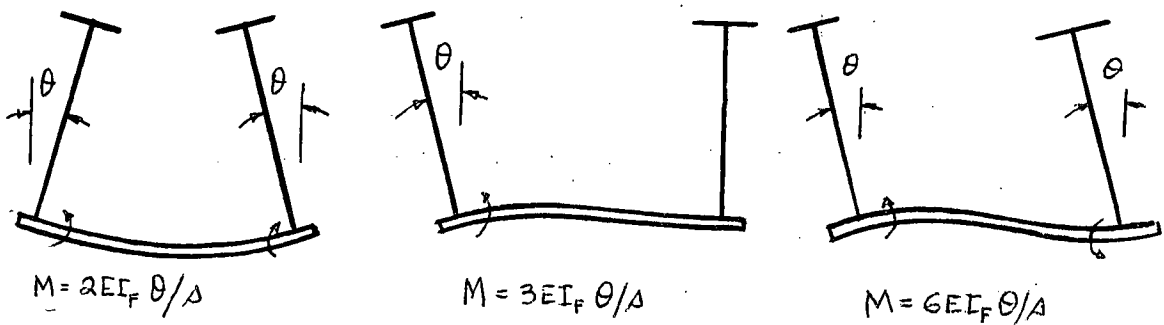
torsional restraint offered by the floor beams

= $C_o \theta$ /unit length or along the bridge

$C_o = 6EI_F/\Delta a$ $C_o = 3EI_F/\Delta a$ $C_o = 2EI_F/\Delta a$

Fig. 5.12. Values of elastic floor stiffness arising from different
initial crookedness patterns.

5.4.3 Lines of First Yield.

The problem still remains of deciding the safe working load of
the bridge. The measured values of rotation (Fig. 5.8) indicate that
a reasonable ultimate load carrying capacity of the bridge is that load
which will just cause yielding of the outer tip of the top flange.
Working loads can then be chosen as some fraction of this load to cause first
yield. Two methods of predicting the load to first yield the structure
are now outlined.

A measured line of first yield, (that is the locus of all points
with central load and central rotation for which yielding of the outer
tip of the top flange first occurs as co-ordinates,)is shown in
Fig. 5.14. Several different initial crookedness values are shown for
the same size model.

Calculated lines of first yield are also shown in Fig. 5.14.
The first line is obtained by considering the elastic deformations
of the bridge, and using the equivalent initial crookedness as
measured by the Southwell Plot. Then the yield strain on the outer
tip of the top flange is found by expressing the strain in terms of
the rotation of the I beam.

Thus, the final rotation θ is given by equation (3.12).

$$\theta = a_1\theta_1/[1-(P/P_1)^2]$$
(5.12)

and the strain, ϵ , in the top flange given in terms of this rotation,
i.e.

ϵ = [lateral curvature x $\frac{1}{2}$ width of top flange] + [vertical

curvature x $\frac{1}{2}$ height of the I beam.]

= $\frac{1}{2}$ b d^2y/dz^2 + $\frac{1}{2}$h d^2u_T/dz^2 .

The expression for lateral curvature is obtained by using the second
derivative of the expression for the lateral movement of the top
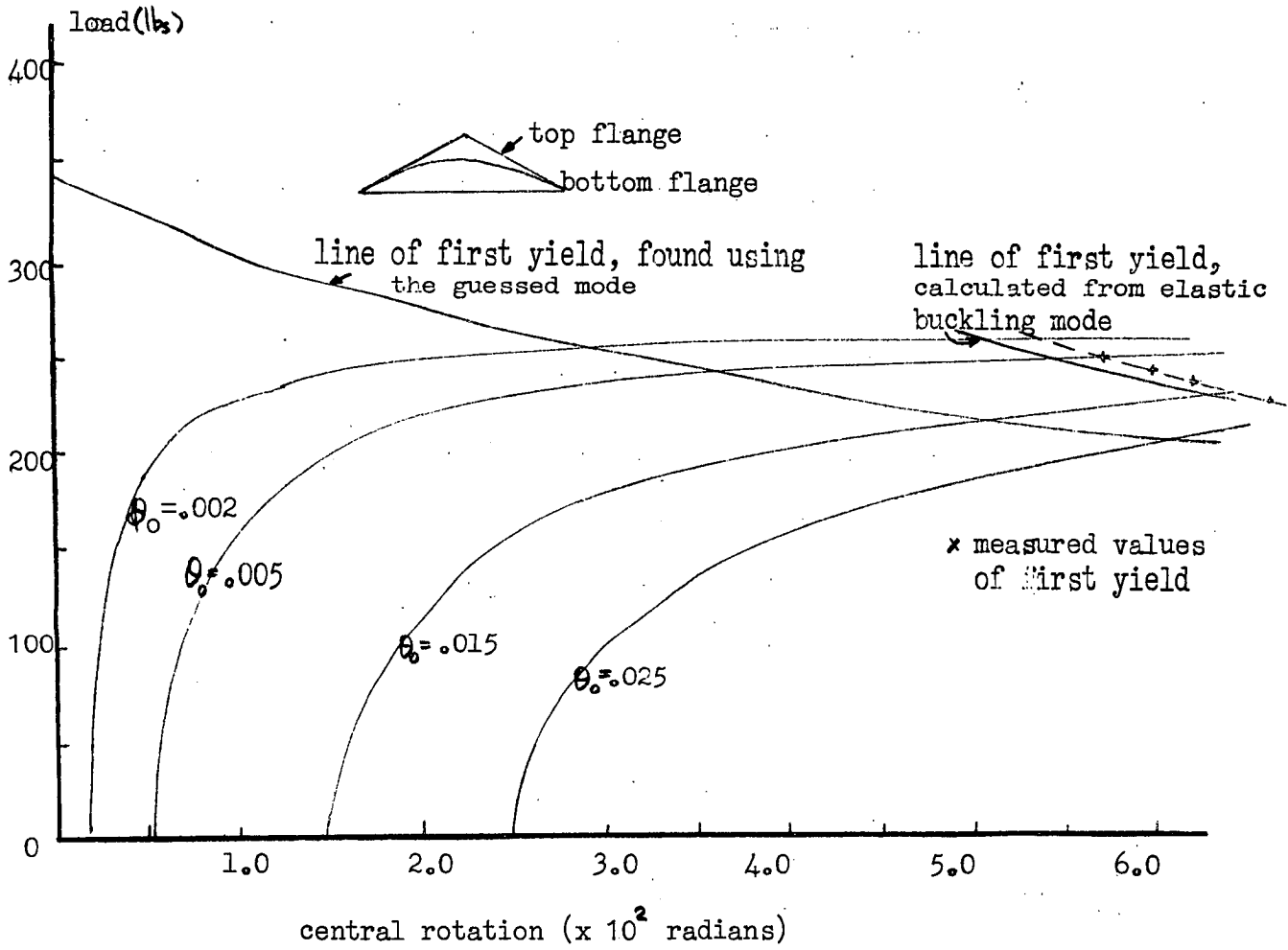
flange, $U_T = \frac{1}{2}h\theta + u$.

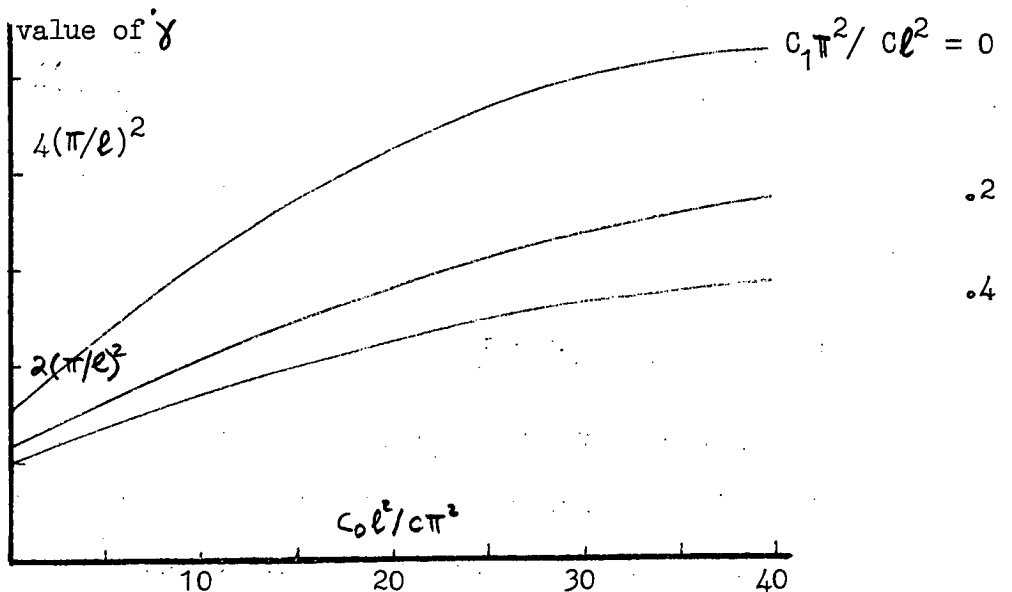Fig. 5.14. Comparison of the two methods of finding lines of first yield.

Fig. 5.15 Values of $\dot\gamma$ in $d^2\theta/dz^2 = \dot\gamma\theta$ at $z = 0$.

The individual components of the lateral curvature of the top flange are found as follows:

(a)   an approximation for $d^2\theta/dz^2$ is obtained from the expression for θ , and is given by the equation

$$d^2\theta/dz^2 = d^2[g_1 \cos\pi z/\ell + g_3 \cos 3\pi z/\ell + \ldots]/dz^2 .$$

Values for this component of curvature, at the centre of the bridge, are given in the form of a graph in Fig. 5.15 and values of are found such that

$$d^2\theta/dz^2 = \gamma\theta_{(z=0)} .$$

(b)   The curvature along the centre line of the I beam, $d u/dz^2$, is obtained from equation (3.4) ie.

$$EI_\eta d^2u/dz^2 = \tfrac{1}{2}P(\tfrac{1}{2}\ell - z)\theta .$$

Using these values, the maximum strain   in the top flange is given by the equation

$$\epsilon_{max} = \theta(\tfrac{1}{2}h\gamma + P\ell/4EI_\eta)\tfrac{1}{2}b + (P\ell/4EI)\tfrac{1}{2}h .$$

Therefore, the maximum measured strain in the top flange ϵ_{meas} is found by using the equation (5.12) to find the measured change in central rotation $(\theta - a_1\theta_1)$ and

$$\epsilon_{meas} = [a_1(P/P_1)^2\theta_1/(1-(P/P_1)^2)] [\tfrac{1}{2}h\gamma + P\ell/4EI_\eta]\tfrac{1}{2}b + P\ell h/8EI .$$

An alternative, and simpler approach, to find a line of first yield is as follows:

The line is calculated by using the approximate measured shape as given in (e), section 5.4.1. The rotation of the web is given by the equation

$$\theta = 1.75\,\theta_{z=0} \left[\tfrac{1}{2}\pi - \pi z/\ell - \cos \pi z/\ell \right]. \tag{5.14}$$

The strain at the tip of the top flange is obtained by estimating the vertical and lateral bending effects. The corresponding bending moments are given by the expressions M and $M\theta$, respectively. Thus the strain at the top of the top flange ϵ is

$$\epsilon = M\theta t/2EI_\eta + Mh/2EI.$$
$$= [P\ell\theta t/8EI_\eta] + P\ell h/8EI. \tag{5.15}$$

It can be seen from Fig. 5.14, that little difference exists between the measured line of first yield and the two calculated lines of first yield. However the second method of calculation, using the shape that the bridge takes up when yielding occurs as the describing shape, is easier to calculate and visualize. It is felt that this method also gives a closer description of the structural behaviour when the bridge is made of a deck that has a large lateral stiffness.

5.5   Comparisons between the Mathematical Model of 5.4 and

existing Mathematical models.

The proportions of the model bridges tested were such that the buckling load corresponding to the Timoshenko model for through bridges, as outlined in "Theory of Elastic Stability", (Ref. 30) was comparatively large when compared with the measured lateral torsional buckling load. It would be expected that as the stiffness of the floor beams is increased, the difference between the buckling load of the Timoshenko model and the buckling load of the model proposed in Chapter Three would decrease. In the following paragraphs a comparison between the Timoshenko model and the lateral torsional buckling model is presented, and a simple relationship between the two buckling loads is found.

In any through bridge it is likely that the deformation shown in Figs. 5.2, 5.7a, 5.7b, 5.7c and 5.7d are present. The magnitude of the component deformations in each mode is dependent on the type and size of bridge, the applied loading, and the initial crookedness.

The central point loading on each I beam necessary to provide the buckling load for deformations shown in Fig. 5.2 is found from equation (5.3) and the Euler column buckling expression.

Then

$$P = (4h/\ell)P_T \tag{5.16}$$

$$= (4h/\ell)(\pi^2 EI_T/4.0\sqrt{EI_T \, a\delta})\quad,$$

The value of the virtual lateral displacement δ of the compression flange nearest midspan of the bridge consists of the contributions from the movement of the sides of the frames and the floor of the frames. A good approximation for δ given in B.S. 153 is

$$\delta = (h_1^3/3EI_S + h_2^2 \, s/2EI_F)$$

which may be expressed in the form

$$\delta = k(h_2^2 s/2EI_F)\quad, \tag{5.17}$$

where h_1 = distance of the centroid of the compression chord

from the top of the floor beam cross member

EI_S = lateral flexural stiffness of the vertical side of the bridge

h_2 = distance of the centroid of the compression chord from the

neutral axis of the floor beam cross member

a = width of the bridge

EI_F = vertical flexural stiffness of the floor system in the plane

of bending of the floor

k = a factor dependent on the ratio of the contributions to the

virtual displacement, and is given by the ratio of the total

lateral movement of the top flange of a through bridge

(sustained by a unit horizontal force applied at the top

flange of the bridge) to the magnitude of the lateral

movement of the top flange that results from the deformation

of the floor beams.

Equations (5.16) and (5.17) can be simplified. The central point loading P on each I beam necessary to provide the buckling load for the deformations as shown in Fig. 5.2 is then given by the equation

$$P = (\pi/\ell)^2 \sqrt{EI_T \, EI_F \, (\ell/a)(\ell/s)}\; 1.42(h_2/h)/\sqrt{k}\quad. \tag{5.18}$$

The central point loading on each I beam necessary to provide
the buckling load for deformations shown in Fig. 5.7a is found from
equation (5.11). The approximations

$$EI_\eta = 2EI_T$$

and

$$C_o = 2EI_F/sa$$

are used and equation (5.11) simplifies. The central load is then
given by

$$P = (\pi/\ell)^2 \sqrt{EI_T\ EI_F\ (\ell/a)\ (\ell/s)} \ . \tag{5.19}$$

Thus from equations (5.18) and (5.19) the two buckling
loads are equal when the critical value of k is given by the
equation

$$k_{crit} \approx 2(h_2/h)^2. \tag{5.20}$$

When k is less than k_{crit} , that is when most of the lateral
deformation (sustained by a unit lateral load applied on the top
flange) results from the deformation of the floor beams, the buckling
load for the mode shown in Fig. 5.7a is less than the buckling load
for the mode shown in Fig. 5.2. When k is greater than k_{crit} , that
is when most of the lateral deformation results from the deformation
(sustained by a unit lateral load applied on the top flange) of the
sides of the bridge the buckling load for the mode shown in Fig. 5.2
is less than the buckling load for the mode shown in Fig. 5.7a.
Values of k and k_{crit} for various existing through bridges are
tabulated in the Appendix F to show that bridges have been
designed in both regions.

A model bridge was designed so that the two buckling loads
were equal, that is k = k_{crit} . The resulting deformations contained
both buckling modes. However, because the measured buckling load of
the system was within 10% of the predicted buckling load, it was
assumed that there is little interaction between the two types of
deformation.

The ferry terminal bridge at Devonport has for the critical

value of $k \approx 2.42$; the actual value of k is 1.67. This indicates a

floor system which is more flexible than the critical value. Therefore

the buckling load corresponding to the mode shown in Fig. 5.7a is the

lowest buckling load. The low value of k indicates that for this bridge

it is unncessarry to design against a mode of buckling similar to that

mode shown in Fig. 5.2.

In the following section a detailed analysis of the behaviour

of the ferry bridge at **Devonport** is presented. This analysis is based

on deformations similar to those shown in Fig. 5.7a and a design

procedure is indicated.

5.6   Analysis of an Existing Bridge Structure

For the bridge ferry terminal at Devonport, as shown in Fig. 5.3,

the relevant constants are

$$I = 61{,}000 \text{ lb in}^4$$

$$(I/y) = Z = 1{,}900 \text{ lb in}^3$$

$$C = 4.45 \times 10^8 \text{ lb in}^2$$

$$EI_\eta = 3.0 \times 10^{10} \text{ lb in}^2$$

$C_0 = 2EI / \Delta a$ (as crookedness is in the mode $\int \, \downarrow$)

$$= 1.0 \times 10^6 \text{ lb in}$$

> (In this calculation the concrete deck has been assumed not
>
> to restrain the rotation of the floor. This estimate gives
>
> an underestimate of the buckling load of the structure).

$$C_0 \ell^2 / C\pi^2 = 200$$

$$C_1 = 3.0 \times 10^{13} \text{ lb in}^6$$

$$C_1 \pi^2 / c\ell^2 = 0.68.$$

The buckling load, calculated from equation (5.11), is a central

loading on the total bridge structure of 720 tons. The buckling mode

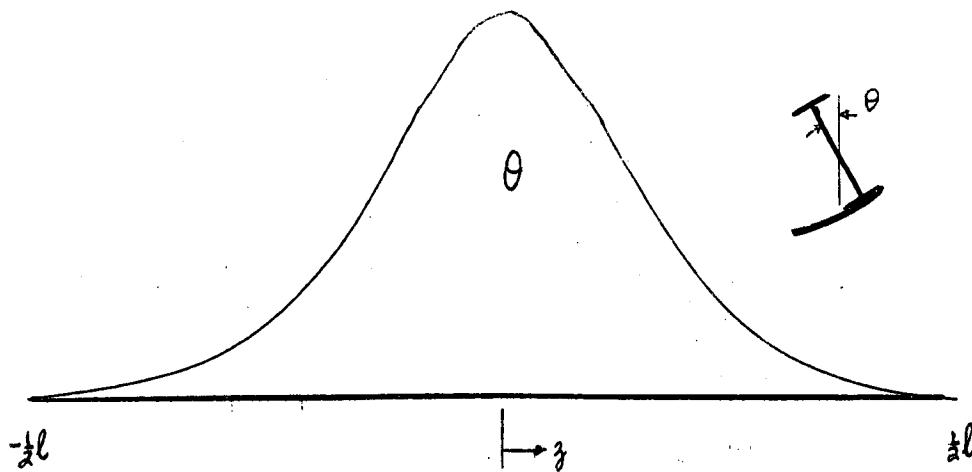found from Fig. 3.18 is sketched in Fig. 5.16.

Fig. 5.16. Rotational buckling mode of the through
bridge at Devonport, Tasmania, calculated from
the column of equation (5.10).

The dead weight of the bridge is approximately sixty tons.
It has been pointed out earlier in this Chapter that this uniform
load is approximately equivalent to a central point load of fourty
tons, that is $60/1.5 = 40$.

The initial rotational crookedness of both webs of the
bridge consisted of a first buckling mode specified by a central
rotation value of 6×10^{-3} radians, together with higher order
buckling modes which represented approximately a further central
rotation value of 3×10^{-3} radians. These estimates were obtained
by noting the difference from the vertical indicated by placing an
engineer's spirit level against the web of the bridge *.

---

* Measurement of four other through bridges, each approximately
sixty feet in length, indicated that these values of initial
rotational crookedness are reasonable. The bridges measured
included a railway bridge, a pedestrian overpass and a large
truss bridge used for motor traffic. The usual value of the
maximum rotational crookedness of the web was 10^{-2} radians.
Means of deciding an economic value of initial crookedness
are investigated in the appendix G. There exists scope for
some valuable work to be done to determine a reasonable
practical value of crookedness at which fabricators could
aim.

The initial lateral crookedness of the bridge was of the order of $\ell/1000$, These readings indicate an equivalent first mode ~~initial~~ rotational crookedness of 6.25×10^{-3} radians. (See Appendix D for further details).

From equation (5.12) the central rotation and applied central load relationship is of the form

$$\theta = a_1 \theta_1 / [1 - ((P_{LL} + 40)/720)^2] \quad , \tag{5.21}$$

Where P_{LL} is the total central live load (in tons) applied to the bridge. A graph showing the relationship between the central rotation and central live load is shown in Fig. 5.17.

However, the instability deformations resulting from loads applied to the centroid of the I beams are not the only deformations which are measurable. The bridge is loaded on the deck as shown in Fig. (5.18). This loading results in deformations approximately similar to the first buckling mode.
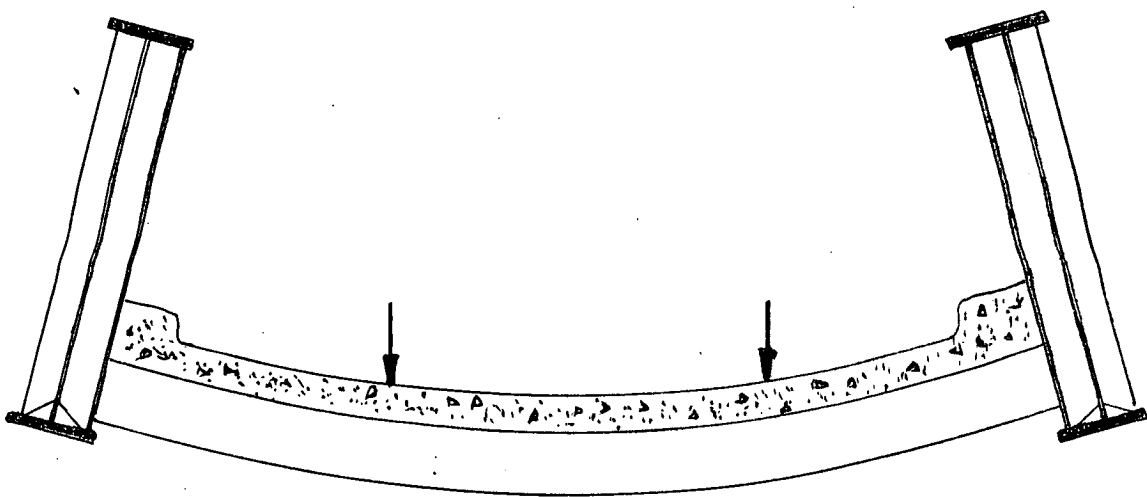

Fig. 5.18. Deformations of the bridge resulting from a method of loading other than through the centroid of the I beam sides. In this case the loading was applied by driving a loaded fork lift truck on to the bridge.

The deformations induced by this loading can be calculated in the manner indicated in Chapter Four. This loading introduces rotations, given by the equation

$$\theta_{z=0} = k_2 \, (P/\lambda)(s/8) \, 4EI_\eta \Big/ (P_1\ell)^2 \, (1-(P/P_1)^2) \; . \tag{5.22}$$

where k_2 = factor, from Chapter Four, depending on the ratio

$C_0 \ell^2 /C\pi^2$, and the distribution of loadings. In the

case of a central point load, k_2 is approximately 13.

When the ferry terminal bridge constants are specified, equation (5.22) reduces to the equation

$$\theta = 2 \times 10^{-4} \, P_{LL}/[1-(P_{LL}/720)^2] \; . \tag{5.23}$$

Equation (5.23) is plotted in Fig. 5.17.

A line of first yield, using the approximate yielded shape outlined in section 5.4.3, is also plotted in Fig. 5.17. The load to cause first yield is obtained as the intercept of this line with the line formed from the addition of the rotations caused by the buckling instabilities (i.e. equation 5.21) and the torsional deformations (i.e. equation 5.23).

5.7   Comparisons between Measured and Predicted Results.

It can be seen from Fig. 5.17 that the instability effects are not large in the lower range of loads and most of the rotation of the I beam is caused by the torsional loadings imposed by the floor system. However, the load to first yield the bridge is considerably affected by the torsional deformations induced by the deformed floor, and this effect must be considered if safe and reasonable load carrying capacity for the bridge is to be determined.

These predicted results are now compared with measurements taken on the actual bridge structure. A central load of approximately 34 tons, applied by driving a loaded fork lift truck on to the bridge, resulted in a central rotation increase of 4×10^{-3} and 3×10^{-3} radians on the two I beams, with no measurable distortion of the

total live load (tons)

Euler buckling load

600

500

400

300

$\phi = \phi_o / \left[1 - (P/P_{crit})^2 \right]$

predicted rotations from torsional loadings

200

calculated load-
rotation relation
(elastic)

100

calculated line of
first yield

BS153 working load

suggested working
range

measured results

0

dead
load

0   1.0   2.0   3.0   4.0   5.0
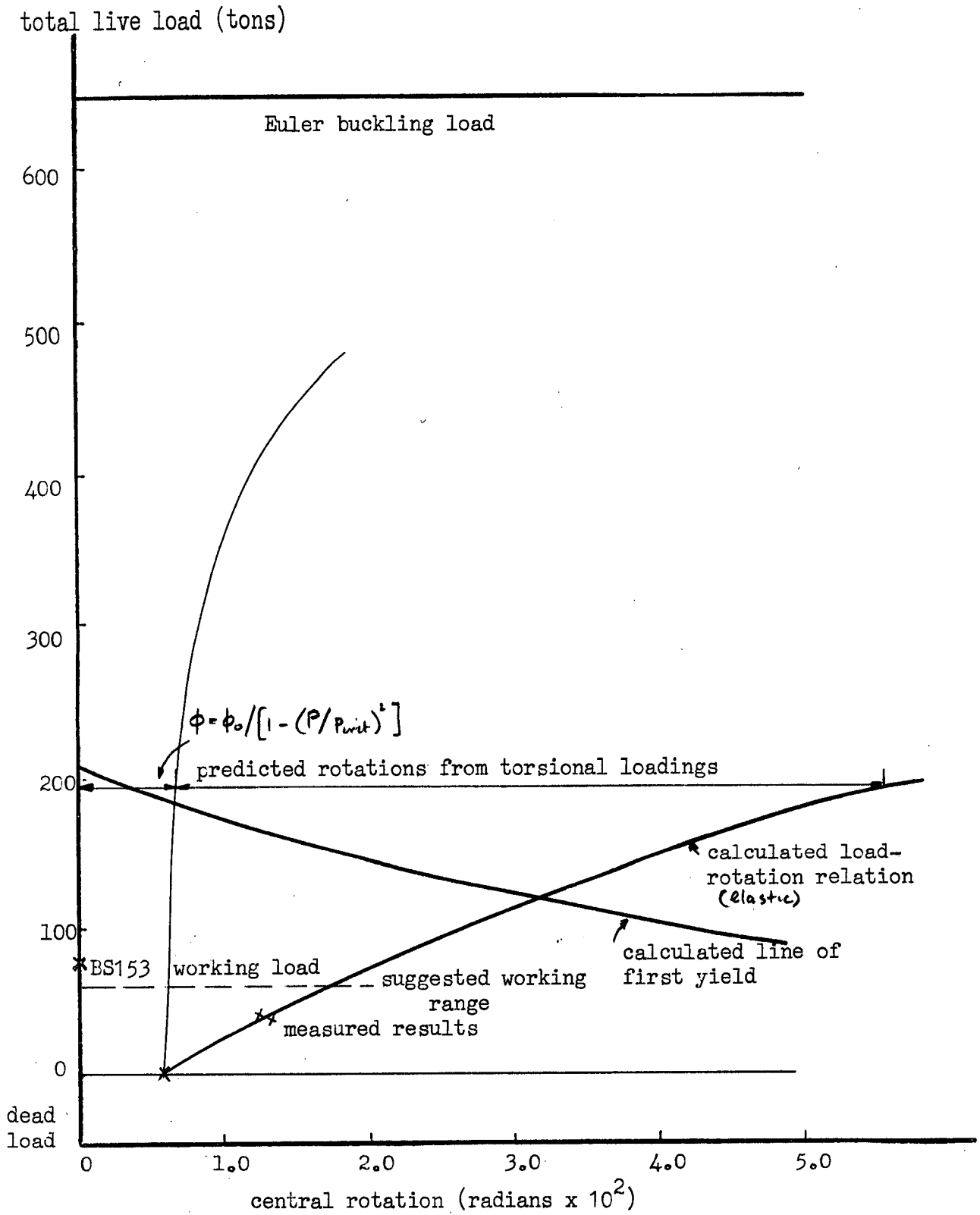
central rotation (radians x 10^2)

Fig. 5.17. Plots of loads and central rotation of the I beam sides
of the ferry terminal bridge at Devonport, Tasmania.

cross section of the I beams. Measurement of rotation changes was made with a spirit level held against the web. This reading was checked by a spirit level placed on the flanges.

For the same change in load, strain measurements obtained from Huggenberger mechanical strain gauges indicated strains of 0.20×10^{-3} and 0.25×10^{-3} on the edges of the top flange of one I beam, and 0.17×10^{-3} and 0.10×10^{-3} on the other I beam. All readings were taken at midspan.

The measured results are within 10% of the values. predicted by the mathematical model developed in this chapter. This mathematical model (based on picturing the deformations of the structure as it deforms,) is used in the following section to estimate safe working loads for the bridge.

5.8   Working Loads.

The designer has a choice in deciding the design criteria he wishes to specify. Two possible criteria are outlined in section 2.10 and are

(b)   a working load for the material, and

(c)   a maximum deformation of the structure.

Consider the working load criteria. At a load of 120 tons (Fig. 5.17) the structure begins to yield, and as the model tests show there is little load increase after first yield, this load is a good estimate of the maximum load that the structure could carry. A working load of approximately 60 tons i.e. $(120 \div 2)$ tons appears reasonable. At this load the nominal stress in the top flange, corresponding to vertical bending alone, is 15,000 psi.

At a loading of 60 tons, the central rotation increases by approximately 1.4×10^{-2} radians from the initial no load position, and the increase in lateral deflection of the top chord is approximately 2.0 ins., that is $\ell/500$ from the initial position. These deformations at 60 ton load are reasonable, as they do not

appear unsightly, and do not interfere with the function of the structure. Therefore, use of either criteria (b) or (c) in the design of this bridge structure is satisfactory as both criteria indicate similar working loads.

5.9   Conclusion.

The behaviour of an existing through bridge has been measured and reasonable mathematical descriptions suitable for design purposes have been developed.

It is recommended that existing code recommendations be modified in the light of this work. A suggested form is as follows:

DESIGN OF THROUGH BRIDGES.

Through bridges should be designed to resist likely modes of lateral instability. The type of lateral instability is dependent on the relative values of the stiffness of the sides of the bridge and the stiffness of the floor of the bridge. A through bridge will be called a light through bridge when the stiffness of the floor is small in comparison to the stiffness of the sides of the bridge. The predominant modes of overall deformation then are
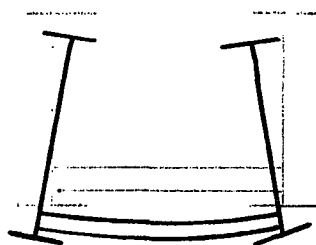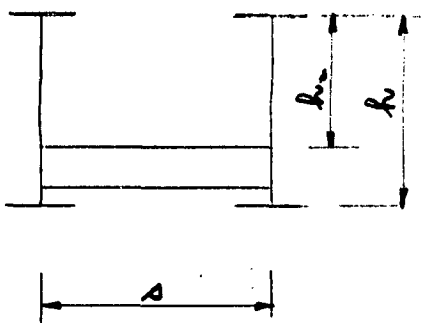
	k < k crit	k > k crit
	light through bridge	heavy through bridge
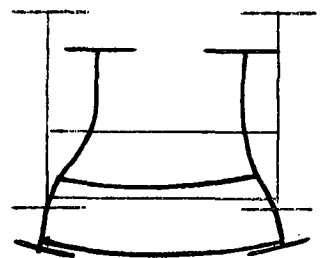
CALCULATION OF BUCKLING LOADS.

The buckling loads applied through the centroid of each beam needed to sustain these two types of deformation for the initially straight bridges are

(a) for light through bridges

central point load $P_1 = 5/\ell \sqrt{EI_\eta \, C_o}$

where C_0 = equivalent floor stiffness

$$= 2EI_F/sa$$

EI_η = lateral bending stiffness of one I beam

a = distance between floor beams

ℓ = length of the bridge

EI_F = vertical bending stiffness of one floor beam

s = width of the bridge

distributed load $(\frac{1}{2}p\ell) = (7.5/\ell)\sqrt{EI_\eta \ C_0}$

and (b) for heavy through bridges

central point load $P_1 \approx (4h/\ell)\left(\pi^2 EI_T / 4\sqrt{EI_T \ a \ s}\right)$,

where h = height, at midspan, of the I beam

ℓ = length of the bridge

EI_T = lateral stiffness of the top flange, at midspan

a = distance between floor beams

δ = value of the virtual lateral displacement of the

top flange, under the action of a unit horizontal

force

$$\approx h_2^3/3EI_s \ + \ h_2^2 A/2EI_F$$
$$= k\left(h_2^2 A/2EI_F\right)$$

where h_2 = distance of the compression chord from the centroid

of the floor beam cross member

EI_s = lateral flexural stiffness of the side of the bridge

s = width of the bridge

k = the ratio of the total lateral movement of the top

flange of a through bridge (sustained by a unit

horizontal force applied at the top of the bridge)

to the magnitude of the lateral movement of the top

flange that results from the deformations of the

floor beam.

$$k_{crit} \ = 2(h_2/h)^2.$$

distributed load $(\frac{1}{2}p\ell) = (8h/\ell)\left(\pi^2 EI_T / 4\sqrt{EI_T \ a \ s}\right).$

The buckling loads corresponding to modes (a) and (b) are equal

when $k = k_{crit}$

DEFORMATIONS.

(a) light through bridges

The value of the rotation of the I beam at midspan, in the plane of the cross section, be calculated from the equation

$$\theta = 10^{-2} / \left[1 - \left((P_{LL} + P_{DL}/1.5)/P_1 \right)^2 \right]$$

where P_{LL} = live load applied to one I beam

P_{DL} = half the dead weight of the bridge.

A line of first yield be found by using the forces of the deformed shape

$$\theta = 1.75 \, \theta_{3=0} \left[\tfrac{1}{2}\pi - \pi_{3}/\ell - \omega \pi_{3}/\ell \right]$$

where z is measured along the bridge, from midspan. The load corresponding to first yield be taken as the load carrying capacity of the bridge.

(b) heavy through bridges.

The deformations of this type of bridge be taken as small.

The load carrying capacity be taken as the buckling load or the load to cause first yield, which ever is smaller.

LATERAL AND TORSIONAL LOADINGS

(a) light through bridges.

Lateral loadings (including wind) and loadings applied to the deck be considered as affecting the rotational and lateral deformations of the buckling mode of the bridge. A description of their effects is given in Chapter Four of this thesis.

(b) heavy through bridges.

Lateral loadings and loadings applied to the deck be considered as not affecting the rotational and lateral deformations of the buckling mode of the bridge. However, the strains induced by these loadings should be linearly added to the strains induced by the vertical loadings. (see Appendix H of this thesis) .

FORCES PRESENT AS THE BRIDGES DEFORM.

(a) light through bridges.

Floor beams should be designed to resist the vertical loading, together with the forces induced by the torsional deformation of the bridge. (The torsional moment at the I beam-floor junction is less than the moment given by the equation

$$M = 6EI_F \theta / \Delta \approx 0.2 EI_F / \Delta \ ),$$

Web stiffness should be proportioned to have greater stiffness than those used for an I beam with deformations in the plane of the web only. No allowance should be made for increases in buckling loads as a result of the stiffness effects.

(b)   heavy through bridges.

Vertical members designed to resist the bending of the I beams, together with the forces induced by the lateral bending of the top flange. (To allow for the lateral bending, the vertical members should be designed to resist, by a cantilever action, a lateral force F equal to 1% axial load in the top flange).

WORKING LOADS.

(a) light through bridges.

Working load = $\frac{1}{2}$ load to cause first yield (calculated by considering the deformations of the structure)

(b) heavy through bridge.

Working load = $\frac{1}{2}$ load to cause first yield, (assuming the structure does not deform) or

$\frac{1}{2}$ buckling load, which ever is least.

CHAPTER SIX

TORSION

6.1   Introduction

It has been shown in the previous chapters that after a

clear picture of the deformations of the structure is established,

the forces to sustain these deformations can be found easily.

However, in the case of twisted members with open or closed

cross section, other than circular or elliptical, no clear

picture of the deformations has been presented. An original

contribution to this subject is now presented to fill this

gap in our understanding of torsion problems. For coherence,

the early work is first summarized.

The method is to measure and describe the movement

of a line on the twisted member. Coulomb (Ref. 4) used

this approach and obtained the good approximation for a

twisted circular bar that plane sections perpendicular to the

longitudinal axis of the bar remained plane and that radii

in those cross sections remained straight. Later, Navier

used the same assumptions to describe the geometric

deformations within a bar of non circular cross-section

and poor estimates of the torsional stiffness of the

member were obtained. Improving estimates of the

deformations within twisted bars of cross-section other

than circular could not be found, and a more mathematical

approach was developed by St. Venant. (Ref. 57).

St. Venant noted that for a non-circular bar the

cross section did not remain plane and movements, or warping,

out of the plane perpendicular to the longitudinal axis,

were present. In the St. Venant approach, this warping

is specified by a warping function, ψ , and the equations

of statical equilibrium for the forces in the longitudinal direction
acting on an element, that is

$$\partial^2\psi/\partial x^2 + \partial^2\psi/\partial y^2 = 0, \tag{6.1}$$

and the boundary conditions that no external forces act on the
lateral surface of the bar, that is

$$(\partial\psi/\partial x - y)\, dy/ds - (\partial\psi/\partial y + x)\, dx/ds = 0 \tag{6.2}$$

are satisfied. In these equations x, y are the rectangular
coordinates in the plane of the undeformed cross-section and
s defines the arc length along the boundary. These two equations,
(6.1), (6.2) are of the same form as the differential equations
describing the purely membrane effects of a thin membrane and
this analogy has been used, together with associated soap film
measurements, as a means of obtaining a solution to the torsion
problem. However, as happens with analogies, a true picture of
the behaviour of the actual problem is often lost, and a
fundamental understanding of the overall geometrical and
statical action is not obtained.

In this chapter the torsional behaviour of some
structural sections is examined. The overall deformations
are measured and an an analysis using these measurements
(similar to the approach of Coloumb) is used. With this
approach it is possible to establish a picture of the
deformations, and as a result an original, simple and basic
view of the torsion problem is obtained.

6.2.1   First Simple Model

The first step in the inverse approach as outlined
in Chapter One is to load the strip with four balanced forces
and measure the surface shape of the strip. The surfaces are
found to deform (using the Ligtenberg moire technique,, Ref. 8)
such that lines of constant slope in the x, z directions are
straight to a first approximation, and are related by

$\partial w/\partial z = \text{constant}.$
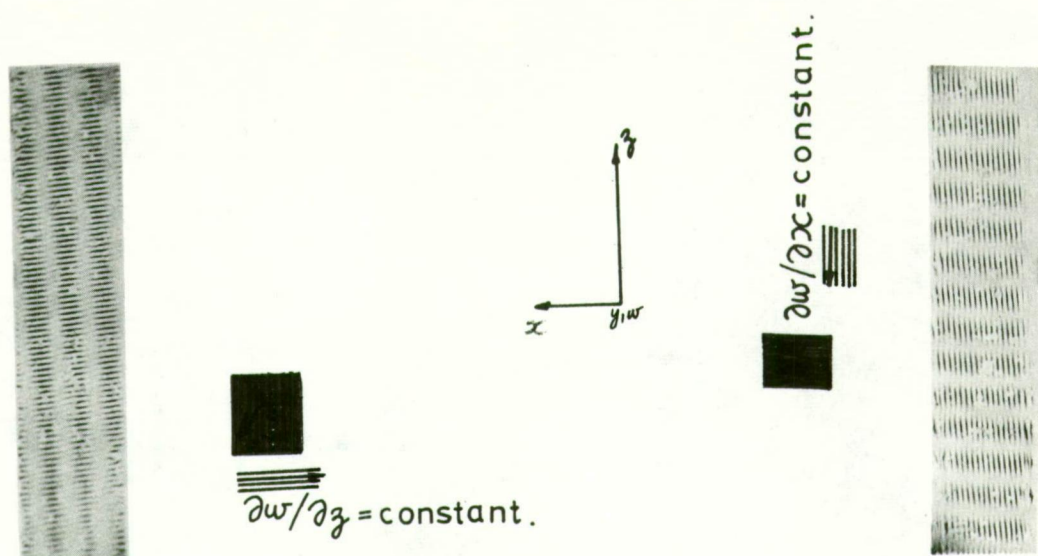
$\partial w/\partial x = \text{constant}.$

Fig. 6.1 Lines of constant slope on the surface of a twisted strip.

$\frac{1}{2}\gamma_s\,dz$

dz

top surface

$\frac{1}{2}t$

mid-plane

$\frac{1}{2}t$

$d\theta_{xy}$

Fig. 6.3b The mould, made from twisted strips, used in the manufacture of half deformed elements

$\frac{1}{2}\gamma_s$

bottom surface

$\frac{1}{2}\gamma_s$

Fig. 6.3a A deformed element.

$$\partial w/\partial x = kz \tag{6.3}$$

and
$$\partial w/\partial z = kx, \tag{6.4}$$

where w is the displacement parallel to the y axis as shown in Fig. 6.1. The closeness of these two relationships to the actual deformations can be seen by placing a straight edge perpendicular and parallel to the longitudinal axis of the twisted strip. When the straight edge is placed on the surface of the strip and is rotated it can be seen that the surface shape is anticlastic; that is, the principal curvatures are opposite in sign. An estimate of the relative magnitudes of these curvatures is obtained as follows. * Choose the axis of reference in the centre of the strip. Integrate equations (6.3), (6.4), originally obtained from the form of the moire fringe patterns. The shape is then given by

$$w = kx\, z. \tag{6.5}$$

Rotate the reference axes through forty five degrees to new axes x_1 , z_1 and the surface is then given by

$$w = \tfrac{1}{2}k(x_1^2 - z_1^2) \quad , \tag{6.6}$$

and thus the two prinicpal curvatures $\partial^2 w/\partial x_1^2$ and $\partial^2 w/\partial z_1^2$ are equal in magnitude but opposite in sign. The surface described by the equation (6.6) will be called a simple anticlastic surface.

The internal displacements are the next to be investigated. Observations of clear rubber models indicate that lines originally perpendicular to the midplane of the strip remain straight after deformation, but that the cross-section defined by these lines warps about the mid plane, as shown in Fig. 6.2.

---

* The magnitude of the curvatures can also be obtained directly from the Ligtenberg photographs, and a Mohr circle of curvatures.

(a)

(b)

Measured surface deformations

First approximation to the surface deformations
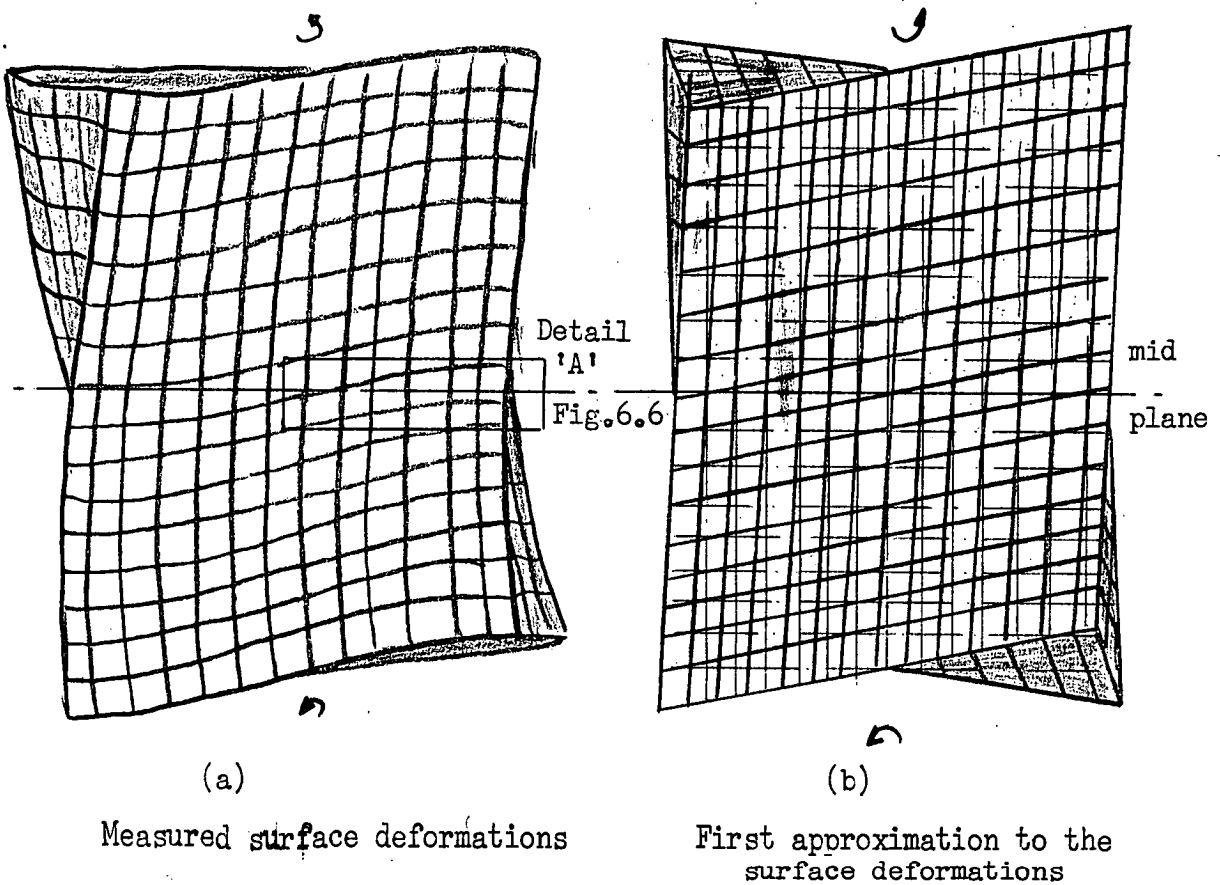
Fig. 6.2 Observations and Approximations to the Surface

Deformations of a Twisted Strip.

Plots of Mohr circles of strains, using the estimate for the surface displacements equation (6.6) and the estimate of straight lines through the model remaining straight after deformation, indicate that a rectangular element with sides parallel to the sides of the strip, deforms in a shearing manner. Various combinations of shearing deformations can be tried, but it is found that only elements with pure shearing deformations (Fig. 6.3) fit together and define a continuous surface.*

Thus, the twist of the strip can be obtained from the shape of the element. From Fig. 6.3a the twist in the xz plane K_{xz} is found from the twist of the sides of the element. Then

$$K_{xz} = d\theta_{xy}/dz = d\theta_{yz}/dx = \tfrac{1}{2}\gamma s/\tfrac{1}{2}t \quad , \tag{6.7}$$

---

* A simple means of performing the three dimensional integration required to fit the elements together, while still maintaining contact

TOP SURFACE

$\frac{1}{2}\gamma_s dz$

trans-lated

$\frac{1}{2}\gamma_s dz$

mid-plane

top surface

$\frac{1}{2}t d\theta_{xy}$

$\frac{1}{2}t$

translated

CROSS - SECTION

mid-plane

a   b   c
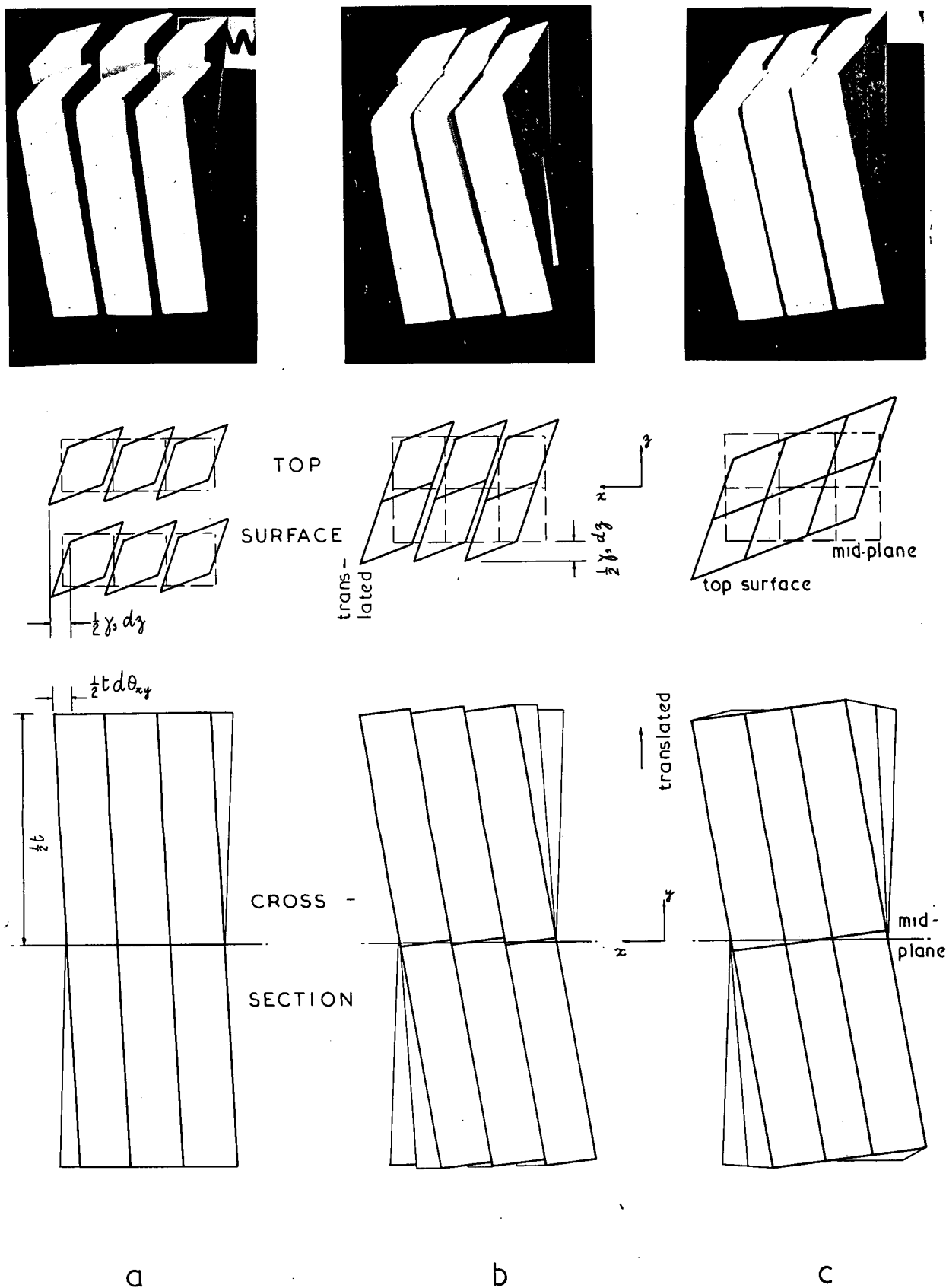
The half elements are stood upright with the midplanes resting on a flat surface representing the initial shape of the bar (Fig. 6.4a). Elements on the face, of width b, are rotated in the xy plane, relative to adjacent elements having the same z, (Fig. 6.4b), by an amount $d\theta_{xy} = \frac{1}{2}\gamma_s\,(dz/\frac{1}{2}t)$, where γ_s is the surface shear strain and t is the thickness of the plane, each element is then translated in the xz plane (Fig. 6.4b) to make all points on the face of width b alsmot continuous. Each element is then rotated in the yz plane, relative to adjacent elements with constant x (Fig. 6.4c), an amount $d\theta_{yz} = \frac{1}{2}\gamma_s\,(dx/\frac{1}{2}t)$, to remove the steps in the surface. It can be seen from the result of this integration (i.e. Fig.6.4c) that the functional form satisfies the geometric conditions of the simple anti-clastic surface, with all cross sections parallel to the sides of the strip being warped into a simple anticlastic surface. Thus the twisted strip itself is the same shape as the element.

Fig. 6.4

with the problem, is obtained by making several of these deformed

elements from plaster of paris (Fig. 6.3a and Fig. 6.3b) and

fitting them together mechanically and is shown in Fig. 6.4.

Half the element, representing the element from the

midplane to the top surface of the strip is easily made, as each

surface of the element is itself an anticlastic surface under the

geometric conditions of Fig. 6.3a. The mould is made by twisting

three metal strips of length $\frac{1}{2}t$, width dz($\dot{=}$ dx), to form three

sides which are then held at each end and the surface of the fourth

side is smoothed as the plaster of paris dries. (Fig. 6.3b).

---

where γs is the surface shear strain and t is the thickness of the

strip.

The stresses which will sustain the deformed elements as

shown in Fig. 6.3a are found from the stress-strain relationship

$\tau = G\gamma$, and by considering the overall equilibrium of the strip

the forces needed to sustain the specified deformations are found.

The only external forces required are two twisting moments, Fig.6.5,

the magnitudes of which are given by the equations

$$M_{xy} = (\tau_s \times \tfrac{1}{2}t \times \tfrac{1}{2}) \times (2t/3) \times b = (G\, t^3 b/6)(d\theta_{xy}/dz) \quad , \qquad (6.8)$$

and

$$M_{yz} = (\tau_s \times \tfrac{1}{2}t \times \tfrac{1}{2}) \times (2t/3) \times \ell = (G\, t^3\ell/6)(d\theta_{yz}/dx) \quad ,$$

and the twisting moments per unit length in each case is equal.

This set of twisting moments must be statically equivalent to the

applied force system, with

$$M_{xy}/b = M_{yz}/\ell = \tfrac{1}{2}\ F \quad , \qquad (6.9)$$

and thus the end torque Fb is given by

$$Fb \quad = Gt^3 b/3\ (d\theta_{xy}/dz) \quad ,$$

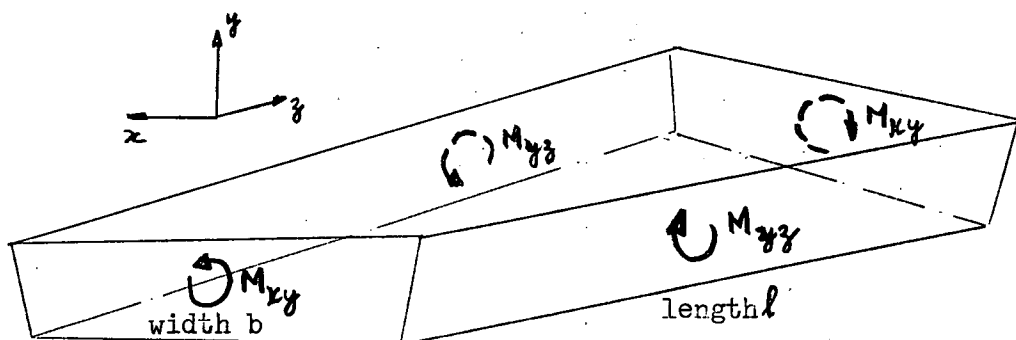the well known relationship for thin rectangular sections.

Fig. 6.5 Forces necessary to sustain the twisted strip.

In problems of torsion the torque is often applied by a series of couples at each end, with no twisting moments on the longitudinal sides of the section. This problem is considered in the next section.

6.2.2   Improvements in the Model for the Torsion of a Thin Rectangular Strip.

When a couple is applied at each end of a thin strip, and the surface geometry is measured, the lines of constant slope are again, to a good first estimate, straight. Measurements of the displacements of lines on the surface near the edges, indicates that these lines deform according to Fig. 6.2(a), and Fig. 6.6.
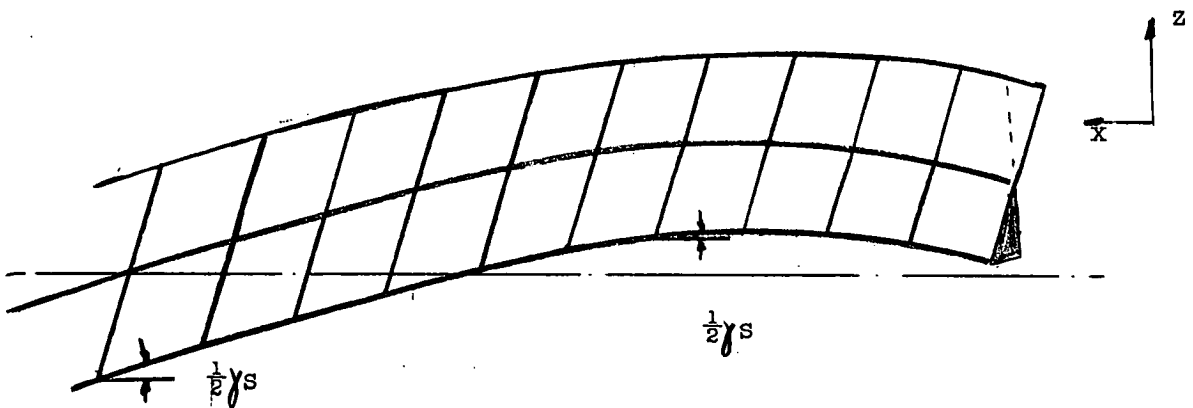
Fig. 6.6. Deformations of square elements on the surface of a twisted strip (see also Fig. 6.2a)

A geometric model of this behaviour is that away from the edges the deformed elements are the same as in the previous problem, but that near the edges the shear strains taper off from approximately one half thickness of the bar away from the edge and are zero at the edge. For this geometric model, the relative rotation of each cross section is similar to that used in the previous problem and thus the geometry is specified by the relationships $d\theta_{xy}/dz = \frac{1}{2}\gamma \, s/\frac{1}{2}t$, $d\theta_{yz}/dz = \frac{1}{2}\gamma \, s/\frac{1}{2}t$. As a means of producing the necessary change of shape of the elements near the edges, a second set of stresses, as shown in Fig. 6.7 must be applied, in a manner satisfying statical equilibrium of the elements in the z direction, that is

$$\partial \tau_{xz}/\partial x \; + \; \partial \tau_{yz}/\partial y = 0 \qquad\qquad (6.10)$$

Fig. 6.7. Deformations of the bar, and the forces

necessary to sustain these deformations.
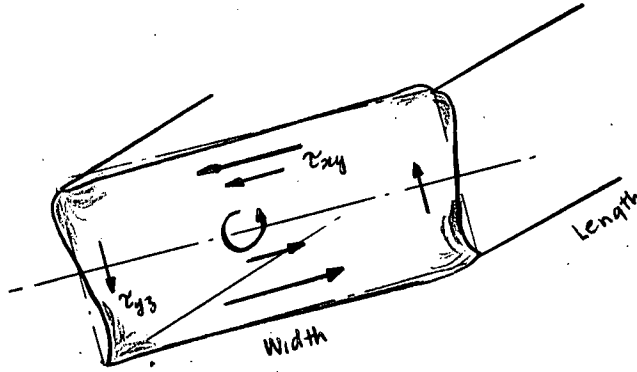
Overall statical equilibrium then gives the end torque as

$$T = \iint \tau_{xz} \, y \, dx \, dy \quad - \quad \iint \tau_{yz} \, x \, dx \, dy$$

and can be simplified (Ref. 57) to

$$T = 2 \iint \tau_{xz} \, y \, dx \, dy \quad , \tag{6.11}$$

when the integration is performed over the complete cross section, and the boundary conditions on shear stress are imposed.

This second set of stresses does not alter the overall geometry significantly, as the strains are localized near the corners, and thus the simple anticlastic surface shape of the surface geometry, and the shape given by Fig. 6.6 for the deformed shape through the thickness is sufficient to describe the geometric behaviour. The warped shape of the cross-section is again close to a simple anticlastic surface (Fig. 6.2a).

A reasonable estimate of the value of the integral $\iint_A \tau_{xy} \, y \, dx \, dy$ is obtained from the previous problem and

$$\tfrac{1}{2}T = \iint \tau_{xz} \, y \, dx \, dy = (G \, t^3 b/6) \, (d\theta_{xy}/dz) \quad . \tag{6.12}$$

The end torque twist relationship is again given by

$$T = (G \, t^3 b/3) \, d\theta_{xz}/dz \quad . \tag{6.13}$$

This model is now extended to describe the deformations within a split conduit, and the torsional stiffness of the conduit is estimated.

6.3   Torsion of a Split Conduit.

A means of describing the deformations of the split conduit, twisted in a manner such that the warping of the cross section is not restrained, is obtained by choosing an element similar in shape to the flat strip, but taking into account the curved nature of the surface (Fig. 6.8).
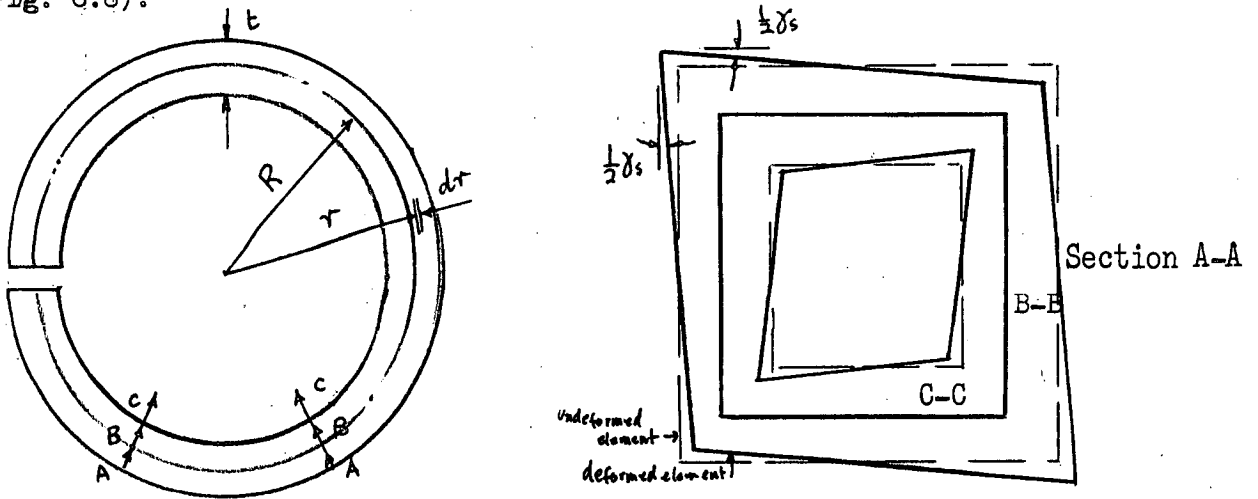
Fig. 6.8   Shear deformations of a split conduit.

Then, by specifying the deformed shape such that lines originally perpendicular to the midplane of the conduit remain straight after deformation, the shear strains are defined and are given by the equation

$$\tfrac{1}{2}\gamma = (r - R)\, d\theta_{xy}/dz \ , \tag{6.14}$$

where γ is the shear strain at any radius r,

r is the radius of the element,

and   R is the average radius of the ring.

As in the previous examples, the elements fit together, to a first approximation. The stress-strain relationships are then used to define the stresses, and the edge stresses are introduced in a similar manner to the previous example. The only force necessary to sustain the deformed shape is an end torque and is given approximately by the expression

$$T = \int_{R-\frac{1}{2}t}^{R+\frac{1}{2}t} (2\pi r t\, dr)\, r \ , \tag{6.15}$$

where the reference point used is the geometric centre of the ring, and
the effect of the edge stresses is neglected (Fig. 6.9). The equation
(6.15) can be simplified using equation (6.14) and the load deformation
relationship $\tau = G\gamma$, and becomes

$$T = G(2\pi R t^3/3) (d\theta_{xy}/dz) , \qquad (6.16)$$

once again the well known relationship (Ref. 57).
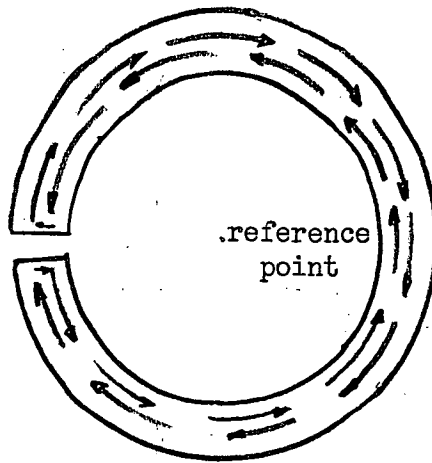
Fig. 6.9. Reference Point, and shear stresses.

Similar results can be obtained for any thin strip, by specifying
the geometric conditions that the midplane remains twisted only,
straight lines originally perpendicular to the midplane remain
straight after deformation, and an element of the same shape as
the strip deforms in a condition of shearing strain.

6.4   Torsion of Rectangular Bars.

6.4.1. Solid Rectangular Bars.

This foregoing model for the thin strip can be extended to
describe the behaviour of rectangular bars of any proportions.
From the previous model it was seen that there were two distinct
strain distributions, only one of which contributed to the end
rotation, as the other was localized at the edges. However, as
the difference between side dimensions of the rectangular section
decreases, the contribution to the rotation of the both shear strain

distributions must be included in order to obtain a model which describes rectangular bars more generally.

In the improved model the twist of the section $d\theta_{end}/dz$ is determined from the addition of the twist resulting from the shear strain distribution in the xz plane, that is $d\theta_{xy}/dz$, to the shear strain distribution in the yz plane, that is $d\theta'_{xy}/dz$ (Fig. 6.10). The total twist is then given by the equation

$$d\theta_{end}/dz = d\theta_{xy}/dz + d\theta'_{xy}/dz$$
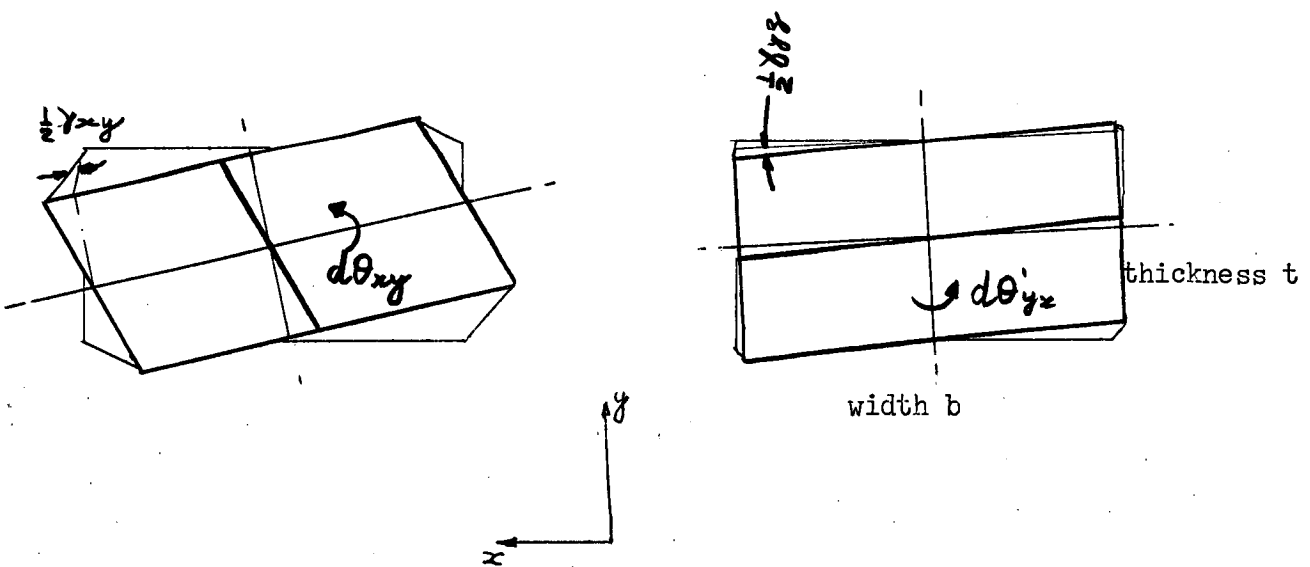
Fig. 6.10. Shear strains, and resulting rotations, for a rectangular bar. (Also see Fig. 6.12a)

It was also seen from the previous model that a general result for any bar under torsion that was sustained by two orthogonal stress distributions, subject to the boundary conditions that the lateral surfaces are free from external forces, is that these two distributions contribute equally to the total torque. Then in the rectangular bar a slight overestimate of the torque twist properties can be obtained by linearizing the two separate stress distributions and superimposing them. (Fig. 6.11).
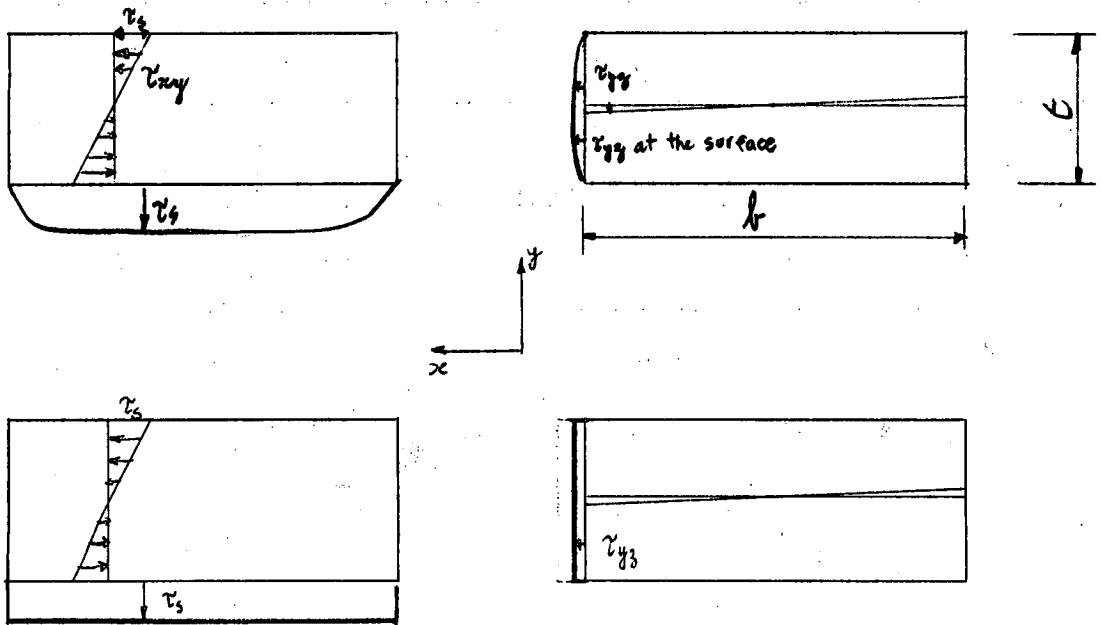
Fig. 6.11. Linearization of the Two Stress Distributions.

Under this simplification the torque is given by the equation

$$\text{Torque} = G\, t^3 b/6 \; (d\theta_{xy}/dz) + Gb^3 t/6 \; (d\theta'_{xy}/dz) \qquad (6.17)$$

and thus $(d\theta_{xy}/dz)t^2 = (d\theta'_{xy}/dz)b^2$. $\qquad (6.18)$

The rotation of one end relative to the other is defined by

$$d\theta_{end}/dz = d\theta_{xy}/dz \; (1 + (t^2/b^2)) \, , \qquad (6.19)$$

with the warped cross-section consisting of two superimposed anticlastic surfaces.

Under these conditions the torque twist relationship at the end is

$$T = Gt^3 b/3 \; (d\theta_{end}/dz) \; / \; (1 + (t^2/b^2)) \; . \qquad (6.20)$$

A table of values (Table 6.1) shows that the mathematical model, as developed by St. Venant (Ref. 57), and this model, derived from geometric functional form, agree closely, with the greatest difference of 15%, at $b/t = 1.0$.

b/t		1.0	2.0	3.0	4.0	5.0	10.0	∞
$1/3 \, (1+(t^2/b^2) \,)$		.167	.267	.30	.314	.32	.33	.333
St. Venant		.1406	.229	.263	.281	.291	.312	.333

Table 6.1. Comparisons of torsional stiffness between

St. Venant expression and the solution 6.20.

The reason for the difference is seen when an examination is made
of the specified deformations. The warping of the cross section is taken
as being separable into two distinct simple anticlastic surfaces (Fig. 6.12)
corresponding to the two sets of shear strains. The super-position of
these warped cross sections then determine a final warped cross section,
as shown in Fig. 6.12. As the ratio of the width of the bar to the
thickness of the bar is decreased the surface resulting from the super-
position of the two anticlastic surfaces tends towards a plane section.
In the limit, when the width of the bar is equal to its thickness, the
geometric model specifies that plane sections remain plane. Navier
assumed that when a square bar was twisted, plane sections remained
plane, but he also used a strain distribution which increased linearly
with the distance from the centroid of the bar. In the model proposed
in this thesis, the strain distributions increase linearly with the
perpendicular distance from one principal axis of bar. Measurements
indicate that this specification is not a good estimation near the
corners of the square. Therefore the next step in the successive
improvement of the model is to use a better estimate of the geometric
functional form to satisfy the measured geometry near corners (Fig. 6.6)
and from this new form to recalculate the statical actions. However,
as a reasonable estimate of the behaviour has been obtained, the process
is terminated at this stage.
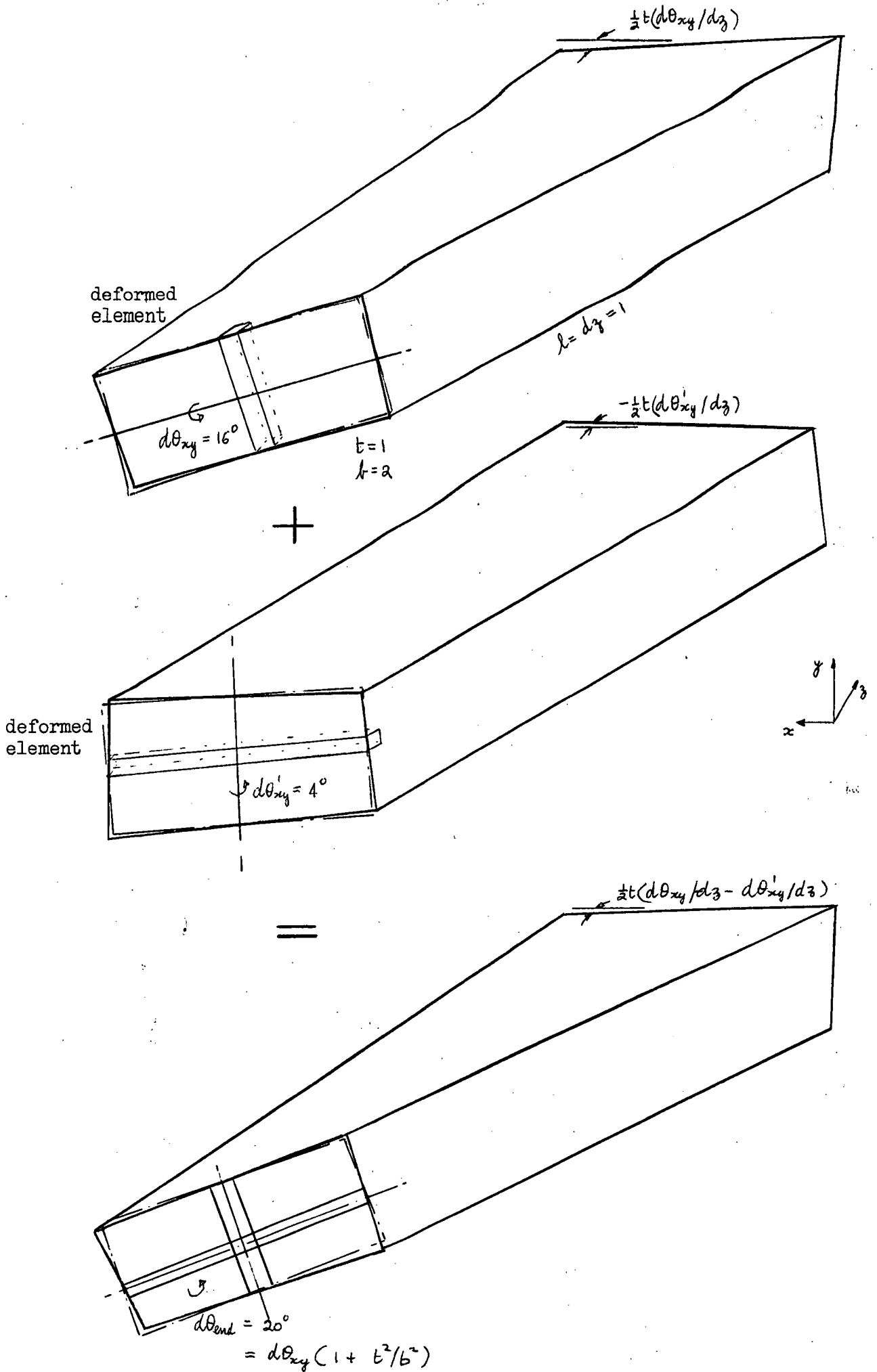
Fig. 6.12a. Combinations of the orthogonal strain distributions for a rectangular
section width b = 2, thickness t = 1. (A valuable comparison is
obtained by comparing this shape with the actual deformed shape of
a rectangular bar b = 2, t = 0.25, in Fig. 6.2a, and a square bar
in Fig. 6.12b).

$\frac{1}{2} t \, d\theta_{xy}/dz$

$d\theta_{xy} = 16°$

deformed element

$-\frac{1}{2} t \, d\theta'_{xy}/dz$

deformed element

plane sections

remain plane

$d\theta'_{xy} = 16°$

$d\theta_{end} = 32°$
$= d\theta_{xy} + d\theta'_{xy}$
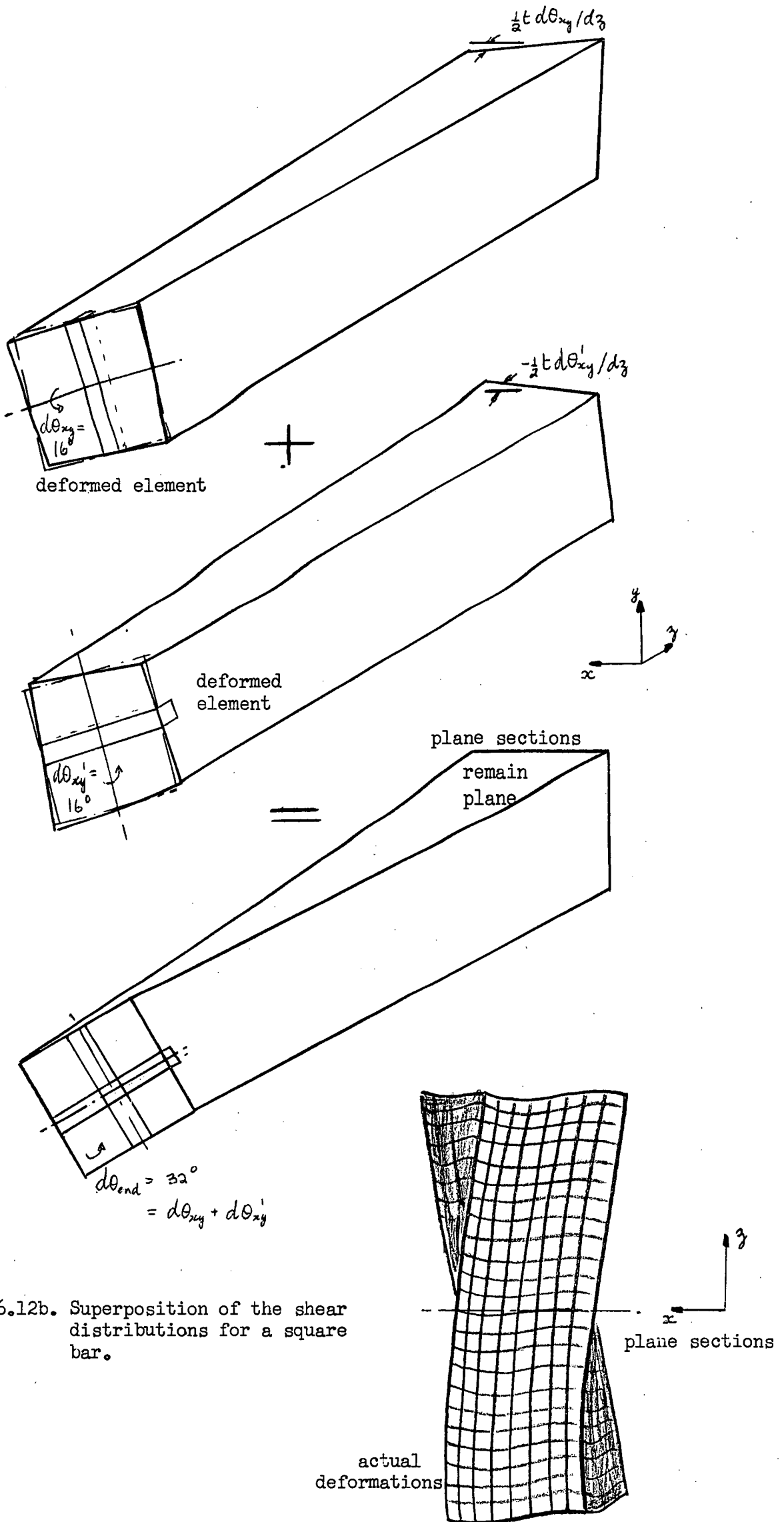
Fig. 6.12b. Superposition of the shear
distributions for a square
bar.

plane sections

actual
deformations

6.4.2 Hollow Rectangular Bars

A simple model describing the behaviour of hollow rectangular bars is obtained as an extension of the previous model for the solid bar.

Measurements of the surface shape indicate that the simple anticlastic surface, with equal but opposite principal curvatures, is again a reasonable approximation. Also, lines on the surface of the bars deform in a manner which is similar to the solid rectangular bar of the same external dimensions. A good first model is obtained by approximating the form of the deformations of the hollow bar as being similar to the deformations of the solid bar.

Then, the twist and shear strains are linked, as before, by the equations

$$d\theta_{xy}/dz = \tfrac{1}{2}\gamma s/\tfrac{1}{2}t \; ,$$

$$d\theta'_{xy}/dz = \tfrac{1}{2}\gamma s/\tfrac{1}{2}b \; ,$$

(6.21)

and
$$d\theta_{end}/dz = d\theta_{xy}/dz + d\theta'_{xy}/dz \; .$$
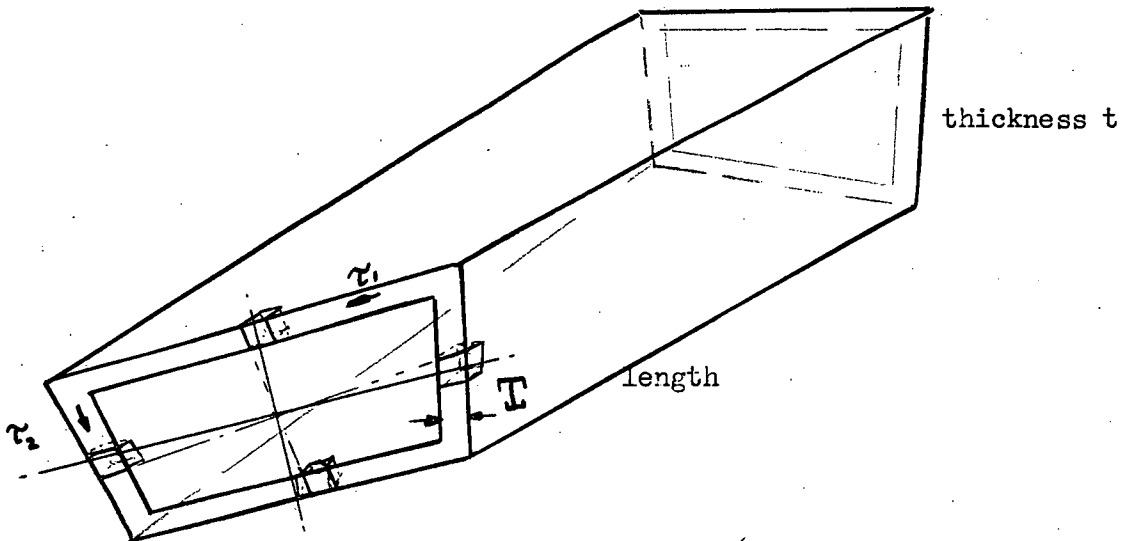

Fig. 6.13 Twisting Deformations of a Hollow Rectangular Bar.

The forces necessary to sustain the deformed shape are easily found For the hollow thin section of thickness T, (T/t is small) the shear stresses necessary to sustain the shapes shown in Fig. 6.13 are approximately constant. Therefore, the total torque is found from the contributions of the two shear distributions and

$$T = (\gamma_1 \Bbb{I} b) t + (\gamma_2 \Bbb{I} t) b. \qquad (6.22)$$

When we assume that the two contributions to the torque are equal (as was the case with the solid rectangular bar), then the two shear stresses γ_1 and γ_2 are equal. Substituting the load deformation relationship $\tau = G \gamma$ into equation (6.21) we then obtain the relationship between the two contributions to the total end rotation $d\theta_{end}/dz$, and

$$t(d\theta_{xy}/dz) = b(d\theta_{xy}'/dz)$$

$$d\theta_{end}/dz = (1 + t/b)(d\theta_{xy}/dz) \quad . \qquad (6.23)$$

The total torque is then

$$T = 2\tau \Bbb{I} bt$$

$$= G \Bbb{I} bt^2 (d\theta_{xy}/dz)$$

and from equation (6.23)

$$T = G \Bbb{I} bt^2 (d\theta_{end}/dz) /(1 + t/b) \quad . \qquad (6.24)$$

This approximation is close to measured results, and is identical with the usual approximation obtained by using a shear flow analysis (Ref. 57). The advantage of the foregoing method is that it provides a visual picture of the deformations.

6.5 Large Torsion of Sections: All stresses elastic.

6.5.1 Introduction

A further understanding of the geometric deformations of a twisted strip is obtained by examining the deformed member when large twists are applied.

When large twists are applied to an open cross section member, and the ends of the member are unrestrained against warping, the member

shortens and the longitudinal fibres that were straight before the member was twisted, distort into helices. An axis common to these helices can be found, and this axis has been defined by Ashwell (Ref. 58) as the distortion axis.

The properties of this axis can be seen by examining the behaviour of a circular section.

6,5.2 The Circular Section.

The shortening effect was first observed in 1807 by Thomas Young (Ref. 57), who noted that when circular bars were twisted, the applied torque was balanced mainly by shear stresses, but that an additional resistance to torque, proportional to the cube of the angle of twist, was furnished by the longitudinal stresses in the fibres, which were assumed to bend into helices.
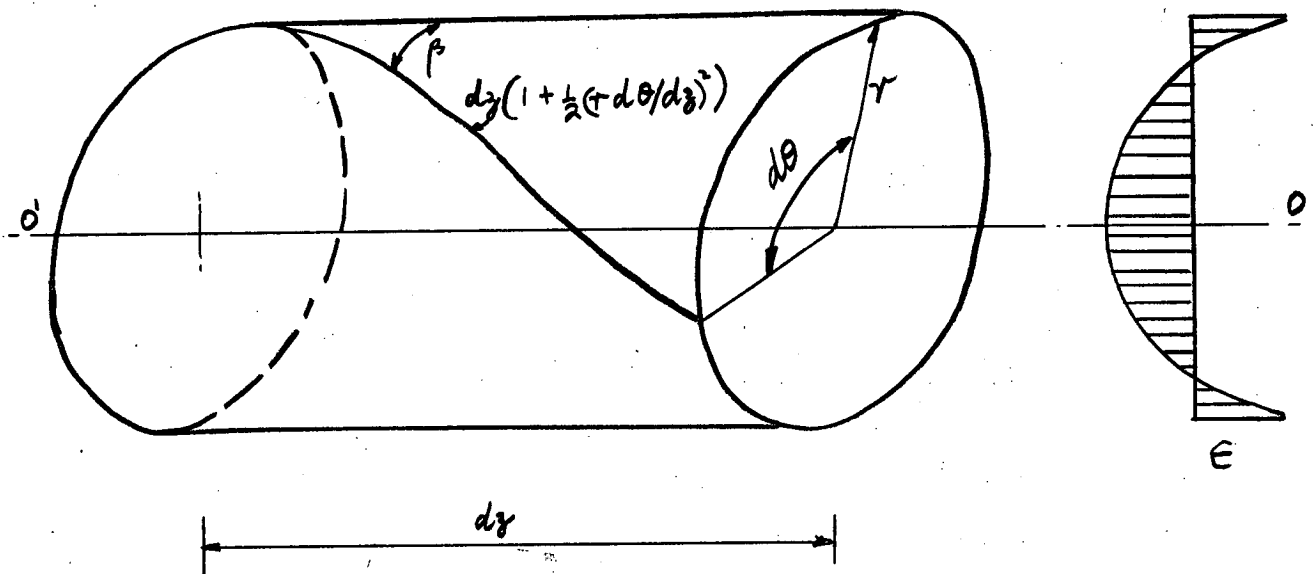

Fig. 6.14. Twisting Deformations of a Circular Bar.

The geometric mechanism is seen in Fig. 6.14. Plane sections, originally perpendicular to the longitudinal axis OO' are assumed to remain plane, while the cross sections rotate relative to each other. The axis OO' is assumed to remain straight, but allowed to shorten.

The longitudinal strains, measured relative to this axis OO' are given by the equation

$$\epsilon_z - \epsilon_{oo'} = \tfrac{1}{2}(r\, d\theta/dz)^2 - \tfrac{1}{8}(r\, d\theta/dz)^4 + \cdots \qquad (6.25)$$

where $\epsilon_{oo'}$ and ϵ_z are the longitudinal strains at O, and at z respectively. When the value of $(r\, d\theta/dz)$ is small, a good approximation for equation (6.25) is

$$\epsilon_z - \epsilon_{oo'} = \tfrac{1}{2}(r\, d\theta/dz)^2.$$

The stresses at any distance from OO' are found from equation (6.25) and the stress strain relationship, $f = E\epsilon$, where E is Young's modulus. In this formulation, the resistance to lateral contraction is assumed to be small. This approximation is reasonable when the cross section is open or closed and hollow. For a solid section the differential lateral contractions have a more pronounced effect, but this effect is not considered in this thesis.

Integration of the required stress pattern determines the forces necessary to sustain the deformed shape. As no resultant axial force is applied, the constant $\epsilon_{oo'}$ is given by the equation

$$\epsilon_{oo'} = -\tfrac{1}{2}(d\theta/dz)^2\, I_p/A \quad , \qquad (6.26)$$

where I_p is the polar second moment of area and A is the area of the bar. The total torque resisted by the section is given by the equation

$$T = GJ(d\theta/dz) + \tfrac{1}{2}(d\theta/dz)^2 \int_A E(r^2 - I_p/a)r\, dA \sin\beta \qquad (6.28)$$

and simplifies to

$$T = GJ(d\theta/dz) + \tfrac{1}{2}(d\theta/dz)^3 E\ (H_p - I_p^2/A) \qquad (6.29)$$

when $H_p = \int_A r^4\, dA$

and $\sin\beta = r\, d\theta/dz$.

6.5.3 Sections Built up from Flat Strips.

Buckley (Ref. 59) extended the above analysis to describe the behaviour of flat strips. Weber (Ref. 60) added a further extension for the description of doubly symmetric sections. Both authors take the centroidal axis as axis of reference and this line is assumed to remain straight.

However, for singly symmetric sections the best choice of an axis of reference is more difficult. Weber (Ref. 60), Cullimore (Ref. 61), Ashwell (Ref. 62), and Gregory (Ref. 63 and 64) have proposed various models. These models are examined using an equal sided angle section as an example.

Weber assumed that there existed one longitudinal line which remained straight, relative to the deformed member. (Fig. 6.15). When the lines AS, A'S, BS, B'S', are taken as remaining straight, the longitudinal strains can be found. Denoting the co-ordinates of the line WW' by x, y, the longitudinal strains, measured relative to the line WW' are given by

$$\epsilon_z - \epsilon_{ww'} = \tfrac{1}{2}(r_w d\theta/dz)^2,$$

$$(6.30)$$

where r_w is the perpendicular distance from the line WW' to the point z on the section.
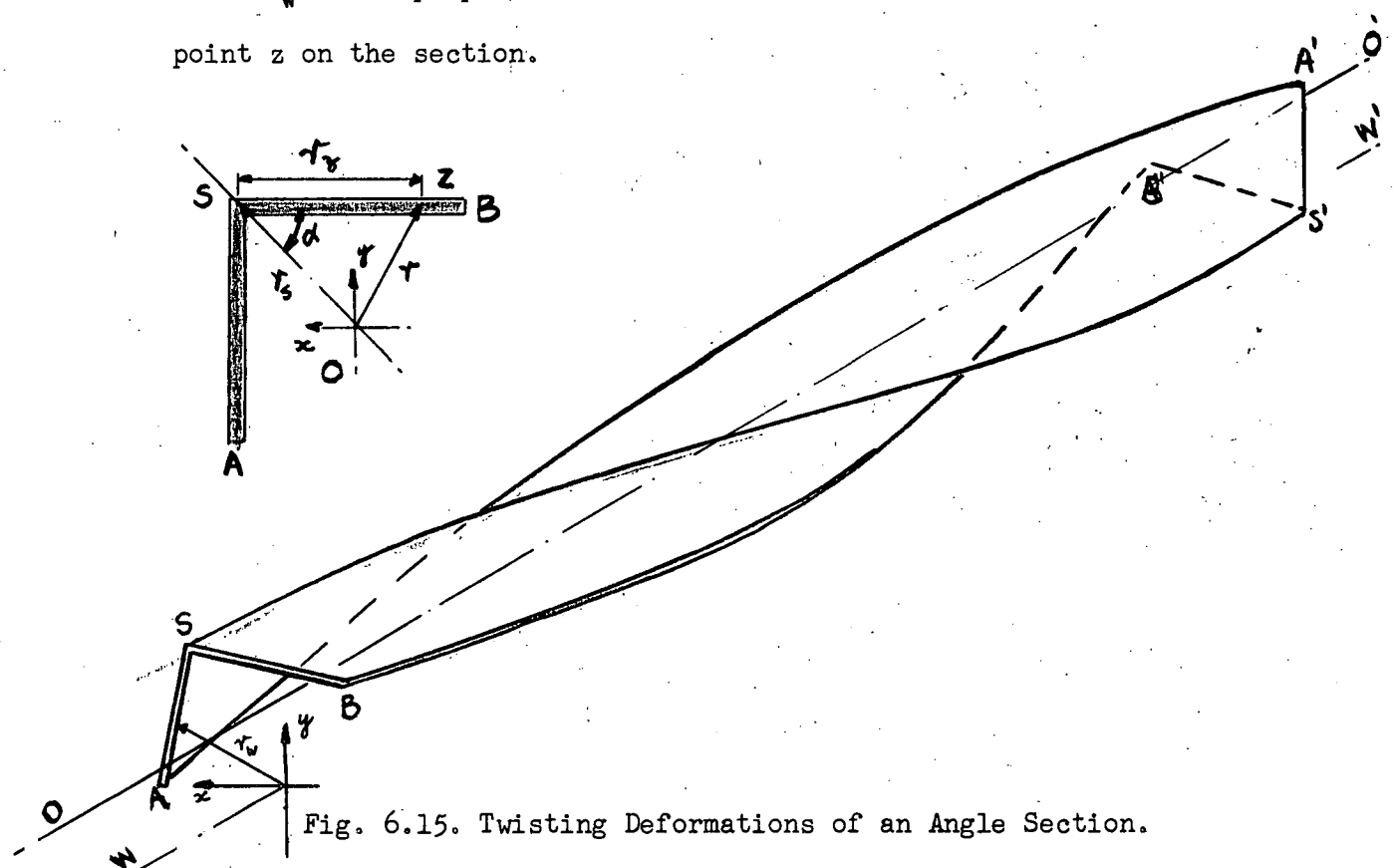

Fig. 6.15. Twisting Deformations of an Angle Section.

In the Weber model, the position of the straight line WW' is moved until a point is found for which no bending moments and axial force need be applied to the section to sustain the deformed shape.

Cullimore (Ref. 61) used the equation (6.30), and the co-ordinates x, y were moved until a potential energy integral was minimised. This minimization can be shown to be equivalent to satisfying the corresponding equations of statics (Ref. 65). The equations of statics satisfied by Cullimore are the conditions of zero bending moments.

Ashwell (Ref. 62) observed the behaviour of a twisted strip arranged as a cantilever, and noticed that points on the free end of the cantilever moved laterally and vertically. Measurements were made of these deflections, and described in terms of the longitudinal fibres twisting into a helices with a common axis. Ashwell considered much larger displacements than previous authors and showed that the magnitude of the twist and the ratio of the bending stiffness to torsional stiffness affect the position of the distortion axis. Ashwell arrives at this conclusion after carrying out an analysis which uses as reference axis the deformed centroidal axis. The position of the straight distortion axis is then determined as a calculated distance from the centroidal axis.

Gregory (Ref. 63 and 64) concluded that longitudinal lines must bend relative to each other when the section is twisted. The axis of reference was taken at the corner of the legs, (Fig. 6.15), and, to allow for the bending of the longitudinal lines, the longitudinal strains were specified by the equation

$$\epsilon_z - \epsilon_{ss'} = \frac{1}{2}(r_z \, d\theta/d_3)^2 + d\,r_z, \qquad (6.31)$$

where d is a constant to be determined. The constants $\epsilon_{ss'}$ and d were again determined from the overall statical condition that neither axial forces nor bending moments were applied.

Gregory wrongly criticizes Weber, Cullimore, and Ashwell for not including this bending strain in their mathematical models. He did not realize that the bending of a member could be combined with twist about some assumed axis to produce twist (without bending) about a different axis. Gregory was mistaken, and the results obtained by Weber, Cullimore, Ashwell and Gregory are all identical, as can be seen by the following example, (also Ref. 66 and 67).

Consider the angle, (Fig. 6.15) with the axis OO' defining the distortion axis. The longitudinal strains at the points z, s with the axis OO' as reference are

$$\epsilon_z - \epsilon_{oo'} = \tfrac{1}{2}(r \, d\theta/dz)^2, \tag{6.32}$$

and

$$\epsilon_{ss'} - \epsilon_{oo'} = \tfrac{1}{2}(r_o \, d\theta/dz)^2. \tag{6.33}$$

The difference between the strain at point z, and the strain at point s, is obtained from the difference of equations (6.32), (6.33) and the use of the cosine rule in triangle osz. Then

$$\epsilon_z - \epsilon_{ss'} = \tfrac{1}{2}(r_z \, d\theta/dz)^2 - r_o r_z \cos\alpha \, (d\theta/dz)^2. \tag{6.34}$$

Equation (6.34) is similar to Equation (6.31), when the constant d is evaluated, and Gregory's method therefore gives similar results to those obtained by Weber.

6.5.4 The Axis of Distortion and the Shear Centre

The axis of distortion is defined by Ashwell (Ref. 58) as the axis which co-incides with the longitudinal fibre, inside or outside the section, which does not distort into a helix, but remains straight when the bar is twisted. This axis should not be confused with the axis of displacement (as defined by Ashwell) or the shear centre axis. The axis of displacement of a prismatic elastic cantilever, built in at a support at one end and twisted

by a torque at the other, is the axis about which the cross sections of

the cantilever rotate in their planes relatively to the support;

while the shear centre axis of a prismatic elastic cantilever, built in

at a support at one end and bent by a load at the other, is the axis

through which the load must be applied in order that the cross sections

do not rotate.

As has been shown previously, the axis of distortion for a twisted

section, with warping of the cross section completely unrestrained, is

found by considering the effect of non linear geometric deformations.

However, the axis of displacement and the shear centre axis are

based on essentially linear ideas. Therefore the existence of a reciprocity

is possible. A reciprocity does exist when the linear terms dominate, and

is outlined by the well known Maxwell Reciprocal Theorem (Biezeno and

Grammel Ref. 44), i.e. if the cantilever is loaded through the shear

centre the cross section does not rotate or if the cantilever is twisted

there exists an axis about which the cross sections of the cantilever

rotate in their planes relative to the support (i.e. does not move).

This reciprocity has been the subject of investigations for many authors

including Duncan, Ellis, and Scrutton (Ref. 68), Lockwook Taylor (Ref.69),

Hoff (Ref. 70) and Ashwell (Ref. 58). It is not proposed to detail their

work, but a short tabulation of the similarities which give rise to the

reciprocity is given to outline the basic ideas. *

---

* It would appear that there exists a linear differential equation which

describes the behaviour of an open section which is twisted and bent.

This differential equation, and associated boundary conditions is

possibly self adjoint, as the reciprocity is only another way of showing

this condition. At present however, the nature of this differential

equation appears illusive.

Shear strains, and hence stresses calculated by assuming that plane sections originally perpendicular to the longitudinal axis remain plane.

Warping and hence longitudinal stresses calculated by assuming lines originally perpendicular to longitudinal axis remain straight.

For a channel

Assume a point exists such that when loaded through the point, the section goes straight down.

Assume a point exists which does not move. Draw the relative warping between the ends.
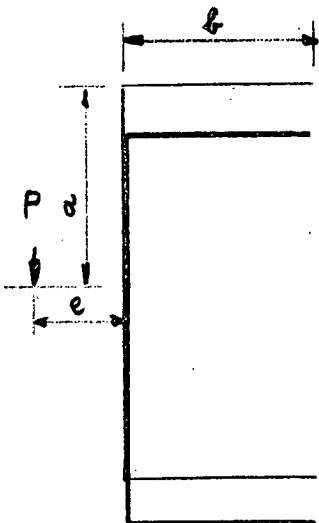
change of warping per unit length

$$\propto d^2\theta/dz^2$$

curvature

$$\propto e \, d^2\theta/dz^2$$
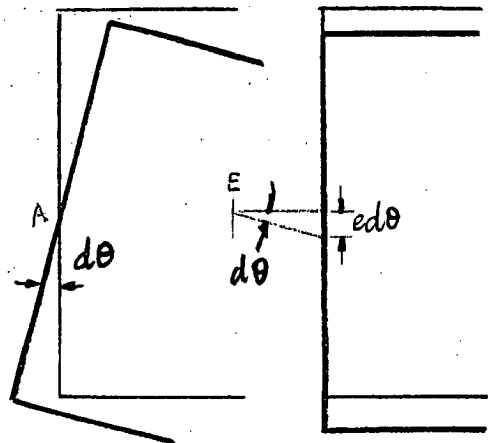
rotating about A

Point of zero movement moved from A to E

shear stresses

longitudinal stresses
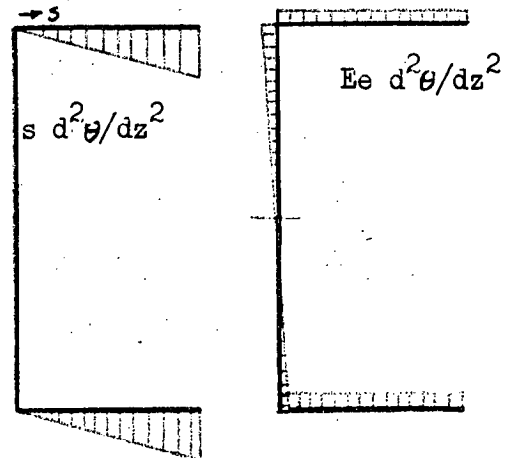
$$s \, d^2\theta/dz^2$$

$$Ee \, d^2\theta/dz^2$$

$$T = 0 = Pe - Pa \int_0^\ell s \, ds / I_{xx}$$

$$M = 0 = (d^2\theta/dz^2)\int_0^\ell s \, ds + e(d^2\theta/dz^2) I_{xx}$$

Clearly no twisted section satisfies either the conditions of completely unrestrained warping (i.e. giving rise to an axis of distortion) or of complete restraint of warping at one end (i.e. giving rise to an axis of displacement). Thus, when any section is twisted, it will depend on the relative magnitudes of the non linear geometric deformations and the manner in which the warping changes, as to the way in which the section deforms. Similarly, when any section is bent, the non linear geometric deformations will determine the way in which the section deforms. Consider the behaviour of an angle section and a channel section, both arranged as built in cantilevers.
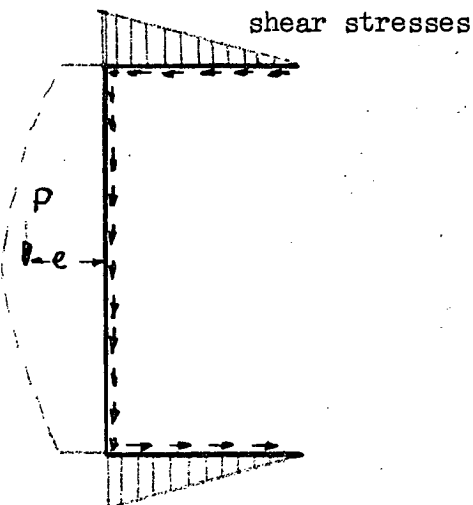
The twisted angle member deforms so that lines perpendicular to the longitudinal axis remain straight. Hence, as only one plane is defined by these two lines, little primary warping exists; (there is a small amount of warping across the thickness of the leg). Therefore, the angle member arranged as a built in cantilever, and twisted, deforms so that non-linear shortenings are important and an axis of distortion is soon defined. This axis is not in the same position as the shear centre as the linearity has been lost, and therefore reciprocity does not hold.

The twisted channel section deforms with a large primary warping. When arranged as a built in cantilever the resistance of this warping by the support gives rise to comparatively large warping stresses, compared to the stresses arising from the longitudinal shortening stresses. Therefore the channel section deforms so that an axis of displacement is defined. Since the linear twisting deformations are dominant, then the reciprocal theorem is a good estimate of the behaviour, and hence the shear centre is in the same position as the axis of displacement.

From the tabulation it is seen that the shear centre and the axis of distortion are section properties. However, the nature of the warping restraint is important in determining the relative importance of the linear and non linear terms. The general influence

of boundary conditions, and of warping restraints introduced along the member, is at present unanswered. However, when warping restraints are introduced along the member, the shear centre and axis of distortion move. For example, when the length of the split of a split conduit is gradually decreased (by welding adjacent sides of the split together) the axis of distortion and shear centre both move towards the centroid of the section; when the split is covered in, and a closed hollow circular section is obtained, the centroid coincides with the shear centre and the axis of distortion.

6.6 Large Torsion of Sections, with Plastic stresses.

6.6.1 Introduction

The previous section illustrates that the distortion axis is an important sectional property for twisted members.

To find the position of the distortion axis for a large range of sections, the author has found that it is unnecessary to solve algebraically the conditions of no axial load and no applied bending moment, as a particular symmetry about the distortion axis can be used.

Consider again the angle section. The longitudinal stresses resulting from the longitudinal strain pattern have no stress resultants. By taking moments about each leg in turn, it is seen that the resultant moments on each leg must be zero. For zero resultant moment on each leg, there must exist points of no longitudinal stress nor strain. These points of longitudinal strain are on a circle, of radius R, as found from equation (6.32) by equating ϵ_z to zero, and the radius is then given by the equation

$$R = \sqrt{2\epsilon_{oo}} \, / (d\theta/dz) \qquad \bullet \qquad (6.35)$$

By the particular symmetry of the angle section, these points of zero longitudinal strain must be equally spaced about the perpendicular bisectors of the leg, and hence the position of the

distortion axis is at the junction of the two perpendicular bisectors of the legs of the angle. Similarly for the equal sided channel, the distortion axis is at the junction of the perpendicular bisectors of the sides.

The approach developed above is useful to describe the behaviour of an open cross section member once the material yields.

The yielding is an interaction between the longitudinal strains and the St. Venant torsional shear strains. Certain approximations are made in order to obtain a quick and reasonable formulation of the problem. The approximation is made that the stress strain relationship of combined compression and shear is similar to the stress strain relationship in combined tension and shear. The approximation is also made that under conditions of full plasticity the average of the longutidinal stresses across the thickness of the section is constant, in all parts of the member and is independant of the longitudinal or shearing strains. *

---

* The following comment was contributed by the Reviewer of the author's paper "The Axis of Distortion, accepted for publication by the International Journal of Mechanical Sciences."

"The yielding is due to both the longitudinal stresses f_z and the St. Venant - type shear stresses q. Let a small increment of twist produce, at a point in the member, increments of longitudinal strain $\delta\epsilon_z$ and shear strain $\delta\gamma$. Then, by assuming all stresses zero expect f_z and q, it can be deduced from the Tresca yield condition and the Levy-Mises flow rule, that

$$ f_z = \frac{6\,q_p\,\delta\epsilon_z}{\sqrt{9\,\delta\epsilon_z^2 + 4\,\delta\gamma^2}} $$

where q_p is the shear stress to produce yield. As the twist increases into the range of plastic behaviour, it can be expected that the strains (which are proportional to the square of the twist) will greatly exceed the strains (which are proportional to the twist). Thus, except close to the positions of zero ϵ_z,

$$ \delta\epsilon_z \gg \delta\gamma $$

and hence

$$ f_z \approx \pm 2\,q_p $$

where the sign is the same as the local sign of ϵ_z ".
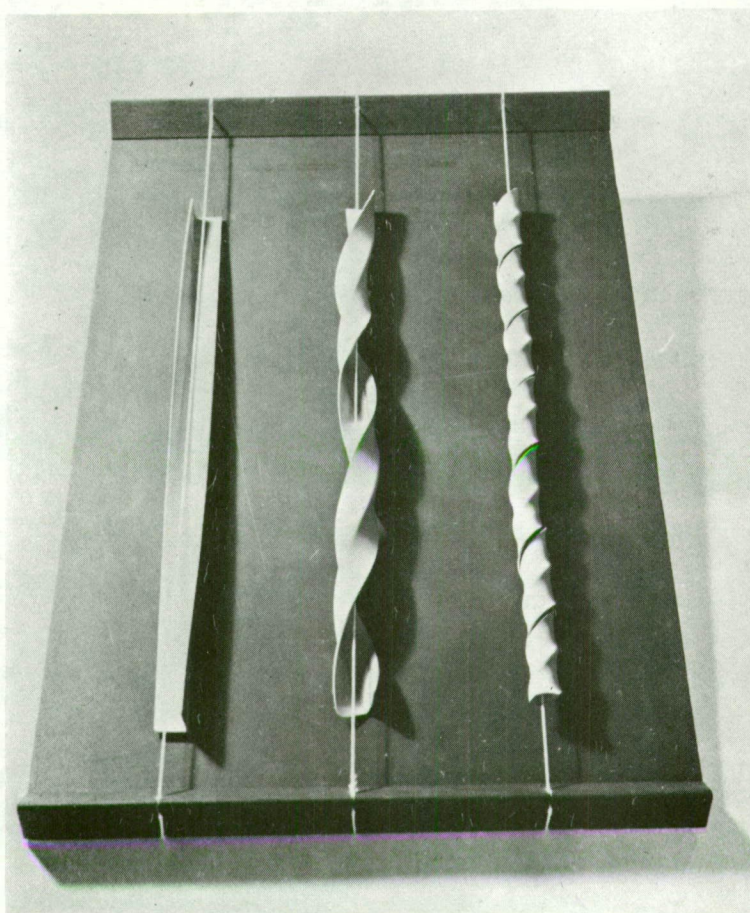
Fig 6.16 Twisted angle sections. The position of the axis of distortion is indicated by the white string.
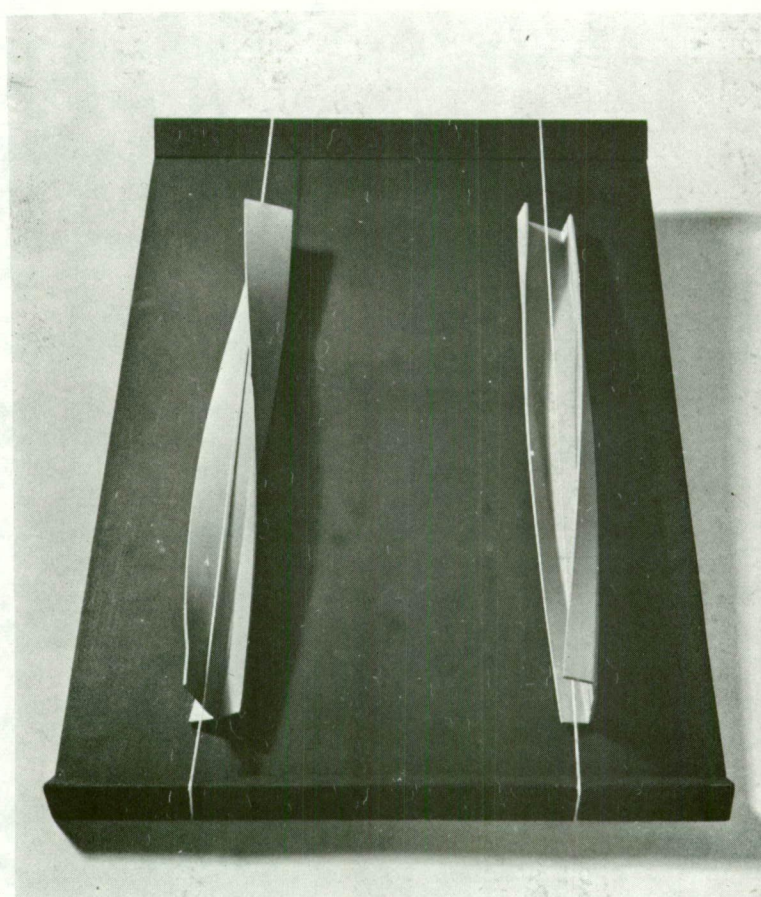
Fig. 6.18c. Other twisted sections, showing the position of the axis of plastic distortion.

Further, the geometric approximations made are that the value of
the longitudinal shortening of the member ($\epsilon_{oo'}$) and the warping of the
member measured relative to the plane perpendicular to the distortion
axis (rdθ/dz) are small when compared with unity.

From experimental observations, it appears that over a large
range of twist, longitudinal lines drawn on the surface of open cross
section members deform into helices. In Fig.(6.16), for example
the permanent twist deformation of an aluminium angle section is
shown.

When the existence of a distortion axis is postulated,
the points of zero strain must be equally spaced about the
perpendicular bisectors of the legs of the angle as this statement
is consistent with a distribution of longitudinal stresses
satisfying the conditions of zero bending moment and zero axial
force, (Fig. 6.17). The positions of the points of no longitudinal
strain are shown in Fig. 6.17 for the assumed plastic stress
distribution.

a elastic
b elastic plastic
c plastic

locus of points
of zero longitudinal strain

longitudinal strains   longitudinal stresses

Fig. 6.17. Longitudinal strains and Stresses, for a Twisted
angle section.

The mathematical model outlined above indicates that the axis of distortion remains in the same position relative to the section for all values of twist through the elastic range and until full plast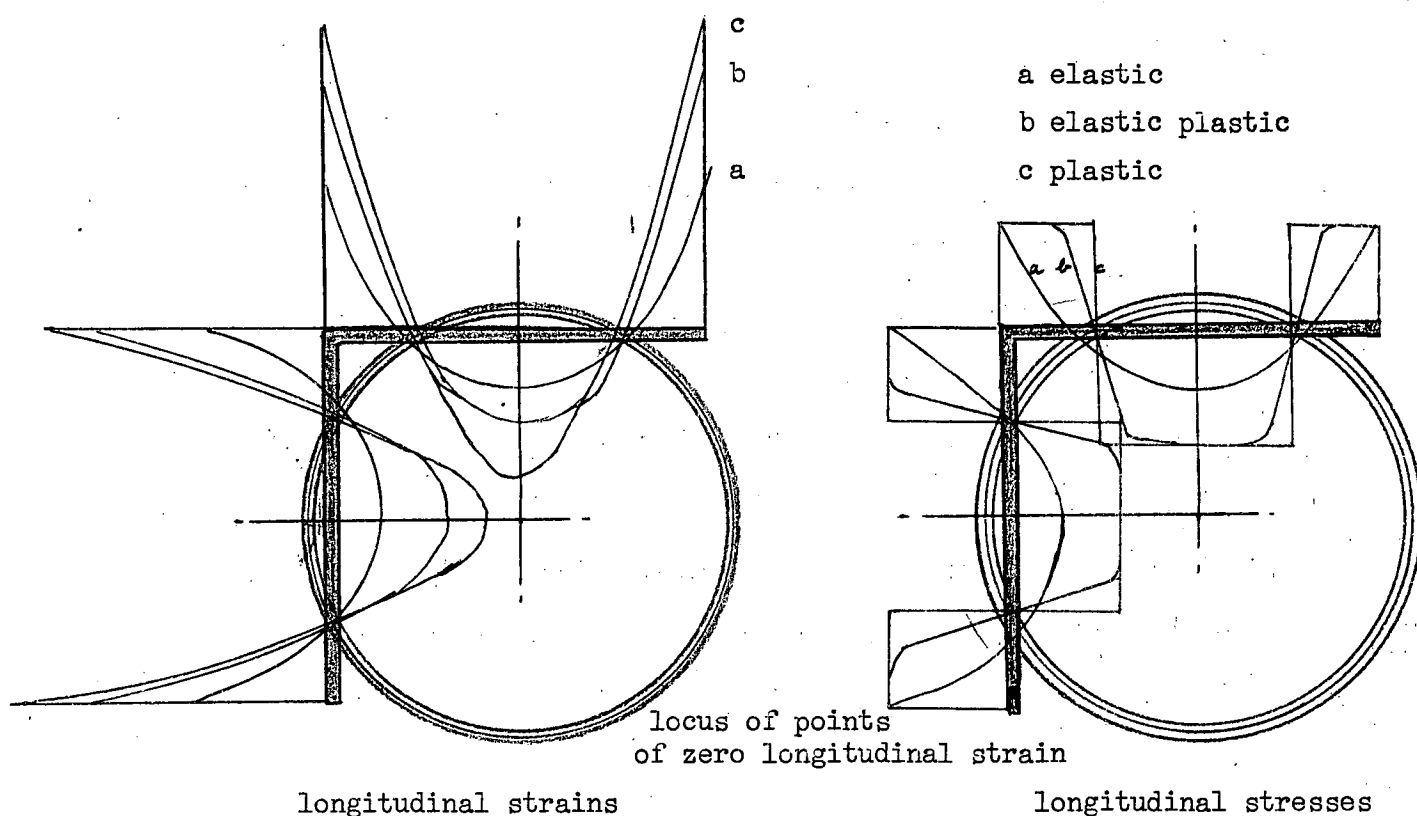icity is developed. However, for very large angles of twist, it is found from measurement that the value of the angle between the legs of the angle member is not constant. Nevertheless, the axis of distortion for the new shape is at the junction of the perpendicular bisectors of the sides, as can be seen in Fig. 6.16 where the white string indicates the measured positions of the axis of distortion.

When the position of the axis of distortion can be found from the symmetry of the longitudinal strains, the position of this axis remains constant, as the section is twisted. The sections satisfying this condition include the equal-sided channel, the I section, a sector of a circle section, and the Z section. For other sections, the position of the axis of distortion as determined when all strains are elastic differs from the position of the axis of distortion determined when full plasticity is assumed. To the author's knowledge, the estimation of the position of a fully plastic distortion axis has not previously been established.

6.6.2 The Axis of Distortion of the Channel Section, height 2a, flange width b.

Ashwell (Ref. 62) gives the position of the axis of distortion as in Fig. 6.18a and the particular case of a = b = 1.0 is considered. The position of the axis of distortion under conditions of full plasticity is found by noting first the form of the longitudinal strains. The idealized plateau type plastic longitudinal stress system mentioned previously and based on the pattern of the longitudinal strain system is used, but the exact positions of the points of zero stress are not specified.

When the statical conditions of no bending moments, and no axial force are satisfied, that is when
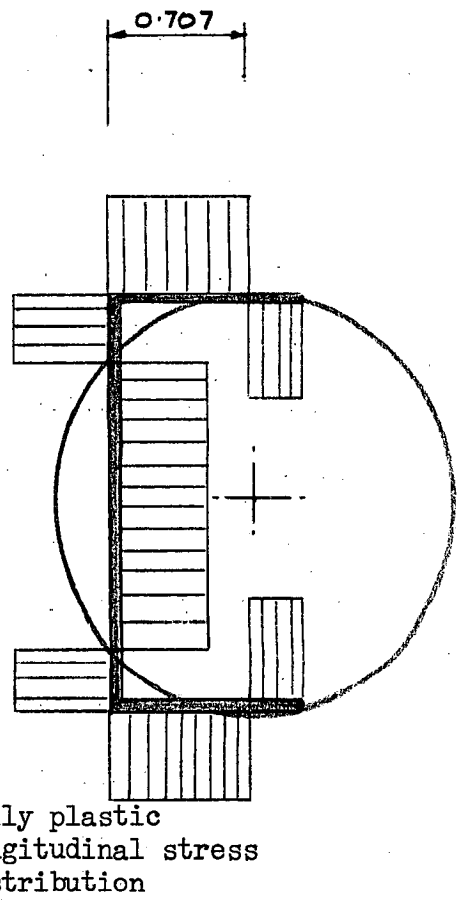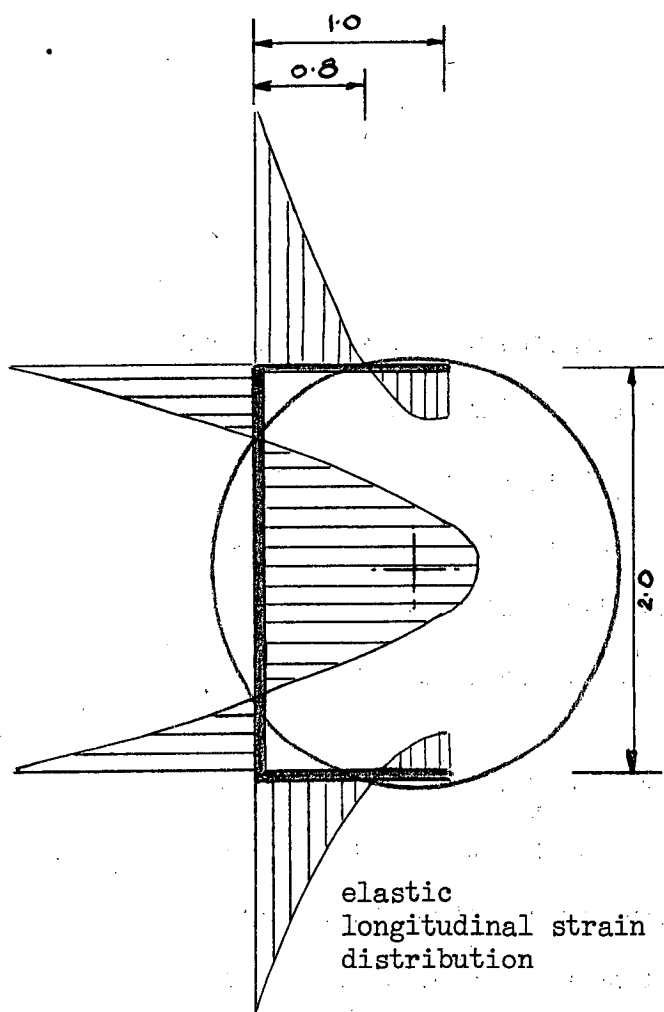
elastic
longitudinal strain
distribution

fully plastic
longitudinal stress
distribution

Fig. 6.18a.

elastic
longitudinal strain
distribution

fully plastic
longitudinal stress
distribution
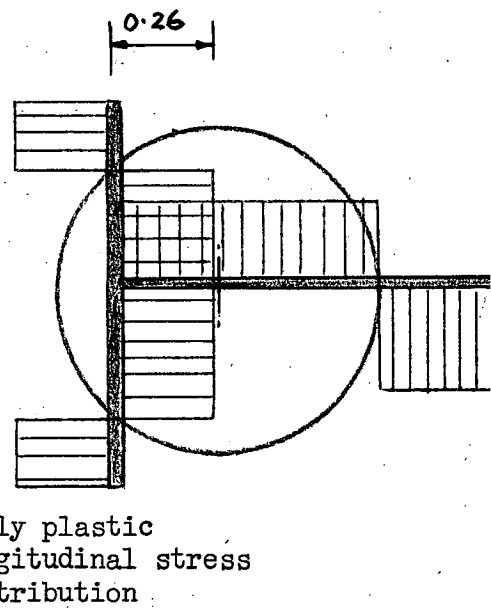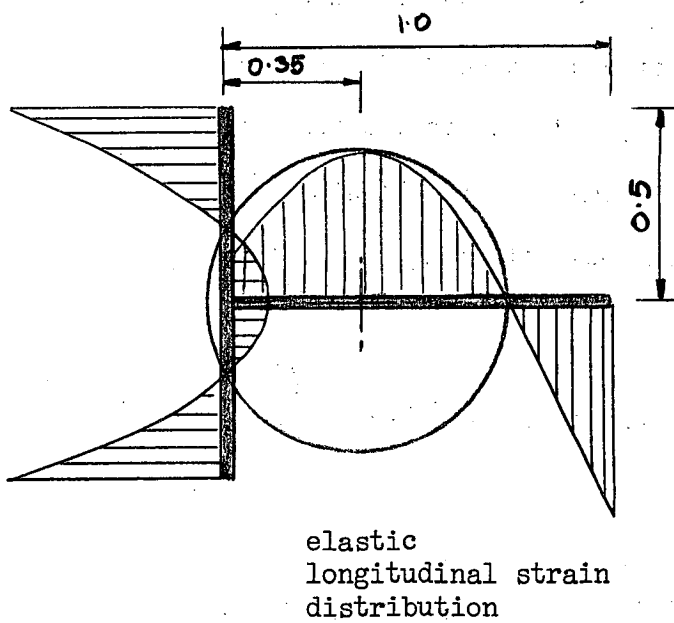
Fig. 6.18b.

$$\int_A f_z \, dA = 0, \qquad\qquad (6.36)$$

$$\int_A f_z \, x \, dA = 0,$$

and

$$\int_A f_z \, y \, dA = 0,$$

the co-ordinates of these points of zero longitudinal stress, and hence strain can be found. If a plausible distribution has been established the points of zero longitudinal strain lie on a circle. The locus of the centre of this circle is a straight line, and this line will be called the axis of plastic distortion, to distinguish it from the axis of distortion which is derived from considerations of elasticity.

For the channel section, with a = b = 1, the position of the axis of distortion axis (elastic) is at a distance of 0.8 form the vertical side. The form of the strain distribution (Fig. 6.18a) indicates an approximate stress distribution and the equations (6.36) are used to find the points of zero stress. The points of zero longitudinal strain and hence the position of the axis of plastic distortion is then determined. For this channel section the position of the axis of plastic distortion is at a distance 0.707 from the vertical side. Thus there exists a longitudinal line, defined in terms of the section properties, which remains straight after the section has been twisted into the fully-plastic range.(Fig. 6.18c).

6.6.3 The Axis of Distortion of the T-section, flange 2a, stem b.

From Ashwell's table, (Ref. 62) for a T-section with a = 0.5, b = 1.0 the position of the axis of distortion is at a distance 0.35 along the stem (Fig. 6.18b), while the position of the axis of plastic distortion is at a distance 0.264 along the stem. (see also Fig. 6.18c

Other sections examined included unequal sided channel and Z sections, and all confirmed the existence of a plastic distortion axis. The co-ordinates of the position of this axis were calculated

from the mathematical model developed in 6.6.2 and were compared with results obtained from experimental observations, (Fig. 6.18c). The difference between the position of the calculated and the experimental axis of plastic distortion was small.

6.7 Torsion of Sections, with Applied Constraints.

The position of the axis of distortion for all asymmetric sections changes with the applications of axial loads and bending moments.as may be seen easily when the effects of an axial load P, and bending moments M_x and M_y are included in the elastic mathematical model. In analytical terms, the co-ordinates of the position of the axis of distortion are found when the following equations are satisfied:

$$\int_A E(\tfrac{1}{2}(r \ d\theta/dz)^2 - \epsilon_{WW\ell}) \ dA = P$$

$$\int_A E(\tfrac{1}{2}(r \ d\theta/dz)^2 - \epsilon_{WW\ell}) \ x \ dA = M_x \qquad\qquad (6.37)$$

and $$\int_A E(\tfrac{1}{2}(r \ d\theta/dz)^2 - \epsilon_{WW\ell}) \ y \ dA = M_y.$$

The general behaviour of the asymmetric section, under the combined action of twist and applied forces, can be seen when the particular example of the angle section is considered.

Assume that the axis of distortion is at the perpendicular bisectors of the two legs, Fig. 6.19a. Then, the longitudinal strain and hence longitudinal stress system satisfying equations (6.37) is maintained by a zero axial force and zero bending moment system.

When we assume a different position for the axis of distortion, axial forces and bending moments consistent with equations (6.37) must be applied. Assume that the position of the axis of distortion is half way between the position of the centroidal axis and the position of the axis, of distortion for no applied axial force and bending moment. A trial and error solution is satisfactory
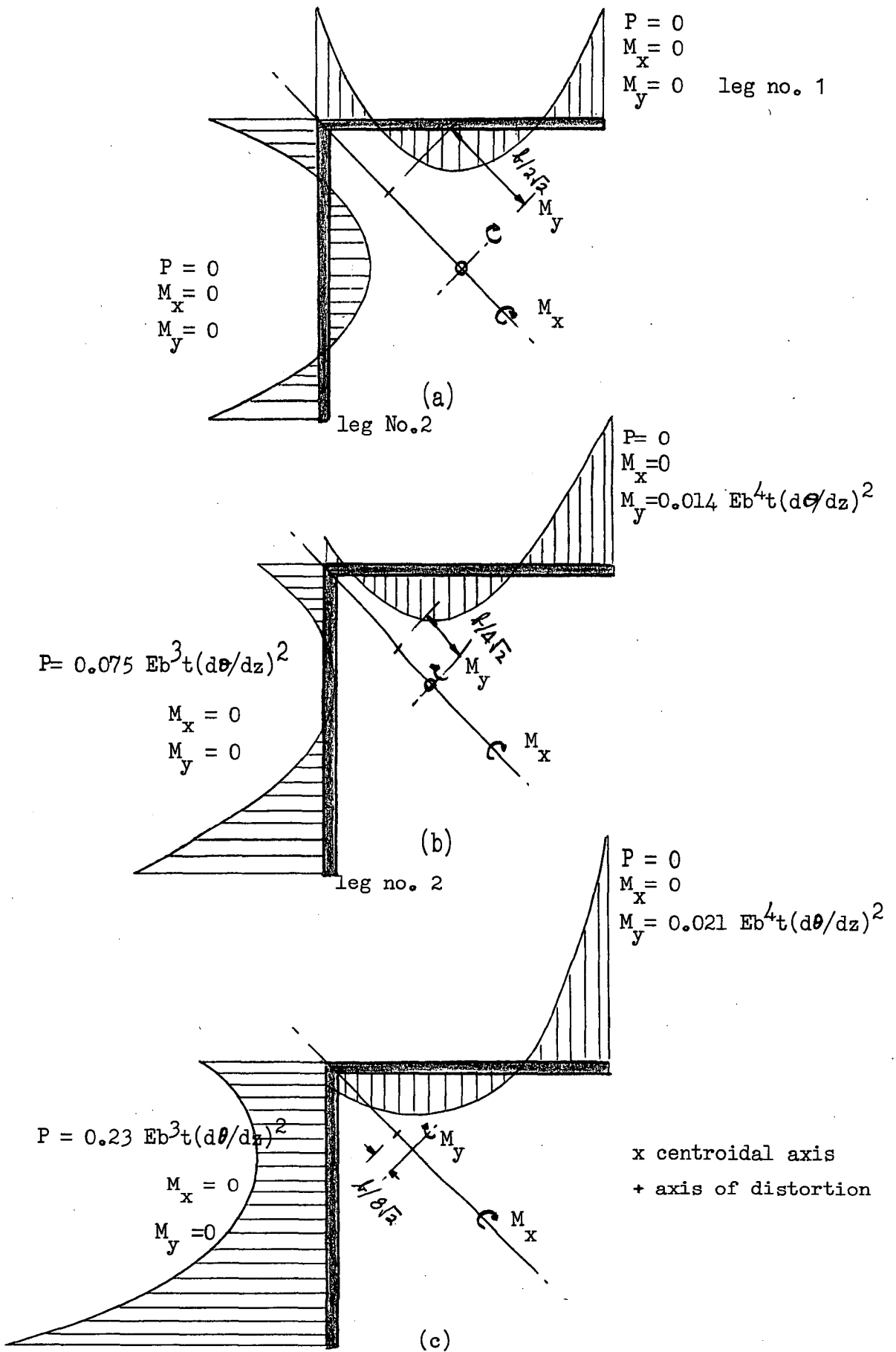
Fig. 6.19. Positions of the distortion axis corresponding to different elastic longitudinal stress distributions.

to find the forces required to maintain the deformed shape. One possible solution is shown sketched in Fig. 6.19b on the leg No. 1, and is given by the equations

$$M_x = P = 0$$

and

$$M_y = 0.014 \, Eb^4 t (d\theta/dz)^2 \quad.$$

Thus, the axis of distortion will remain straight, and in the specified position, when the bending moment My is applied. The moment must be applied to the cross section of the angle at the ends, and a constant intensity (per unit length) moment must be applied through the distortion axis in a direction which rotates with the cross section. The above solution is not the only combination of forces which will sustain the specified deformations, and there exists a range of solutions for the bending moments and axial forces. Another solution, sketched in Fig. 6.19b on leg No. 2, is given by the equations

$$M_x = My = 0$$

and

$$P = 0.075 \, E \, b^3 t (d\theta/dz)^2 \quad.$$

The axial force (a tension force) must be applied through the distortion axis, in a manner which does not restrict the warping of the cross section.

Assume another position for the axis of distortion, closer to the centroidal axis. (Fig. 6.19c). The two extreme solutions are

$$M_x = P = 0$$

$$M_y = 0.021 \, E \, b^4 t (d\theta/dz)^2 \qquad \text{(leg No. 1)}$$

and

$$M_x = My = 0$$

$$P = 0.23 \, E \, b^3 t (d\theta/dz)^2 \qquad . \qquad \text{(leg No. 2)}$$

A pattern in the results for the particular combination of twist and applied axial loads is obtained from Fig. 6.20, where the ratio of the axial load to the square of the angle of twist is plotted against different positions of the axis of distortion.

In the limiting case, as the twist is decreased and the axial tension force is increased the axis of distortion converges to the centroidal axis. Under these conditions, a uniform finite axial tension stress system is needed to sustain the distortion axis close to the centroidal axis. This result is consistent with the definition of the centroidal axis, and is as would be expected. However, the establishment of the rate of movement is, to the author's knowledge, original.
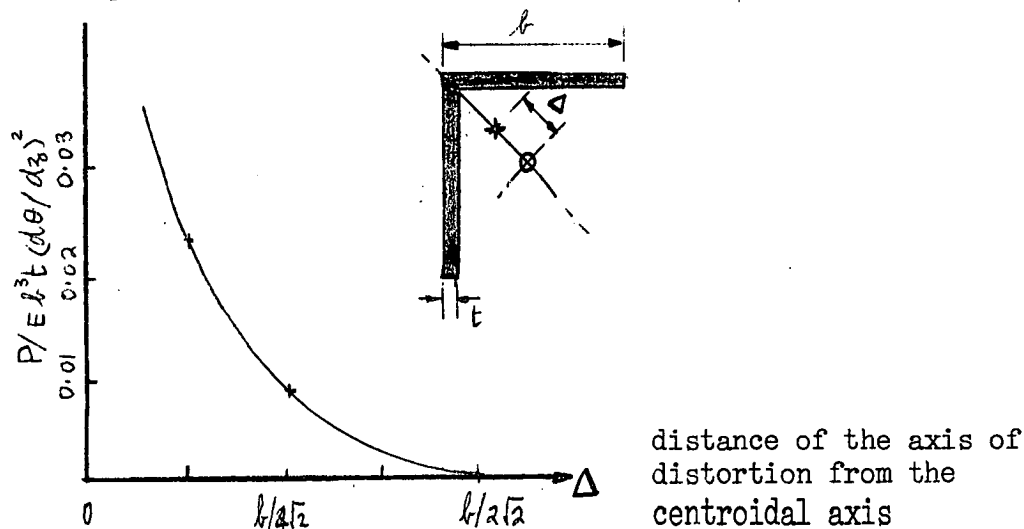
Fig. 6.20. A Graph of axial force, and twist, showing the position of the axis of distortion for an angle section.

The longitudinal strains, sustained by an applied axial tension * force affect the torsional stiffness of the section.

---

* It is possible to assume positions of the axis of distortion for which it is necessary to apply compressive axial forces. However, these compressive axial forces are likely to introduce buckling deformations. Tests carried out at the University of Tasmania with angle sections indicate that when a combination of compressive axial force and no twist are applied, the initial crookedness of the angle member is sufficient to induce buckling deformations. (Ref. 72). For short thin angle members, the line of shear centres appears to be the only line which remains reasonably straight. Hence the analysis developed above is limited to describing the effects of tensile axial forces. The overall effect of combined compressive axial forces and twist is a field in which further investigation is needed.

For very small angles of twist and large axial loads, it is convenient
to choose the centroidal axis as the axis of reference and neglect the
shortening effect of the twist. The approximate effect of the axial
load on the torsional stiffness of the section is then easily found.
Biot (Ref. 71) has shown that, under these conditions, the torque
carrying capacity is given by the equation

$$T = (GJ + PI_c/A) (d\theta/dz) \qquad , \qquad (6.38)$$

where P/A is the applied axial tension, and I_c is the polar
second moment of area taken about the centroid. This expression
does not allow for the bending of the centroidal axis.

However, using the co-ordinates of the distortion axis
for the particular combinations of axial load and twist, we may
evaluate the torsional stiffness, and allow for the bending of
the centroidal axis, and the shortening effects.

The applied torque is balanced by two effects; the
St. Venant shearing stresses and the inclined longitudinal stresses.
The St. Venant stresses have been discussed in Section 6.2, while
the magnitude of the longitudinal stresses (inclined at an angle
to the distortion axis) is given by equation (6.37). Then, the
torque is given by the equation

$$T = GJ(d\theta/dz) + \int_A E[\tfrac{1}{2}(r \, d\theta/dz)^2 + \epsilon_{oot}] \, r \, dA \sin\beta \qquad , \qquad (6.39)$$

and using equation (6.37) to find the axial shortening,
equation (6.39) becomes

$$T = GJ(d\theta/dz) + \int_A E[\tfrac{1}{2}(r \, d\theta/dz)^2 + P/EA - \tfrac{1}{2}(I_p/A)(d\theta/dz)^2] r \, dA \sin\beta \quad .(6.40)$$

When the approximation is made that $\sin\beta = r \, d\theta/dz$, equation
(6.40) simplifies, and the torsional stiffness is

$$T = (GJ + PI_p/A)(d\theta/dz) + \tfrac{1}{2}(d\theta/dz)^3 E[H_p - I_p^2/A] \qquad , \qquad (6.41)$$

where $H_p = \int_A r^4 \, dA$, and is taken about the axis of
distortion determined from the particular axial tension loading.

6.8   A Functional Description of Torsion.

It has been shown in sections 6.1 to 6.5 that the deformations of a member subject to small twist can be described by a simple functional form. With small twists, and with the warping of the ends of the member unrestrained, a reasonable functional form is "all straight lines originally parallel to the sides of the strip (that is lines across the width, through the thickness, and along the length of the strip) remain straight after the member has been twisted."

In sections 6.6 and 6.7 it has been shown that the deformations of a member subject to large twists, axial tensile forces, and particular bending moment combinations can also be described by a simple functional form. In this case the approximation is "all straight lines originally parallel to the sides of the cross section, (that is lines across the width and through the thickness) and one longitudinal line (either inside or outside of the section) remain straight after the section has been subject to large torsion".

6.9   General Comments.

The problem of the torsional behaviour of elastic rectangular bars has thus been solved by the inverse approach, i.e. by first establishing experimentally a simple geometric model of the behaviour, then by using the load deformation relationships to obtain stresses, and finally by using these stress resultants to examine equilibrium. The discrepancies in equilibrium are then used to estimate the next simple geometric model and an iterative cycle is established. The power of this method is that only the important effects are considered at each level, and a model of the behaviour of the structure or member is developed as the step by step solution proceeds. This method is thus suitable for teaching the engineering approach to the solution of a difficult problem, i.e. by estimating in an ordered manner the important effects, understanding the significant simplification at each stage, and knowing what is the next step in the improvement of the solution.

CONCLUSION

Characteristic geometric describing shapes, or functional forms, have been used throughout this thesis to approximate and predict structural behaviour. The ideas involved were first introduced in Chapter One, and the well known examples of stretched, bent, and twisted bars were discussed. In the remaining chapters these basic ideas were used in a variety of structural contexts.

In Chapter Two, a description of structural stability in terms of characteristic describing shapes, that is buckling modes, was advanced. This description was sufficient to justify the use of a generalized Southwell Plot to estimate buckling loads and buckling modes for a range of structural behaviour.

Next, in Chapter Three, Four and Five the design of a through plate girder bridge was outlined in terms of the patterns of geometric behaviour observed in simple model tests. A mathematical model to describe the lateral and torsional instability deformations exhibited by these model tests was developed, and solutions were found. With this deformation behaviour in mind, the current methods used to design through bridges were outlined and it was shown that these existing methods are suitable for the design of through bridges which have very heavy floors. In these designs the lateral deformations of the top flange of the bridge are considered and the web and floor is assumed to resist the lateral movement of the top flange.

However, these methods were shown to provide an unsatisfactory description of the behaviour of through bridges which have very light floors. In these cases the lateral and torsional deformations of the entire side of the bridge becomes the dominant deformation. The floor then provides torsional resistance against these movements. Measurement

of the behaviour of a loaded full-size through bridge, which had a light floor, was then described. It was shown that these measurements are described reasonably well by the mathematical model developed in this thesis. The experience gained from the entire study was then summarized into the form of a recommendation for the design of through bridges.

Finally, in the concluding chapter, a geometric description of torsion was developed. This description was based on measurement, and subsequent approximation and simplification, and the twisting behaviour of a large range of sections was described in terms of anticlastic surfaces, helices and straight lines.

APPENDIX A

A closer look at the self adjoint property.

For the differential equation

$$EI\ d^4y/dx^2\ +\ P\ d^2y/dx^2\ =\ 0\ ,$$

the self adjoint form is

$$\int_a^b EI(d^4y_1/dx^4)\ y_2\ dx\ =\ \int_a^b EI\ d^4y_2/dx^4\ y_1\ dx$$

and

$$\int_a^b Pd^2y_1/dx^2\ \ y_2\ dx\ =\ \int_a^b P\ d^2y_2/dx^2\ y_1\ dx\ .$$

Using the boundary conditions $x = a, b$ $y = 0$, $\sum EI\ d^2y/dx^2 = 0$, and simplifying, as in equations 2.52 and 2.53, we obtain the orthogonality relations

$$\int_a^b (EI\ d^2y_1/dx^2)\ d^2y_2/dx^2\ =\ 0\ ,$$
$$\qquad\quad \uparrow \qquad\qquad\quad \uparrow$$
$$\qquad\quad \text{moment} \qquad\quad \text{curvature}$$

and $\quad \int_a^b P(dy_1/dx\ \ dy_2/dz)\ =\ 0\ .$

$$\qquad\quad \uparrow \qquad\qquad \nwarrow$$
$$\qquad\quad \text{load} \qquad\qquad \text{vertical deflection}$$

The property of self adjointness is useful because it allows a separation of variables. Separating variables is not strange in engineering solutions, as the aim in analysis is always to reduce the number of variables that must be considered at any one time.

Thus, in the theory of elasticity, we use

$$\sigma_1 \gamma_2\ =\ \tau_2 \epsilon_1$$
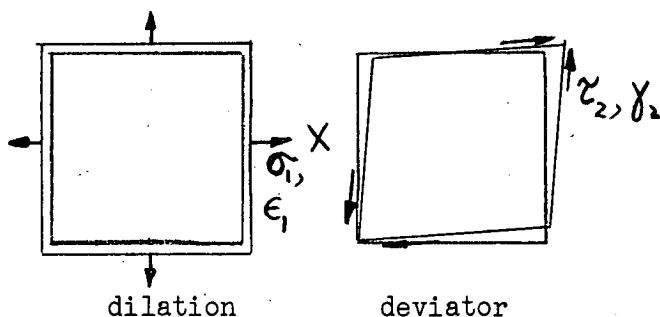
dilation   deviator   energy is separable along these paths.

and these ideas are carried over to yielding problems, or in the analysis
of frames (Ref. 80)
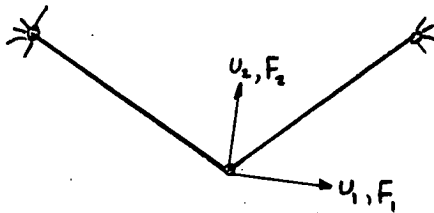
$$u_1 F_2 = u_2 F_1$$

Pull in either u_1 or u_2 direction
and structure moves in the same
direction

energy separable along these
paths

Typical problems which are not necessarily self adjoint include:

follower systems which depend
on the previous path,

systems which depend on the
previous deformations, for
example when yielding occurs,
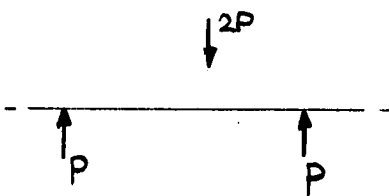
and some systems where the
applied force does not act
on the centroid of the section,
(for example the lateral
torsional buckling of an I beam
considered in Chapter Three
exhibits this property).

Means to handle non self adjoint terms are gradually appearing in
the literature (Refs. 73 - 79). Probably a great future field of study
lies in the further investigation of non self adjoint systems, as one of
the big problems in structural analysis is the adequate description of
yielding and the ideas outlined in this thesis furnish a method for
attaching the problem.

The general problem could be simplified to a simple system with
two rigid links and a hinge, with a variable but defined moment and
change of slope properties.

moment

change of angle
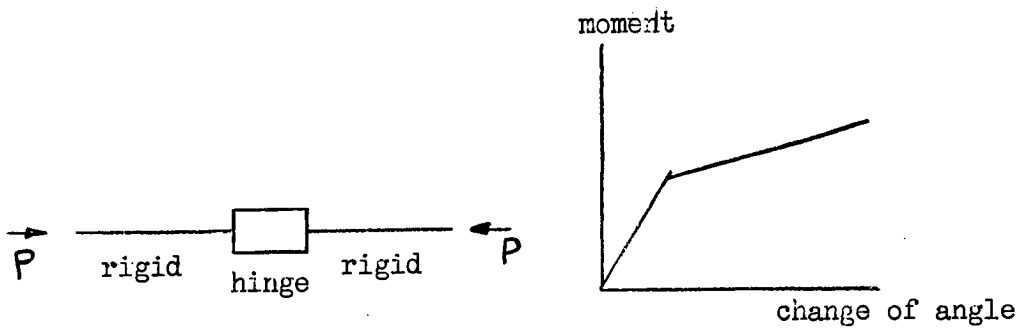
The shape of the initially crooked system for each loading can be

defined in terms of the previous shapes. The method of determining

these shapes is then dependant on a choice of orthogonal functions

which apply in the range of deformation over which the previous shape

is defined.

APPENDIX B

Convergence of an infinite Fourier Series Expansion.

The establishment of the convergence of the infinite series

expansion

$$\phi = \sum_{n=1}^{\infty} a_n \phi_n$$

where

$$a_n = \int_a^b \phi N(\phi_n)\, dz / \int_a^b \phi_n N(\phi_n)\, dz, \quad \text{or} \quad \int_a^b \phi L(\phi_n)\, dz / \int_a^b \phi_n L(\phi_n)\, dz$$

and ϕ is a solution of the differential equation $L(\phi) - \lambda N(\phi) = 0$

requires some elegant mathematics.

The differential equation approach separates the boundary

conditions from the conditions inside the boundaries. When checking

for convergence it is easier to examine a reformulation of the

mathematical statements in terms of one equation. Thus, the

differential equation

$$L(\phi) - \lambda N(\phi) = 0,$$

with associated boundary conditions is transformed into the

Fredholm integral equation

$$\phi - \lambda \int_a^b K(z, s)\, \phi(s)\, N(\phi)\, ds = 0$$

where a, b define the domain.

$K(z, \Delta)$ is a symmetric (as the differential equation is self

adjoint) kernel and z, Δ are points within the domain.

The convergence properties of eigen functions is examined by

exploring the properties of integral equations . The classic

theorem which arises from the study of integral equations is the

Hilbert-Schmidt theorem (Miklin, Ref. 16, p. 79) and states:

"Hilbert-Schmidt theorem: Let $\lambda_1, \lambda_2, \lambda_3 \ldots \ldots$ be

the eigen values of a symmetric kernel $K(x, \Delta)$, and $\phi_1, \phi_2, \phi_3 \cdots$

be the corresponding eigen functions. Let $h(x)$ be a function, the square
of which is absolutely integrable in (a, b). If $\int_a^b |K^2(x, s)| ds$
is bounded, then the function

$$f = Kh = \int_a^b K(x, s)\, h\,(x)\, ds$$

may be expanded as a uniformly and absolutely convergent Fourier series
with respect to the orthonormal system ϕ_n, that is

$$f(x) = \sum_{n=1}^{\infty} f_n\, \phi_n(x) \quad \text{where} \quad f_n = (f, \phi_n)$$

The coefficients of f are related to the coefficients of h by the
equation

$$f_n = h_n / \lambda_n$$

Thus, it is necessary to find the kernel, $K(x, s)$, (called the Green's
Function) to establish convergence. The kernel is found by finding the
deformations needed to sustain a unit force at the point s. An integration
of the total force applied then determines the total deformation.

Consider again the pin-ended column,

$$EI\, d^2y/dx^2 + Py = 0$$

with boundary conditions $y = 0$, $x = 0$ and $x = \ell$. To construct this well
known Green's Function, apply a unit discontinuity in bending moment at
a point s, while satisfying the load deformation relationship for the
member.

Then $EI\, d^2y/dx^2 = 0$ at all points except $x = \ell$

$$\therefore \quad y = \begin{cases} a_1\, x + b_1 & 0 \leqslant x \leqslant s \\ a_2\, x + b_2 & s \leqslant x \leqslant \ell. \end{cases}$$

Satisfying the boundary conditions leads to the equations

$$y = \begin{cases} a_1\, x & 0 \leqslant x \leqslant s \\ a_2\, (\ell - x) & s \leqslant x \leqslant \ell \end{cases}$$

Satisfying the continuity of deflections at $x = s$, gives the equation

$$a_1\, s = a_2\,(\ell - s)\,.$$

Satisfying the condition that a unit moment is applied across the
gap at $x = s$ gives the equation

$$\int_{s-\xi\delta}^{s+\xi\delta} EI\, d^2y/dx^2\, d\delta = 1 \qquad , \text{ as } \delta \to 0$$

$$\therefore \quad EI\, dy/dx\bigg]_{s+\xi\delta} = EI\, dy/dx\bigg]_{s-\xi\delta} + 1$$

$$\therefore \quad EI\, a_1 = -EI a_2 + 1$$

$$\therefore \quad a_1 + a_2 = 1/EI \quad .$$

The two equations in a_1 and a_2 are then used to determine the deflection of the column when a unit moment is applied at the point $x = s$, and the deflection y is

$$y = G(x, s) = \begin{cases} x(\ell - s)/EI & 0 \leqslant x \leqslant s \\ s(\ell - x)/EI & s \leqslant x \leqslant \ell \end{cases}.$$

A statical consideration of the external moments applied to the section, give the actual moment at each point s , and

$$M = P\, y(s) \; .$$

Thus, the total deflection of the column is found by summing the effects of deflections caused by these applied moments, and

$$y = \int_0^\ell Py\,(s)\, G(x, s)\, ds.$$

Clearly the real kernel $G(x, s)$ is bounded and thus from the Hilbert-Schmidt theorem the expansions of eigen functions of the differential equation for the pin ended column are absolutely convergent.

Proceeding in a manner similar to that outlined above it is possible to examine some of the mathematical models for the through bridge.

The differential equation

$$C\, d^2\theta/dz^2 + (P^2/4EI_\eta)(\tfrac{1}{2}\ell - z)^2 \theta = 0,$$

with boundary conditions $\theta = 0$; $z = \tfrac{1}{2}\ell, \tfrac{1}{2}\ell$ has the same kernel as the pin ended column. Then

$$\theta = \int_{\frac{1}{2}\ell}^{o} G(z,s)(P^2/4EI_\eta)(\tfrac{1}{2}\ell-z)^2\,\theta(s)\,ds + \int_{\theta}^{-\frac{1}{2}\ell} G(z,s)\,(P^2/4EI_\eta)(\tfrac{1}{2}\ell+z)^2\theta(s)\,ds\,,$$

where $\quad G(z,\,s) = \begin{cases} z(\ell-s)/C & 0 \le z \le s \\ s(\ell-z)/C & s \le z \le \tfrac{1}{2}\ell\,, \end{cases}$

The differential equation

$$C\,d^2\theta/dz^2 - C_o\theta + (P^2/4EI_\eta)(\tfrac{1}{2}\ell-z)^2 = 0$$

with boundary conditions $\theta = 0$, $z = \pm\tfrac{1}{2}\ell$, may be shown to have a kernel

$$G(z,\,s) = \begin{cases} n(\sinh n\,s - \cosh n\,s \tanh n\ell)\sinh nz/C_o \tanh n\ell & 0 \le z \le s \\ \\ n(\sinh n\,z - \cosh n\,z \tanh n\ell)\sinh ns/C_o \tanh n\ell & s \le z \le \ell \end{cases}$$

where $\quad n^2 = C_o/C$.

The differential equation

$$C_1 d^4\theta/dz^4 - C\,d^2\theta/dz^2 + C_o\theta - (P^2/4EI_\eta)(\tfrac{1}{2}\ell-z)^2\theta = 0$$
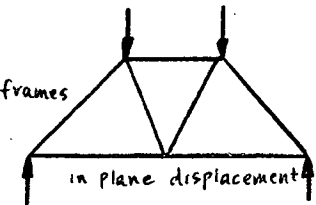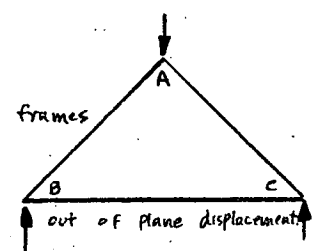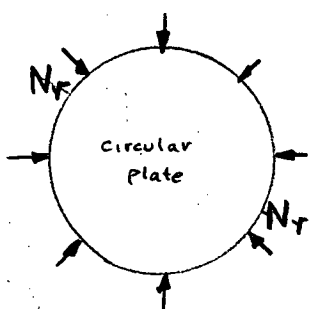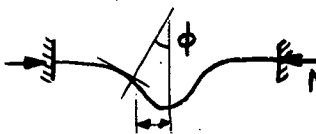
may be shown to have a similar kernel, but with n defined by the equation

$$C\,n^2 = C_o + C_1\,n^4\,.$$

These kernels, $G(z,\,s)$, are real, and bounded, and thus by the Hilbert-Schmidt theorem the expansions of infinite series eigen functions corresponding to solutions of the corresponding differential equations are absolutely convergent.

Mathematical Models for which a Southwell Plot is a useful device to measure buckling loads and modes.

Typical structure	differential equation of undeformed structure	differential equation of initially deformed structure	boundary conditions	Southwell Plot variables ϕ	λ
frames — in plane displacement Ref 13	$EI\, d^4y/dx^4 + P\,d^2y/dx^2 = 0$	$EI\, d^4(y-y_0)/dx^4 + P\,d^2y/dx^2 = 0$	(a) $x=0, \ell;\ y=0,\ EI\,d^2y/dx^2=0$ (b) $x=0, \ell;\ \lessgtr EI\,d^2y/dx^2=0,$ $\quad \lessgtr(EI\,d^3y/dx^3 - P\,dy/dx)=0$	$y,\ dy/dx,\ d^2y/dx^2$:	P
frames — out of plane displacement Ref 11	$EI\, d^4y/dx^4 + P\,d^2y/dx^2 = 0$ $T = GJ\theta/\ell$	$EI\, d^4(y-y_0)/dx^4 + P\,d^2y/dx^2 = 0$ $T = GJ(\theta-\theta_0)\ell$	(a) $x=0, \ell;\ M_{AB}=-M_{AC},\ M_{BC}=-M_{CB}$ (Moments) $\quad M_{BA}=-M_{CA}$ $T_{AB}=-T_{AC}=T_{BA}=-T_{CA}$ (torques) (b) $x=0,\ell;\ M_{AB}=M_{AC},\ M_{BC}=M_{CB},$ $\quad M_{BA}=M_{CA}$ $T_{AB}=T_{AC},\ T_{BA}=T_{AC}=0$	$y,\ dy/dx,\ d^2y/dx^2$:	P
circular plate Ref 30	$[r^2 d^2\phi/dr^2 + r\,d\phi/dr - \phi] +$ $N_r\, r^2\phi/D = 0$	$[r^2 d^2(\phi-\phi_0)/dr^2 + r\,d(\phi-\phi_0)/dr - (\phi-\phi_0)] +$ $N_r\, r^2\phi/D = 0$	$r=0, R;\ \phi=0$	$\phi,\ d\phi/dr,\ d^2\phi/dr^2$:	N_r

cylindrical shell

$$\left[D\, d^4w/dx^4 + E h w/a^2\right] + N_x\, d^2w/dx^2 = 0$$

$$\left[D\, d^4(w-w_0)/dx^4 + E h(w-w_0)\right] + N_x\, d^2w/dx^2 = 0$$

$x=0, l$; $w=0$, $D\, d^2w/dx^2 = 0$

$w, dw/dx, d^2w/dx^2$: N_x

Ref 30

flat plate
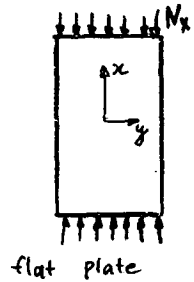
$$w = f(y)\,\sin m\pi x/a$$

$$w = \left[f(y) - f(y_0)\right]\sin m\pi x/a$$

$$\left[d^4 f/dy^4 - A\, d^2 f/dy^2 + B f\right] - C N_x f = 0$$

$$\left[d^4(f-f_0)/dy^4 - A\, d^2(f-f_0)/dy^2 + B(f-f_0)\right] - C N_x f = 0$$

$x=0, l$; $w=0$, $d^2w/dx^2 + v\, d^2w/dy^2 = 0$

$w, dw/dx, d^2w/dx^2$: N_x
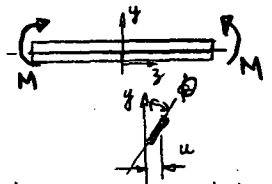
Ref 30

beam liable to lateral and torsional instability.

$$\left[c_1\, d^4\theta/dz^4 - c\, d^2\theta/dz^2\right] + M^2\theta = 0$$

$$\left[c_1\, d^4(\theta-\theta_0)/dz^4 - c\, d^2(\theta-\theta_0)/dz^2\right] + M^2\theta = 0$$

(a) $z = \pm\frac{1}{2}l$; $\theta=0$, $c_1\, d^2\theta/dz^2 = 0$

(b) $z = \pm\frac{1}{2}l$; $\theta=0$, $d\theta/dz = 0$

$\theta, d\theta/dz, d^2\theta/dz^2$: M^2

Ref 30
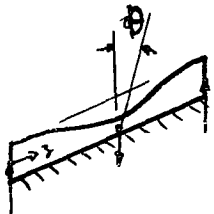
beam liable to lateral instability, bottom flange restrained.

$$\left[c_1\, d^4\theta/dz^4 - c\, d^2\theta/dz^2\right] + P\left[w\, d^2\theta/dz^2 + d\theta/dz\right] = 0$$

$$\left[c_1\, d^4(\theta-\theta_0)/dz^4 - c\, d^2(\theta-\theta_0)/dz^2\right] + P\left[w\, d^2\theta/dz^2 + d\theta/dz\right] = 0$$

$z=0, l$; $\theta=0$, $c_1\, d^2\theta/dz^2 = 0$

$\theta, d\theta/dz, d^2\theta/dz^2$: P

Ref 56

APPENDIX D

The Effect of an Initial Lateral Curvature in Equation 3.9.

The effect of the lateral initial crookedness can be included in the mathematical model for the initially deformed structure by using the ideas as outlined in Chapter Four and only a brief summary of the analysis is given. The mathematical model is

$$C_1 d^4(\theta-\theta_o)/dz^4 - C d^2(\theta-\theta_o)/dz^2 + C_o(\theta-\theta_o) - (P^2/4EI_\eta)(\tfrac{1}{2}\ell-z)^2\theta = \tfrac{1}{2}P(\tfrac{1}{2}\ell-z)d^2u_o/dz^2$$

The right hand side of this equation is then expressed as an infinite series expansion of the form

$$k_1\theta_1(\tfrac{1}{2}\ell-z)^2 + k_2\theta_2(\tfrac{1}{2}\ell-z)^2 + \ldots = \tfrac{1}{2}P(\tfrac{1}{2}\ell-z)d^2u_o/dz^2.$$

The value of k_r is found using the orthogonality relationship

$$\int_{\tfrac{1}{2}\ell}^{o} \theta_r\theta_s(\tfrac{1}{2}\ell-z)^2\,dz = 0$$

and thus the value of k_1 is given by the equation

$$k_1 = \int_{\tfrac{1}{2}\ell}^{o} \tfrac{1}{2}P(\tfrac{1}{2}\ell-z)\,d^2u_o/dz^2\,\theta_1\,dz / \int_{\tfrac{1}{2}\ell}^{o}(\tfrac{1}{2}\ell-z)^2\theta_1^2\,dz$$

Assuming that the initial lateral crookedness is of the form

$$u_o = a_o \sin \pi x/\ell$$

we obtain the value of k_1. This value is approximately a constant for all values of C, C and C and

$$k_1 \approx 6.1\,Pa_o/\ell^3 .$$

The solution of the equation is then obtained by using the infinite series expansions

$$\theta = m_1\theta_1 + m_2\theta_2 + \ldots$$

and

$$\theta_o = a_1\theta_1 + a_2\theta_2 + \ldots$$

and is of the form

$$\theta = [a_1 + (25\,EI\,Pa_o/\ell^3\,P_1^2)]\theta_1/[1-(P/P_1)^2] + \ldots$$

Again using the first term of the expression, we have

$$\theta = [a_1 + 25 \text{ EI } Pa_0/\ell^3 P_1^2] \, \theta_1/[1-(P/P_1)^2] \quad .$$

As the Southwell Plot is usually taken over a small range of loads, close to $P = P_1$; the top line of this expansion will be approximately constant in this range. Thus, the initial lateral curvature can be considered as being approximately equivalent to an initial rotational effect.

For full size light through bridge $\quad C_0\ell^2/C\pi^2 \approx 100$

then from Chapter Five the value of the buckling load P is approximately

$$P_1 = (100/\ell^2)\sqrt{\text{EI}_\eta \ C}$$

Thus the lateral deflection term is approximately

$$25 \text{ EI } P \ a_0/(100\sqrt{\text{EI}_\eta C}) \ P_1 \ell$$
$$= 0.25\sqrt{\text{EI}_\eta/C}(P/P_1)(a_0/\ell) \ .$$

Making further approximations; namely

$$\text{EI}_\eta = 2 \ (b^3 t/12) \ E$$
$$C = 2 \ (t^3 b/3) \ E/2(1 + \nu)$$
$$b/t = 15$$
$$P/P_1 = 0.8$$
$$a_0 = 1/1000$$

then

$$0.25\sqrt{\text{EI}_\eta/C} \ (P/P_1) \ (a_0/\ell) = 2.4 \times 10^{-3} \text{ radians.}$$

For a full size bridge, the equivalent initial rotational crookedness is of the order of $(a_1 + 2.4 \times 10^{-3})\theta_1$. For the average bridge $a_1 = 10^{-2}$ radians and thus the equivalent rotational crookedness is approximately 1.24×10^{-3} radians.

For the model bridge $\quad C_0\ell^2/C\pi^2 = 3$ $\quad\quad$ and $P_1 = (30/\ell^2)\sqrt{\text{EI}_\eta \ C}$, the equivalent rotational crookedness is thus approximately (see Fig D1),

$$[a_1 + (25 \text{ EI } P \ a_0/\ell^3 \ P_1^2)] \, \theta_1 = [0.02 + 0.005]\theta_1$$
$$= 0.025 \, \theta_1 \ .$$

Load (lbs)

P_{crit} measured from Southwell Plot

P_i calculated from mathematical model

(a) $\theta = a_1\theta_1 / [1 - (P/240)^2]$; $a_1 = 2.0 \times 10^{-2}$, measured value of the initial crookedness of the web

(b) $\theta = [a_1 + 25EI_\eta\, Pa_0 / \ell^3 (240)^2]\, \theta_1 / [1 - (P/240)^2]$; $a_1 = 2.0 \times 10^{-2}$ or $a_0 = .050$ in, measured lateral crookedness

(c) $\theta = a_1\theta_1 / [1 - (P/240)^2]$; $a_1 = 2.4 \times 10^{-2}$, obtained from a Southwell Plot of θ/p^2, θ

(d) θ, P measured, using $a_1\theta_1$ as 2.4×10^{-2} radians.

CENTRAL ROTATION (RADIANS)
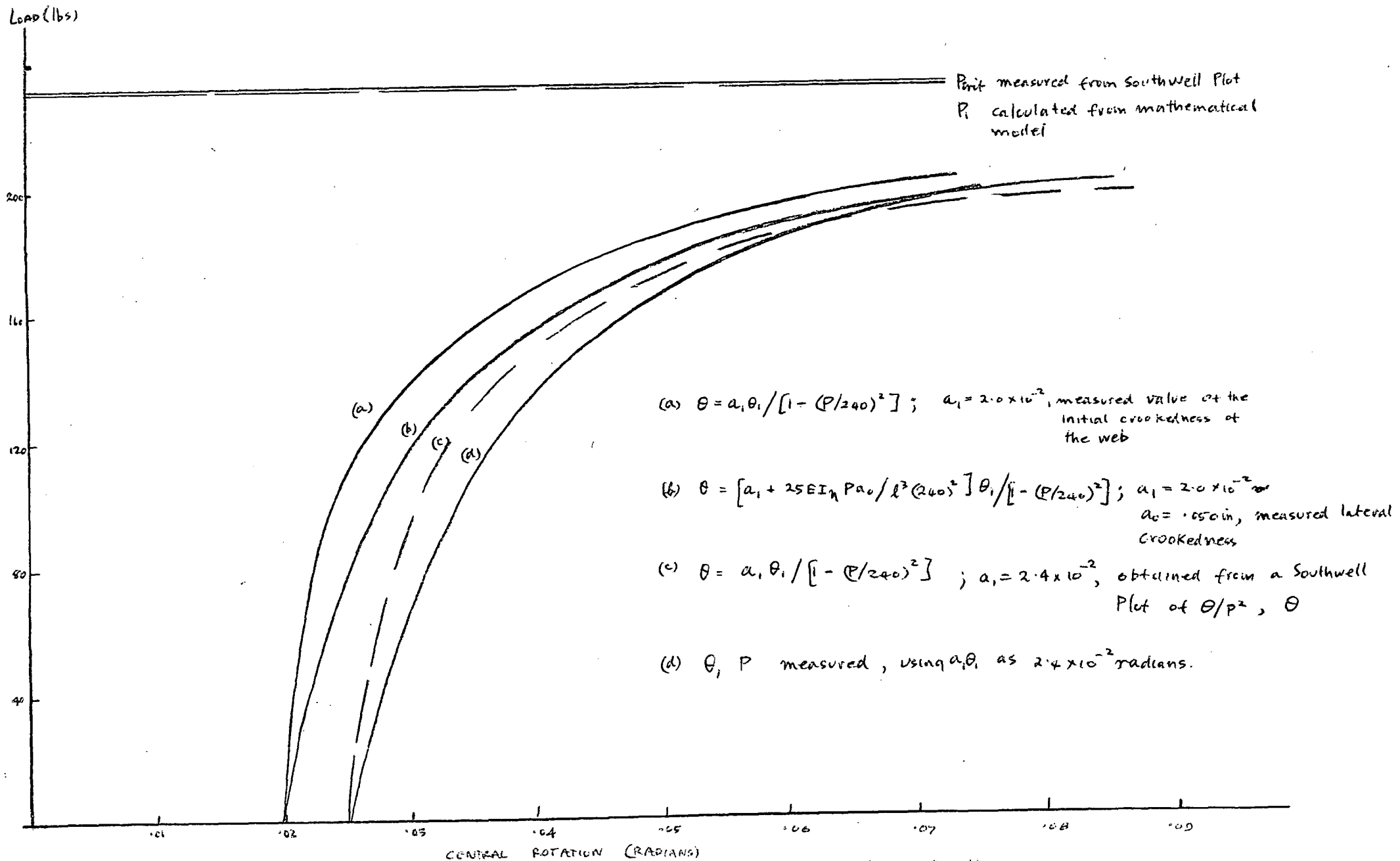
FIG D1   Mathematical models for the brass model bridge, allowing for the effect of initial lateral crookedness

Detailed Measurement of model through plate girder bridges.

LOAD (lbs)

Combined Graphs for different models for M.S. Bridge with no bracing.

Line of first yield, calculated from the deflected shape
$$\theta = 1.75\,\theta_{300}\left[\tfrac{5}{11} - \tfrac{73}{e} - \cos\tfrac{\pi}{5}/e\right]$$

Puit, calculated Bridge B

Puit, calculated, measured, Bridge A

Puit, measured Bridge B

Top Flange deflected

Y_s calculated from measured crookedness, elastic mathematical model

0.38 in from initial position

Y_s measured first yield of top flange

$\theta = a_0/(1 - (P/P_{crit})^2)$

a_0 from initial rotation of the web

Puit/calculated

Y_s measured first yield of top flange

Y_s, calculated from measured crookedness, elastic mathematical model

Y_s, calculated from S.P and elastic mathematical model

top Flange deflected 0.47 in from initial position

BRIDGE 'B'

BRIDGE 'A'

θ, P Measured.
θ_0 from measured initial rotation of the web

$\theta = a_0/(1 - (P/P_{crit})^2)$, from S.P.

$\theta = a_0/(1 - (P/P_{crit})^2)$
Puit calculated
θ_0 from initial rotation of the web

$\theta = a_0/(1 - (P/P_{crit})^2)$; a_0 from S.P
Puit from S.P

BUCKLING LOAD IF NO RESTRAINT OFFERED BY THE BOTTOM CHORDS

Measured θ, P
θ_0 from measured initial rotation of the web.

0.01 0.02 0.03 0.04 0.05 0.06 0.07 0.08 0.09 0.10

ROTATION AT THE CENTRE OF THE BRIDGE (RADIANS).

- 202 -

Mild Steel Bridges

Bracing of the bottom flanges.

APPENDIX F

Typical through bridge dimensions.

Location	Type	ℓ /s	ℓ /a	h/ℓ	k	k_{crit}
Brooker Highway	single lane railway bridge; plate girder	60/15	60/15	5/60	10	2.5
Brooker Highway	pedestrian foot bridge; truss	60/6	60/6	4/60	1.2	3.0
Devonport	ferry terminal bridge; plate girder	86/15	86/5.3	5/86	1.67	2.42
Hobart	ferry terminal bridge; plate girder	81/15	81/5	5/81	4	2.5
Westerway	road bridge; truss	36/20	36/6	7/36	2.15	2.15

ℓ = length, s = width, h = height, (in feet) of the bridges.

TABLE 1, Comparison of values of k for
different types of through bridges.

APPENDIX G.

An Economic Value for the Initial Rotational Crookedness.

The first mode initial crookedness for the ferry bridge was of the order of 0.6×10^{-2} radians, with a maximum value of 10^{-2} radians. These figures, in comparison with figures obtained from similar structures appears a reasonable average.

For this particular bridge it is possible to determine the benefit gained by increasing the rotational straightness, in the fabrication stage.

A decrease in first mode rotation from 0.6×10^{-2} radians to 0.3×10^{-2} radians increases the load carrying capacity by 10%. (Fig. G1.)
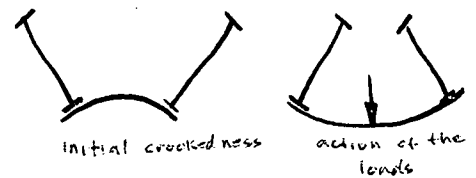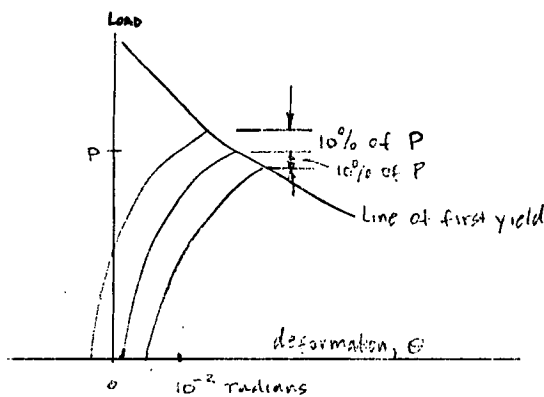
Fig. G2.

Fig. G1. Load deformation relations for varying crookedness values.

If this increase in load carrying capacity results in a corresponding decrease in steel area of the flanges, the resulting steel saved is 10% of the weight of the flanges.

Another possible means to obtain higher working loads is to deliberately make the bridge crooked in a manner which is opposite to the deformations induced by the loads. Thus, if the bridge is made as in Fig. G2 higher working loads for the frame lateral deformation can be achieved. (Fig. Gl).

Then, if the value of steel saved is greater than the cost of fabrication of the girder with controlled rotational straightness, it is economically worthwhile to produce the improved girder.

APPENDIX H.

The Effect of Lateral Loads on the Heavy Through Bridge.

This model describes the extreme type of deformation leading to instability which is characteristic of through bridges with rigid decks; that is a model describing a structure which is most unlikely to move bodily in the lateral direction. In this model the top flange moves more than the rest of the structure, (Fig. H1) and hence conditions describing the lateral stability of the top flange are considered.
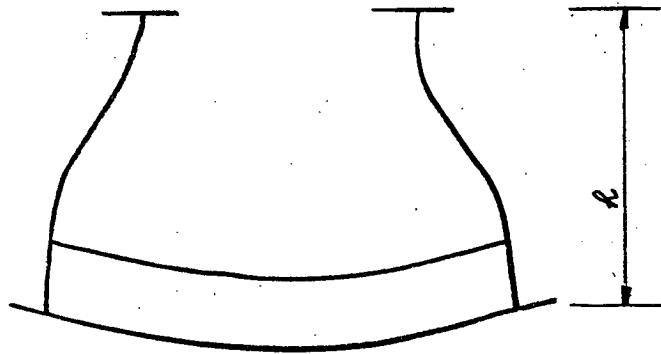
Fig. H1. Deformations of a through bridge, when the bottom chords provide restraint against rotation, and prevent translation.

For the bridge uniformly loaded along the bottom flanges, and for the origin taken at the end, the force P_T at z in the top flange, in a single beam is given by the equation

$$P_T \, h = \tfrac{1}{2} \, w \, \ell \, z - \tfrac{1}{2} \, w z^2 \; , \tag{H1}$$

where w is the uniform load for each I beam per unit length of the bridge. This relationship is shown in Fig. H2.
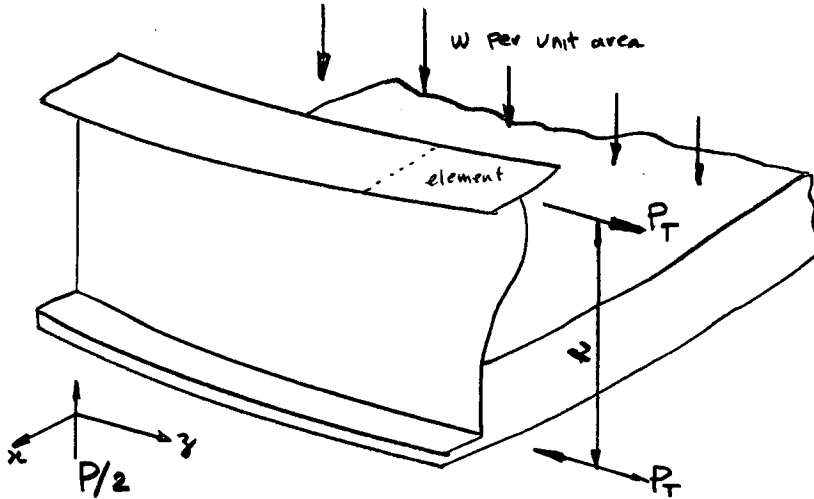
Fig. H2. An element of the bottom chord, web and flange for the
bridge shown in Fig. H1.

When the flange is slightly disturbed from its initially straight
position the equations of statical equilibrium are obtained by examining
the shear per unit length acting on an element, as shown (Fig. H3), and
we obtain the differential equation

$$d^2(EI_T \, d^2x/dz^2)/dz^2 + d(P_T(dx/dz)/dz + \beta x = 0 \tag{H2}$$

and if the flexural rigidity is constant along the length, equation (H2)
simplifies to the differential equation

$$EI_T \, d^4x/dz^4 + \beta x + (w/2h)d[z(\ell-z)dx/dz]/dz = 0 \tag{H3}$$

When the boundary conditions

$$z = 0 \text{ and } \ell \; ; \quad x = 0, \quad EI_T d^2x/dz^2 - 0 \; ,$$

are specified, a mathematical system which has an infinity of eigen
function solutions x_n , and corresponding eigen values w_n is specified
(see Chapter Two).

Fig. H3. An element of the top flange for the bridge shown in
Fig. H1.

A solution of the differential equation (H3) and associated boundary conditiins is obtained by Timoshenko, Ref. 2, who uses an energy method. The final shape, x, is expressed in a Fourier sine series, i.e.

$$x = a_1 \sin \pi z/\ell + a_3 \sin 3\pi z/\ell + \ldots$$

for the symmetric mode, and

$$x = a_2 \sin 2\pi z/\ell + a_4 \sin 4\pi z/\ell + \ldots$$

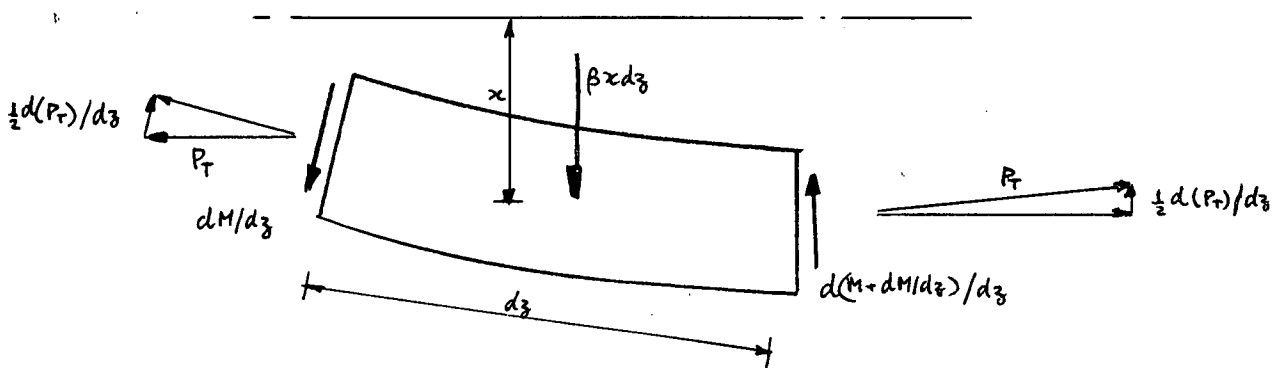for the antisymmetric mode. The values for a_1, a_3, a_5, are shown in Fig. H4 and values for w_1, w_2 are shown in Fig. H5.

The lowest buckling load is obtained from fig. H5, and it/is seen that sometimes this mode is symmetric and sometimes antisymmetric. However, the difference in buckling loads, corresponding to these two different modes is small.

2.2.6 Lateral loading effects on equation (H3).

The effect of a distributed lateral shear force, h(z) applied to the top flange, is to alter the differential equation (H3) to the differential equation

$$EI_T d^4x/dz^4 + x + (W/2h)d[z(\ell-z)dx/dz]/dz = h(z) \quad , \tag{H4}$$

where h(z) is a function of the applied loading.

This model is solved by replacing the loading by the series

$$c_1 d[z(\ell-z)dx_1/dz]/dz + c_2 d[z(\ell-z)dx_2/dz]/dz + \ldots = h(z)$$

The value of c_m is obtained as the ratio

$$c_n = \int_0^\ell x_n h(z)dz / \int_0^\ell d[z(\ell-z)dx_n/dz]/dz \; x_n \; dz$$

when both sides of the series are multiplied by the function x and the equation is integrated between the boundaries. The final solution

$$x = b_1 x_1 + b_2 x_2 + b_3 x_3 + \ldots$$

is obtained by substitution of the values of $c_n x_n$ into equation (H4).
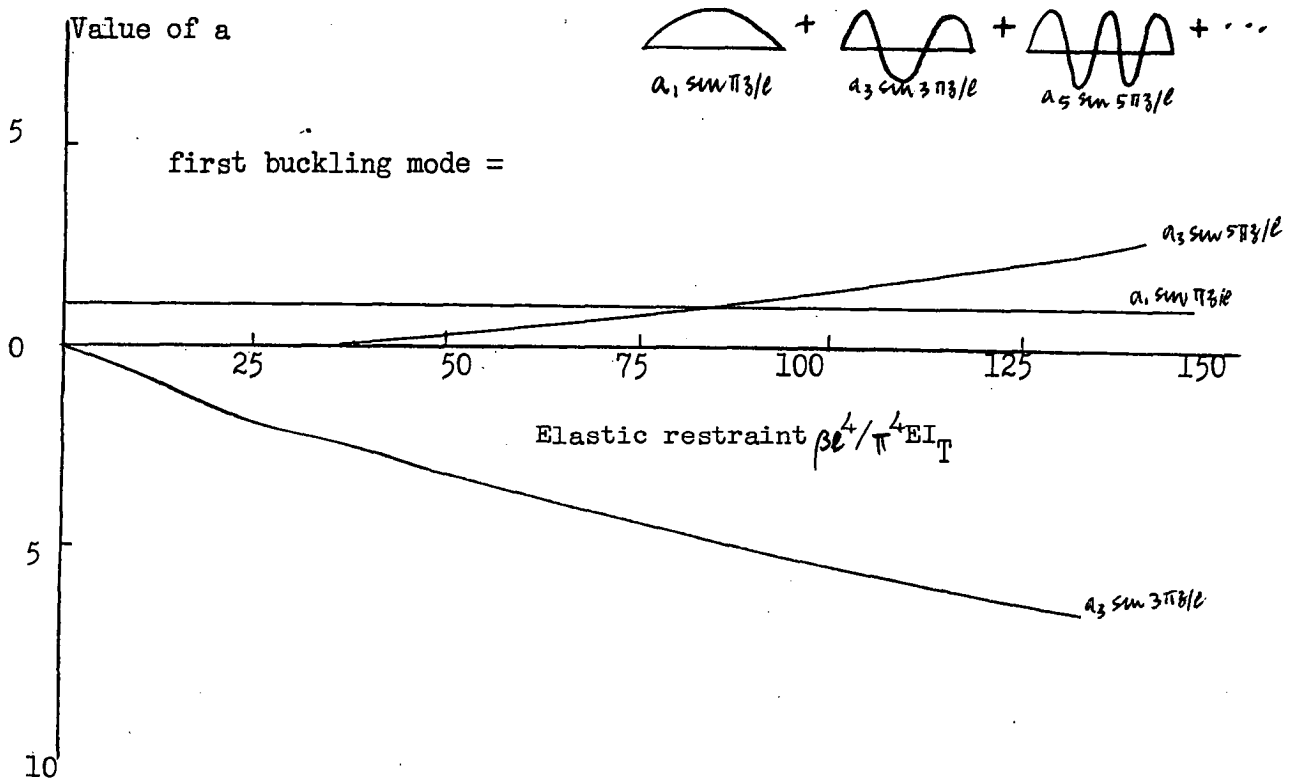
Fig. H4. First buckling mode components for a solution of equation H
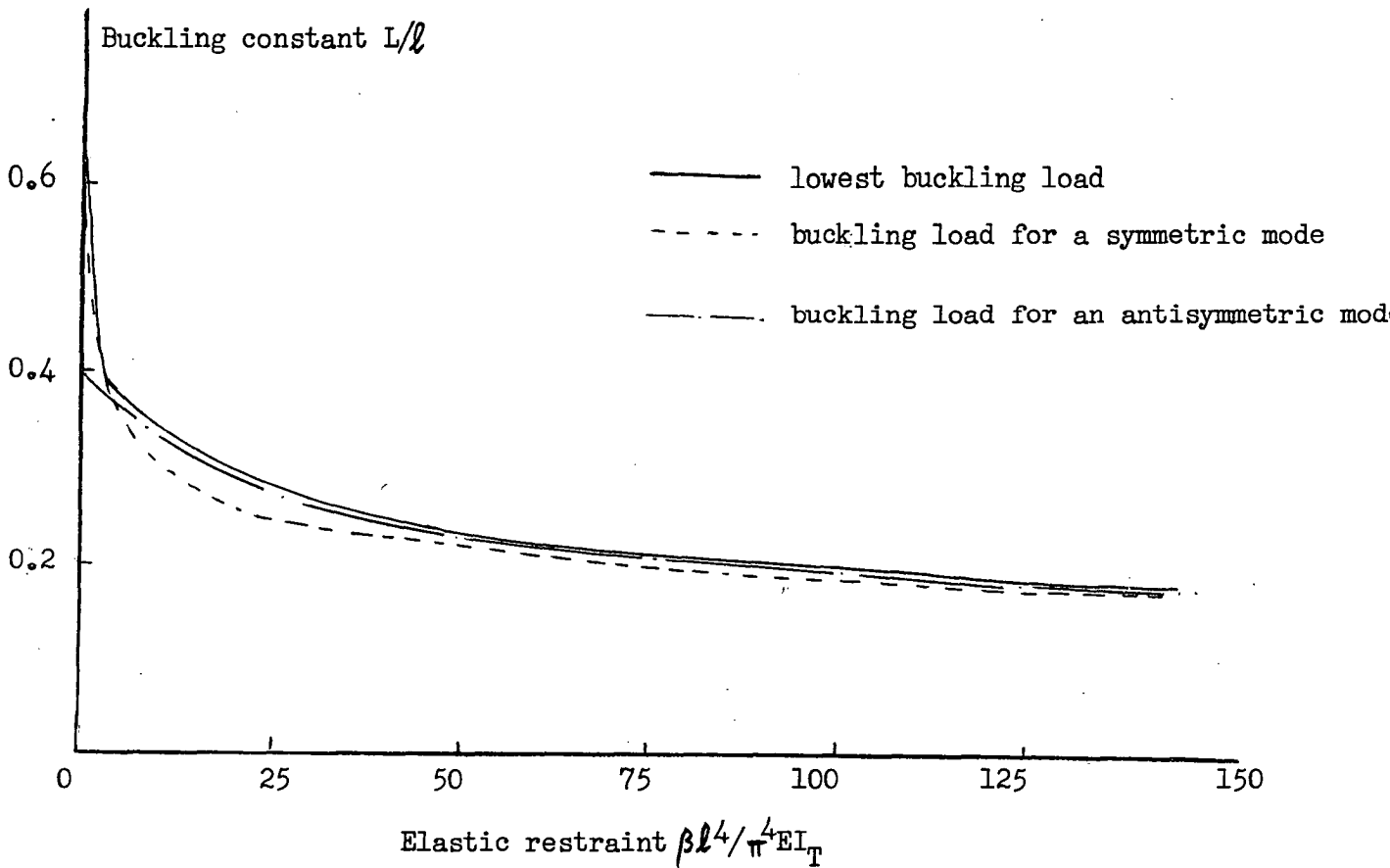
Fig. H5. Values of (L/ℓ) to use in $P_T = \pi^2 EI_T/(L)^2$ for a solution of equation H3.

When a lateral point load F is applied to the top flange at a point in the middle of the bridge, and the vertical loading applied to the bridge is increased until it is close to the buckling load of the bridge, the final shape of the top flange x is given approximately by the first term in the infinite series, that is

$$x \approx k \; x_1 \, (F/2\ell)(w_1/2h)/(1-w/w_1) \; .$$ (H5)

Values of k are plotted in Fig. H6 for a range of values of elastic restraint $\beta\ell\,4/\pi^4 EI_T$.
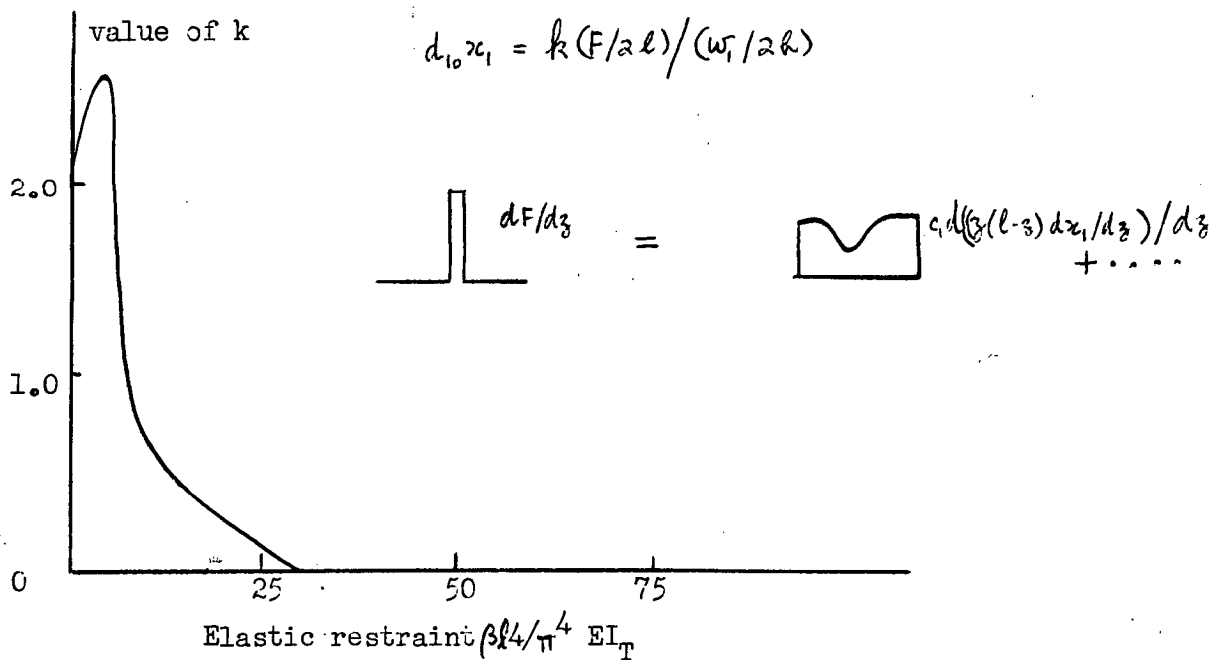
Fig. H6. Values of k for lateral loading as given by equation H5.

Examination of other forms of loading, indicate that of all the likely forms of lateral loading that might be applied to the bridge the central lateral point loading induces the maximum first mode deformation. However, it is seen from Fig. H6 that these deformations quickly diminish as the lateral restraint is increased. Therefore, even when large vertical loads are applied to the bridge, it is unnecessary to allow for any decrease in the lateral stiffness of the top flange.

Because the first buckling mode is not a good representation of the deformations induced by the lateral loadings, a large number of terms in the infinite series are required to specify accurately

the final deformations.   It is easier therefore to use existing methods
of superposition to find the final deformed shape of the bridge, i.e.
find the deformations induced by the lateral loadings using usual bending
theory, and add linearly these deformations to the buckling deformations.

APPENDIX J.

<u>Notation.</u>

A	$=$	area of the section
a	$=$	spacing of the floor beams
$a_n y_m$	$=$	components of the n buckling mode
$[A]$, $[B]$	$=$	$n \times n$ matrices
B	$=$	bimoment
b	$=$	width of strip, leg width of an angle section
C	$=$	St Venant torsional stiffness
C_o	$=$	equivalent torsional restraint provided by the floor beams
C_1	$=$	warping stiffness
C_{10}, C_{oo}	$=$	values of C_1 , C_o along a beam
E	$=$	modulus of elasticity, Young's modulus
EI	$=$	flexural stiffness of a pin ended column
EI_η	$=$	flexural lateral stiffness of an I beam
EI_F	$=$	flexural vertical stiffness of a floor system
EI_T	$=$	flexural lateral stiffness of the top chord of an I beam
F	$=$	force
f_z	$=$	longitudinal stress at the point z
G	$=$	shear modulus
g_1 , g_2	$=$	constants
$h(z)$	$=$	lateral shear force
H_P	$=$	fourth moment of area, taken about the Weber centre
h	$=$	depth of I-section beam
I_c	$=$	polar second moment of area taken about the centroid
I_P	$=$	polar second moment of area taken about the Weber centre
K	$=$	force
$K(x, s)$	$=$	kernel
k	$=$	the ratio of the total lateral movement of the top flange of a through bridge (sustained by a lateral force applied at the top flange of the bridge) to the magnitude of the lateral movement of the top flange that results from the deformation of the floor beams

ℓ	=	length of column section, strip
L	=	effective length of the top flange of the I beam
$L(\phi), N(\phi)$	=	differential operators
M	=	moment
M_{xy}, M_{yz}	=	twisting moments in the xy and yz planes
P	=	load applied to a single I beam, column
P_1, P_2	=	eigen values
P_a	=	Euler buckling load of a column of length a
P_T	=	the axial force in the top flange of the I beam at z
P_{crit}	=	first critical load as measured by a Southwell Plot
p	=	line loading
q_p	=	shear stress to produce yield
r, R	=	radii
r_s, r_z, r	=	distance measurements
s	=	arc length along a boundary
S	=	width of bridge
T_z	=	torsional loading
T	=	torque
t	=	thickness of the strip
u	=	lateral deflection of the centroid of the beam
u, v	=	movements in the xy plane
w	=	vertical movement in the z direction
w	=	uniform loading
w_1, w_2	=	eigen values
x	=	the lateral movement of the top flange
x_1, x_2	=	eigen functions
$[x]$	=	column vector
x, y, z		
	=	systems of axes
x_1, y_1, z_f		
y	=	final deformed shape
y_1, y_2	=	eigen functions
y_o	=	initial crookedness in y
α, β	=	angles

β = the lateral shear force restraint per unit displacement provided by the web and bottom chords of the through bridge

γ = $(EI - EI_\eta)/EI$, taken as 1.0 for the problems examined in this thesis

ϵ_z = longitudinal strain at the point z

ϵ_{od} = longitudinal strain a the point 0

ϵ_x, ϵ_y = direct strains in the x, y directions

γ_{xy} = shear strain in the xy plane

γ_s = shear strain on the surface of a strip

σ_x, σ_y = direct stresses in the x, y directions

$\tau_{xy}, \tau_{yz}, \tau_{zx}$ = shear stress in the xz, xy, yz planes

θ_{xy}, θ_{yz} = rotations in the xy and yz planes

θ = rotation of the beam

θ_1, θ_2 = eigen functions

λ = loading constant

λ_1, λ_2 = eigen values

ϕ = deformation

ϕ_o = initial deformation

REFERENCES

1. Rowe, R.E. and Base, G.D. "Model Analysis and Testing as a Design
        Tool",
        <u>Proc. I.C.E.</u> Vol 33. Feb 1966 and discussion Vol 36, March
        1967.

2. Pugsley, Sir Alfred, "The Way of Research", Presidential Address
        Institution of Structural Engineers, 1957.
        <u>Structural Engineer</u>, Nov 1957.

3. Southwell, R.V., "On the Analysis ofExperimental Observations in
        Problems of Elastic Stability", <u>Proc. Roy. Soc.</u>, London,
        Series A, Vol 135, 1932.

4. Timoshenko, S.P. "History of Strength of Materials", <u>McGraw-Hill</u>,
        1953.

5. Oliver, A.R., "University Training of an Engineer", <u>Inst. Eng.</u>
        <u>Aust. Tasmanian Div. Bulletin</u>, No 156, July 1965.

6. Gregory, M.S. "Teaching Engineering Attitude to Students",
        <u>Proc. A.S.C.E. Journ. Proff. Pract.</u> Jan. 1965 .

7. Middleton, E. & Jenkins, C.J. "A Moire Method of Strain Analysis
        for Student Use". <u>Bulletin of Mechanical Engineering</u>
        <u>Education</u> Vol 5 No. 3, July- Sept. 1966.

8. Ligtenberg, F.K. "The Moire Method - a new experimental method
        for the determination of moments in small slab models"
        Vol XII No. 2 <u>Proc. Soc. Experimental Stress Analysis</u>,
        1955.

9. Vlasov, V.Z. "Thin Walled Elastic Beams". 2nd Edition. <u>Israel</u>
        <u>Program for Scientific Translations</u>, 1961.

10. Wilkin, J.K. "Decked Rockfill Dams", <u>Tasmanian Division Bulletin</u>.
        <u>The Institution of Engineers</u>, Australia Feb. 1967.

11. Gregory, M.S. "The Buckling of Structures" Ph.D. Thesis <u>Univ. of</u>
        <u>Tas.</u>, Aust. 1960.

12. Gregory, M.S. "Elastic Instability" <u>Spon, London</u>, 1967.

13. Ariaratnam, S.T. "The Southwell Method of Predicting Critical
        Loads of Elastic Structures", <u>Quart. J. Mechs. and</u>
        <u>Appl. Maths</u>, 14, 1961.

14. Crandall, S.H. "Engineering Analysis" McGraw Hill, 1956.

15. Courant, R., and Hilbert, D., "Methods of Mathematical Physics"
      Vol. 1, Interscience Publishers, New York, 1953.

16. Mikhlin, S.G. "Integral Equations" Pergamon Press 1957.

17. Donnell, L.H. "On The Application of Southwell's Method for
      the Analysis of Buckling Tests" Stephen Timoshenko
      60th Anniversary Volume, The MacMillan Co., 1938.

18. Dumont, C. and Hill, H.N., "The Lateral Stability of Equal
      Flanges Aluminium Alloy "I" Beams subjected to Pure
      Bending", N.A.C.A. TN 770, 1940.

19. Massey, C. "Elastic and Inelastic Instability of I-Beams",
      The Engineer, p. 672, Oct. 25, 1963.

20. Galletly, G.D. and Reynolds, T.E. "A Simple Extension of Southwell's
      Method for Determining the Elastic General Instability
      Pressure of Ring-Stiffened Cylinders Subject to
      External Hydrostatic Pressure", Proc. S.E.S.A.
      Vol XIII No. 2. 1956.

21. Gregory, M.S. "The Application of the Southwell Plot on Strains
      to Problems of Elastic Instability of Framed Structures
      where Buckling of Members in Torsion and Flexure occurs"
      Aust. J. Appl. Sci. 11 (1) 1960.

22. Gregory, M.S. "The Use of Measured Strains to obtain Critical
      Loads", Civil Engrg. Lond. Vol 55, No. 642; p.80-82.

23. Southwell, R.V. "Theory of Elasticity", Oxford University Press
      1941.

24. Thompson, J.M.T., "Basic Principles in the General Theory of
      elastic Stability". J. Mech. Phys. Solids 11, 1963.

25. Johnston, Bruce G., "The Column Research Council Guide to
      Design Criteria for Metal Compression Members",
      Second Edition, John Wiley & Sons, 1966.

26. O'Connor, C. "Residual Stresses and their Influence on Structural
      Design", Journ. Inst. Engineers, Aust. Vol 27, Dec. 1955.

27. Tall, L. (editor) "Structural Steel Design". The Ronald Press Co.,
      1964.

28. National Association of Australian State Road Authorities, Highway Bridge Design Specification, 1958.

29. Bleich, F. "Buckling Strength of Metal Structures" McGraw-Hill, 1952.

30. Timoshenko, S.P. and Gere, J.M., "Theory of Elastic Stability", McGraw-Hill, Second Edition, 1961.

31. Lamb, H. and Southwell, R.V. "The Vibrations of a Spinning Disc", Proc. Royal Soc. London, Series A, Vol 99, 1921.

32. Mitchell, A.G.M. "Elastic Stability of Long Beams Under Transverse Forces". Philosophical Mag. Vol 48, 298. 1899

33. O'Connor, C., "The Buckling of a Monosymmetric Beam Loaded in the Plane of Symmetry". Aust. Jounr. of Applied Science. Vol 15, no . 4, Dec. 1964.

34. Lee, G.C., "A Survey of Literature on the Lateral Instability of Beams". Welding Research Council Bulletin Series. Aug. 1960.

35. Finlayson, B.A. and Scirven, L.E., "The Method of Weighted Residuals - A Review". App. Mech. Review Article, Vol 19, No. 9. Sept. 1966.

36. Temple, G. and Bickley, W.G., "Rayleigh's Principle". Oxford University Press. 1933.

37. Frazer, R.A., Jones, B.A. and Skan, S.W. "Approximations to Functions and to the Solution of Differential Equations" Great Britain Aeronaut. Research Comm. Dept. and Mem. 1799, 1937.

38. Kjar, A.R., "A Summary of Buckling with particular regard to the Buckling of a Through Plate Girder Bridge". Honours Degree Thesis, University of Tasmania, March 1965.

39. Taylor, A.C., and Ojaluo, M. "Torsional Restraint of Lateral Buckling". Journal Struct. Div., Proc ASCE. April, 1966.

40. Schwarz, H.A., "Gesammelte Mathematische Abhandlungen", Berlin Vol 1, 1890.

41. Temple, G. "The Computation of Characteristic Numbers and Characteristic Functions". Proc. Lond. Math. Soc. (2) 29. 1928.

42. Collatz, L. "Z angew Math u Mech., 19 p 239. 1939.

43. Collatz, L. "Eigenvertaufgaben mit Fechnischen Anwendung" Akademische Verlagsgescllschaff m.l.H. Leipzig. 1949.

44. Biezeno, C.B. and Grammel, R. "Engineering Dynamics", Blackie & Sons Ltd. Vol 1, 2,1955.

45. Timoshenko, S.P. and Woinowsky-Krieger, S. "Theory of Plates and Shells". McGraw-Hill, 1959.

46. Gaylord, E.H. and Gaylord, C.N. "Design of Steel Structures" McGraw-Hill 1957.

47. Timoshenko, S.P. "The Collected Papers of" McGraw-Hill 1953.

48. Dooley, J.F. "On the Torsional Buckling of Columns of I-Section Restrained at Finite Intervals". Int. J. Mech. Sci. Vol 9, 1967.

49. O'Connor, C., Goldsmith, P.R. and Ryall, J.T. "The Reinforcement of Slender Steel Beams to Improve Beam Buckling Strength". Trans. Inst. Eng. Aust.CE7, No. 1. April 1965, and discussion CE7, No. 2 Oct. 1965.

50. Horne, M.R. and Merchant, W. "The Stability of Frames". Pergamon Press, 1965.

51. British Standard 153: "Steel Girder Bridges". British Standards Institution.

52. Column Research Council. "Design Criteria for Metal Compression Members, Second Edition" edited by Bruce G. Johnston. John Wiley & Sons, 1966.

53. Deutsche Norman DIN 4114: "Steel Structures, Stability, (Buckling, Overturning and Bulging)". 1952.

54. American Association of State Highway Officials. "Standard Specifications for Highway Bridges". 1961.

55. National Association of Australian State Road Authorities "Highway Bridge Design Specification", 1958.

56. Schmidt, L.C., "A Problem of Elastic Lateral Stability" Quart. Journ. Mech. and Applied Math., Vol XVIII, Pt 4, 1965.

57. Timoshenko, S.P. and Goodier, J.N. "Theory of Elasticity"
   McGraw- Hill, Second Edition 1951.

58. Ashwell, D.G. "The two axes of Twist in Elastic Prisms",
   Engineering, Dec. 18 1953.

59. Buckley, J.C., "The Bifilar Property of Twisted Strips",
   Phil. Mag. Series 6, vol 28: 1914.

60. Weber, C. "Die Lehre der Drehungsfestigkeit", Forschungsarbeiten
   No. 249. V.d. I 1921.

61. Cullimore, M.S.G. "The Shortening Effect; A non linear feature
   of Pure Torsion", Research Engineering Structures
   Supplement. Butterworths Scientific Publications 1940.

62. Ashwell, D.G. "The Axis of Distortion of a Twisted Elastic Prism",
   Phil. Mag. Series 7, vol 42, 1951.

63. Gregory, M.S. "A Non Linear Bending Effect when certain
   Unsymmetrical Sections are Subject to a Pure Torque",
   Aust. Journal of Applied Science, Vol 11, No. 1, 1960.

64. Gregory, M.S. "Elastic Torsion of Members of thin Open Cross
   Section", Aust. Journal of Applied Science, Vol 12,
   No. 2, 1961.

65. Oliver, A.R. "Energy Methods in Structural Analysis": Civil
   Eng. Trans. Inst. Eng. Aust. March 1961.

66. Mitchell, L.H. Private Communication to M.S. Gregory 4/10/61.

67. Ashwell, D.G. Private Communication to M.S. Gregory 14/2/63.

68. Duncan, W.J., Ellis, D.L. and Scruton, C. "The Flexural Centre
   and the Centre of Twist of an Elastic Cylinder",
   Phil. Mag. S.7 Vol 16. No 104. August 1933.

69. Lockwood Taylor, J. "Theory of Torsion Bending", Aircraft Eng.
   Oct., 1938.

70. Hoff, N.J. "Stresses in Space Covered Rings in Monocoque
   Fuselages". Journ. of Royal Aero. Soc. Feb. 1943.

71. Biot, M.A. "Increase ofTorsional Stiffness of a Prismatic
   Bar due to Axial Tension", Journal of Applied
   Physics 10, 1939.

72. Green, R.T.G. "Stability of Angle Section Members",
   Master of Eng. Science Thesis, University of Tasmania,
   August, 1967.

73. Hilderbrand, F.B. "Methods of Applied Mathematics" <u>Prentice-Hall</u>
      Inc., 2nd Edition, 1965.

74. Caughey, T.K. and O'Kelly, M.E.J. "Classical Modes in Damped
      Linear Dynamic Systems". Trans ASME <u>Journ. App. Mech.</u>
      Sept., 1965.

75. Hermann, G. "Stability of Equilibrium of Elastic Systems Subjected
      to Non-Conservative Forces". <u>Applied Mech. Reviews</u>, Feb.1967.

76. Maybee, J.S. "Normal and Quasi Normal Modes in Damped Linear
      Systems". Trans ASME <u>Journ. App. Mech.</u>, June 1966.

77. Atkinson, C.P. "On the Stability of the linearly Related Modes of
      Certain non-linear two degree of freedom Systems".
      <u>Journ. App. Mech.</u> 28, 1961.

78. Saravanos, B., "Finite Difference Approximation to a Non-Self
      Adjoint Eigen System". Tech. Note, <u>Journ. Royal Aero. Soc.</u>
      Nov. 1964.

79. Bolitin, V.V., "Non Conservative Problems of the Theory of Elastic
      Stability". <u>Pergamon/MacMillan</u>, 1963.

80. Gregory, M.S. "Framed Structures". <u>Longmans</u>, London, 1966.

The following is a list of <u>papers published by the author</u> in
connection with this thesis. Most of the published work is
embodied in this thesis:

<u>Kjar, A.R.</u> Discussion to "The Reinforcement of Slender Steel Beams to
Improve Beam Buckling Strength". by O'Connor etc.
<u>I.E. Aust. CE No 7 No 1 April 1965,</u> appearing in
<u>CE No 7, No 2,</u> Oct 1965, p. 162.

<u>Kjar, A.R.</u> Discussion to "Torsional Restraint of Lateral Buckling" by
Taylor, A.C., and Ojalvo, M. <u>Proc. ASCE Struct Div.,</u> April
1965, appearing in Feb. 1967, p. 569.

<u>Kjar, A.R.</u> Discussion to "Computer Analysis of a 600 ft. Three Dimensional
Frame Building, <u>I.E. Aust CE No 8, No 1,</u> April, 1967,
appearing in CE No 8, No 2, Oct 1967. p. 169.

<u>Kjar, A.R.</u> "Large Field Measurement of Geometry"
<u>I.E. Aust, Tas Div. Bulletin</u> Nov 1965.

<u>Kjar, A.R.</u> "The Axis of Distortion" <u>Intern. Journ. Mech. Sciences</u>
(in the hands of the printer).

<u>Kjar, A.R.</u> "Approximate Methods in Structural Analysis"
"First Australasian Conference on Structural Analysis",
<u>University of New South Wales.</u> August 1967.

The following papers have been submitted for publication, and are
at present in the hands of the reviewer:

Kjar, A.R. <u>"Lateral Instability of I-section Beams".</u>

Kjar, A.R. <u>"Southwell Plot Extensions".</u>

Kjar, A.R. <u>"The Design of Through Bridges".</u>

Kjar, A.R. <u>"A Geometric Approach to Torsion of Thin Strips".</u>

- oOo -